Mechanisms of Recovery in incomplete Spinal Cord Injury

Dissertation

zur

Erlangung der naturwissenschaftlichen Doktorwürde
(Dr. sc. nat.)

vorgelegt der

Mathematisch-naturwissenschaftlichen Fakultät

der

Universität Zürich

von

Björn Zörner

aus Deutschland

Promotionskomitee

Prof. Dr. Martin E. Schwab (Vorsitz, Leitung der Dissertation und verantwortliches Fakultätsmitglied)
Prof. Dr. Wolf Blanckenhorn
Prof. Dr. Armin Curt
Prof. em. Dr. Volker Dietz

Zürich, 2014

Für meine Eltern Helga und Wolfgang

„Nicht Kunst und Wissenschaft allein, Geduld will bei dem Werke sein.“

Mephistopheles in
Johann Wolfgang von Goethes
Faust I, Hexenküche, 1808

Table of contents

Chapter 5

Basic mechanisms of functional recovery in multiple sclerosis

Summary

Animals and humans can show extensive spontaneous functional recovery after brain or spinal cord injury. Mechanisms mediating this recovery include different forms of neuronal plasticity such as sprouting of lesioned and spared nerve fibers and the formation of detour pathways bypassing the lesion. In animals, this is described for the corticospinal tract and propriospinal connections. Very little is known about plastic changes in the brainstem with its wide-spread spinal projections and its outstanding role for locomotion in all vertebrates. In adult rats, we studied anatomical plasticity, specifically, compensatory sprouting of spared fibers, in the major descending brain regions after cervical unilateral hemisection injury. We identified a highly plastic region in the phylogenetically oldest and functionally most important part of the brainstem, the reticular formation. We also found evidence that changes of the spinal projection pattern of reticular neurons were accompanied by remodeling of their input from a “higher” locomotor center in the midbrain, the mesencephalic locomotor region. We developed and validated a testing apparatus for precise, quantitative and objective assessment of different types of locomotion in rodents with brain or spinal cord injury and used this set-up to demonstrate the functional relevance of the observed anatomical changes in the brainstem. In behaviorally recovered spinal cord injured rats, inactivation of the plastic reticular nucleus led to the reappearance of some of the deficits seen acutely after hemisection. Our results suggest that anatomical modifications in the brainstem represent a key element for spontaneous recovery of locomotor function after incomplete spinal cord injury. Such spontaneous anatomical plasticity can be further enhanced in spinal cord injured rodents and primates by blocking endogenous inhibitory factors of axonal growth such as the protein Nogo-A. For clinical trials investigating this approach, early identification of eligible patients is crucial. Based on data from a multicenter cohort study, we generated a clinical algorithm improving outcome prediction and patient stratification in incomplete spinal cord injury to further open up paths towards clinical application of those promising therapies.

Zusammenfassung

Tiere und Menschen können spontan eine erhebliche Erholung nach Verletzung des Gehirns oder des Rückenmarkes zeigen. Die zugrundeliegenden Mechanismen für diese Erholung beinhalten verschiedene Formen der neuronalen Plastizität, wie das Aussprossen von verletzten und unverletzten Nervenfasern und die Ausbildung von Umgehungen. Dies ist im Tier eindrücklich für Fasern, die von der Großhirnrinde in das Rückenmark projizieren, und für Verbindungen innerhalb des Rückenmarkes dokumentiert. Nur sehr wenig ist über plastische Veränderungen im Hirnstamm bekannt, der viele und weitreichende Verbindungen in das Rückenmark entsendet und dem eine herausragende Bedeutung für die Fortbewegung in Wirbeltieren zukommt. In erwachsenen Ratten untersuchten wir nach einer halbseitigen Durchtrennung des Halsrückenmarkes die anatomische Plastizität, insbesondere das kompensatorische Aussprossen von unverletzten Nervenfasern, in den wichtigsten das Rückenmark innervierenden Hirnregionen. Wir identifizierten eine stark plastische Region in einem der entwicklungsgeschichtlich ältesten und funktionell wichtigsten Teilen des Hirnstamms, der retikulären Formation. Zudem fanden wir Hinweise darauf, dass die Veränderungen des spinalen Innervationsmusters dieser retikulären Nervenzellen von einer Umgestaltung ihrer Afferenzen aus einem „höheren“ lokomotorischen Zentrum im Mittelhirn begleitet war. Wir entwickelten und validierten ein Messsystem für die präzise, quantitative und objektive Auswertung verschiedener Formen der Fortbewegung in Nagetieren mit Gehirn- oder Rückenmarkverletzung. Dies ermöglichte es uns, die Auswirkungen der beobachteten anatomischen Veränderungen im Hirnstamm auf die motorischen Funktionen zu untersuchen. In Ratten, die sich von der halbseitigen Rückenmarkverletzung erholen konnten, führte die Inaktivierung des plastischen retikulären Kerns im Hirnstamm zum Wiederauftreten von einigen Defiziten, die schon akut nach der Rückenmarkverletzung zu beobachten waren. Unsere Resultate legen nahe, dass die anatomischen Veränderungen im Hirnstamm ein wesentliches Element der spontanen Erholung von Lokomotion nach inkompletter Rückenmarkverletzung darstellen. Die spontane anatomische Plastizität kann zusätzlich durch die Blockierung von körpereigenen Nervenwachstumshemmstoffen, wie das Protein Nogo-A, in rückenmarkverletzten Nagetieren und Primaten gesteigert werden. Für die Durchführung von klinischen Studien, die diesen Ansatz verfolgen, ist eine frühe Identifizierung von geeigneten Patienten entscheidend. Basierend auf Daten aus einer multizentrischen Kohortenstudie entwickelten wir einen klinischen Algorithmus zur verbesserten Prognose und Einteilung von Patienten mit inkompletter Rückenmarkverletzung, um den Weg hin zur klinischen Anwendung dieser aussichtsreichen therapeutischen Ansätze weiter vorzubereiten.

General introduction

Epidemiology, consequences and therapy of spinal cord injury

Spinal cord injury is a devastating neurological condition affecting primarily young men. The global incidence lies between 10 to 83 cases per million inhabitants a year[1]. Trauma, ischemia, tumor or degenerative processes can result in spinal cord lesions that sever ascending and descending nerve fibers and destroy local spinal neurons and glia. Falls are the leading cause of traumatic spinal cord injury in the United States[2]. In one third (up to one half) of the cases the cervical spinal cord is injured resulting in tetraparesis or tetraplegia. About half of the subjects with spinal cord injury have a complete lesion. Impairments commonly observed after spinal cord injury are paresis, sensory disturbances, spasticity as well as bladder, bowel and sexual dysfunction. In particular in incomplete spinal cord injury, outcome is highly variable ranging from subjects that rely on lifelong permanent assistance to individuals without any restrictions in everyday life[3]. In the absence of pharmacological or surgical therapies enabling direct spinal cord repair in humans[4], the current strategy to improve deficits in spinal cord injured subjects comprises an interdisciplinary approach including physiotherapy, occupational therapy and symptomatic medical treatment. Thus, neurorehabilitation intends to improve functional outcome by permitting, promoting and enforcing spontaneous recovery, for example by training, and optimizing compensational strategies. A better understanding of the mechanisms underlying spontaneous recovery after spinal cord injury is essential to improve current therapies and to develop new effective treatments for spinal cord injury (***see Chapter 1***).

Animal models in neurorehabilitation research

The identification of these mechanisms mediating spontaneous recovery following injury to the central nervous system (CNS), for example spinal cord injury, is one major objective of basic neurorehabilitation research. To progress in this field, basic neurorehabilitation research relies on animal models, although there are issues challenging the translation of results obtained from animals studies into humans[4]. Such concerns include the use of invalid injury paradigms, bipedal walking in humans and quadrupedal locomotion in experimental animals like rodents and differences in neuroanatomy and body (and CNS) size between species. Anatomical studies at the level of single cells and axons are, so far, only feasible in animals, but are indispensable for understanding the complex processes leading to functional recovery after CNS injury. To correlate even subtle anatomical changes with functional outcome in

animal models of CNS injury, a detailed analysis of the animals' behavior is required. However, previous methods to assess motor function like scoring systems suffered from several limitations, for example subjectivity and low sensitivity. Therefore, we developed a behavior set-up that allows comprehensive, quantitative and objective evaluation of motor functions in rats and mice (***see Chapter 2***). Using this set-up, our group characterized in detail the behavioral deficits and the recovery pattern after cervical unilateral spinal cord hemisection in rats[5]. Injured rats showed excellent recovery of basic hindlimb motor functions but poor recovery of the ipsilesional forelimb and persistent deficits in fine motor control. Thus, rats demonstrated a comparable pattern of impairment and recovery as humans with unilateral spinal cord injury, i.e., Brown-Séquard syndrome[6,7]. Therefore, we used this highly reproducible and conferrable rat spinal cord injury paradigm to further study the mechanisms underlying functional recovery after CNS injury (***see Chapter 3***).

Current concepts on the mechanisms mediating recovery after spinal cord injury

The degree of the initial deficit and the extent of recovery after CNS damage, for example spinal cord injury, is influenced by the type of the lesion, its location and its size as well as by additional factors such as the age of the injured individual. In the acute phase, resolution of edema, adjustments of metabolic disturbances and restoration of axonal or synaptic conduction failure may contribute to improvements observed early after injury[8]. Axonal demyelination can occur after spinal or brain injury and remyelination of these axons by oligodendrocytes may account, in part, for functional recovery in the subacute phase[9]. Synaptic and dendritic modifications, sprouting of lesioned ("regenerative sprouting") and unlesioned fibers ("compensatory sprouting") and the formation of new connections and pathways are known as "neuronal plasticity". Such plastic changes are most likely present from early until late stages after injury and are associated with functional recovery in animals[10-16]. The contribution of each of these processes to recovery may vary depending on the nature of the injury but these mechanisms may also act in concert to eventually improve function.

Anatomical changes in the adult CNS of spinal cord injured animals were demonstrated at different levels. Following transection of the dorsal half of the thoracic spinal cord, severed corticospinal fibers contact propriospinal neurons bridging the lesion site to convey supraspinal information to neurons located in the lumbar spinal cord[12]. Also, spinal interneurons were shown to rewire in response to staggered thoracic spinal hemisection

injuries relaying supraspinal input to lumbar spinal circuits[15]. In addition, there is evidence from experiments in cats that spinal locomotor networks such as the central pattern generator reorganize after incomplete spinal cord injury to become more independent from supraspinal control[17]. Finally, one remarkable finding in rats was that collaterals of unlesioned corticospinal axons spontaneously sprout across the spinal cord midline after spinal hemisection injury or pyramidotomy to innervate new target neurons in the denervated hemicord[18,19]. Such a side-switch of projections of a corticospinal neuron has far-reaching consequences. Further "secondary" modifications may be needed such as adaptations of the input the crossed neuron receives from other neurons. However, such transsynaptic rearrangements in the CNS after spinal cord injury remain to be demonstrated. Up to now, spontaneous compensatory sprouting over the spinal cord midline was exclusively described for corticospinal neurons. Despite their outstanding physiological roles for locomotion in animals and humans, the descending brainstem systems are grossly understudied in the present literature on spinal cord injury, recovery and plasticity. Therefore, we investigated spontaneous anatomical plasticity - specifically, spontaneous compensatory sprouting over the spinal cord midline - of descending brainstem motor systems after unilateral hemisection injury in rats (***see Chapter 3***). We also asked whether changes of the spinal projection pattern of a given brainstem nucleus were accompanied by modifications of its input and whether anatomical plasticity in the brainstem contributed to the observed recovery of locomotor function after spinal cord injury.

Despite all these abovementioned processes, spontaneous recovery after spinal cord injury is often incomplete, especially following large lesions. The identification of factors hindering functional improvement is another key objective in basic neurorehabilitation research in order to discover new therapeutic targets[20-22]. For example, neutralization of the neurite-outgrowth inhibitor Nogo-A improves outcome after incomplete spinal cord injury in rats and monkeys by increasing anatomical plasticity[23-25]. This approach is currently studied in humans with spinal cord injury in a multicenter clinical trial (***see also Chapter 1***). Therapies inducing neuronal plasticity or even long-distance regeneration require bridges of spared nervous tissue at the lesion site to be effective. Therefore, it seems reasonable to investigate this approach in individuals with incomplete spinal cord injury but little prospect of good spontaneous recovery. Identification of these patients at an early time point after injury requires improved outcome prediction and patient stratification. Based on data from a multicenter cohort study, we generated a clinical algorithm for early identification of patients with incomplete spinal cord injury and poor functional outcome (***see Chapter 4***).

Finally, the basic mechanisms mediating functional recovery in traumatic spinal cord injury may be conferrable to other diseases of the CNS. Multiple sclerosis (MS) is a chronic inflammatory disease of the CNS characterized by demyelination of nerve fibers, axonal injury and neuronal degeneration in the brain and, in particular, in the spinal cord. In ***Chapter 5***, we discuss the mechanisms that may also be crucial for recovery from MS lesions.

Aims of the thesis

Studies in rodents with CNS injury
(Chapter 2 and 3)

- To establish a new behavior testing set-up that allows comprehensive, quantitative and objective evaluation of different types of locomotion after CNS damage in rodents.
- To undertake a systematic and comprehensive evaluation of the effects of various insults to the CNS for the validation of the new behavior testing set-up in rats and mice.

- To demonstrate spontaneous anatomical plasticity, i.e. an increase of midline crossing fibers, in descending brainstem systems after incomplete cervical spinal cord injury (unilateral hemisection) in adult rats.
- To demonstrate that changes in the spinal projection pattern of a “plastic” region are accompanied by anatomical remodeling of its input from other CNS centers.
- To demonstrate the relevance of these anatomical changes in the brainstem for functional recovery after incomplete cervical spinal cord injury by investigating the behavioral consequences of inactivation of the “plastic” region in recovered rats.

Study in humans with spinal cord injury
(Chapter 4)

- To identify predictors of walking outcome in a population of individuals with tetra- or paraparesis allowing reliable prognosis and subgrouping of patients for future clinical trials and studies on functional recovery in incomplete spinal cord injury.

Chapter 1

Anti-Nogo on the go: from animal models to a clinical trial

Björn Zörner and Martin E. Schwab

Brain Research Institute, University of Zurich and Dept. of Health Sciences and Technology, ETH Zurich, Zurich, Switzerland

The original article was published in *Ann N Y Acad Sci* 2010 (1198, Suppl 1, E22-34).

Author contributions

BZ wrote the manuscript. MES revised the manuscript.

1.1. Abstract

Smaller lesions of the brain and spinal cord often have a good prognosis with extensive functional recovery based, in part, on spontaneous neuritic sprouting and rearrangements of projections. This is well documented for the cortex, but compensatory fiber growth and formation of new connections and “detour pathways” can also occur in the spinal cord, where they contribute to functional recovery. Extent and length of fiber growth is, however, very limited in the adult central nervous system (CNS). Our group discovered Nogo-A, a neurite growth inhibitory protein present in CNS myelin. Function blocking antibodies were generated and administered to rats and macaque monkeys with spinal cord injuries (SCI) or cortical lesions. Biochemical readouts showed an up-regulation of growth specific proteins after CNS lesion and anti-Nogo-A antibody treatment. On the anatomical level, enhanced regenerative and compensatory sprouting of fibers was demonstrated resulting in the formation of new functional connections in the spinal cord. In animals with unilateral sensorimotor cortex lesions, fibers from the intact corticofugal system crossed the midline, supplying innervation to the denervated brain stem or spinal cord. Behavioral tests of locomotion as well as skilled forelimb reaching showed marked improvements of functional recovery in the Nogo-A antibody treated injured animals. In collaboration with Novartis, a human anti-human Nogo-A antibody was generated and tested in adult monkeys. A Phase I clinical trial applying this anti-Nogo-A antibody to subjects with acute SCI has been successfully conducted. Phase II is currently in preparation including European and North-American networks of spinal cord injury centers.

1.2. Introduction

Spontaneous, functionally relevant regeneration or replacement of lost nervous tissue is limited or even absent following injury to the central nervous system (CNS). Despite these restrictions, patients who have suffered a stroke or a spinal cord injury (SCI) as well as animals which underwent experimental CNS injury often show some time-dependent recovery of initial impairments. Most functional improvements can be observed at acute and subacute stages after CNS injury, the recovery curve plateaus after several months and in the chronic phase only minor improvements occur. In the first few days after injury, functional recovery is attributed to processes such as reperfusion of the penumbra, edema resolution, reversal of conduction block and spinal shock, remyelination of demyelinated fibers and compensation for metabolic disturbances. In the ensuing period, improvements are likely to be due to several other compensatory mechanisms which are grouped under the umbrella term "neuronal plasticity". Randolph J. Nudo, a pioneer in the field of neuroplasticity, recently noted “plasticity refers to the phenomenon of change, not to the specific underlying mechanisms”[26]. Today, ample evidence exists that plastic changes can occur at different CNS levels such as cortex, subcortical regions or the spinal cord, by numerous ways ranging from biochemical and molecular to synaptic and anatomical adaptations potentially culminating in rewiring and reorganization of entire neuronal networks. Changes in signal transduction, neuronal membrane excitability, synaptic strength, synapse and dendritic spine generation and elimination, recruitment of functionally homologous but separate anatomical pathways as well as axonal and dendritic sprouting resulting in the formation of new neuronal connections are examples of different mechanisms of neuronal plasticity. All of them can contribute to functional improvements occurring during the recovery process. One prerequisite for such adaptive processes to take place after CNS injury is that a number of neurons or fibers remain unaffected by the lesion. This is supported by the notion that in patients and animal models of CNS injury functional recovery is strongly dependent on the extent of CNS damage. After small lesions, strong or even complete functional recovery can be achieved. In contrast, very large CNS lesions, such as complete spinal cord injuries or strokes affecting the whole sensory-motor cortex, are associated with poor functional outcome. This leads to the assumption that functional recovery depends mainly on the amount of spared CNS tissue and on the potential of the unaffected central systems to functionally compensate through plastic adaptations. Both factors are again influenced by numerous other aspects such as the location of the lesion, additional collateral damage and the age at which the CNS injury occurs. Therapeutic interventions attempt to decrease the secondary damage (neuroprotection), and to

increase spontaneous plastic adaptations to enhance functional recovery after CNS injury. Neuroplasticity as well as axonal regeneration are restricted in the adult CNS by growth inhibitory molecules[27-30]. The most potent currently known of these is the myelin-associated protein Nogo-A. After CNS injury, neutralization of Nogo-A or suppression of its effects enhances regenerative sprouting and long-distance regeneration of lesioned axons as well as compensatory sprouting of unlesioned fiber tracts both in rodents and in monkeys[24,27,29-32]. In these studies anatomical findings were accompanied by increased functional recovery. Encouraged by the beneficial effects in animal studies, a clinical trial was initiated whereby Nogo-A blocking antibodies were given to subjects with acute spinal cord injury, discussed below. In addition to myelin associated molecules, regeneration failure has been attributed to factors present in the glial scar, in particular to a major family of inhibitory extracellular matrix molecules, the chondroitin sulphate proteoglycans (CSPGs)[27,28,33]. The inhibitory effects of CSPGs can be diminished *in vitro* and *in vivo* by treatment with chondroitinase ABC, an enzyme which digests CSPGs. Chondroitinase administered after CNS injury leads to axonal regeneration and increased neuronal plasticity associated with improved functional recovery[34].

This review first describes spontaneous, plastic changes at the anatomical and system level in animal models of small, focal injuries in the adult CNS. The second part focuses on the effects of Nogo-A neutralization on neuronal regeneration, plasticity and functional outcome in animal models of SCI and stroke, and, finally, we will discuss the ongoing Phase I/II clinical trial investigating this approach in acute SCI patients.

1.3. Mechanisms of spontaneous functional recovery after CNS injury

Spontaneous regenerative sprouting

CNS injuries cause damage to neuronal and glial cells in the CNS gray and white matter. In addition to destruction of local neuronal circuits at the injury site, disruption of ascending and descending fiber tracts is common, especially after SCI. Transection of axons in the adult mammalian CNS induces Wallerian degeneration of the axonal parts separated from the cell bodies while the proximal endings, which are still connected to their perikarya, form terminal retraction bulbs after an initial phase of axonal die back of several millimeters[35]. In contrast to the situation in development or after peripheral nerve injuries where long-distance regeneration can occur, only a minority of injured axons attempt to re-grow in the adult CNS. Regenerative sprouting is suspended after 0.2 to 2 millimeters[36,37]. Research over the last two decades has demonstrated the presence of inhibitory factors in adult CNS myelin and scar

tissue that actively block axonal regeneration. Therefore, spontaneous long-distance regeneration of ascending or descending axons is limited or even absent and does not significantly contribute to spontaneous functional recovery after CNS injury. However, recent findings in adult cats showed that cut commissural spinal interneurons spontaneously regenerate through the injury site even though inhibitory molecules such as CSPGs were present[38]. This indicates that in the adult mammalian CNS the potential to regenerate after lesion, and thus the degree of responsiveness to an inhibitory environment, might differ between neuronal cell subtypes. Nevertheless, the functional relevance of regenerating interneurons after SCI remains to be determined and also other mechanisms, such as compensatory plastic changes and extensive reorganization processes, accounting for remarkable improvements observed after smaller CNS injuries have to be considered.

Detour pathways and network reorganization

Mid-thoracic dorsal hemisections of the spinal cord disrupt the main component of the corticospinal tract (CST). Similarly, a focal inflammatory lesion can specifically target the thoracic dorsal CST. Adult rats lesioned in these ways showed initial impairments in hindlimb motor functions which were followed by some functional recovery[12,39]. In these animals, new collaterals of severed hindlimb CST fibers sprouted into the cervical spinal gray matter, as demonstrated by anterograde and retrograde neuroanatomical tract tracing (Figure 1.1 B)[12,16,40]. Intracortical electrical stimulations in the hindlimb area induced movements of whiskers, shoulder and forelimb muscles[40]. Most of the axotomized hindlimb cells with newly formed cervical projections were located at the rostral border of the cortical hindlimb area[16]. Interestingly, functional imaging demonstrated an expansion of the sensory representation of the forelimbs including this rostral hindlimb region. Consequently, stimulation of the forepaws evoked action potentials in axotomized hindlimb cells[16]. This indicates that after thoracic transection of the CST, a number of axotomized cortical hindlimb cells rewired to the cervical spinal cord and were functionally incorporated into forelimb sensory-motor circuits. However, this extensive anatomical reorganization of cortical forelimb networks probably does not contribute to the observed improvements of hindlimb function in CST specific behavioral tests. Therefore, what are the mechanisms that could lead to hindlimb recovery after partial thoracic SCI?

Three weeks after mid-thoracic dorsal SCI, an increased number of close appositions indicated the formation of new synaptic contacts between the cervical sprouts of transected hindlimb CST fibers and cervical interneurons (Figure 1.1 B)[12,40].

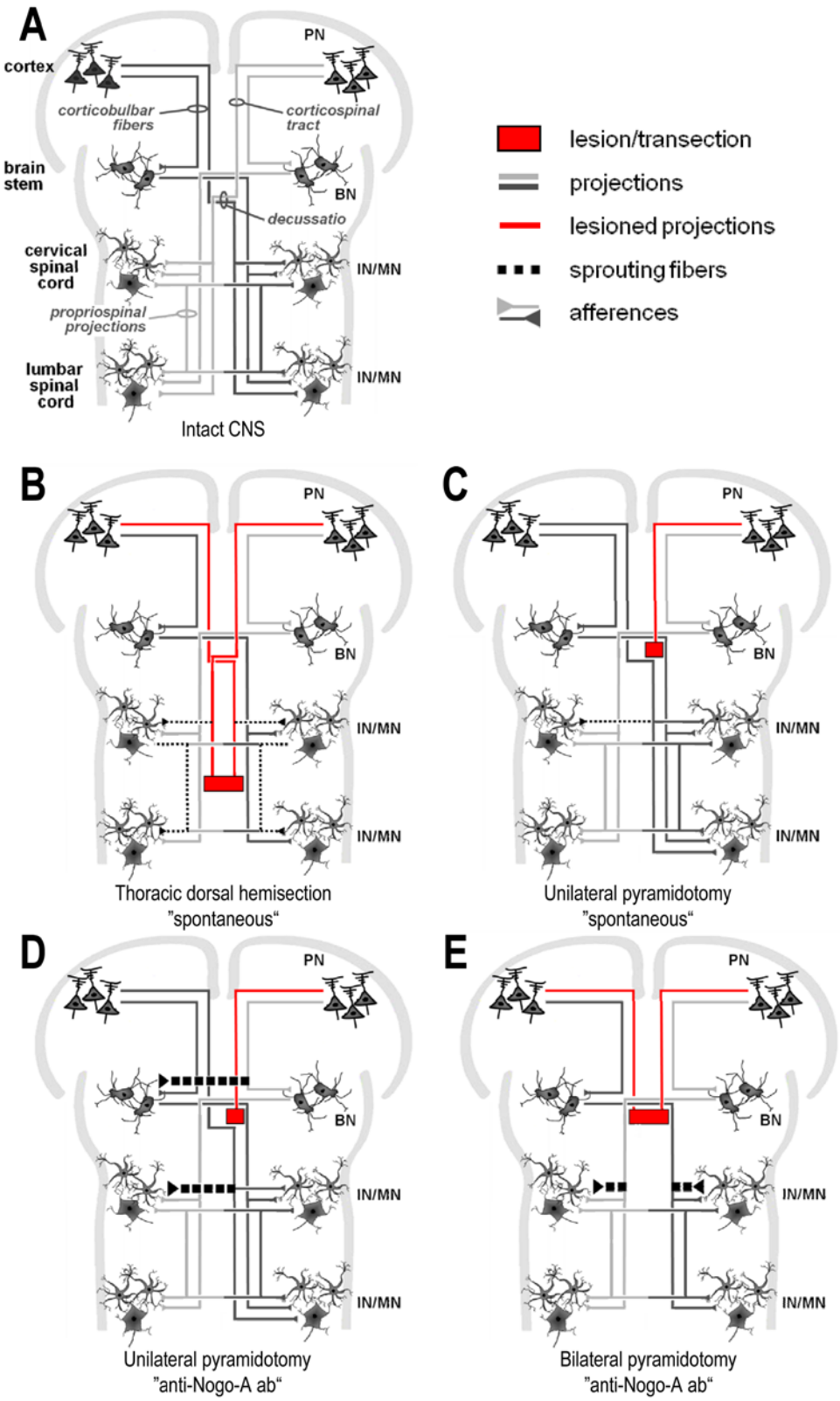

Figure 1.1. Spontaneous and anti-Nogo-A antibody induced fiber growth after different types of CNS injuries in the adult rat. (**A**) Schematic overview of the anatomy of several descending fiber tracts important for initiation and control of movements such as walking, swimming, or grasping. Dark-gray and light-gray lines indicate projections originating on the left and right side, respectively. (**B**, **C**) Lesioned fibers are shown in red and spontaneous structural changes observed in different CNS lesion paradigms are illustrated by dotted lines. Compensatory sprouting of uninjured systems leads to formation of new connections ("detour pathways") and strengthening of existing pathways and is likely to contribute to spontaneous functional recovery after CNS tract lesion. (**D**, **E**) Anti-Nogo-A antibody treatment results in enhanced compensatory sprouting after CNS injury which is associated with increased functional improvements assessed in different motor-related behavior tasks. ab, antibody; PN, pyramidal neuron; BN, brain stem neuron; IN, interneuron; MN, motoneuron.

In the cervical spinal cord, different types of interneurons can be distinguished. Short propriospinal interneurons (PSNs) project either directly onto cervical motoneurons or into the gray matter of adjacent spinal segments, whereas projections of long PSNs descend mainly in the ventral and lateral funiculus to innervate lumbar target neurons. Interestingly, both types of cervical interneurons were contacted by the hindlimb CST collaterals three weeks after injury, implicating a rather unspecific initial collateral sprouting response of lesioned CST fibers. This sprouting response was dependent on the amount of lesioned CST fibers; the more fibers damaged after focal inflammatory CST lesions, the more pronounced the collateral sprouting into the cervical gray matter[39]. Twelve weeks after injury, the number of contacts between CST collaterals and long descending PSNs was unchanged compared to the amount at three weeks post-lesion, whereas the number of contacts on short PSNs decreased significantly. This indicates a subsequent refinement or pruning of the initial innervation pattern[12]. In addition, connections of long cervical PSNs onto lumbar motoneurons increased after thoracic dorsal SCI (Figure 1.1 B). A second CST lesion at the level of the medulla oblongata in the brain stem (pyramidotomy) reversed partially the observed improvements of hindlimb function. Retrograde trans-synaptic tracing by injecting GFP-labeled pseudorabies viruses in the hindlimb muscles confirmed the existence of a new pathway from the hindlimb motor cortex to the lumbar spinal cord and, again, revealed adaptations of the cortical representation maps[12,41]. Further evidence that propriospinal neurons can relay supraspinal input across the lesion site and are important for functional recovery after incomplete SCI was provided by the finding that pharmacological ablation of spinal interneurons located directly above a thoracic unilateral spinal hemisections or between two staggered hemisections abolished the previously recovered hindlimb function in mice[15].

Spontaneous compensatory sprouting of unlesioned descending fiber tracts, associated with functional improvements, has been documented extensively in several CNS injury models. After transection of the dorsal components of the CST in the cervical spinal cord, compensatory sprouting of spared ventral CST fibers was detected in adult rats[11]. These sprouts re-innervated motoneuron pools, in the cervical gray matter, below the lesion site. Functional recovery, in a skilled forelimb task, accompanied the anatomical changes. Behavioral improvements were reversed by an additional transection of the ventral CST thus indicating that compensatory sprouting of the ventral CST contributed to the observed recovery after dorsal CST transection. Brus-Ramer and colleagues reported that a CST lesion, electrical stimulation and, specifically the combination of both led to outgrowth of spared CST fibers[42]. Transection of one CST induced projection changes of the other, unlesioned

CST whereby a number of spared fibers recrossed the midline at spinal levels and innervated the opposite gray matter which was deprived of its main cortical input (Figure 1.1 C). Artificial activation of theses fibers by electrical stimulation[42] or forced limb use[19] augmented the compensatory sprouting response of the unlesioned CST. For the latter intervention, also referred to as constrained-induced movement therapy in the clinics, anatomical changes in the corticospinal projections were accompanied by almost full recovery of the impaired forelimb in a behavior task requiring cortical control[19]. Similar results were obtained after a unilateral transection of the cervical spinal cord[18]. Anterograde and retrograde tracing revealed that unlesioned CST fibers descending in the contralesional spinal cord and originating from the ipsilesional cortex recrossed the midline at cervical and lumbar levels below the injury (Figure 1.1 C). Adjustments of corticobulbar and bulbospinal projections might also play an important role for functional recovery after CNS injuries but plasticity of these systems is only poorly understood at present. In contrast, Barriere *et al.* clearly demonstrated that spontaneous adaptations in local spinal circuitries like the spinal locomotor pattern generator networks contribute to functional improvements following SCI[17,43]. In summary, numerous animal studies provide evidence that functional improvements after SCI might be due to time- and activity-dependent plastic changes at all levels of the CNS.

In contrast to large cortical lesions, small, focal injuries to the cortex are often associated with substantial functional recovery both in animal models and stroke patients[44]. Human and animal data suggest that plastic adaptations in perilesional as well as in remote cortical areas are involved in recovery. Functions previously performed by damaged cortical regions might be adopted, at least partially, by other in parallel acting cortical systems such as secondary motor regions[45,46]. Another strategy might involve enhanced recruitment of alternative descending pathways. Here, compensation mediated by different brain stem systems, for example the reticulo-, vestibulo- or rubrospinal system, have to be considered[47].
Animal studies demonstrated that recovery after stroke is accompanied by substantial functional reorganization and anatomical changes in regions adjacent to the lesion[44,48,49], in ipsilesional secondary motor regions[10,13,50] as well as in the contralesional hemisphere[51-55]. This led to the currently predominant concept that plastic adaptations in various systems distributed throughout the CNS can contribute to functional recovery after CNS damage[44]. In an important study performed in adult macaque monkeys, Liu and Roullier showed that the ipsilesional premotor cortex is involved in the recovery process after primary motor cortex lesion[10]. Injury to the cortical hand representation area in M1 led to initial severe deficits in manual dexterity followed by functional improvements over 4-5 months. Transient

pharmacological deactivation with muscimol of several cortical areas of both hemispheres revealed that only deactivation of the ipsilesional premotor region re-induced the initial deficit in manual dexterity. Other primate studies emphasized that the size of the hand representation area in the premotor region was related to the extent of the lesion in the M1 primary motor area[50,56]. Functional changes in the hand representation regions were associated with anatomical alterations: new projections between the primary somatosensory cortex and the premotor region were established suggesting an enormous potential for intracortical rewiring and network remodeling in the adult primate CNS in response to small strokes[13]. Human data supported the notion that ipsilesional secondary motor systems, in particular the premotor cortex, can contribute to functional recovery after stroke[57-59] whereas the role of contralesional motor regions is less clear[46,60,61]. Again, the extend of the cortical damage probably determines which systems are recruited to compensate for the lost functions[44,62].

Accordingly, small lesions of the primary motor cortex might be compensated sufficiently by reorganization processes in perilesional areas. Moderate lesions could induce compensatory plastic adaptations in secondary motor regions in the ipsilesional hemisphere. In contrast, motor regions in the contralateral hemisphere may contribute to the very limited functional recovery in severely affected patients after large cortical lesions[44,59,62,63]. Thus, observations made in animal models of CNS injury and human studies lead to the conclusion that inducing axonal regeneration and enhancing neuroplasticity in ipsilesional and contralesional cortical areas, brain stem systems and in spinal networks are promising therapeutic goals in order to increase rewiring and functional recovery even after large CNS injuries.

1.4. Nogo-A inactivation enhances recovery after CNS injury

Endogenous neurite growth inhibition

Almost 20 years ago, central myelin and differentiated oligodendrocytes were found to inhibit axonal outgrowth *in vitro*[64], even in the presence of appropriate neurotrophic support[65]. Membrane proteins of CNS myelin, in particular a high molecular weight compound (NI-250, now Nogo-A) and an immunologically related protein (NI-35, probably a fragment of NI-250 in rat material) were shown to account for a large part of the nonpermissive and growth-inhibitory properties of central myelin[66,67]. Antibodies, in particular the immunoglobulin type M (IgM) antibody IN-1, were able to neutralize the inhibitory properties of both protein fractions and facilitated axonal outgrowth on CNS myelin and oligodendrocytes. Nogo-A (NI-220/250) was purified in 1998[68] and its cDNA cloned in 2000[69-71]. Currently several

additional molecules restricting axonal growth *in vitro* have been identified in CNS myelin and the astroglial scar, including CSPGs, Ephrins, Netrins, Semaphorins, MAG (myelin-associated glycoprotein) and OMgp (oligodendrocyte myelin glycoprotein)[27,28,72]. For most of these, the *in vivo* role in restricting axonal outgrowth after CNS injury remains unclear.

Nogo-A is one of three main splice forms derived from the *nogo* gene. It is expressed by differentiated oligodendrocytes and by developing subpopulations of neurons[73]. Nogo-B (55 kDa) has a widespread expression pattern while Nogo-C (25 kDa) can be found primarily in skeletal muscles. The function of the latter two is unknown. All isoforms share a common C-terminal domain, the so called reticulon-homology domain (RHD), and were therefore assigned as reticulon (RTN)-4/Nogo to the reticulon family[70,74]. The growth inhibitory properties of the transmembrane protein Nogo-A are attributed to at least two extracellular regions: the C-terminal Nogo-66 domain, located in the RHD and present in all isoforms, and a sequence unique to Nogo-A designated as delta 20[70,75,76]. The existence of a neuronal binding site for the Nogo-A specific domain has been shown biochemically, but has not been identified molecularly so far[76]. The Nogo-66 domain binds to a leucine-rich repeat glycoprotein, the Nogo-66-receptor (NgR), which is linked to the neuronal membranes via a glycosylphosphatidylinositol (GPI)-anchor[75,77]. MAG and OMgp also bind to and activate NgR[78-81]. NgR interacts with other membrane bound co-receptors such as Lingo-1, TROY and the low-affinity neurotrophin receptor p75. The resultant receptor complex can mediate signal transduction via p75. The Nogo-A specific fragment delta 20 is internalized into neuronal cells by a Pincher-dependent process and activates intracellular pathways including intracellular calcium as well as the small GTPase RhoA and its downstream target ROCK[82]. LIM kinase and the actin-binding protein cofilin can transmit the signals to the axonal cytoskeleton[83]. In addition, delta 20 was found to be retrogradely transported to the cell body after endocytosis into neurites where it may have further growth inhibitory functions[82]. The consequences of activation of these pathways are growth cone collapse, growth arrest and axonal retraction[82,84-88].

Nogo-A neutralization induces axonal regeneration and recovery after spinal cord injury

In the early 1990's, our group described the ability of injured CNS axons in adult rats to regenerate over several millimeters after SCI in the presence of anti-Nogo-A antibodies (IN-1) produced by transplanted hybridoma cells[36]. These findings were reproduced by other laboratories using different CNS lesion paradigms and treatment regimes in various species

including adult macaque monkeys[31,32,89,90]. In particular, new anti-Nogo-A antibodies (11C7 and 7B12), the NgR blocking peptide NEP1-40 or soluble NgR-Fc and Lingo-Fc fusion proteins were shown to reduce myelin inhibition and enhance regenerative fiber outgrowth[31,89,91-93]. The fact that Nogo-A/Nogo-receptor neutralization or inactivation was consistently associated with enhanced functional recovery after CNS injury was of major importance with respect to future clinical trials.

Delivery of antibodies, peptides or fusion proteins into the cerebrospinal fluid was achieved by implantation of small catheters into the lateral ventricles or the spinal subarachnoidal space. These catheters were then connected to osmotic mini-pumps. Antibodies were detected in the entire spinal cord and brain tissue of adult rats and monkeys after one week of continuous infusion[94]. The antibodies bound to Nogo-A at the cell membrane and were colocalized with endogenous Nogo-A protein in vesicles and lysosomes inside Nogo-A expressing cells such as oligodendrocytes. This implies a mechanism of protein-antibody complex internalization which eventually leads to a significant downregulation of the Nogo-A tissue levels *in vivo*. After transection of the major components of the thoracic CST in rats, blockade of Nogo-A by intrathecally infused antibodies resulted in significantly enhanced regenerative sprouting of lesioned CST fibers rostral to the lesioned site[31]. In contrast to the restricted sprouting response in control animals, which usually halted after a millimeter, lesioned fibers in anti-Nogo-A antibody treated rats showed substantial long-distance regeneration and bypassed the lesion site in spared tissue bridges[31]. CST fibers grew in irregular courses, were often located at unusual anatomical sites mainly in the spinal gray matter and were of a very slender or even filiform appearance. Fibers were also observed branching within the gray matter of spinal segments far caudal to the lesion site. Recovery of locomotion as well as precision movements in anti-Nogo-A treated animals occurred more rapidly and was considerably superior to the spontaneous recuperation of control antibody treated animals. Sensory testing provided no evidence for development of negative symptoms such as hypersensitivity or allodynia which are common malfunctions most likely associated with aberrant fiber growth after SCI[31]. In the presence of anti-Nogo-A antibodies, serotonergic fibers originating in the brain stem raphe nuclei were shown to re-establish a lamina-specific projection pattern in the lumbar spinal gray matter after thoracic SCI implicating that Nogo-A neutralization can also influence regeneration or compensatory adaptations of descending fiber tracts besides the CST[93]. A recent study demonstrated efficacy of function blocking anti-Nogo-A antibodies in adult primates after SCI[25,32,95]. Macaque monkeys, which were subjected to unilateral spinal cord transection at

the cervical level including the CST, progressively recovered manual dexterity of the ipsilesional hand[32,95]. Amongst other tests, recovery of hand function was assessed in a finger prehension task ("modified Brinkman board" and drawer task). Animals which had received intrathecal application of anti-Nogo-A antibodies over a period of four weeks showed an almost complete recovery of hand function in this paradigm, irrespective of the lesion size. In contrast, functional performance of control antibody treated monkeys was inversely correlated with the lesion extent and was significantly lower compared to anti-Nogo-A antibody treated animals. Importantly, neither adverse side effects related to the anti-Nogo-A treatment nor signs of increased pain were reported in the postlesional period. Anatomical analysis revealed higher numbers of axonal swellings caudal, and increased axonal arbor length rostral, to the lesion site in monkeys treated with the Nogo-A blocking antibody[25,32]. In addition, the number of axonal retraction bulbs formed by transected CST axons rostral to the lesion was reduced while the number of axons growing medially from the white matter towards the cervical gray matter was increased after anti-Nogo-A antibody treatment[25]. This probably reflects the first part of the irregular course which regenerating axons choose in order to bypass the lesion site and innervate target neurons in spinal segments caudal to the injury. Similar results were reported after inhibiting different components of the Nogo-66 receptor complex[89,90,92] and its signaling pathway in rat models of spinal cord injury[85,96].

Results obtained in Nogo knockout mice were initially controversial. In two mutant mouse lines, either lacking Nogo-A or Nogo-A and Nogo-B, enhanced sprouting and axonal regeneration were demonstrated after SCI in two independent laboratories[97,98]. Due to high variability a third laboratory could not confirm these observations when investigating both Nogo-A/B and Nogo-A/B/C knockout mice[99]. Study discrepancies were explained by dissimilar gene targeting strategies, compensatory upregulation of other growth inhibitory proteins during development and usage of different lesion paradigms and mice strains. Back-crossing experiments indicated that differences in the genetic background of mice play an important role regarding neurite outgrow and axonal regeneration[100]. Finally, enhanced regenerative fiber growth in Nogo-A knockout mice was confirmed in two different pure background strains[100]. Transgenic mice lacking NgR or Nogo-A/B demonstrated better recovery of motor functions accompanied by increased compensatory sprouting of unlesioned CST fibers in a stroke lesion paradigm[101]. All transgenic mouse lines lacking one, two or all three Nogo-isoforms were viable, had no obvious developmental or birth defects and did not show detectable motor or sensory deficits later in adulthood.

Extracellular matrix molecules, such as CSPGs, are up-regulated after CNS injury and contribute considerably to the inhibitory environment that lesioned axons have to overcome in order to regenerate[27,28,102]. Recently, the first receptor, a transmembrane protein tyrosine phosphatase, PTPσ, mediating the inhibitor effects of CSPGs has been identified[103]. Digestion of CSPGs by chondroitinase resulted in enhanced axonal regeneration of ascending and descending fibers accompanied by improved functional outcome[104,105]. Combinatorial treatment regimes might therefore help to maximize the amount of regenerating axons following complete or incomplete SCI in the future[106].

Nogo-A blockade increases neuronal plasticity

Inhibitors of axonal growth not only impede axonal regeneration after injury, but also play a major role in restricting compensatory plasticity and reorganization processes after SCI or stroke. Sprouting of unlesioned fiber tracts often contributes to the functional recovery after CNS lesions at perinatal and postnatal stages in animal models and probably also in human infants[107,108]. The decline of the plastic potential and compensatory capacity of central networks during maturation is correlated with the onset and progression of CNS myelination[109]. Consequently, we could demonstrate that neutralization of the myelin-associated growth inhibitor Nogo-A enhances compensatory sprouting of unlesioned CST fibers after unilateral pyramidotomy in adult rats, a process which was accompanied by almost complete functional recovery in motor and sensory tests[23]. Collaterals of the spared CST recrossed the midline via the dorsal commissure at spinal levels and re-innervated the hemicord deprived of its major cortical input due to the lesion. Anti-Nogo-A treated rats showed a twofold increase of spinal midline crossing fibers compared to injured animals treated with control antibodies (Figure 1.1 D). These collaterals terminated mainly in Rexed's laminae VI and VII of the spinal gray matter suggesting a topographically appropriate CST projection pattern. The novel spinal projections might be utilized to relay cortical information to spinal targets and to re-gain control over the lesion-impaired body parts, as suggested by the observed improvements in food pellet reaching or rope-climbing tests[23]. When both CSTs were transected at the pyramid level in adult rats, rubrospinal fibers were shown to sprout into the deafferented spinal gray matter after treatment with anti-Nogo-A antibodies (Figure 1.1 E)[110]. The compensatory sprouting response in the rubrospinal system was associated with functional improvements and suggests that after Nogo-A inactivation functionally related but anatomical separated systems can overtake, at least partially, functions of another system. In addition, treatment with chondroitinase led to an increased sprouting response of lesioned

(CST) and spared systems (serotonergic) after SCI[111]. This finding can be explained by treatment effects on CSPG-containing perineuronal nets which are thought to constrain the formation of new connections[34,102].

Whether combining treatments which boost neuroplasticity with physical rehabilitation can further promote functional recovery after injury has been investigated only recently in two animal studies. After thoracic dorsal SCI, either acute treatment with anti-Nogo-A antibodies or intensive treadmill training improved locomotor function in rats. Interestingly, the combination of both treatments starting simultaneously in the acute phase after injury did not result in a synergistic effect[112]. This finding suggests that determining the appropriate rehabilitative training paradigm as well as the optimal time window for each therapy is crucial for a successful combination of different approaches. In contrast, combining chondroitinase treatment with a specific skilled-reaching rehabilitation resulted in increased recovery of manual dexterity after a partial cervical SCI[113]. However, the putative benefit of combining therapies after CNS injury needs to be further investigated emphasizing important issues such as the appropriate type and the correct application of rehabilitative training and the optimal treatment windows for each individual therapeutical approach[114].

In different unilateral stroke models affecting the sensorimotor cortex such as middle cerebral artery occlusion (MCAO) or photothrombotic cortical injuries, an increase of spinal midline crossing fibers emanating from the unlesioned motor cortex were found in adult rats after acute and even after one week delayed treatment with anti-Nogo-A antibodies and NgR blocking fusion proteins compared to animals treated with control antibodies or proteins, respectively[101,115]. Grasping skills with the impaired forelimb were significantly correlated with the amount of cervical midline crossing fibers after recovery from injury[115]. These results show that Nogo-A inactivation after unilateral sensorimotor cortex lesion can enhance compensatory processes in the contralesional hemisphere potentially mediated via novel double-crossed pathways. After unilateral aspiration lesion of the sensorimotor cortex, reorganization of the intact cortex was reported in Nogo-A antibody treated rats leading to more frequent ipsilateral forelimb movements elicited by intracortical microstimulation[116]. Functional MR-imaging 8 weeks after unilateral MCAO revealed adaptations in the somatosensory system induced by anti-Nogo-A antibodies[117].

Anatomical changes could also be detected at different brain stem levels in adult rats after injuries affecting the cortex or its projections. In the intact rat, the parvocellular part of the red nucleus and the basilar pontine nuclei receive major inputs from the ipsilateral cortex through strictly topographically organized direct corticobulbar fibers or CST collaterals. Both,

the red nucleus and the pontine nuclei, are important motor centers in the brain stem mediating and modulating motor functions either via direct spinal projections (rubrospinal tract) or via the cerebellum. After pyramidotomy or unilateral sensorimotor cortex lesion, animals treated with Nogo-blocking substrates (antibodies or function blocking NgR fusion proteins) showed a significant increase of midline crossing fibers at the brain stem level innervating the contralateral parvocellular part of the red nucleus as well as the contralateral basilar pontine nuclei and performed significantly better in a skilled forelimb reaching task even when initiation of treatment was delayed for one week (Figure 1.1 D)[23,101,118-121]. Interestingly, the new corticopontine projections maintained the somatotopically organized projection pattern typical for the ipsilateral corticopontine innervation[118,119]. The axons were of smaller diameter, unmyelinated, contained vesicle-like structures and contacted almost exclusively, via axonal boutons, dendrites of the pontine target neurons[119]. Following unilateral aspiration lesion of the sensorimotor cortex a higher number of fibers originating in the spared cortex were found to innervate the ipsilesional striatum after Nogo-A inactivation compared to animals which received control antibodies or were left intact[122]. In NgR and Nogo-A/B knockout mice, compensatory axonal sprouting of unaffected cortical fibers was enhanced at cervical spinal and brain stem levels after unilateral sensorimotor cortex lesion resulting in bilateral cortical projections[101]. Thus, findings in different unilateral stroke paradigms indicate that neuroplasticity, i.e. large-scale structural adaptations in spared corticofugal fibers, are enhanced in the presence of Nogo-A function blocking antibodies leading to new connections in the brain stem and the spinal cord which contribute to functional improvements.

The putative mechanisms underlying the described spontaneous or treatment-induced anatomical adaptations of lesioned and spared neuronal projections after different types of CNS injuries are complex and not entirely clear. An upregulation of neurotrophic factors and/or other growth permissive molecules in denervated regions of the CNS might induce spontaneous compensatory sprouting of unlesioned fiber tracts[123]. Blocking the growth-inhibitory properties of Nogo-A or CSPGs generates a more permissive environment for plastic adaptations. Mechanisms of target selection in the spinal cord and brain stem may involve re-expression of developmental guidance molecules after CNS lesions[20,124]. In addition, the refinement of newly established (detour-) pathways may be due to activity-dependent mechanisms and/or competition for target derived factors, also mechanisms which are fundamental for precise assembly and subsequent adjustments of neuronal networks during development[29,42,124-126].

Clinical trial of an anti-Nogo-A antibody

Three different antibodies (IN-1, 11C7, 7B12) raised against Nogo-A have proved efficient in enhancing regenerative and compensatory neurite growth *in vitro* and in several *in vivo* models of CNS injury as summarized above. In collaboration with Novartis (www.nibr.novartis.com) a human anti-human Nogo-A antibody (ATI 355) has been produced. Extensive toxicological studies with respect to the antibody application were performed in two species including primates. Major efforts were undertaken to standardize diagnosis and measures of functional outcome[4,127]. Networks collecting clinical data of spinal cord injured subjects were established in Europe (European Multicenter Study about Spinal Cord Injury, EMSCI, www.emsci.org) and North America (North American Clinical Trials Network, NACTN, financed by the Spinal Cord Consortium of the Christopher and Dana Reeve Foundation, Springfield, NJ, USA). Patient data collected in such databases can serve as historical control datasets and can be employed to design future clinical studies[128]. Phase I of the anti-Nogo-A-trial started in 2006 coordinated by Novartis in the EMSCI network clinics (www.clinicaltrials.gov, NCT00406016) and in a North-American network of spinal cord injury centers. The Phase I clinical trial investigated mainly pharmacokinetics, safety, tolerance and correct dose of the antibody and was successfully completed in 2009. Subjects with thoracic and cervical injuries either functionally complete or incomplete (ASIA A-C) were enrolled and treated with the function blocking human anti-human-Nogo-A antibody within the first 14 days after injury. In accordance with our animal studies, antibodies were delivered intrathecally into the lumbar liquor space via a pump or injections. Application lasted for different time periods ranging from 24 hours to four weeks. During Phase I, 50 subjects with SCI were treated and the tolerance was excellent and no side effects ascribed to the anti-Nogo-A antibody have been observed. We hope to enroll the first of 120 subjects for Phase II soon testing the efficacy of the anti-Nogo-A antibody treatment after spinal cord injury in human supported by an interdisciplinary and international alliance of experts.

1.5. Conclusion

Basic and clinical research of the last two decades has led to an increasing understanding of basic mechanisms underlying spontaneous functional recovery after CNS injury. Plastic adaptations include structural changes, rewiring processes and circuit reorganization at different levels of the injured CNS. In the absence of axonal regeneration, collateral sprouting in lesioned and spared fiber tracts can result in the formation of new connections and detour pathways which are important parts of compensatory strategies used by the adult CNS to re-

establish function after smaller cortical and spinal injuries. Interventions which increase axonal regeneration and compensatory fiber growth in the injured CNS will open new avenues for treatment of even large injuries. Inactivation of restrictors of regeneration and neuronal plasticity present in the adult CNS has proven effective in animal models of spinal cord injury and stroke. Blockade of Nogo-A by antibodies induced axonal regeneration, enhanced structural compensatory adaptations and substantially improved functional recovery in animals subject to different models of CNS injury. A clinical trial using anti-Nogo-A antibodies in paraplegic patients is currently ongoing. A beneficial effect of anti-Nogo-A-antibody application on the functional outcome of spinal cord injured individuals would be a major breakthrough with regard to treatment options after CNS injuries in humans and a successful example of “bench-to-bedside” research.

Chapter 2

Profiling locomotor recovery: comprehensive quantification of impairments following CNS damage in rodents

Björn Zörner [1,3] and Linard Filli [1,3], Michelle L. Starkey [1], Roman Gonzenbach [1], Hansjörg Kasper [1], Martina Röthlisberger [1], Marc Bolliger [2] and Martin E. Schwab [1]

[1] Brain Research Institute, University of Zurich and Dept. of Health Sciences and Technology, ETH Zurich, Zurich, Switzerland

[2] Spinal Cord Injury Center, Balgrist University Hospital, Zurich, Switzerland

[3] authors contributed equally to the study

The original article was published in *Nature Methods* 2010 (7, 701-708).

This article was also published in the Ph.D. thesis presented by Linard P. Filli which was accepted by the ETH Zurich in 2011 (DISS. ETH No.: 20062).

Author contribution

BZ designed the study, refined the testing set-up, performed surgeries (spinal cord injuries), collected and analyzed data, made the figures and wrote the manuscript.

2.1. Abstract

Rodents are frequently used to model damage and diseases of the central nervous system (CNS) that lead to functional deficits. Impaired locomotor function is currently evaluated by using scoring systems or biomechanical measures. These methods often suffer from limitations such as subjectivity, non-linearity and low sensitivity, or focus on a few, very restricted aspects of movement. Thus, full quantitative profiles of motor deficits after CNS damage are lacking. Here, we report the detailed characterization of locomotor impairments after applying common forms of CNS damage in rodents. Numerous objective and quantitative readouts were obtained from rats with either spinal cord injuries or strokes and transgenic mice (*Epha4*$^{-/-}$) during skilled walking, overground walking, wading and swimming resulting in model-specific locomotor profiles. Our testing and analysis method provides comprehensive assessment of locomotor function in rodents and has broad application in various fields of life science research.

2.2. Introduction

A common consequence of damage to the central nervous system (CNS) caused by trauma, ischemia, or neurodegenerative or inflammatory diseases is impairment of motor functions. In the corresponding animal models accurate and comprehensive functional testing is not only important to determine whether a novel therapeutic approach is successful but is also indispensable for understanding complex CNS processes such as the mechanisms leading to spontaneous recovery[47,129]. In neuroscience research, models based on rodents are commonly used and locomotion is one of the most frequently investigated motor functions[130-132].

For evaluation of locomotor deficits, different readouts such as endpoint measures[133,134] (scores), biomechanical measures[135-137] (kinematics, kinetics) or electromyography (EMG)[136,138] are commonly used. However, these readouts suffer from several limitations. The most commonly used scores are neither linear nor objective and often have a low sensitivity especially with regards to treatment effects or compensatory strategies[131,139]. Established scoring systems are generally developed for a particular type of injury and thus are not easily transferred to other models[134]. Highly sensitive biomechanical measurements or EMG recordings usually focus on a few, very specific aspects of a movement, for example joint angles or timing of muscle activity, whilst other aspects, like changes in body posture are rarely assessed. Since the overall functional status of the animal is often ignored, data obtained from these approaches can be difficult to interpret[139]. Furthermore, application of these methods is mainly limited to a few specialized laboratories. The use of several endpoint measures combined with quantitative biomechanical readouts has been emphasized in the literature as a priority and might help overcome some of the above mentioned problems, but this is usually expensive, time- and space-consuming and not standardized hindering comparison of results between laboratories[131,139]. Adding an additional level of difficulty to the behavior analysis, rodents show various forms of locomotion depending on their environment. This includes skilled walking, normal walking on even ground or, in an aquatic environment, wading through shallow water or swimming. All of these types of locomotion differ considerably with regards to the motor pattern produced, sensory input and participating CNS networks [140-143] and, therefore, might be differentially affected by a given CNS injury. Thus, a comprehensive analysis of the animals' behavior, including different forms of locomotion, is necessary for a full assessment of the consequences of a lesion and is a prerequisite to link neuroanatomical changes to functional outcome. However, studies investigating the effects of a given CNS injury by assessing full, quantitative locomotor profiles are lacking.

The objective of this study was to undertake a systematic and comprehensive evaluation of the effects of various insults to the CNS using four motor tasks that test different aspects of locomotion in rats and mice. By assessing a number of objective and quantitative outcome measures, we generated locomotor profiles characteristic for the investigated models of CNS damage. Thus, the dataset presented here can guide the selection of the appropriate lesion paradigm and the corresponding outcome measures for future animal studies.

2.3. Methods

Animals

We performed all experiments with the approval of and in accordance with the guidelines of the Veterinarian Office Zurich, Switzerland. CNS lesions and behavioral testing were performed on 14 adult female Lewis rats (200-250 g, R. Janvier, Le Genest-St Isle, France). In addition, we evaluated locomotor function in three EphA4-receptor knockout (*Epha4*$^{-/-}$, C57BL/6 background, provided by R. Klein, Martinsried, Germany) and three wild-type C57BL/6 mice. Mice were 4-5 months old and of both sexes. Rats and mice were housed in groups of 3-5 per cage, 12:12 h light:dark cycle with food and water *ad libitum*.

Surgery and animal care

We performed all surgeries (rats only) under general anesthesia achieved by subcutaneous injections of Hypnorm and Dormicum (Hypnorm: 120 µl per 200 g body weight, Janssen Pharmaceutics; Dormicum 0.75 mg per 200 g body weight, Roche Pharmaceuticals). Spinal cord injuries were either: a bilateral dorsal cut lesion at T8 vertebral level (n = 5 rats), a large bilateral ventral lesion at T8 (n = 2 rats), or a cervical unilateral right-sided complete hemisection at C4 (n = 4 rats). The lesions were performed as described previously[18,144]. Rats with an ischemic lesion to the cortex (stroke, n = 3 rats) received 14 stereotactic injections of the vasoconstrictor endothelin-1 (ET-1, 0.3 µg/µl, Sigma-Aldrich) into the left motor cortex (fore- and hindlimb areas). We injected a volume of 500 nl at a depth of 1.2 mm with a rate of 6 nl/sec. After each injection, we left the needle in place for 3 min before it was carefully removed. After the final injection of ET-1, or after SCI, the rats were sutured and returned to a heated blanket to recover from surgery. One day before and for two days after surgery, rats received subcutaneous injections of analgesic (Rimadyl, 2.5 mg per kg body weight, Pfizer AG). In addition, postoperative care included daily subcutaneous injections of antibiotics (Baytril, 5 mg per kg body weight, Bayer AG) for one week to prevent bladder or wound infections. We checked the rats' health twice daily for the entire experiment. After SCI,

bladders were manually expressed until normal bladder function returned. As expected, stroke lesions did not affect bladder function.

Testing apparatus

For evaluation and analysis of locomotor function in rats and mice, we used a single custom designed set-up, the *MotoRater* (Figure 2.1 A). The complete set-up is now commercially available at TSE-systems GmbH (http://www.tse-systems.com/). We tested the rats and mice in a clear Plexiglas basin, 150 cm in length, 13 cm in width and 40 cm in height. At one end a small footbridge allowed the rats and mice to exit the basin into a cage. A temperature sensor was installed to measure the water temperature. For testing skilled locomotion, we placed a horizontal ladder (for rats: length of 113 cm, width of 13 cm; for mice: length of 113 cm, width of 7 cm; 15 cm above ground) with regularly (training) or irregularly (testing) spaced, round metal rungs into the basin. We used a Plexiglas runway (length of 123 cm, width of 13 cm, 15 cm above ground) to assess overground locomotion and wading. For wading and swimming, the water temperature was 23 °C. Water depth for wading was 3 cm (rats) or 1 cm (mice) above the runway's surface; for swimming, water depth was 25 cm. For mice, we restricted the width of the testing corridor to 7 cm by two additional Plexiglas walls. To allow evaluation of the performance from the left and right side and from below at the same time, we placed one mirror (100 cm x 16 cm) on the basin's floor at an angle of ~ 90 ° and positioned two perpendicularly arranged mirrors (100 cm x 18 cm) behind the long side of the basin (Figure 2.1 B). We used high frame rates to film the performance in the testing basin (see below). This required an additional strong light source that was comprised of four commercially available 36 Watt fluorescent lamps emitting cool white light. During testing, the lighting rack was located between the camera and the testing apparatus illuminating the basin from above (one lamp) and below (three lamps). More detailed information is provided in section 2.6. Supplementary Notes.

Electromyographic recordings

For EMG recordings during the locomotor tasks, we placed a cableway system on top of the basin enabling a motile wire connection between a preamplifier and the rats' head adapter (Figure 2.1 C). Bipolar Teflon-coated stainless steel wires (Cooner Wire) were chronically implanted into the left and right musculus tibialis anterior and musculus vastus lateralis as described previously[145]. The distance between the electrode tips was between 1-2 mm. Implanted wires were led subcutaneously to the head and attached to a connector that was

fixed on the rats' skull with dental cement. One wire served as a ground electrode and was placed subcutaneously in the neck region of the rat. Pre-amplified signals were digitized (sampling rate of 1 kHz), amplified (1000 x) and high-pass filtered (30 Hz). We processed the data with DIAdem academic 8.1 software (National Instruments Engineering GmbH & Co. KG).

Preparation of the animals

After acclimatization to the testing apparatus, we trained the rats and mice in 5 daily sessions (every other day, about 10 passages per animal and task) until they crossed the testing basin with a constant speed. Rats and mice were trained on the ladder with a regular arrangement of metal rungs. For testing, rung sequences were irregular and varied to avoid habituation to a particular rung pattern. Before baseline recording, the skin overlying defined anatomical landmarks on the lateral side of the forelimbs and hindlimbs was shaved and tattooed with a commercially available tattooing kit (Hugo Sachs Elektronik, Harvard Apparatus GmbH). We marked the following bony structures of the forelimb: vertebral border of the scapula (shoulder blade); tip of the humerus (shoulder joint); wrist and the 5th metacarpal head (digit)[146]. We also labeled the following hindlimb structures: iliac crest; greater trochanter (hip); lateral malleolus (ankle); metatarsophalangeal joint of 5th toe (MTP) and the tip of toe[146]. On the ventral surface of the tail, we marked four points with tattoos, these were: the base of the tail, the first and second thirds of the tail and the tip of the tail.

Data acquisition and kinematic analysis

We tested rats with strokes and dorsal SCIs before (baseline) and 3, 7 and 28 days after injury. Locomotor performance of rats with ventral and cervical SCIs was evaluated at baseline and 7, 14 and 28 days following lesion. In these rats, we removed the early session (3 days) as rats are more severely impaired after ventral and cervical lesions than they are after stroke or dorsal SCI. We tested *Epha4*$^{-/-}$ and wild-type mice in a single session. Before every testing session, we reinforced visualization of the tattoos with a fluorescent dye (for example fluorescent, fast drying nail polish) or a black marker in case of albino rats. For each animal (rats and mice) and each task, we recorded 3-10 passages and analyzed at least three of them. The analysis was based exclusively on video recordings captured with a high-speed color camera (Basler A504kc Color Camera, Basler AG, 1280 x 1024 pixels). We filmed rats and mice at a frame rate of 50, 100 or 200 f/s (Hz) for skilled walking on the ladder, overground walking and wading or swimming, respectively.

To increase the number of pixels per marker, we placed the camera close to the basin (distance of 100-150 cm), thereby limiting the field of view to about one third of the length of the testing track. By moving the camera on a guide rail along the testing track, we recorded the full distance covered by the animals. We attached a commercially available flashlight pointer to the camera that indicated the camera's field of view. This provided visual feedback to the experimenter who manually moved the camera thus allowing reliable recordings of moving rats and mice. Locomotor behavior was only analyzed in a central, 60 cm long region of the testing apparatus to avoid artifacts due to acceleration and deceleration at the beginning and end of the track, respectively. For each task only passages with similar and constant movement velocities and without lateral instability were used for kinematic analysis.

In collaboration with a software engineering company (ALEA Solutions GmbH), a color-based automated tracking software ClickJoint, V5.0 was developed (now commercially available at ALEA Solutions GmbH, www.aleasol.ch) and used for offline analysis of the video recordings. For calibration of the software, we placed three 5 cm long pieces of tape on the walls of the testing basin so they were visible from all perspectives (direct view and mirror images). As the camera was moved during recordings to follow the rats and mice on their journey through the testing basin, normalization of the spatial measurements to the position of the iliac crest (for hindlimb analysis) or the shoulder blade (for forelimb analysis) was required. The software automatically tracked frame by frame the markers on the skin of rats and mice and generated two-dimensional coordinates (x, y) for every marker and time point. Based on these coordinates, the software modeled body segments as rigid straight lines between markers. For kinematics, movements were automatically reconstructed from changes in the marker location between consecutive frames. Angles and distances were calculated directly by the software allowing the generation of stick diagrams and spatial displacement plots. For angle measurements, we used the smaller angle of the two alternatives; typically this was the angle at the flexor side of a limb joint. We analyzed the side and the bottom views of the rats and mice separately. Data were smoothed by applying an integrated supplementary function of the ClickJoint software using a cubic-spline function. Data were then imported into Microsoft Office Excel 2007 (Microsoft) and further analyzed with pre-assembled Excel sheets determining, for example joint angles or distances between joints at a given time point, range of motion, coordination parameters or movement velocities. To minimize artifacts due to divergent movements of the skin over the underlying bony structures[147], we defined the knee and elbow joints as virtual joints, that is their positions were indirectly computed by the ClickJoint software. For the knee, the calculation was based on

both the position of the markers over the hip and ankle and the length of the femur (rat = 2.5 cm, mouse = 1.3 cm) and tibia (rat = 3.5 cm, mouse = 2 cm) bones. For the elbow joint, the shoulder and wrist positions and the length of humerus (rat = 2.5 cm, mouse = 1.1 cm) and the lower forelimb (rat = 2.8 cm, mouse = 1.2 cm) were used. For more detailed information about camera settings, software application and data processing see section 2.6. Supplementary Notes.

Locomotor parameters

We defined the movement phases of a limb during locomotion in accordance with the literature[136,148]. In brief, for walking and wading, a gait cycle was defined as the time period between two consecutive ground contacts of the paw of one limb. The time point of paw contact was identified visually. The stance phase lasted from the initial paw contact until lift off and this was followed by the swing phase which started with lift off and terminated with ground contact of the paw. We defined mid-stance as the time point in the middle of the stance phase. For swimming, we defined a stroke cycle as the time period between two consecutive hip angle minimums of one limb. This was determined based on kinematic joint angle measurements. Within a stroke cycle, two phases were distinguished, the “power stroke” and the “return stroke”. The power stroke started with the minimum hip angle and ended when the maximum hip angle was reached. The onset and ending of the return stroke was determined by the maximum and minimum hip angle, respectively. We defined the body axis which was required for the tail kinematics as a virtual line connecting the nose, two virtual points midway between fore- and hindlimbs and the genital area.

For evaluation of skilled walking over the horizontal ladder, steps were counted and classified as: functional paw placement (a weight-bearing step on a rung); slip (a step with initial contact of the rung followed by a slip off the rung) or miss (a step that missed the rung completely). We quantified fore-hindlimb coordination by assessing how often the same rung was targeted (touched) first by the forelimb and subsequently by the ipsilateral hindlimb; a pattern that is usually observed in intact rodents crossing a ladder (baseline)[141]. Numbers were expressed as a percentage of total steps or targeting attempts and were an average of at least three passes.

For wading and walking, we defined the base of support as the distance between the paws during the stance phase. For the hindlimbs, base of support was calculated by adding the distances measured between the MTP of the 3rd toe and the body axis for consecutive left-right hindlimb steps. We assessed external rotation of the hindlimb at the beginning of the

stance phase by measuring the angle between the body axis and the paw axis defined by a virtual line connecting the third MTP and the heel. For evaluation of base of support and external rotation, we used the bottom view. On the basis of the side views, horizontal protraction and retraction of hind- and forelimbs in the sagittal plane were quantified by measuring the maximal and minimal toe or wrist excursions relative to the iliac crest or shoulder, respectively. The number of steps with paw dragging (defined as digits touching the ground during the swing phase) were counted and expressed as a percentage of total steps. We determined the height of the iliac crest by measuring the vertical distance between the iliac crest and the surface of the runway during mid-stance.

For swimming, the number of forelimb strokes was assessed manually. Forelimb strokes that touched the walls of the Plexiglas basin and thus were mainly used for navigation were excluded from the analysis. We evaluated left-right coordination by measuring the time interval between the onset of the stroke cycle of the ipsilateral and contralateral hindlimb. This time interval was then normalized to the duration of the complete stroke cycle of one of the hindlimbs, usually the right, and expressed as a percentage[136,149]. Thus, 0 % indicates simultaneous hindlimb movements whilst 50 % suggests a perfect, alternating “out-of-phase” rhythm. Deviation from the perfect “out-of-phase” rhythm was used as a readout of left-right coordination. Stick diagrams, spatial displacement plots and angle-angle plots were typically generated for a time period of 1sec (4-5 stroke cycles in intact rats) per pass. We evaluated tail-hindlimb coordination by determining the temporal relation between the time point of the most extreme angular displacement of the base of tail to the left or the right side and the time point of the maximal hindlimb extension.

Statistics

We performed the statistical analysis with the SPSS software package for Windows (version 14.0; SPSS) and GraphPad Prism 5 for Windows (version 5.01; GraphPad Software). For the behavioral data obtained from rats with a CNS injury, one-way repeated-measures ANOVA followed by *post hoc* Bonferroni tests were used to assess lesion effects (baseline vs. 3 or 7 days after injury) and functional recovery (3 or 7 vs. 28 days after injury). To detect correlations between parameters, we calculated Pearson’s correlation coefficients. For rats with a ventral SCI, only descriptive statistics were applied due to the fact that only two rats were evaluated. In these cases, results for individual rats are shown with black and white dots representing individual animals in the Figures. To test differences between *Epha4*$^{-/-}$ mice and wild-type mice, we performed Student’s *t*-test (two-tailed, unpaired). Data are presented as

group mean values for every testing session and error bars represent s.e.m.. The level of statistical significance for all tests was determined *a priori* at $P < 0.05$.

Preparation of Figures

We generated the data graphs in Microsoft Office Excel 2007. Stick diagrams were generated by the ClickJoint software, version 5.0. Photographs, diagrams and all data graphs were processed in Microsoft Office PowerPoint 2007 (Microsoft) and Adobe Photoshop CS3 Extended (Adobe).

2.4. Results

Set-up for locomotor testing in rodents

We evaluated locomotor function in rats and mice in a rectangular Plexiglas basin. By changing the conditions within the basin, we investigated four different types of locomotion (Figure 2.1 A). To test skilled locomotion, we used a horizontal ladder. For assessment of overground locomotion, we replaced the ladder by a Plexiglas runway. For wading, the basin was filled with water to be 3 cm (rats) or 1 cm (mice) above the runway's surface since we found that these water levels were adequate to provide weight support for impaired animals without eliciting swimming movements. Finally, we evaluated swimming after filling the entire basin with water. Testing of a single animal in all four locomotor tasks was possible within 15 minutes. Three mirrors were arranged inside and outside of the basin such that the animals performance was recorded simultaneously from three sides (left, right and below) with one camera (Figure 2.1 B, Figure 2.2 A - Figure 2.5 A). We used a color-based tracking software for automatic tracking of markers tattooed on the rat or mouse's skin overlying anatomical landmarks (Figure 2.1 A). In addition, there was the possibility to perform EMG recordings during the locomotor tasks (Figure 2.1 C). A large number of parameters describing locomotor outcome could be assessed in the four different tasks as summarized in Table 2.1. However, for efficient analysis of locomotor ability, we chose a set of the most relevant parameters for each locomotor task (see Table 2.1). Precise paw placement[150] and fore-hindlimb coordination[141] were evaluated on the horizontal ladder whereas basic aspects of locomotor function were assessed during normal walking or wading. In addition, during wading, rats and mice tended to raise themselves as much as possible out of the water thus maximally extending their limbs. Therefore, we assessed body height and joint angles in this task and interpreted them as measures of strength. During swimming, rats and mice

demonstrated consistent, stereotypical hindlimb and wave-like tail movements which allowed reliable kinematic assessment of different forms of coordination and movement patterns.

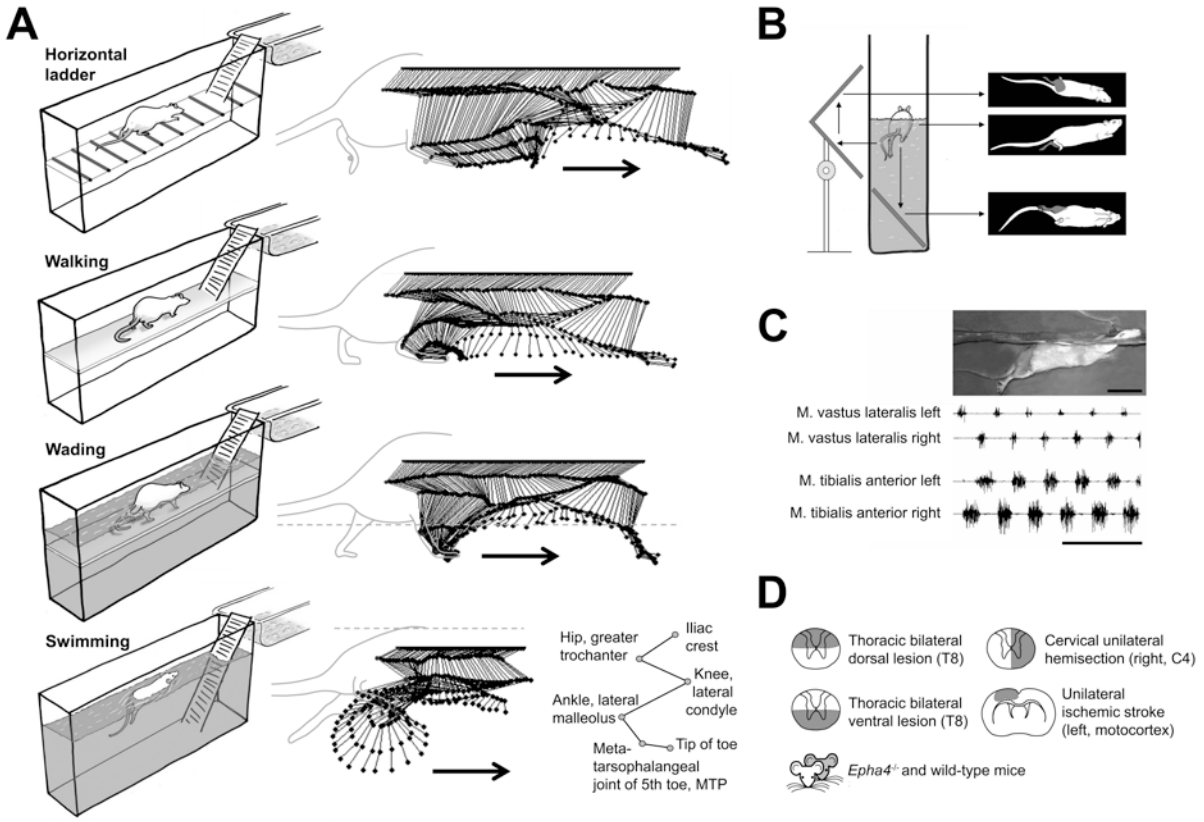

Figure 2.1. Experimental set-up for detailed evaluation of locomotor function in rodents after different forms of CNS damage. (**A**) We test locomotion in four different behavioral tasks by introducing different elements (horizontal ladder, shelf, water) into a basin. Tasks evaluated are "walking over an irregular horizontal ladder", "overground locomotion", "wading through shallow water" and "swimming". Stick diagrams of a single hindlimb step or swim cycle obtained from an uninjured rat illustrate that movement patterns differ considerably between tasks. Arrows indicate direction of movement and dashed line illustrates water level during wading and swimming**.** Bony landmarks for kinematic analysis of hindlimb movements are shown. (**B**) An arrangement of 3 mirrors enables recording of the performance with a high-speed camera from the left, right and bottom view, simultaneously. (**C**) Photograph of a swimming rat with head adapter for EMG recordings; scale bar, 5 cm. Sequences of amplified EMG illustrate hindlimb muscle activity of an uninjured rat during swimming; M, musculus; scale bar, 500 ms. (**D**) Schematic representations illustrate paradigms of CNS damage evaluated in this study, also used in Figure 2.2-2.5. CNS injuries are either bilateral dorsal spinal lesions at thoracic vertebral level 8 (T8), bilateral ventral spinal lesions at T8, unilateral right-sided spinal hemisections at cervical level 4 (C4) or ischemic strokes in the left motor cortex. *EphA4*-receptor knockout mice (*Epha4*$^{-/-}$) are compared to wild-type mice.

Evaluation of locomotor impairments

To model different types of CNS injury, adult female Lewis rats received surgical dorsal thoracic, ventral thoracic or unilateral right-sided cervical spinal cord injuries (SCI) or unilateral left-sided ischemic strokes in the motor cortex induced by stereotactic injections of endothelin-1, a potent vasoconstrictor (Figure 2.1 D). We also assessed locomotion in a

genetically modified mouse line, EphA4-receptor knockout (*EphA4*$^{-/-}$), with a characteristic hopping gait[151] and compared them to wild-type mice.

In the horizontal ladder task, trained intact rats (Figure 2.2 A) and mice crossed the ladder almost without slips or missteps and hindlimbs were always placed on the rung that was previously occupied by the ipsilateral forepaw indicating perfect coordination of fore- and hindlimbs. After bilateral dorsal thoracic SCI, rats demonstrated significant deficits in accurate hindpaw placement typically due to short targeting ($P < 0.0001$, one-way repeated-measures ANOVA, $n = 5$ rats; Figure 2.2 B, C). Rungs used by the ipsilateral forepaw were less frequently targeted by the respective hindlimb (49 ± 14%, 3 days after injury, group mean ± s.e.m., $n = 5$ rats) suggesting impaired fore-hindlimb coordination (Figure 2.2 D). No substantial recovery of either skill was detected at 28 days after injury. Rats with thoracic bilateral ventral SCI or cervical hemisections had very low performance on the ladder; precise hindpaw placement and fore-hindlimb coordination were virtually absent post-injury (not shown). After cervical hemisection, the ipsilesional forelimb was strongly impaired and only passively dragged over the rungs. Left cortical strokes resulted in slight and transitory, but significant deficits in skilled placement of the right fore- and hindpaw (forepaw: $P = 0.0122$, hindpaw: $P = 0.0344$, one-way repeated-measures ANOVA, $n = 3$ rats) while left limbs were unimpaired (Figure 2.2 E). Fore-hindlimb coordination was unchanged after unilateral strokes (Figure 2.2 F). When crossing the horizontal ladder, precise paw placement was not impaired in the *Epha4*$^{-/-}$ mice (Figure 2.2 G). *Epha4*$^{-/-}$ mice demonstrated synchronous steps with both, forelimbs and hindlimbs whereas fore- hindlimb coordination was normal (Figure 2.2 H).

During overground walking (Figure 2.3 A), rats with dorsal thoracic SCI consistently showed weight bearing steps. However, the gait was unstable leading to a significantly increased base of support ($P = 0.0275$, one-way repeated-measures ANOVA, $n = 5$ rats; Figure 2.3 B) and increased hindpaw exorotation ($P = 0.0002$, one-way repeated-measures ANOVA, $n = 5$ rats; Figure 2.3 C). Kinematic analysis revealed a significant backwards shift of hindlimb excursions although the total extent of movement remained unchanged (protraction: $P = 0.0008$, retraction: $P = 0.0041$, total: $P = 0.6693$, one-way repeated-measures ANOVA, $n = 5$ rats; Figure 2.3 D). In addition, fore-hindlimb coordination ($P = 0.0003$, one-way repeated-measures ANOVA, $n = 5$ rats; Figure 2.3 E) and toe clearance ($P < 0.0001$, one-way repeated-measures ANOVA; 70 ± 12 % of steps with paw dragging, 3 days after injury, group mean ± s.e.m., $n = 5$ rats; Figure 2.3 F) was significantly impaired. Seven days after either ventral thoracic lesions or cervical hemisections the walking pattern of the hindlimbs were massively impaired.

Parameter	Measure	Horizontal ladder	Walking	Wading	Swimming
General locomotor function					
Velocity of locomotion	meters/second	+	+	+	+
Trunk instability	seconds, centimeters	+	+	+	+
Body height, body angle	centimeters, degrees	+	++ (Fig. 2.3g)	++ (Fig. 2.4b,e,g)	+
Duration of tail or abdominal dragging	seconds	+	+	+	-
Base of support (distance between paws)	centimeters	+	++ (Fig. 2.3b)	-	+
Forelimb activity during swimming	number of FL strokes/run	-	-	+	++ (Fig. 2.5b)
Tail position, tail height, tail movement pattern, tail oscillation, tail motion velocity	centimeters, second^{-1}, centimeters/second	+	+		++ (Fig. 2.5i,j)
Basic and skilled limb movement					
Correct stepping, accurate paw placement	percent of plantar or functional steps	++ (Fig. 2.2b,c,e,g) +	+	+	-
Step or swim cycle duration, phase duration	seconds	+	+	+	+
Linear displacement (for example, limb pro- and retraction, step height)	centimeters	+	++ (Fig. 2.3d)	++ (Fig. 2.4d,f)	+
Angular displacement (for example, range of motion, minimal and maximal joint angles)	degrees	+	+	++ (Fig. 2.4b)	+
Velocity or acceleration of displacement	centimeters/second, radian/second, centimeters/second^2, radian/second^2	+	+	+	++ (Fig. 2.5c)
Toe clearance (paw dragging)	percent of steps with paw dragging, percent of step cycle duration	+	++ (Fig. 2.3f)	++ (Fig. 2.4c)	-
Paw position and rotation	centimeters, degrees		++ (Fig. 2.3c)	+	+
Coordination					
FL-HL coordination					
Coordinated placement of fore- and hindpaws on ladder	percent of identical rungs targeted	++ (Fig. 2.2d,f,h)	-	-	-
Ratio of FL and HL cycle duration	seconds/seconds	+	++ (Fig. 2.3e)	+	-
Phase dispersion, footfall diagram	percent deviation	+	+	+	-
Left-right coordination					
Ratio of left and right limb cycle duration	seconds/seconds	+	+	+	+
Phase dispersion, footfall or phase diagram, polar plot	percent deviation	+	++ (Fig.2.3h)	+	++ (Fig. 2.5d,e)
Timing of muscle activity (EMG recordings)	seconds	+	+	+	++ (Fig. 2.1c)
Intralimb coordination					
Timing of joint excursions	seconds	+	+	+	+
Limb motion patterns (for example, stick diagram, spatial displacement plot, angle-angle plot)	centimeters, degrees	+	+	+	++ (Fig. 2.5f,g)
Timing of muscle activity (EMG recordings)	seconds	+	+	+	++ (Fig. 2.1c)
Tail-HL coordination					
Timing of hindlimb excursions in relation to tail motion	seconds	+	+	+	++ (Fig. 2.5h)
Intratail coordination					
Timing of motion of different tail segments	seconds	-	-	-	+

(-) parameter not applicable or measurable; (+) parameter measurable; (++) recommended outcome parameter

Table 2.1. Parameters of locomotor function. Summary of parameters and possible measures for quantification of locomotor function in the different locomotor tasks. A large number of established quantitative parameters, as well as new readouts, can be assessed with the set-up. For locomotor profiling after CNS damage, we recommend a set of the most relevant outcome parameters and give references to the Figures illustrating them. We use the horizontal ladder for testing skilled locomotion and fore-hindlimb coordination. Parameters characterizing basic aspects of overground locomotion are assessed during walking and wading. During swimming, we evaluate intralimb and left-right coordination of hindlimbs and tail movements. HL, hindlimb; FL, forelimb.

After ventral injury, weight bearing hindlimb steps were extremely rare, limbs were maximally extended with limb excursions reduced to about 1 cm (Figure 2.3 D). Rats dragged themselves with their forelimbs with minimal hindlimb movements over the runway thus making more detailed analysis of hindlimb function almost impossible. The flat position was reflected by a reduced height of the iliac crest (Figure 2.3 G). However, total hindlimb excursions and limb protraction substantially improved within four weeks (Figure 2.3 D). Animals with a stroke walked almost normally; with only a tendency towards an increased external rotation of the right hindpaw (not shown). Overground walking in *Epha4*$^{-/-}$ mice was characterized by synchronous hindlimb movements (Figure 2.3 H). Coupling between the forelimbs was also observed when mice walked at a constant speed but not during exploration (Figure 2.3 H).

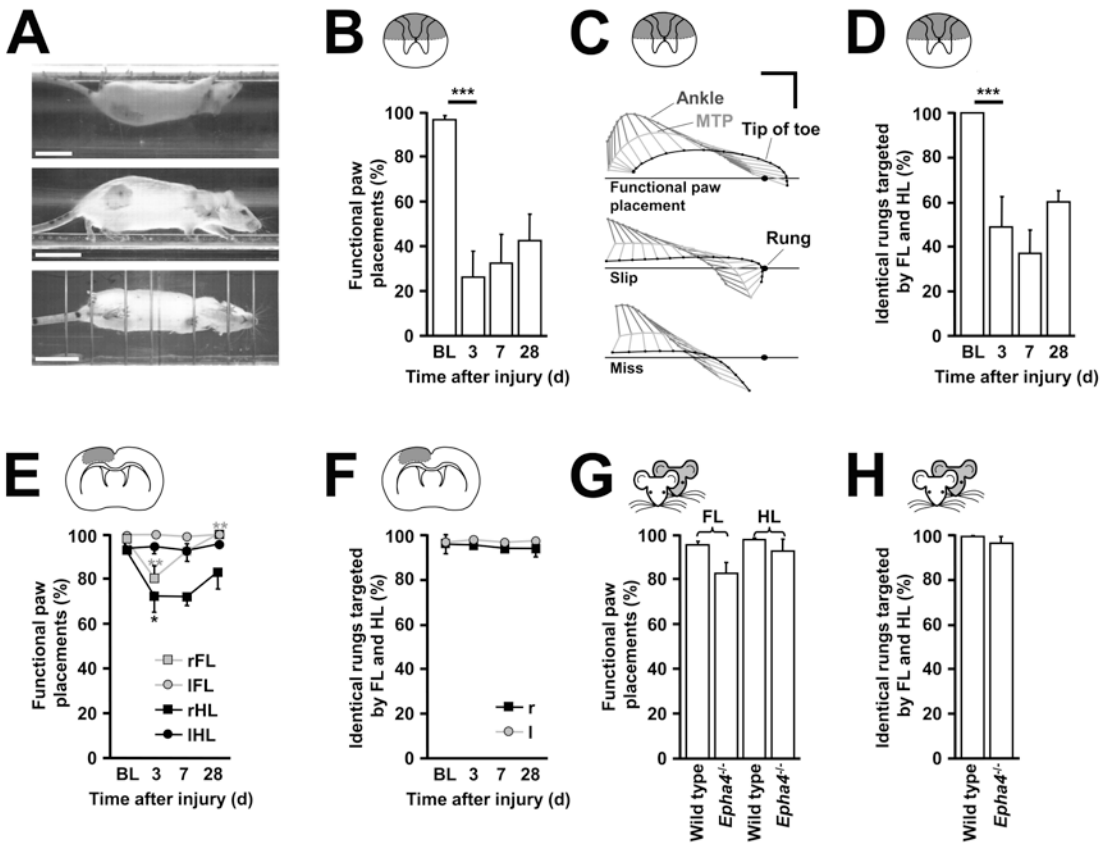

Figure 2.2. Skilled locomotion after CNS damage. (**A**-**F**) We evaluated skilled walking before (baseline, BL) and at several time points after dorsal thoracic SCI (n = 5 rats) or unilateral left-sided cortical stroke (n = 3 rats). (**A**) Image of intact rat crossing horizontal ladder; scale bars, 5 cm. (**B**) Precise placement of hindpaws after dorsal SCI. (**C**) Stick diagrams based on tracking of the ankle, MTP (metatarsophalangeal joint of 5th toe) and tip of toe illustrate typical hindpaw steps, classified as functional paw placement, slip or miss, after dorsal SCI; scale bars, 2 cm. (**D**) Fore-hindlimb coordination after dorsal SCI. (**E**) Precise placement of fore- and hindpaws and (**F**) fore-hindlimb coordination after stroke. (**G**) Precise placement of fore- and hindpaws and (**H**) fore-hindlimb coordination in wild-type (n = 3 rats) and *Epha4*$^{-/-}$ mice (n = 3 mice) assessed in a single testing session. (**B**, **D**-**H**) Bar and line graphs show group mean values for every testing session. (**B**, **D**, **G**, **H**) Values for left and right body side are averaged; (**E**, **F**) separate values for left (l) and right (r) side are presented. (**B**, **D**-**F**) For differences between time points, one-way repeated-measures ANOVA followed by *post hoc* Bonferroni tests were performed. (**G**, **H**) For differences between mice lines, data was subjected to Student's *t*-test (two-tailed, unpaired). ** $P < 0.01$, *** $P < 0.001$ indicate significantly different performances. Error bars, s.e.m.. FL, forelimb; HL, hindlimb.

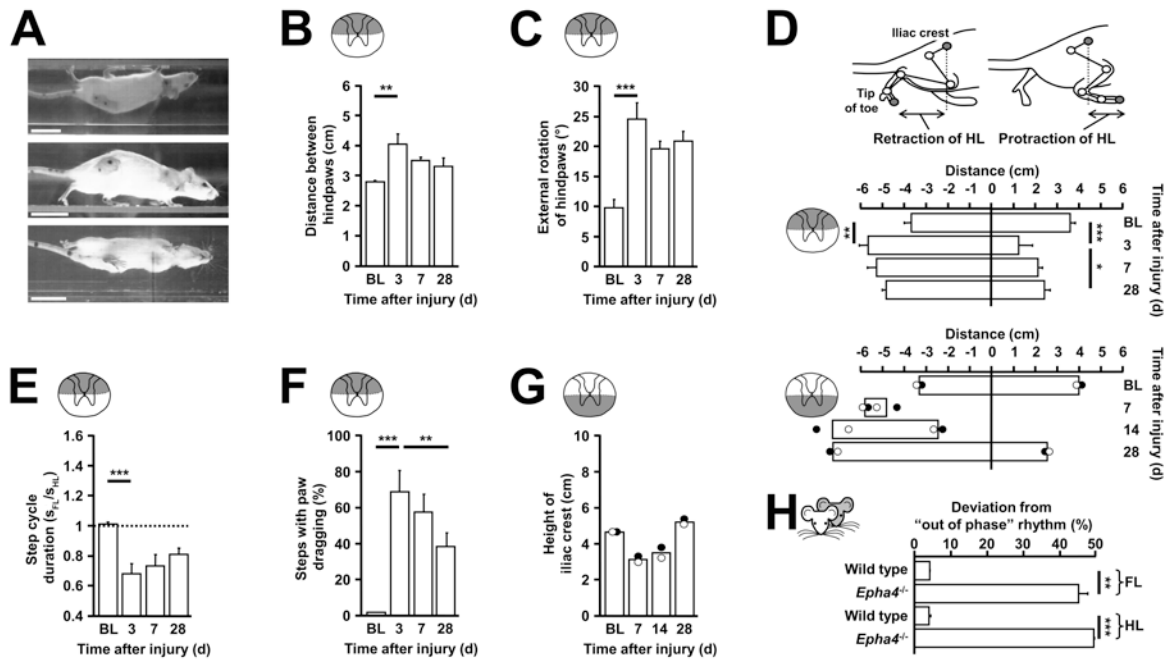

Figure 2.3. Overground walking after CNS damage. (**A**-**G**) Walking was tested before (baseline, BL) and at several time points after dorsal thoracic (*n* = 5 rats) or ventral thoracic SCI (*n* = 2 rats). (**A**) Image of intact rat walking over runway; scale bars, 5 cm. (**B**) Base of support and (**C**) external rotation of hindpaws at initial ground contact after dorsal SCI. (**D**) Horizontal hindlimb excursions described via the maximal protraction (maximal x-value) and retraction (minimal x-value) of the toe relative to the iliac crest after dorsal (upper panel) and ventral (lower panel) SCI. (**E**) Fore-hindlimb coordination and (**F**) toe clearance after dorsal SCI. (**G**) Height of iliac crest at mid-stance phase after ventral SCI. (**H**) Deviation from perfect left-right alternation (out-of-phase) of fore- and hindlimbs in wild-type (*n* = 3 mice) and *Epha4*$^{-/-}$ mice (*n* = 3 mice) assessed in one testing session. (**B**-**H**) Bars represent group mean values for every testing session. (**D** lower panel, **G**) Results for individual rats are shown and black and white dots represent individual rats. (**B**, **C**, **D** upper panel, **E**, **F**) For differences between time points, one-way repeated-measures ANOVA followed by *post hoc* Bonferroni tests were performed. (**D** lower panel, **G**) Data were not subjected to statistical testing. (**H**) For differences between mice lines, Student's *t*-test (two-tailed, unpaired) was applied. * $P < 0.05$, ** $P < 0.01$, *** $P < 0.001$ indicate significantly different performances. Error bars, s.e.m.. FL, forelimb; HL, hindlimb.

During wading in intact rats and mice, characteristic aspects of the locomotor pattern were a tiptoeing gait, elevated body position and increased limb excursions (Figure 2.4 A). After dorsal SCI and unilateral stroke, only minor lesion deficits were observed; the tiptoeing gait disappeared and heels touched the ground in the stance phase. Body height and joint angles of the knee and ankle, but not the hip, were transitorily reduced after dorsal SCI (Figure 2.4 B). Iliac crest height and joint angles of knee and ankle were strongly correlated (r_{knee}=0.87, r_{ankle}=0.91, Pearson's correlation coefficients, *n* = 88 steps of five rats, obtained 3, 7 and 28 days after injury). In contrast to normal overground walking, base of support was unchanged (not shown), paw dragging occurred only occasionally (38 ± 14 % of steps with paw dragging, 3 days after injury, group mean ± s.e.m., *n* = 5 rats; Figure 2.4 C) and hindlimb protraction was not significantly changed (*P* = 0.4883, one-way repeated-measures ANOVA, *n* = 5 rats; Figure 2.4 D). Rats with ventral thoracic lesions or with unilateral cervical injuries produced weight bearing hindlimb steps as early as 7 d after injury during wading, even though steps were characterized by increased retraction and reduced protraction (Figure 2.4

D). Following ventral injury, a gradual increase in iliac crest height during the recovery process was observed (Figure 2.4 E). After unilateral cervical hemisection, ipsilesional forelimb excursions were strongly impaired (Figure 2.4 F) paralleled by a strong reduction in the range of motion in the shoulder and elbow joint (not shown). The *Epha4*$^{-/-}$ mice showed a hopping gait also during wading. Other parameters like iliac crest height at mid-stance phase were unchanged in the mutant (Figure 2.4 G).

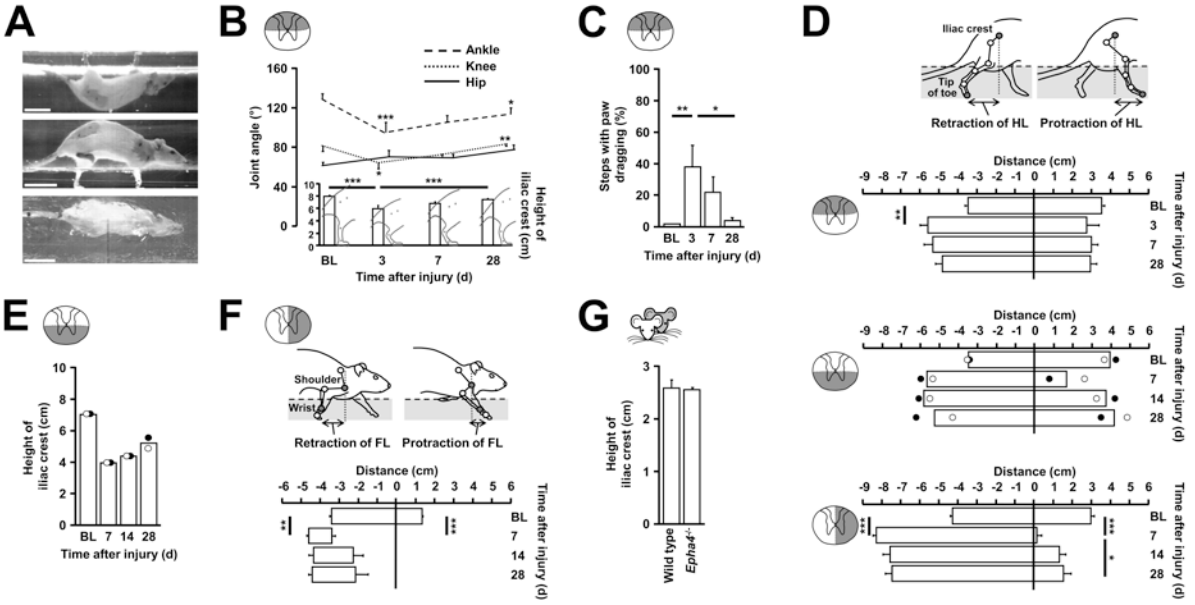

Figure 2.4. Wading after CNS damage. (**A**-**F**) Wading through shallow water was assessed before (baseline, BL) and at several time points after dorsal thoracic (n = 5 rats), ventral thoracic (n = 2 rats) or unilateral right-sided cervical SCI (n = 4 rats). Schematic representations illustrate paradigms of CNS damage (Figure 2.1 D). (**A**) Image of intact rat wading; scale bars, 5 cm. (**B**) Hindlimb joint angles and iliac crest height at mid-stance phase after dorsal SCI. (**C**) Toe clearance in rats with dorsal SCI. (**D**) Horizontal hindlimb excursions during wading are presented as in Figure 2.3 D for rats with dorsal (upper panel), ventral (middle panel) and unilateral cervical SCI (lower panel, ipsilesional hindlimb). (**E**) Height of iliac crest at mid-stance phase after ventral SCI. (**F**) Horizontal excursions of ipsilesional forelimb after unilateral cervical SCI. (**G**) Iliac crest height at mid-stance phase in wild-type (n = 3 mice) and *Epha4*$^{-/-}$ mice (n = 3 mice) measured at a single time point. (**B**-**G**) Bars represent group mean values for every testing session. (**D** middle panel, **E**) Results for individual rats are shown; black and white dots represent individual rats. (**B**, **C**, **D** upper and lower panel, **F**) For differences between time points, one-way repeated-measures ANOVA and *post hoc* Bonferroni tests were applied. (**D** middle panel, **E**) No statistical testing was performed. (**G**) For differences between mice lines, Student's *t*-test (two-tailed, unpaired) was used. * $P < 0.05$, ** $P < 0.01$, *** $P < 0.001$ indicate significantly different performances. Error bars, s.e.m.. FL, forelimb; HL, hindlimb.

Swimming is a stereotypical form of locomotor behavior characterized by powerful hindlimb strokes that are performed in a very consistent and well-coordinated manner providing the main drive for forward motion whilst forepaws are usually immobile below the chest (Figure 2.5 A)[148]. The horizontal sinusoidal oscillations of the tail and occasional forelimb strokes are probably important for navigation and stability during swimming. In infant rats[152] and after SCI in adults[31] extensive use of the forelimbs has been interpreted as a compensatory strategy for immature or impaired hindlimb function, respectively. Accordingly, we found that the

number of forelimb strokes was significantly increased after dorsal thoracic SCI (P = 0.0098, one-way repeated-measures ANOVA, n = 5 rats; Figure 2.5 B).

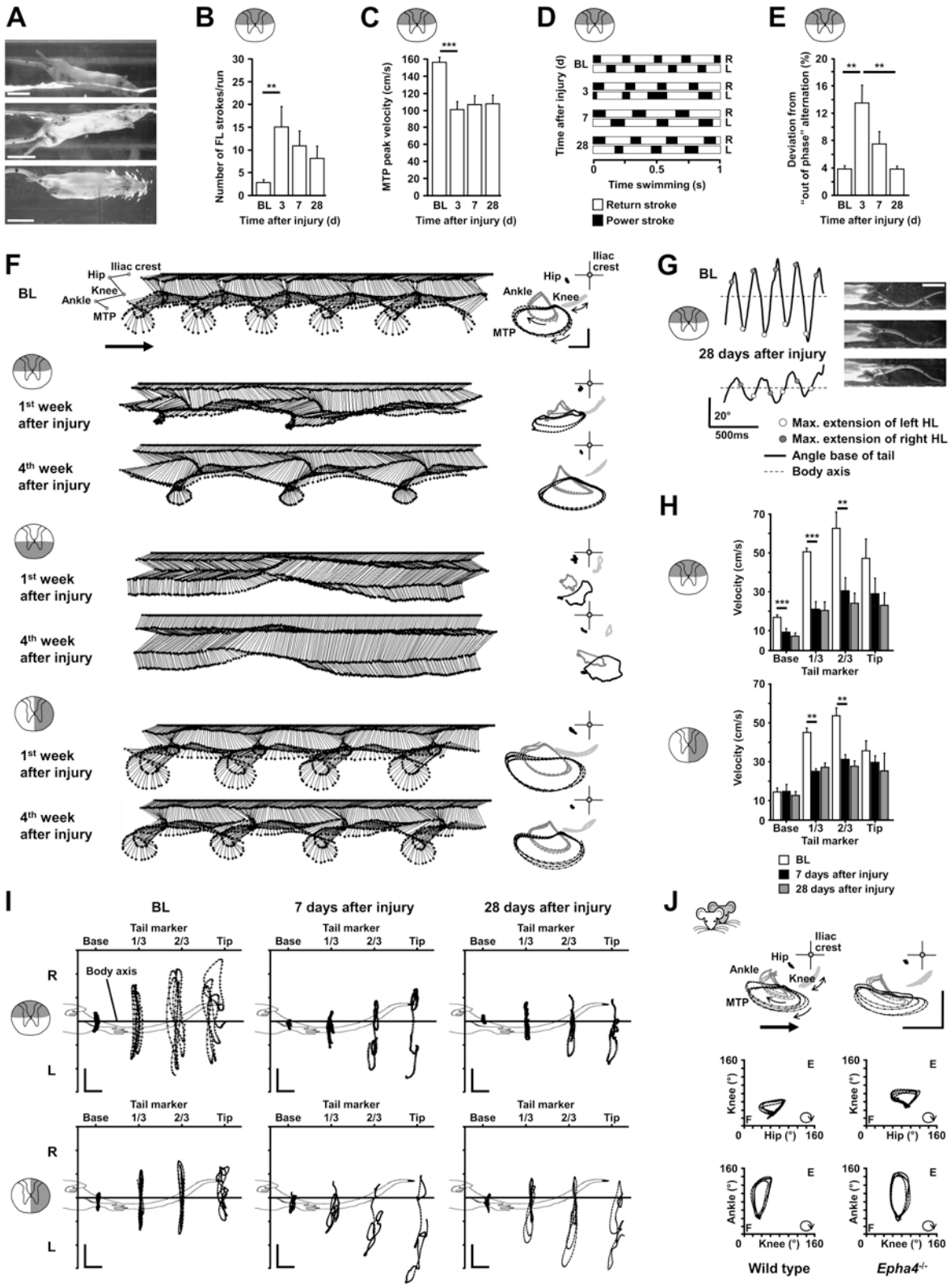

Figure 2.5. Swimming after CNS damage. (**A-I**) Swimming was tested before (baseline, BL) and at several time points after dorsal thoracic (n = 5 rats), ventral thoracic (n = 2 rats) or unilateral right-sided cervical SCI (n = 4 rats). (**A**) Intact rat swimming; scale bars, 5 cm. (**B**)

Forelimb (FL) strokes and (**C**) peak velocity of metatarsophalangeal joint (MTP) after dorsal SCI. (**D**) Phase diagram illustrating left-right alternation of hindlimbs after dorsal SCI. (**E**) Deviation from perfect hindlimb alternation (out-of-phase) after dorsal SCI. (**F**) Stick diagrams and spatial displacement plots illustrate swimming performance after dorsal, ventral or unilateral SCI over a period of 1 s. Thick arrows, swimming direction; thin arrows, temporal progression of movements; scale bars, 2 cm. (**G**) Disturbed synchrony of tail base excursions and hindlimb (HL) extension after dorsal SCI. (**H**) Mean movement velocity of tail markers (base, first third, second third, tip of tail) after dorsal and unilateral SCI; scale bar, 5 cm. (**I**) Lateral movements of tail markers over a period of 1 s after dorsal and unilateral SCI; scale bars, 2 cm. R, right; L, left. (**J**) Spatial displacement and angle-angle plots of an *Epha4*$^{-/-}$ and wild-type mouse; scale bars, 2 cm. E, Extension; F, Flexion. (**B**, **C**, **E**, **H**) Bars represent group mean values for every testing session; one-way repeated-measures ANOVA and *post hoc* Bonferroni tests; ** $P < 0.01$, *** $P < 0.001$. Error bars, s.e.m.. (**D**, **F, G, I**) Results of single rats and (**J**) of single mice representative for their experimental group.

Hindlimb movements were slower as indicated by significantly reduced peak toe velocities ($P = 0.001$, one-way repeated-measures ANOVA, $n = 5$ rats; Figure 2.5 C) and longer stroke cycle durations with extended power and return stroke phases (Figure 2.5 D). A transient disturbance of the left-right coordination was present (Figure 2.5 D, E) and hindlimb excursions were initially smaller and of irregular shape (Figure 2.5 F). Hindlimb function during swimming recovered impressively which was reflected in most of the parameters assessed. In contrast, the strongly impaired tail-hindlimb coordination (Figure 2.5 G), tail movement velocity (Figure 2.5 H) and tail motion patterns (Figure 2.5 I) did not improve over time. Throughout the testing period, rats with ventral thoracic SCI demonstrated massive impairments in hindlimb (Figure 2.5 F) and tail function (not shown) and strong lateral instability in the swimming task. Forward motion was only achieved by excessive forelimb use. After cervical hemisection, kinematic analysis showed transiently exaggerated joint excursions of the ipsilesional hindlimb (Figure 2.5 F). Tail movements were slower (Figure 2.5 H) and strongly deviated towards the uninjured side (Figure 2.5 I) suggesting an imbalance of tail muscle activity in favor of the intact side. Accordingly, rats with cervical hemisections suffered from lateral instability during swimming. After unilateral stroke, no deficits in swimming were detected (not shown). *Epha4*$^{-/-}$ mice showed consistent coupling of hindlimbs resulting in an uneven, bumpy swimming style that appeared less efficient than the regular left-right alternating pattern demonstrated by wild-type mice. A shift in the angle-angle plots towards higher degrees indicated increased extension of the hip and knee joint (Figure 2.5 J). In addition, *Epha4*$^{-/-}$ mice showed an extensive and coupled use of both forelimbs during swimming.

2.5. Discussion

We used a set of physiological, objective and quantitative parameters to generate comprehensive locomotor profiles for some of the most common models of CNS insult. We found that these profiles were highly dependent on lesion type and severity. Some parameters were more sensitive to or more affected by one particular lesion than another allowing for the selection of suitable combinations of locomotor task, readouts and lesion type in future studies.

After dorsal thoracic SCI, rats were able to perform weight-bearing hindlimb steps and demonstrated only transitory deficits in left-right and intralimb coordination during swimming indicating that the lumbar spinal central pattern generator (CPG) networks and their main modulatory inputs were unaffected by the injury[153,154]. However, damage to major components of the cortico- and rubrospinal tract and the gracile fasciculus led to strongly impaired paw placing, seen during skilled walking and overground locomotion, with respect to accuracy, strength and velocity. This suggests that these tracts play an important role in skilled and distal hindlimb motor function in rats[150]. In addition, after this lesion type fore-hindlimb coordination and tail movements were also impaired, possibly due to damage of components of the propriospinal system[155] and bulbospinal tracts, respectively. In line with these findings, unilateral strokes comprising the fore- and hindlimb sensorimotor region resulted in contralateral deficits in fine motor control without affecting other basic aspects of locomotion during swimming, walking or wading. Ventral thoracic SCIs disrupt, among other systems, vestibulospinal fibers and main portions of the reticulo- and raphespinal tracts. The latter are known to be crucial for the initiation and modulation of stepping movements via CPG networks[156,157]. Accordingly, in the first week after injury rats were not able to perform hindlimb swimming strokes or stepping movements during normal overground walking. Interestingly, animals could generate hindlimb movements in the wading test since assistive weight support was provided by the water buoyancy. Although stepping ability improved significantly over time, rats were, even after several weeks, barely able to produce hindlimb strokes during swimming. In the absence of major bulbospinal input, it can be assumed that the rhythmic hindlimb movements generated by the lumbar CPGs rely on or are facilitated by proproiceptive input due to limb loading which is present during wading but not during swimming[158]. Thus, as both proproiceptive input and some weight support seem to be required for hindlimb movements after this lesion, wading is the most appropriate test to demonstrate and evaluate locomotor ability in these rats. After cervical unilateral hemisection, fore- and hindlimbs were differently affected in the four different tasks. Forelimb locomotor

function was extremely poor throughout the entire testing period in all locomotor tasks. In contrast, hindlimb movements were present during wading and swimming within the first week of injury followed by substantial functional recovery indicated by regular weight-bearing hindlimb steps and excellent intralimb coordination. However, rats remained poor in their ability to cross the ladder. These data suggest that the descending fiber tracts in the spared hemicord were at least partially sufficient to compensate for lost supraspinal input. This partial compensation allowed for good basic locomotor function of the affected hindlimb but not forelimb during walking, wading and swimming, however it did not enable skilled movements of either limb. The absence of EphA4, an important axon guidance receptor during development, led to anatomical alterations of corticospinal projections and locomotor networks in the lumbar spinal cord[151,159]. These changes are considered responsible for the previously described synchronous hindlimb movements ('hopping') during walking[151]. Interestingly, we found additionally that forelimb movements were synchronously coupled during overground locomotion. No deficit in precise paw placement was detected on the horizontal ladder. These behavioral data suggest that important anatomical changes are also present on the level of cervical CPG networks[160], but that the anatomically altered corticospinal system is able to control precise targeted movements. These conclusions were based on testing in several locomotor tasks, highlighting the importance of broad screening.

Our data were comprehensive in several ways. We provided information about "whether" and "how" a task was performed after a variety of CNS insults in rats and mice. The battery of readouts used ranged from "very basic" to "very specific". We assessed movements of all relevant body parts (forelimbs, hindlimbs, trunk and tail) as well as the most important characteristics of locomotion - for example different forms of coordination. In addition, our analysis was highly sensitive as it was able to detect compensatory strategies, such as the finding that during swimming, slower, less powerful and uncoordinated hindlimb strokes were compensated for by extensive forelimb use and exaggerated hindlimb movements in rats with SCI. A number of established as well as novel parameters were assessed. For the established parameters, our results are in line with data from earlier studies using comparable lesion types and testing conditions[18,31,143,150]. In this study, we concentrated on commonly used CNS injury paradigms in adult rats and on one transgenic mouse line. However, our method is not limited to these situations and could also be used to study models of peripheral nerve injury, muscular diseases, and neuroinflammatory or neurodegenerative diseases.

Our results, derived from a systematic evaluation of different types of CNS damage in rodents, emphasize the importance of detailed locomotor profiling in animal research. Broad

application of these sets of objective and quantitative readouts will improve and standardize behavioral assessment.

2.6. Supplementary Notes: Description of the locomotor testing set-up

Testing box

The testing box (basin) was entirely made of Plexiglas and 150 cm in length, 13 cm in width (inside) and 40 cm in height. The walls (thickness: 0.8 cm) and the floor plate (thickness: 1.5 cm) of the box were attached to each other using an adhesive solution (Acrifix 106, Röhm GmbH). At one side, the wall was 10 cm lower and a small footbridge (rigid PVC with rough surface) was attached to a ledge (Figure 2.6 A) so that the animals could exit the testing box and enter a cage placed next to the testing box. On the opposite side of the box, a hole was drilled in the Plexiglas wall close to the floor plate and a ball valve was installed for water drainage (Figure 2.6 A). A temperature sensor was installed to measure water temperature.

Elements to test different types of locomotion

The horizontal ladder (rats: length of 113 cm, width of 13 cm; mice: length of 113 cm, width of 7 cm) was composed of thin Plexiglas side rails (thickness of 0.5 cm), metal rungs (round, length of 13 cm (rats), 7 cm (mice); diameter of 0.3 cm (rats), 0.2 cm (mice)) and two PVC plates (height of 22 cm, width of 13 cm, thickness of 1.5 cm) as supporting legs (Figure 2.6 B). Side rails were attached to the PVC plates at both ends so that the ladder was at least 15 cm above ground. A number of small holes separated by 1 cm were drilled into both stringers to insert the metal rungs. Therefore, it was possible to change the sequence of the metal rungs before every testing session. Animals were trained on the ladder with a regular arrangement of metal rungs (rung in every 4^{th} hole). For testing, rung sequences were irregular and varied (rungs in every 3^{rd}-5^{th} hole) to avoid habituation to a particular rung pattern and, thus, to ensure correct testing of skilled walking[150,161]. During training and testing on the horizontal ladder, the box was filled with water to approximately 1 cm below the rungs, to prevent the animals from climbing underneath the ladder.

The runway used to test overground walking and wading consisted of a clear Plexiglas shelf (length of 123 cm, width of 13 cm, thickness of 0.5 cm) which was attached at both ends to PVC plates (height of 22 cm, width of 13 cm, thickness of 1 cm) holding the runway 15 cm above ground (Figure 2.6 B). When inserting the runway into the testing box, sagging of the Plexiglas shelf was prevented by placing two small, but robust, PVC plates attached to each other by a double ended screw onto the floor of the testing box, just between the

supporting elements of the runway and the walls of the testing box. By turning the screw, the total length of the two attached PVC plates could be altered thereby changing the pressure exerted on the lowest parts of the supporting stands. This simple tool allowed us to adapt the tension of the runway and thus avoid sagging of the shelf.

For mice, passages were altered to 7 cm in width by two additional Plexiglas walls (length of 100 cm, height of 14 cm, thickness of 0.5 cm; Figure 2.6 B). The upper sides of the walls were fixed to each other with three metal bars (length of 7 cm) used as spacer pieces to form a 7 cm wide Plexiglas corridor. For swimming, the bars served as suspension point for hooks to hang the Plexiglas corridor into the water. For walking and wading, the corridor was simply placed on top of the runway. The corridor was not used for the evaluation of skilled locomotion in mice since the width of the mouse ladder was already 7 cm.

Arrangement of mirrors

The arrangement of the three mirrors used in this study allowed recording and evaluation of the animals performance in the testing box simultaneously from three sides (left, right and below) with only one camera. The first mirror (100 cm x 16 cm, thickness of 0.4 cm) was placed on the basin's floor at an angle of ~ 90° (bottom view). The other two mirrors (100 cm x 18 cm, thickness of 0.4 cm) were connected via an adjustable hinge-joint and fixed to an aluminum rack (extrusion connecting system**,** Kanya AG) that was placed directly behind the long side of the testing box to visualize the side of the animals hidden from the camera (Figure 2.1). One mirror was placed at the level at which the animals performed the locomotor task, while the other one was higher and positioned almost perpendicular to the lower mirror (Figure 2.6 C).

Light system

The high frame rates used to record the animals required an additional strong light source (see below). We built a light system that was comprised of four commercially available 36 Watt fluorescent lamps emitting cool white light. The lamps were attached to an aluminum rack (extrusion connecting system**,** Kanya AG). To direct the light onto the testing box and diminish light loss, reflecting foils were placed behind the lamps. During testing, the rack was located between the camera and the testing apparatus illuminating the basin from above (one lamp) and below (three lamps). Since the light was directed onto the testing box, the escape cage at the end of the box was less strongly illuminated. The additional light did not seem to affect the animals' motivation to cross the testing box nor their locomotor behavior. In

contrast, they were rather animated to cross the basin in order to enter the darker escape cage at the end of the apparatus. This side effect of the light system emerged as a rather positive feature for locomotor function testing.

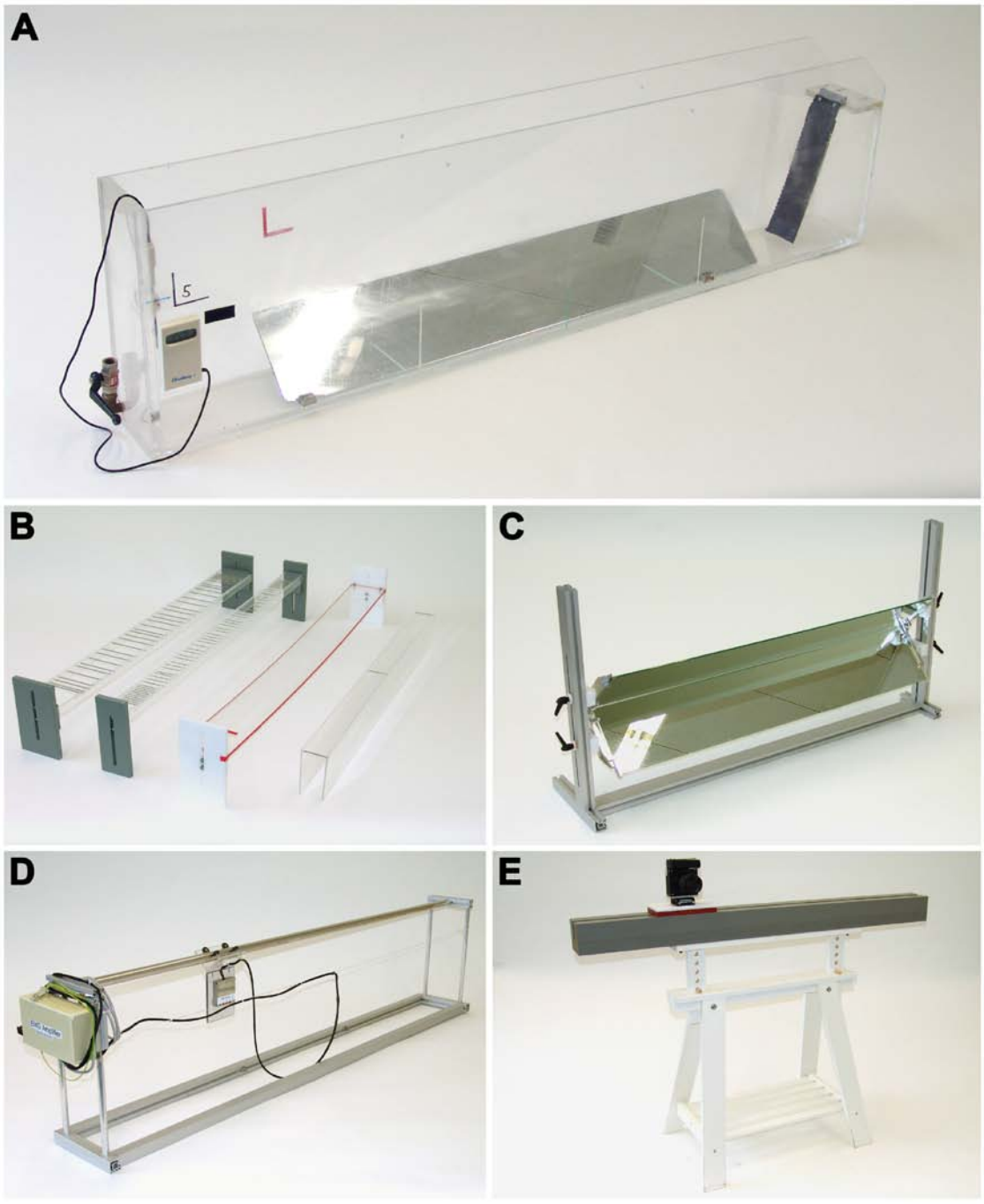

Figure 2.6. Different components of the locomotor testing system. (**A**) Testing box. (**B**) Horizontal ladders for rats and mice, runway, Plexiglas corridor for mice. (**C**) Mirror system. (**D**) EMG set-up. (**E**) Camera mounted on a guide rail.

EMG set-up

For EMG measurements, an aluminum frame that was 159 cm in length, 15 cm in width and 36 cm in height (extrusion connecting system**,** Kanya AG) was built. This frame could be plugged on top of the walls of the testing box and served as suspension for a round and smooth aluminum beam (Figure 2.6 D). A mobile preamplifier was attached to a hanger unit running on four small wheels over the beam. This assembly resulted in minimal friction so that rats, connected to the preamplifier via wires to their head adapter, were easily able to pull the preamplifier with them when crossing the testing box. The preamplifier was connected to a second amplifier fixed to the frame. The second amplifier relayed the data to a working station for further processing with DIAdem academic 8.1 software (National Instruments Engineering GmbH & Co. KG).

Prerequisites for successful automated tracking

Based on pilot experiments, we decided to film the animals with a color high-speed camera (Basler A504kc Color Camera, Basler AG), because for successful automated tracking of the markers, several prerequisites had to be fulfilled by the camera and, in addition, also by the set-up.

First, a color camera was required, since marker tracking by the software was based on the color of the markers. This was crucial to enable the software to distinguish between markers that can come close to each other during a given movement and between the markers and the background. Before every testing session, visualization of the tattoos was reinforced with a fluorescent dye (for example fluorescent, fast drying nail polish) or a black marker, in case of albino rats, to increase the contrast and thus optimize tracking.

Second, sufficient temporal resolution was essential since movements of the animals during locomotion can be fast. For instance, the peak velocity of the toe during swimming can reach 160 cm/s in an intact rat. Therefore, recording at high frame rates up to 200 f/s (Hz) was necessary. During swimming, we found that occasionally the automated tracking of markers placed on the distal hindlimbs failed because changes in marker position between one frame and the next were too large even with recordings at 200 f/s. In these cases, manual frame-by-frame tracking was required. In addition, for recordings at high frame rates, an extra light source emitting cool white light in addition to the daylight illumination was essential to ensure good image quality, that is in terms of brightness, and so that the depth of field could be extended by using smaller diaphragm openings of the lens. Depth of field was important for the evaluation of the mirror images. The different locomotor tasks required recordings at

different minimal frame rates (see 2.3. Methods) and so lens openings of f/4, f/5.6 or f/8 were used. Another option would be filming under UV illumination. In our hands, this approach was not satisfying because the light reflected by the markers was not sufficient for filming at high frame rates and most of the animals' body, apart from the markers placed on the skin, was almost invisible making the assessment of other endpoint measures impossible.

Third, good spatial resolution was crucial for the automated tracking. The dimensions of the digital color images obtained with the Basler camera were 1280 x 1024 pixels. To increase the number of pixels per marker, the camera was placed close to the basin (distance of 100-150 cm), thereby limiting the field of view to about one third of the length of the testing track. By moving the camera on a guide rail (Figure 2.6 E), the full distance covered by the animal could be recorded. A commercially available laser pointer (light or flashlight pointer) was attached to the camera indicating the camera's field of view. This provided visual feedback to the experimenter who was manually moving the camera thus allowing reliable recordings of moving animals.

In summary, automated tracking of markers was feasible by using a high-speed color camera with excellent spatial resolution, intensive, colored markers, an additional illumination provided by the light system, small lens openings and high temporal resolution. However, manual tracking was occasionally necessary.

General description of the software, application and data processing

Analysis of video recordings was performed offline with the color-based, automated tracking software ClickJoint (V5.0; ALEA Solutions GmbH, www.aleasol.ch). After the video files were imported into the software, the settings including the number of markers to be tracked, color of markers, size of search field for markers, the virtual joint and a representative distance for calibration (see below) were defined in two separate configuration windows. The knee and elbow joints were defined as virtual joints so that their positions were indirectly computed by the software. For the knee, the calculation was based on both the position of the markers over the hip and ankle and the length of the femur (rat = 2.5 cm, mouse = 1.3 cm) and tibia (rat = 3.5 cm, mouse = 2 cm) bones. For the elbow joint, the shoulder and wrist positions and the length of humerus (rat = 2.5 cm, mouse = 1.1 cm) and the lower forelimb (rat = 2.8 cm, mouse = 1.2 cm) were used.

Before automated tracking could be started, the experimenter had to identify the markers on the animals' skin manually on the first frame of the video file. Then, by automatically tracking the markers frame-by-frame, the software generated two-dimensional

coordinates (x, y) for every marker and time point. Movements could be reconstructed based on the changes of the xy-coordinates over time. Based on the xy-coordinates, the software directly calculated angles and distances and generated stick diagrams and spatial displacement plots. For angle measurements, usually the smaller angle of the two alternatives was used, typically this was the angle at the flexor side of a limb joint. The side and the bottom views of the animals were analyzed separately. For one run, tracking the markers during, for example swimming, took approximately 10-15 minutes per limb (4-5 stroke cycles). During wading and swimming, occasionally interference caused by disturbed water or light reflections on the water surface hindered automated tracking of the markers. In these cases, manual corrections by the experimenter were necessary. All data including the frame, xy-coordinates, angles and distances for every marker was exported, saved and imported into Microsoft Excel. Applying an integrated supplementary function of the ClickJoint software, raw data could be smoothed using a cubic-spline function (internal software value of 50). Data were then further analyzed with pre-assembled Microsoft Excel sheets determining joint angles or distances between joints at a given time point, range of motion, coordination parameters or movement velocities. Currently, the software is being further developed to provide a more comprehensive and convenient data analysis package independent of Microsoft Excel. This new version will be available with the full MotoRater setup at TSE-systems GmbH (www.tse-systems.com).

Practical considerations for animal testing and analysis

To test a single animal in all four locomotor tasks approximately 15 minutes is required. Depending on the task, 3-10 passages were recorded and usually three representative runs were analyzed for every task. Sample selection was based on objective criteria, i.e. comparable locomotion velocity between animals, removal of runs where animals stopped and explored the testing box and, for analysis of limb kinematics, removal of passages in which the animals demonstrated massive lateral instability during locomotion (see below).

Special locomotor parameters: Lateral stability during locomotion

Lateral stability is clearly an important component of all forms of locomotion in rodents and also in humans[162,163]. In this study, lateral stability served on the one hand as a selection criterion for those passages that were used for limb kinematics and on the other hand as a readout of locomotor function. In order to assess lateral stability, both side views of the animal (mirror and direct view) were used. For instance, stability was assumed when both iliac crests were visible during swimming. Here, the time (in percent) that an animal moved

under stable conditions could serve as a functional outcome measure. Other readouts for lateral stability during overground locomotion include the measurement of the animals' base of support[130] (distance between limbs; Figure 2.3) or, possibly more accurately, the variability of pelvis (iliac crest) oscillations in different planes[136].

Chapter 3

Chasing CNS plasticity: the brainstem's contribution to locomotor recovery in spinal cord injured rats

Björn Zörner [1,2,4], Lukas C. Bachmann [1,4], Linard Filli [1,2], Sandra Kapitza [1,2], Miriam Gullo [1], Marc Bolliger [2], Michelle L. Starkey [2,3], Martina Röthlisberger [1], Roman R. Gonzenbach [1,2], Martin E. Schwab [1]

[1] Brain Research Institute, University of Zurich and Dept. of Health Sciences and Technology, ETH Zurich, Zurich, Switzerland

[2] Department of Neurology, University Hospital Zurich, Zurich, Switzerland

[3] Spinal Cord Injury Center, Balgrist University Hospital, Zurich, Switzerland

[4] authors contributed equally to the study

The original article was accepted for publication in *Brain* 2014 (in press).

Parts of this article were also published in the Ph.D. thesis presented by Lukas C. Bachmann which was accepted by the ETH Zurich in 2013 (DISS. ETH No.: 21569).

Author contribution

BZ designed the study, performed surgeries, collected and analyzed data for Figures 3.1-3.5, made the figures and wrote the manuscript.

3.1. Abstract

Anatomical plasticity such as fibre growth and the formation of new connections in the cortex and spinal cord is one known mechanism mediating functional recovery after damage to the central nervous system. Hardly anything is known about anatomical plasticity in the brainstem which contains key locomotor regions. We compared changes of the spinal projection pattern of the major descending systems following a cervical unilateral spinal cord hemisection in adult rats. Like in humans (Brown-Séquard syndrome), this type of injury resulted in a permanent loss of fine motor control of the ipsilesional fore- and hindlimb, but for basic locomotor functions substantial recovery was observed. Antero- and retrograde tracings revealed spontaneous changes in spinal projections originating from the reticular formation, in particular from the contralesional gigantocellular reticular nucleus: more reticulospinal fibres from the intact hemicord crossed the spinal midline at cervical and lumbar levels. The intact-side rubrospinal tract showed a statistically not significant tendency towards an increased number of midline crossings after injury. In contrast, the corticospinal and the vestibulospinal tract as well as serotonergic projections showed little or no side-switching in this lesion paradigm. Spinal adaptations were accompanied by modifications at higher levels of control including side-switching of the input to the gigantocellular reticular nuclei from the mesencephalic locomotor region. Electrolytic micro-lesioning of one or both gigantocellular reticular nuclei in behaviourally recovered rats led to the reappearance of the impairments observed acutely after the initial injury showing that anatomical plasticity in defined brainstem motor networks contributes significantly to functional recovery after injury of the central nervous system.

3.2. Introduction

After injury to the central nervous system (CNS), varying degrees of functional recovery are observed depending typically on the location and size of the lesion. Identification of the underlying mechanisms of spontaneous recovery and the factors that impede further functional improvements is an important prerequisite for the development of effective new therapies for brain and spinal cord injury[21,47,164]. Anatomical plasticity in the CNS ranging from sprouting of lesioned and unlesioned fibres to the *de novo* formation of detour pathways has been shown to mediate functional recovery after brain and spinal cord injury in rodents and primates[12,13,15,165]. After one-sided spinal cord injury (e.g., Brown-Séquard syndrome), spared contralateral tracts are believed to mediate functional recovery through pre-existing or newly formed fibres that cross the spinal cord midline below the level of the injury [18]. Thus far, beneficial, spontaneous neuroanatomical adaptations are almost exclusively described in the sensorimotor cortex and its projections as well as in intraspinal networks[15,44]. Much less is known about adjustments in other brain regions after CNS damage, in particular in the brainstem which contains the phylogenetically oldest and functionally most important centres for basic movement control.

Key structures for the initiation and execution of locomotion are located in the midbrain, pons and medulla oblongata[166,167]. From fish to mammals, locomotor command regions located in the rostral brainstem such as the mesencephalic locomotor region (MLR) are directly connected to bulbar output systems, for example the medial reticular formation[168-171]. The reticular formation, in turn, projects to the spinal cord to initiate and coordinate limb movements and postural support, and to modulate the locomotor rhythm produced by the spinal central pattern generators (CPGs)[156,170,172,173]. The rubrospinal system is involved in the execution of precise limb movements while vestibulospinal tracts primarily control balance and posture[174-176]. Despite the fact that these phylogenetically highly conserved brainstem centres are crucial components of the CNS motor network, only limited information is currently available on their responses to CNS damage[15,110,177,178]. In particular, a comparative analysis of neuroanatomical changes in the different CNS systems after injury is missing.

In this study, we assessed the anatomical plasticity in the major descending CNS systems after cervical unilateral spinal cord hemisections in adult rats. We investigated whether changes in the spinal projection pattern of a plastic region are accompanied by anatomical remodelling of its input from other CNS centres and we evaluated the functional significance of these adaptations.

3.3. Methods

Animals

Adult female Lewis rats ten weeks of age (200-250g, R. Janvier, France) were housed in groups of three to five rats in standardized cages (type 4 Macrolon) under a 12h light/dark cycle with food and water provided *ad libitum*. All experiments were approved by the Veterinary Office of the Canton of Zurich, Switzerland.

Spinal cord injury and animal care

Rats were deeply anesthetized with subcutaneous injections of Hypnorm/Dormicum (Hypnorm: 120µl/200g body weight, Janssen Pharmaceutics, Belgium; Dormicum 0.75mg/200g body weight, Roche Pharmaceuticals, Switzerland) for all surgical procedures described below. For cervical hemisection injury at C4 spinal level, the rats' skin was cut between the occipital bone and the prominent process of the T2 vertebra with a scalpel. Laminectomy of the third cervical vertebra was performed and the dura was opened along the rostrocaudal axis with a fine needle to expose the entire dorsal surface of the spinal cord. A 27 gauge needle was lowered at the spinal cord midline and served as boundary for the hemisection. Since we found no paw preference in the cylinder test in this rat strain (see 4.4. Results), all rats received a right-sided unilateral hemisection injury at cervical level C4. The right spinal hemicord was cut with a sharp sapphire knife (WPI, Berlin, Germany). To ensure completeness of the lesion, cuts were repeated until the ventral surface of the spinal canal was visible. Following the lesion, the muscle layers were sutured and the skin was closed with surgical staples. One day before and for two days after surgery, rats received subcutaneous injections of the analgesic Rimadyl (5mg/kg, Pfizer AG, Zürich, Switzerland). To prevent bladder and wound infections, rats were treated with daily subcutaneous injections of the antibiotic Baytril (5mg/kg body weight, Bayer AG, Leverkusen, Germany) for one week. All rats were checked twice daily for the entire period of the experiment.

To assess a possible role of the myelin-associated neurite growth inhibitor Nogo-A, all chronic spinal cord injured animals received a two weeks intrathecal, thoracic spinal infusion of antibodies (control-IgG or anti-Nogo-A [11C7] antibodies; total amount infused: 6mg) via an osmotic mini-pump (5µl/h, 3.1µg IgG/µl, Alzet 2ML2; Charles River Laboratories, Les Oncins, France) starting at the time of injury. As shown by densitometry of immunostained sections on different levels of the spinal cord rostral to the lesion, antibodies did not efficiently diffuse into the spinal and brain parenchyma, most probably due to a continuous, lesion-induced dura leak at the cervical hemisection site during the time of infusion (data not

shown). The subdural spaces were collapsed all along the spinal cord, supporting the hypothesis of a long-lasting, major cerebrospinal fluid leak in this lesion paradigm. Clinically, large dura mater lesions are known to heal very slowly[179]. Due to the unavailability of the antibody in the tissue, antibody-treatment was disregarded. When control-IgG and anti-Nogo-A antibody treated animals were compared, no differences could be observed for any of the read-outs shown in the present study.

Perfusion and Nissl staining

After completion of the experiments, rats were anesthetized with an overdose of pentobarbital (i.p.) and transcardially perfused with 100ml heparinized Ringer's solution followed by 400ml Ringer's solution containing 4% paraformaldehyde and 5% sucrose. Brains and spinal cords were removed, *post*-fixed in the same fixative over-night at 4°C, cryoprotected in 30% sucrose for 5 days, embedded in Tissue-Tek and frozen in isopentane at -40°C. The tissue was cut on a cryostat and 40µm thick cross-sections were collected on-slide. Completeness of hemisections was confirmed histologically on Nissl stained spinal cord cross-sections of the lesion centre. For staining, dried sections were bathed in Cresyl violet solution for 3min, dehydrated in ethanol, washed in xylol and coverslipped with Eukitt[180]. Rats with incomplete hemisections were removed from analysis.

Behavioural testing and quantification

Rats were familiarized with the behaviour set-ups and trained on the tasks for a total of five to seven sessions within 14 days. Baseline measurements were performed one week before spinal cord injury. To characterize the course of functional recovery after hemisection injury (n=20; 5 rats were excluded retrospectively due to an incomplete hemisection), rats were tested 1, 2, 4, 8, and 12 weeks after lesion. Grooming behaviour was first assessed two weeks after injury and paw preference was tested only once one week before hemisection.

The *paw preference test* ("cylinder test") was performed to detect asymmetries in forelimb use for each individual rat before injury and evaluated according to earlier studies[181]. Also, *air-righting* was assessed and scored as published previously[182,183]. In brief, rats were held in supine position about 30cm above a surface covered with foam material. After being released intact rats land on their paws due to a successive rotation of head, shoulder girdle, thorax and pelvis. Air-righting reaction was tested ten times per time point and video recorded. Scoring was performed based on the posture of the rat at landing[183]: 0 = no rotation, 1 = head rotation only, 2 = head and thorax rotation only, 3 = landing on the side, 4 = full

rotation except hindlimbs, 5 = full rotation. Values represent the mean of ten trials per rat. *Grooming* was assessed immediately after the swimming test (with wet fur) in a transparent Plexiglas cage filled with bedding. Grooming activity was recorded with a video camera for 3min. Each forelimb was evaluated separately. Scoring was performed according to a previously published rating scheme[181,184] based on the most remote part of the head that could be reached by the forepaws: 0 = no contact with the head, 1 = contact with snout (underneath), 2 = contact with the dorsal surface of the snout, 3 = contact with the area between eyes and the front of the ears (forehead), 4 = contact with the ears (front), 5 = contact with the area behind the ears. Over-ground *walking*, *wading* through 3cm deep water, *swimming* and walking over a *horizontal ladder* was tested in a behavioural testing set-up ("MotoRater") described previously[185]. Prior to testing, the rats' skin overlying bony anatomical landmarks on fore- and hindlimbs was tattooed with a commercially available tattooing kit (Hugo Sachs Elektronik, Harvard Apparatus GmbH, Germany) to ensure reliable measurements over time. Locomotor behaviour was filmed with a high-speed video camera (Basler A504kc Color Camera, Basler AG) at 200Hz and analysed with the ClickJoint software (version 5.0; ALEA Solutions GmbH). Parameters assessed during over-ground walking and wading were defined as follows: shoulder and hip height as the vertical distance between the joint and the runway; pro- and retraction of the fore- and hindlimbs as the maximal horizontal distance (forwards and backwards) between the wrist and the shoulder joint or between the toe (MTP) and the hip, respectively; paw dragging was present if toes touched the ground during the swing phase; the paw rotation angle ("external rotation") was defined as the angle between the body axis and the paw axis (line between the third MTP and the heel) and assessed at mid-stance; step width ("base of support") was calculated by adding the distances measured between the body axis and the left and the right heel for two consecutive (left-right) steps. Precise paw placement of fore- and hindlimbs of rats crossing a horizontal ladder with irregularly spaced rungs was assessed[150,185]. The percentage of functional placements, i.e., weight bearing steps without slipping, was used as a parameter and reported for each limb separately. For swimming, the mean swimming velocity was calculated from at least three swims (swimming distance of 60cm per run) per time point. The MTP peak velocity was defined as the maximal velocity of toe movement during hindlimb strokes.

After week 12 *post*-lesion, spinal cord injured rats (n=15) used for the characterization of recovery after hemisection injury (Figure 3.1) were further trained on the locomotor tasks (over-ground walking, wading and swimming) once a week. These rats received an

electrolytic micro-lesion to either the ipsilesional (n=5) or the contralesional (n=10; one rat had to be excluded retrospectively due to incorrect positioning of the lesion) gigantocellular reticular nucleus (with reference to the side of the hemisection) 16 weeks after spinal cord injury. Rats without hemisection (n=7) but electrolytic micro-lesion of the left gigantocellular reticular nucleus served as controls. Functional performance was assessed one day before and two days after the focal brainstem lesion.

Retrograde tracing from the spinal cord

Intact and spinal cord injured rats were deeply anaesthetized (Hypnorm/Dormicum, see above) and fixed in a stereotactic frame after partial laminectomy of the C5, C6 and C7 (spinal segments C6-T1) and T12 and T13 vertebrae (spinal segments L1-L4)[186]. Rats with hemisection injury received unilateral injections of two different fluorescent retrograde tracers into the ipsilesional cervical (tetramethylrhodamine, 3000MW dextran; 10% in injectable water; Invitrogen, UK) and ipsilesional lumbar spinal cord (diamidino yellow dihydrochloride, 2% suspension in 0.1M phosphate buffer and 2% dimethylsulphoxide; Sigma-Aldrich, Switzerland) at 1 week (n=5), 4 weeks (n=10) or 12 weeks *post*-lesion (n=10). Intact rats (n=5) were traced accordingly. Injections were made stereotactically with Nanofil syringes attached to a MicroPump (WPI, Berlin, Germany). A total of 2µl of tetramethylrhodamine administered via ten stereotactic injections of 200nl was injected with a 33 gauge needle along the cervical spinal cord (700µm lateral from the spinal cord midline, in a depth of 1mm from the dorsal surface and a spacing of 1mm between injections). Similarly, a total of 2µl of diamidino yellow dihydrochloride was injected with a 28 gauge needle into the lumbar spinal hemicord (10 injections with 200nl/injection, 500µm lateral from the spinal cord midline, in a depth of 700µm from the dorsal surface and a spacing of 1mm between injections). Rats were perfused 14 days after tracing. Exclusive unilateral spread of the tracers was confirmed *post-mortem* for all injection sites on 40µm thick spinal cord cross sections under a fluorescence microscope. Coronal 40µm thick cryostat sections of the whole brain and cross-sections of the spinal cord rostral to the lesion site were obtained for each rat. Prominent landmarks along the brains' rostrocaudal axis were used as a reference: the anterior commissure (AC), the rostral end of the red nucleus (RN), the central branch of the facial nerve (7N), the rostral end of the inferior olive (IO) and the pyramidal decussation (PD). Each brain region was identified using these landmarks and a rat brain atlas[187]. Retrogradely labelled cell bodies were counted bilaterally in 19 different brain regions by a blinded experimenter. The same number of sections was analysed for each region and each rat. Single

and double labelled cell bodies were quantified on every fourth brain section (i.e., 1 section per 160µm) under a fluorescence microscope and the result was multiplied by four to approximate the actual number of traced neurons. In the present study, we report absolute cell numbers for each region (Table 3.1-3.3). However, since absolute cell counts demonstrated high within-group variability due to the tracing procedure, absolute cell numbers for a given region were normalized to the total number of retrogradely labelled cells of the respective brain for each tracer.

Rostrocaudal coordinates ("+" rostral to landmark, "-" caudal to landmark) used for the individual regions were: the rostral motor cortex (rostr. MCx; start at 4800µm +AC, end at 2560µm +AC, total 2240µm), the caudal motor cortex (caudal MCx; start at 2560µm +AC, end at 4640µm -AC, total 7200µm), the secondary somatosensory cortex (S2Cx; start at 1120µm +AC, end at 4640µm -AC, total 5760µm), the red nucleus (RN; start at RN, end at 1920µm -RN, total 1920µm), the deep mesencephalic reticular formation (MesFR; start at 1280µm +RN, end at 1920µm -RN, total 3200µm), the pontine reticular nucleus, oral part (PnO; start at 1920µm -RN, end at 1120µm +7N, total 2080µm), the pontine reticular nucleus, caudal and ventral part (PnC, PnV; start at 1120µm +7N, end at 7N, total 1120µm), the gigantocellular reticular nucleus (Gi; start at 160µm -7N, end at 1440µm -IO, total 3200µm), the lateral paragigantocellular nucleus, the gigantocellular reticular nucleus (ventral part) and the gigantocellular reticular nucleus part alpha (LPGi, GiV, GiA; start at 160µm -7N, end at 1440 -IO, total 3200µm), the dorsal paragigantocellular nucleus (DPGi; start at 320µm -7N, end at 320µm +IO, total 1440µm), the medullary reticular nucleus, ventral part (MdV; start at 1440µm -IO, end at PD, total 1440µm), the medullary reticular nucleus, dorsal part (MdD; start at 800µm -IO, end at PD, total 1920µm), the medial vestibular nucleus (MVe; start at 320µm +7N, end at 1440µm -IO, total 3680µm), the lateral vestibular nucleus (LVe; start at 160µm -7N, end at 320µm +IO, total 1600µm), the locus coeruleus (LC; start at 1760µm +7N, end at 7N, total 1920µm), the raphe magnus nucleus (RMg; start at 480µm +7N, end at IN, total 2560µm), the raphe obscurus nucleus (ROb; start at 640µm +IO, end at PD, total 3520µm) and the raphe pallidus nucleus (RPa; start at 160µm +IO, end at 640µm +PD, total 2080µm).

For propriospinal neurons located in the rostral cervical spinal cord at C3 and C4 level, labelled neurons were counted on every second to third spinal cord cross-section (thickness of 40µm). Since the number of analysed sections was different for each spinal segment and rat (10-40 sections per segment), the mean number of labelled cells per section was calculated. One intact rat was traced bilaterally from the cervical and lumbar spinal cord

and each brain region analysed in the present study was reconstructed in 3D using Neurolucida 8.0 (MicroBrightField).

Anterograde tracing of reticulospinal fibres

Rats with cervical unilateral hemisection injury (n=15) received a single stereotactic injection of 50nl of the tracer mini-emerald (Fluorescin and biotin tagged 10000MW dextran, 10% in injectable water; Invitrogen, UK) into the contralesional gigantocellular reticular nucleus four weeks after injury. Using a dorsal approach via the cerebellum, a 35 gauge needle was placed slightly dorsolaterally to the centre of the gigantocellular reticular nucleus (4.6mm caudal to lambda, 1.5mm lateral to lambda, 2mm above the base of the skull) to avoid diffusion of the tracer over the midline and damage to the target neurons. In intact rats (n=10, two rats were excluded due to incorrect tracing), the left gigantocellular reticular nucleus was traced accordingly. All rats were sacrificed three weeks after tracing and accurate placement of the injections was confirmed *post-mortem*. Series of 40µm thick cryostat cross-sections of the cervical (C6-T1) and lumbar (L1-L6) spinal cord were analysed under a fluorescence microscope (every fourth section, 10 sections per segment). We counted fibres entering the contralesional (left for intact rats) spinal cord grey matter, midline crossing fibres and fibres in the ipsilesional (right for intact rats) grey matter. The latter were defined as fibres intersecting a virtual vertical line placed in the centre of the spinal cord grey matter at a distance of 600µm from the central canal. To account for the variability induced by the tracing procedure, normalization was performed[188,189]. Therefore, the number of midline crossing fibres was normalized to the number of fibres entering the contralesional/left spinal cord grey matter for each segment. To assess the degree of arborisation of reticulospinal fibres crossing the midline, the number of fibres counted in the ipsilesional/right spinal cord grey matter (see above) was divided by the number of midline crossing fibres.

Retrograde tracing from the gigantocellular reticular nucleus

As described for anterograde tracing, intact rats (n=10) and rats with chronic hemisection injury (n=10, four weeks after injury) received stereotactic tracer injections into the ipsilesional (right in intact rats) and contralesional (left in intact rats) gigantocellular reticular nucleus. Tetramethylrhodamine (3000MW dextran; Invitrogen, UK) was injected into the ipsilesional/right and mini-emerald (10000MW dextran; Invitrogen, UK) into the contralesional/left nucleus. Correct positioning of the needle was checked for each injection site and injections that were off target were excluded from further analysis. For the rostral

cortex, retrogradely labelled cells were counted on every second 40µm thick coronal section (in total 17 sections per rat, starting at the most rostral section with labelled cells). For the MLR, labelled cells were quantified in the area (1.4mm^2) of the cuneiform and pedunculopontine nucleus located laterally to the mesencephalic trigeminal neurons. Again, cells were counted in this area on every second 40µm thick coronal section (in total 12 sections per rat). To normalize for differences in tracing efficiency cell counts were expressed as a lateralization index (number of cells contralateral to injection / number of cells ipsilateral to injection).

Focal lesions of the gigantocellular reticular nucleus

Rats received a local, anodal, electrolytic lesion of the gigantocellular reticular nucleus in the rostral medulla oblongata using platinum-iridium electrodes (118kΩ; Science Products, Germany) attached to a stereotactic frame. The tip of the electrode was placed in the ventromedial part of the gigantocellular reticular nucleus, 4.6mm caudal to lambda, 1mm lateral to lambda and 1.5mm above the base of the skull. An electric current of 200µA was applied continuously for 35s. Only data obtained from rats with histologically confirmed accurate positioning of the lesion were analysed.

Statistics

Statistical analysis was performed using SPSS (V21; SPSS, Inc., IL, USA) and GraphPad Prism 5 (V5.01; GraphPad Software, Inc., CA, USA). The level of statistical significance for all tests was set *a priori* at $P<0.05$ indicated by asterisks in the figures. The exact *P*-values obtained from statistical analyses are given in the text, figures and tables. For analysis of the behavioural data characterizing the time course after spinal cord injury (Figure 3.1), we used one-way ANOVA for repeated measurements. If significant, ANOVA was followed by *post hoc* Bonferroni's Multiple Comparison Test comparing the performance at baseline and one week (or two weeks for grooming) after injury ("lesion effect") and one week (or two weeks for grooming) and 12 weeks after injury ("recovery"). For retrograde tracing from the cervical and lumbar spinal cord (Figure 3.3 and 3.4), the absolute numbers of retrogradely labelled neurons found in a given CNS region were normalized to the total cell number counted per brain (for the same tracer) to reduce within-group variability due to tracing. Statistical analysis on the number of normalized cell counts was performed with one-way ANOVA and followed, if significant, by Bonferroni's Multiple Comparison Test. For anterograde tracing from the contralesional gigantocellular reticular nucleus (Figure 3.5), repeated measures two-

way ANOVA with one repeated factor (“Segment”) and one non-repeated factor (“Injury”) was applied to detect significant differences between each spinal cord segment and between intact rats and rats with hemisection injury. Total mean values were analysed with Student’s unpaired *t*-test (two-sided). For changes of the lateralization index (Figure 3.6), one-way ANOVA was employed to test for significant differences between animal groups. Here, repeated measures ANOVA could not be applied because of the differences in group size due to the exclusion of inaccurate injection sites. If significant, ANOVA was, again, followed by Bonferroni's Multiple Comparison Test. For statistical analysis of the behavioural effects of micro-lesions in the brainstem (Figure 3.7), repeated measures two-way ANOVA with one repeated factor (“Time”, i.e., before and after brainstem lesion) and one non-repeated factor (“animal group”) was used. Only if ANOVA was significant for the repeated measures factor “Time”, *post hoc* analysis was performed with Bonferroni's Multiple Comparison Test (see Table 3.4).

3.4. Results

Behavioural outcome after cervical unilateral spinal cord injury

Adult Lewis rats were tested for their paw preference in the cylinder test and results indicated equal use of both paws (data not shown). Following several days of training and baseline testing in a number of behavioural tasks (see below), all rats received a hemisection injury at cervical level C4 (Figure 3.1 A). Only data from rats with a histologically confirmed complete hemisection (n=15) were included in the analysis.

The air-righting reaction (Figure 3.1 B), i.e., the ability to turn in the air from a supine position in order to land on the paws, was strongly impaired one week after injury ($P<0.0001$, repeated measures one-way ANOVA). At this time point, rats were only just able to rotate their head and shoulder girdle and occasionally their hindlimbs before landing. This was followed by significant recovery of this response starting one to two weeks after lesion ($P<0.0001$, repeated measures one-way ANOVA).

Forelimbs: The ipsilesional, right forepaw was rigid and with flexed, contracted digits (Figure 3.1 C). Starting two to four weeks after lesion, rats used their ipsilesional forelimb like a “walking stick” with only minimal movements in the elbow and wrist, as described previously[5,185]. All assessed parameters including grooming scores (Figure 3.1 D), shoulder height (Figure 3.1 E) and limb excursions (Figure 3.1 F, G) as well as precise paw placement on the horizontal ladder (Figure 3.1 H) indicated very severe deficits in the ipsilesional forelimb acutely after lesion. Starting two weeks *post*-lesion, a small but significant degree of

improvement of crude forelimb movements, such as increased shoulder height (Figure 3.1 E) and limb protraction (Figure 3.1 F), occurred ($P<0.0001$, repeated measures one-way ANOVA). However, performance of the ipsilesional forelimb in general, and on the horizontal ladder in particular, remained far below baseline levels up to 12 weeks *post*-lesion (<20% of baseline performance) indicating persistent deficits of distal forelimb function. The contralesional forelimb was not significantly affected by the lesion (Figure 3.1 H; $P=0.45$, repeated measures one-way ANOVA).

Hindlimbs demonstrated moderate to severe deficits acutely after cervical hemisection injury with the ipsilesional hindlimb being more affected than the contralesional one in most of the behavioural tasks. Locomotor parameters assessed during over-ground walking (toe clearance [Figure 3.1 I], paw rotation [Figure 3.1 J], base of support [Figure 3.1 K]), wading through shallow water (hindlimb excursion [Figure 3.1 L, M], hip height [Figure 3.1 N]) and swimming (swimming velocity [Figure 3.1 O], maximal toe velocity during hindlimb strokes [Figure 3.1 P]) showed significant recovery, often close to pre-lesion levels, four to 12 weeks after spinal cord injury (for all parameters $P<0.01$, repeated measures one-way ANOVA, except for paw rotation of the contralesional hindlimb [Figure 3.1 J]). Precise paw placement on the horizontal ladder was initially very poor for both hindlimbs illustrated by 20-40% (contralesional limb) and less than 10% (ipsilesional limb) functional paw placements on the ladder rungs one week after lesion (Figure 3.1 Q). In contrast to the good recovery of basic locomotor functions, only very limited recovery was observed for both hindlimbs on the horizontal ladder.

Anatomical plasticity of spinal descending tracts after spinal cord hemisection assessed by retrograde tracing

Cervical (C4) hemisection disrupts all descending tracts on the lesioned side. To re-establish functional control over the denervated spinal hemicord below the lesion, fibres from the intact side may sprout across the spinal cord midline or activate pre-existing midline crossing axonal branches. This was studied by injecting retrograde neuroanatomical tracers with different colours into the denervated ipsilesional cervical and lumbar spinal cord grey matter below the lesion (Figure 3.2 A). These tracers were taken up very efficiently by axon terminals, transported retrogradely and accumulated in the cell bodies. Four groups of rats received such tracer injections: 1. intact rats (n=5); 2. rats traced one week after injury (n=5); 3. rats traced four weeks after injury (n=10); and, 4. rats traced 12 weeks after injury (n=10). Retrogradely

labelled cell bodies were counted bilaterally in 19 different brain regions (Figure 3.2 B-E) and in the cervical spinal cord rostral to the injury.

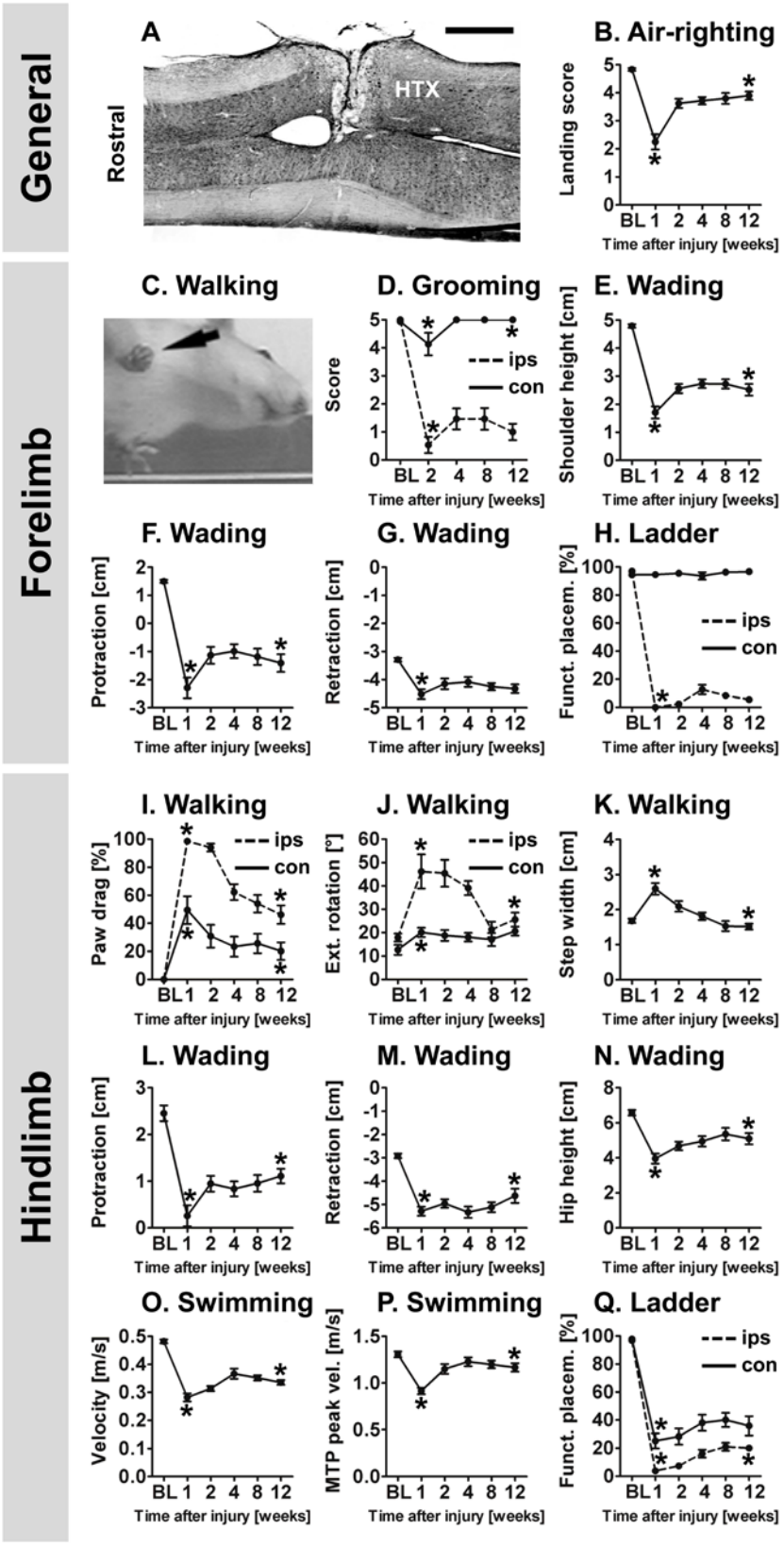

Figure 3.1. Functional outcome after cervical unilateral spinal cord injury. Motor performance of 15 rats was evaluated before (baseline, BL) and at several time points (1, 2, 4, 8 and 12 weeks) after unilateral hemisection injury at cervical level C4 (HTX). (**A**) Nissl staining of

an horizontal longitudinal spinal cord section illustrating the lesion paradigm used. Scale bar, 1mm. (**B**) The air-righting reaction before and after injury was assessed with the landing score ranging from 0 (no reaction) to 5 (full rotation). (**C**-**H**) Performance of the forelimbs was evaluated during walking, grooming, wading and walking over a horizontal ladder. (**C**) An image (bottom view) of an injured rat during over-ground walking 4 weeks after lesion shows that the digits of the ipsilesional forepaw (arrows) are contracted and form a clenched fist while the digits of the contralesional paw are spread and achieve full ground contact. (**D**) Grooming function was assessed for the ipsilesional (ips) and contralesional (con) forelimb separately using a scoring system ranging from 0 (no contact between paw and face) to 5 (grooming of the whole head and neck). (**E**) Shoulder height during wading was determined at midstance of the forelimb gait cycle. (**F**, **G**) Horizontal excursions of the ipsilesional forelimb were described via the maximal protraction (maximal *x*-value) and retraction (minimal *x*-value) of the wrist relative to the shoulder. (**H**) Precise targeting and placement of the ipsi- (ips) and contralesional (con) forepaw was evaluated on a horizontal ladder. The percentage of functional placements (Funct. placem.), i.e., weight bearing steps without slipping, was used as a parameter to assess skilled locomotion. (**I**-**Q**) Performance of the hindlimbs was evaluated during walking, wading, swimming and walking over a horizontal ladder. (**I**) During over-ground walking the number of toe drags were counted for the ipsi- (ips) and contralesional (con) hindlimb and counts were expressed as a percentage of steps with paw dragging. Also, external (Ext) rotation of the ipsi- (ips) and contralesional (con) paw (**J**) and base of support (step width; **K**) was quantified during walking. Base of support was calculated by adding the distances measured between both heels and the body axis during stance phase for consecutive left-right hindlimb steps. (**L**, **M**) Horizontal excursions of the ipsilesional hindlimb during wading were described via the maximal protraction (maximal *x*-value) and retraction (minimal *x*-value) of the toe relative to the hip. (**N**) The hip height during wading was measured at midstance of the hindlimb gait cycle. Overall swimming speed (**O**) and the peak velocity of the ipsilesional metatarsophalangeal joint (MTP; **P**) were assessed during swimming. (**Q**) On the horizontal ladder, precise placement of the ipsi- (ips) and contralesional (con) hindpaw was quantified as described for the forelimbs. Line graphs show group mean values for each time point ± s.e.m. For differences between time points, repeated measures one-way ANOVA followed by Bonferroni's Multiple Comparison Test was performed. Based on *post hoc* analysis, $*P<0.05$ indicates significantly different values between baseline and week 1 (or 2 for grooming) after injury (lesion effect) and between week 1 (or 2 for grooming) and 12 post lesion (recovery).

Although stereotactic tracer injections were performed identically for all rats, absolute cell counts showed high within-group variability (Table 3.1-3.3). Therefore, cell counts for a given region were normalized to the total number of retrogradely labelled cells of the respective brain (Figure 3.3 and 3.4).

After retrograde tracing from the denervated ipsilesional cervical spinal cord below the lesion (Figure 3.3), we found a significant increase of labelled normalized cells in the contralesional gigantocellular reticular nucleus at four weeks after injury compared to the acute state (P=0.023, one-way ANOVA). In terms of absolute numbers, we found 345±146 labelled cells in the contralesional gigantocellular reticular nucleus in rats traced one week after injury compared to 402±158 and 685±280 labelled cells in those rats traced four and 12 weeks *post*-lesion, respectively (Table 3.1). There was a tendency for higher cell numbers in the ipsilesional red nucleus (17±11 cells at one week vs. 59±20 cells at 12 weeks after lesion, Table 3.1) and the contralesional locus coeruleus (50±50 cells at one week vs. 104±61 cells at 12 weeks after lesion, Table 3.1), however, with large inter-individual variations. Spinal projections to the denervated cord were unchanged for the cortex, other reticular nuclei and the vestibular nuclei. The number of raphe neurons projecting to the denervated cervical hemicord from the contralesional raphe was reduced four weeks after injury (P=0.026, one-way ANOVA; Figure 3.3).

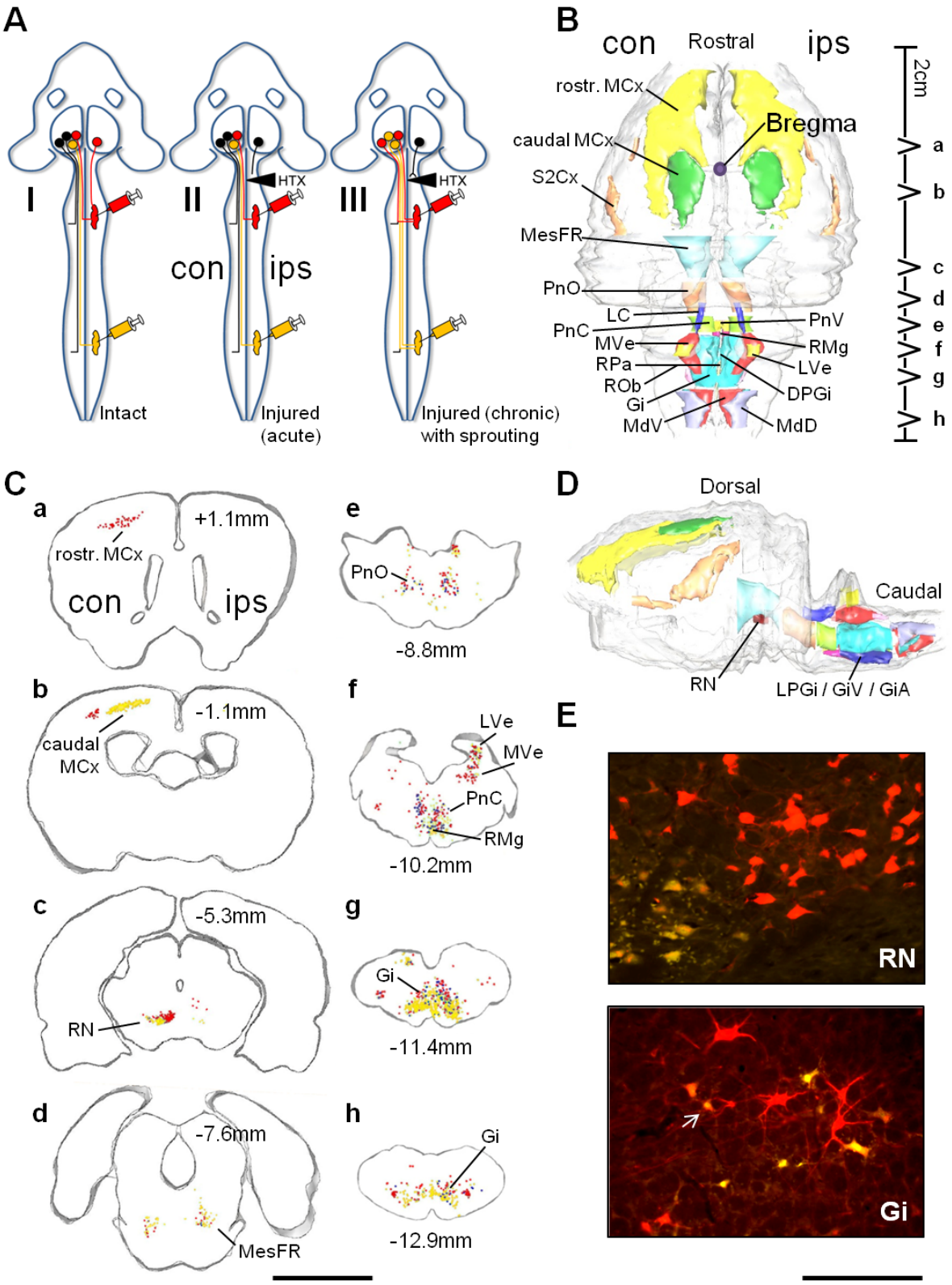

Figure 3.2. Retrograde tracing of brain regions with spinal projections. (**A**) Scheme illustrating the experimental approach. (**A**, **I**) Rats received unilateral spinal injections of two different fluorescent retrograde tracers. Tetramethylrhodamine (TMR, red) and diamidino yellow dihydrochloride (DY, yellow) were injected into the cervical (C5-T1) and lumbar spinal cord grey matter (L1-L6), respectively. Tracers were taken up by axon terminals and transported retrogradely, eventually accumulating in the corresponding cell bodies. Under a fluorescent microscope, neurons projecting into the injected cervical spinal hemicord appeared red while cells with projections into the injected lumbar hemicord were yellow. For the cervical spinal cord, a crossed and uncrossed pathway is illustrated. Neurons without terminals contacting the injection sites remained non-fluorescent (black cells). (**A**, **II**) After unilateral hemisection injury at C4 (HTX), cells located in the ipsilesional half of the CNS with exclusively ipsilateral descending projections lost access to the injection sites due to axotomy and were not labelled

(right black cell). (**A**, **III**) A neuron that changed its spinal projection pattern in response to injury, i.e., sprouting over the midline at cervical or lumbar spinal segments below the lesion site, gained access to the tracer and might be labelled accordingly (one black cell on the left turned red and the other one yellow in the scheme). con, contralesional (left side in intact rats); ips, ipsilesional (right side in intact rats). (**B**) Three-dimensional Neurolucida reconstruction of a rat brain (no lesion) based on bilateral retrograde tracings from the cervical and lumbar spinal cord illustrating the regions analysed, dorsal view. Rostr. MCx, rostral motor cortex; caudal MCx, caudal motor cortex; S2Cx, secondary somatosensory cortex; MesFR, deep mesencephalic reticular formation; PnO, pontine reticular nucleus, oral part; LC, Locus coeruleus; PnC, pontine reticular nucleus, caudal part; MVe, medial vestibular nucleus; RPa, raphe pallidus nucleus; ROb, raphe obscurus nucleus; Gi, gigantocellular reticular nucleus; MdV, medullary reticular nucleus, ventral part; MdD, medullary reticular nucleus, dorsal part; DPGi, dorsal paragigantocellular nucleus; LVe, lateral vestibular nucleus; RMg, raphe magnus nucleus; PnV, pontine reticular nucleus, ventral part; con, contralesional (left); ips, ipsilesional (right). (**C**) Coronal brain slices of an intact rat reconstructed with Neurolucida after right-sided ("ips") unilateral tracing from the cervical and lumbar spinal cord, as illustrated in A. Each coronal plate shown (**a-h**) resulted from the reconstruction of 4 consecutive brain slices with a thickness of 40µm. The location of each coronal plate is indicated by the anterioposterior distance to bregma and also illustrated in B. Red cell bodies were traced with TMR (cervical injections), yellow cell bodies were labelled with DY (lumbar injections) and purple cells were double-labelled. Scale bar, 5mm. Abbreviations as in B. (**D**) Three-dimensional Neurolucida reconstruction of analysed brain regions, lateral view. RN, red nucleus; LPGi, lateral paragigantocellular nucleus; GiV, gigantocellular reticular nucleus, ventral part; GiA, gigantocellular reticular nucleus, alpha part. (**E**) Fluorescence microscopy images of selected brain regions after unilateral cervical (TMR, red cells) and lumbar (DY, yellow cells) tracing. Note the somatotopic organization of the red nucleus (RN) and the presence of double-labelled cells (arrow) in the gigantocellular reticular nucleus (Gi). Scale bar, 200µm.

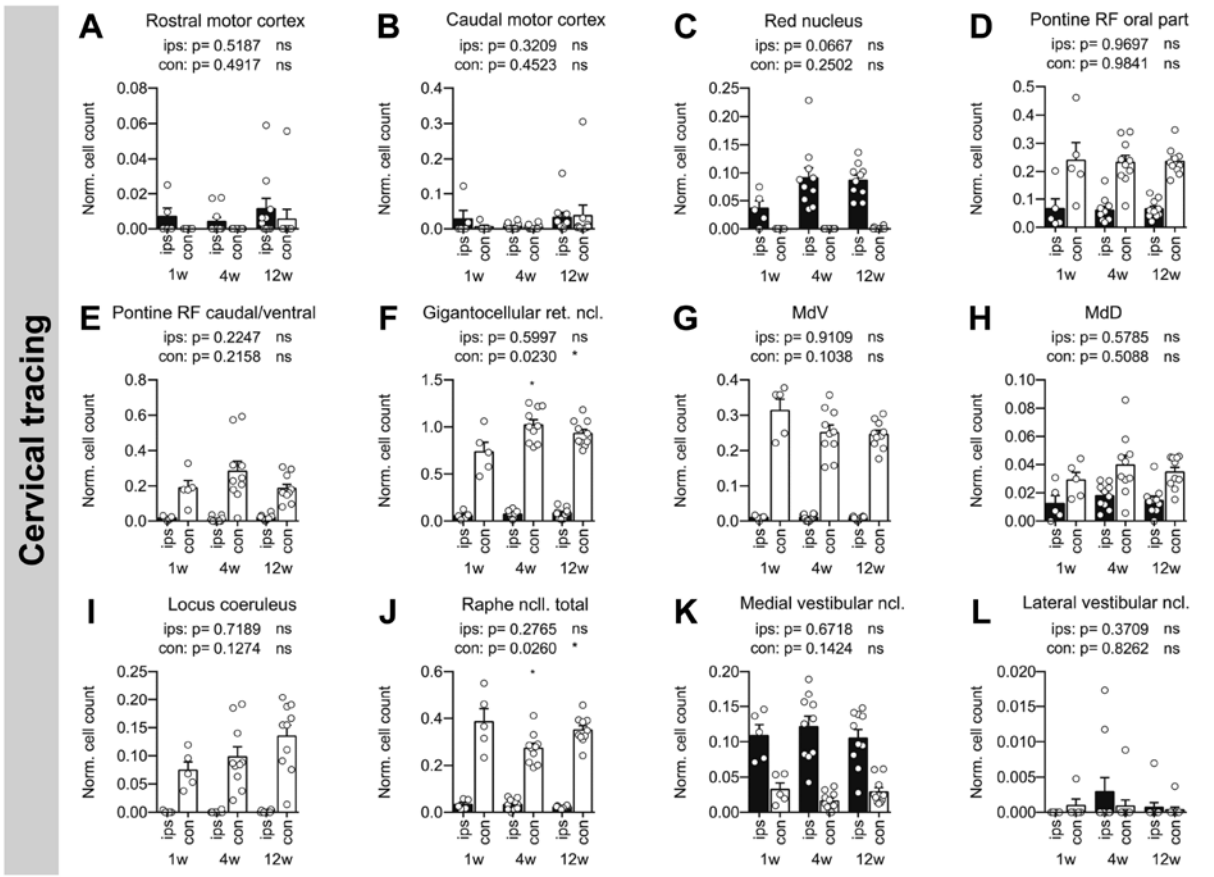

Figure 3.3. Normalized results of retrograde tracing from the ipsilesional cervical hemicord. Normalized cell counts for rats traced 1 (n=5), 4 (n=10) and 12 (n=10) weeks after unilateral hemisection are presented for a number of selected brain regions. Retrograde tracing was performed from the cervical spinal cord as illustrated in Figure 3.2 A. Circles represent single animals. Bars show total group mean values for each time point ± s.e.m. For differences between time points, one-way ANOVA followed by Bonferroni's Multiple Comparison Test was performed. Exact *P*-values derived from the ANOVA are given above the graphs with **P*<0.05 indicating significantly different normalized cell counts between time points. Results from *post hoc* testing are illustrated in the graph with **P*<0.05 denoting significantly different values either between week 1 and week 4 (* above the 4 week column) or between week 1 and week 12 (not present in this figure) after injury. ns, not significant; con, contralesional; ips, ipsilesional; w, week; ret., reticular; ncl., nucleus; ncll., nuclei.

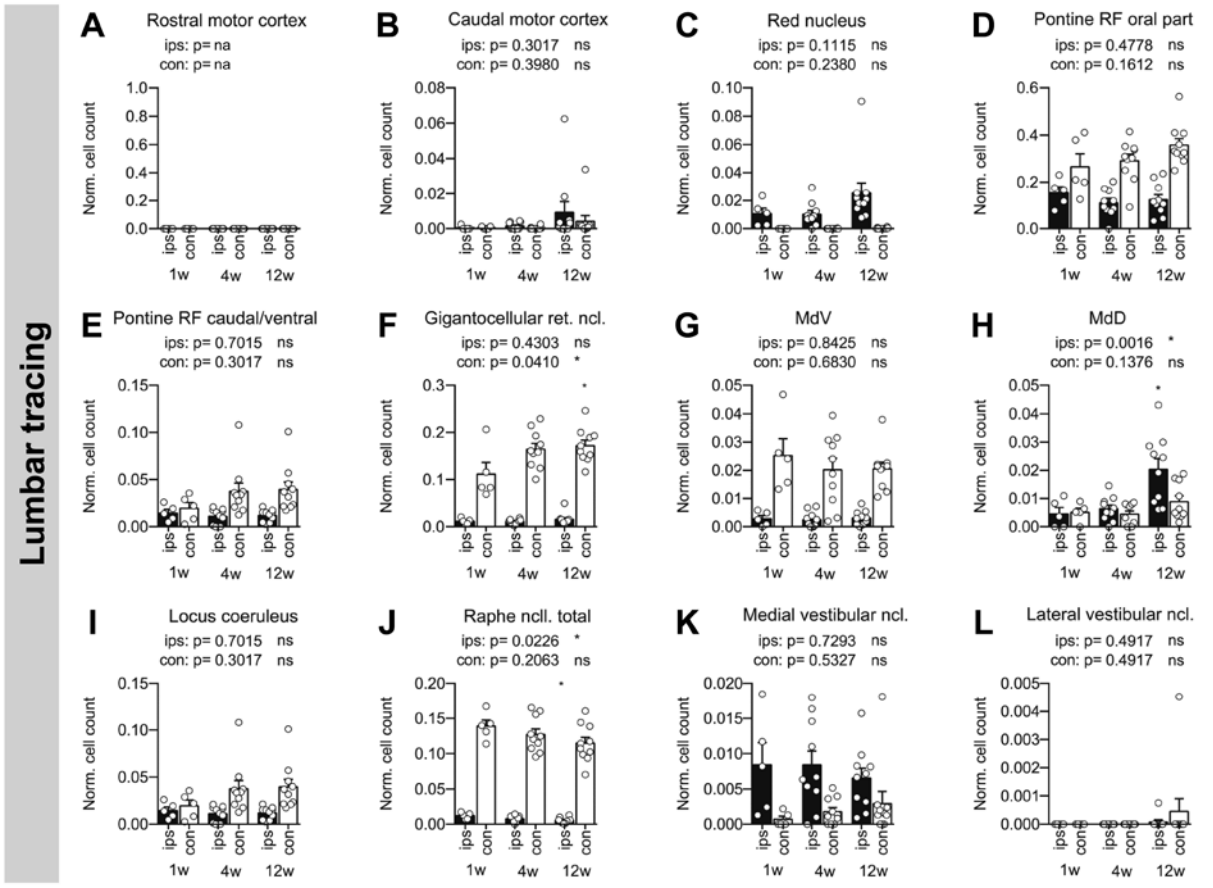

Figure 3.4. Normalized results of retrograde tracing from the ipsilesional lumbar hemicord. Normalized cell counts for rats traced 1 (n=5), 4 (n=10) and 12 (n=10) weeks after unilateral hemisection are presented for the same brain regions as shown in Figure 3.3. Retrograde tracing was performed from the lumbar spinal cord as demonstrated in Figure 3.2 A. Circles represent single animals. Bars show total group mean values for each time point ± s.e.m. For differences between time points, one-way ANOVA followed by Bonferroni's Multiple Comparison Test was performed. Exact *P*-values derived from the ANOVA are given above the graphs with **P*<0.05 indicating significantly different normalized cell counts between time points. Results from *post hoc* testing are illustrated in the graph with **P*<0.05 indicating significantly different values either between week 1 and week 4 (not present in this figure) or between week 1 and week 12 (* above the 12 week column) after injury. ns, not significant; na, not applicable; con, contralesional; ips, ipsilesional; w, week; ret., reticular; ncl., nucleus; ncll., nuclei.

After retrograde tracing from the lumbar denervated hemicord (Figure 3.4), we again found significantly higher normalized cell numbers in the contralesional gigantocellular reticular nucleus in the chronic rats (*P*=0.041, one-way ANOVA). Accordingly, absolute cell numbers for the contralesional gigantocellular reticular nucleus increased from 434±119 labelled cells at one week after injury to almost twice the amount at four and 12 weeks *post*-lesion (Table 3.2). Also, normalized cell numbers were increased in the ipsilesional dorsal medullary reticular nucleus 12 weeks after injury compared to rats traced one week after hemisection (*P*=0.0016, one-way ANOVA; Figure 3.4). Again, the number of normalized cells in the raphe nuclei was reduced in chronic rats after lumbar tracing, however, this time statistical significance was found for the ipsilesional side (*P*<0.0226, one-way ANOVA; Figure 3.4). There was a tendency for increased projections to the denervated lumbar hemicord from the

contralesional cortex and pontine reticular nuclei. No significant changes were detected for the other brain regions. Most double labelled cells, i.e., cells with collaterals in the cervical and lumbar spinal cord, were found in the pontine and medullar reticular formation in intact rats (Table 3.3). After hemisection, the number of double-labelled cells counted in the contralesional reticular formation increased proportionally with the number of single-labelled neurons. Absolute cell counts for all analysed brain and spinal cord regions are given in Table 3.1-3.3.

In summary, these retrograde tracing results show plastic reactions in some but not all brainstem regions. In particular, this is seen in the contralesional gigantocellular reticular nucleus with many neurons whose axons cross the spinal cord midline in response to the hemisection injury. Anterograde tracing of this nucleus was performed to directly visualize these axons.

Time of tracing after hemisection injury:		**No injury**	**1 week**	**4 weeks**	**12 weeks**
Region	**Side**	**Mean ± SD**	**Mean ± SD**	**Mean ± SD**	**Mean ± SD**
Rostral motor cortex	ips	8 ± 12	3 ± 4	2 ± 3	10 ± 21
Rostral motor cortex	con	178 ± 120	0 ± 0	0 ± 0	4 ± 11
Caudal motor cortex	ips	32 ± 24	8 ± 16	4 ± 7	34 ± 55
Caudal motor cortex	con	1545 ± 1138	6 ± 13	3 ± 5	40 ± 110
Motor cortex, total	ips	40 ± 35	11 ± 19	6 ± 9	44 ± 75
Motor cortex, total	con	1722 ± 1241	6 ± 13	3 ± 5	44 ± 121
Sec. somatosensory cortex	ips	0 ± 0	0 ± 0	0 ± 0	1 ± 3
Sec. somatosensory cortex	con	46 ± 47	0 ± 0	0 ± 0	0 ± 1
Red ncl.	ips	22 ± 19	17 ± 11	34 ± 18	59 ± 20
Red ncl.	con	870 ± 158	0 ± 0	0 ± 0	1 ± 3
Deep mesencephalic RF	ips	334 ± 160	6 ± 5	3 ± 5	7 ± 9
Deep mesencephalic RF	con	78 ± 40	28 ± 33	11 ± 8	36 ± 33
Pontine ret. ncl., oral part	ips	349 ± 190	32 ± 28	26 ± 23	46 ± 30
Pontine ret. ncl., oral part	con	310 ± 256	117 ± 76	98 ± 48	174 ± 79
Pontine ret. ncl., caudal / ventral part	ips	465 ± 160	10 ± 13	4 ± 6	16 ± 12
Pontine ret. ncl., caudal / ventral part	con	214 ± 101	100 ± 72	105 ± 61	140 ± 87
Pontine RF, total	ips	814 ± 309	42 ± 33	30 ± 28	63 ± 35
Pontine RF, total	con	524 ± 333	217 ± 144	203 ± 98	314 ± 160
Gigantocellular ret. ncl.	ips	1057 ± 190	30 ± 24	34 ± 25	77 ± 67
Gigantocellular ret. ncl.	con	749 ± 198	345 ± 146	402 ± 158	685 ± 280
LPGi / GiV / GiA	ips	990 ± 333	27 ± 28	17 ± 19	28 ± 18
LPGi / GiV / GiA	con	390 ± 51	742 ± 608	431 ± 266	771 ± 415
Dorsal paragigantocellular ncl.	ips	22 ± 12	10 ± 7	6 ± 5	10 ± 6
Dorsal paragigantocellular ncl.	con	55 ± 25	6 ± 7	4 ± 3	8 ± 6
Medullary ret. ncl., ventral part	ips	347 ± 128	6 ± 10	3 ± 4	9 ± 11
Medullary ret. ncl., ventral part	con	288 ± 95	65 ± 44	47 ± 40	72 ± 50
Medullary ret. ncl., dorsal part	ips	465 ± 120	30 ± 34	29 ± 21	51 ± 49
Medullary ret. ncl., dorsal part	con	409 ± 93	58 ± 40	59 ± 39	106 ± 52
Medull. RF, total	ips	2881 ± 698	103 ± 92	89 ± 61	175 ± 119
Medull. RF, total	con	1891 ± 383	1214 ± 823	943 ± 446	1642 ± 762
RF, total	ips	4029 ± 1102	152 ± 111	122 ± 82	245 ± 146
RF, total	con	2494 ± 700	1459 ± 988	1156 ± 509	1992 ± 930
Medial vestibular ncl.	ips	588 ± 220	62 ± 53	47 ± 24	85 ± 54
Medial vestibular ncl.	con	385 ± 119	13 ± 5	8 ± 8	20 ± 13
Lateral vestibular ncl.	ips	243 ± 117	0 ± 0	1 ± 2	1 ± 3
Lateral vestibular ncl.	con	10 ± 15	1 ± 2	0 ± 1	0 ± 1
Locus coeruleus	ips	128 ± 55	1 ± 2	0 ± 1	1 ± 2
Locus coeruleus	con	42 ± 23	50 ± 50	42 ± 30	104 ± 61
Raphe magnus ncl.	ips	368 ± 141	19 ± 23	14 ± 13	10 ± 7
Raphe magnus ncl.	con	101 ± 35	142 ± 100	71 ± 33	192 ± 109
Raphe obscurus ncl.	ips	107 ± 33	4 ± 5	2 ± 3	6 ± 5
Raphe obscurus ncl.	con	47 ± 26	52 ± 33	33 ± 15	60 ± 21
Raphe pallidus ncl.	ips	11 ± 7	1 ± 2	0 ± 0	0 ± 1
Raphe pallidus ncl.	con	7 ± 7	10 ± 16	6 ± 6	9 ± 11
Raphe Ncll., total	ips	486 ± 125	24 ± 26	16 ± 14	17 ± 9
Raphe Ncll., total	con	155 ± 54	204 ± 142	110 ± 44	262 ± 122
Spinal cord C3 / C4 (mean / section)	ips	29.7 ± 3.5	0.3 ± 0.3	0.1 ± 0.1	0.4 ± 0.4
Spinal cord C3 / C4 (mean / section)	con	21.3 ± 4.7	0.6 ± 0.5	0.3 ± 0.1	0.6 ± 0.5

Table 3.1. Absolute cell counts for all analysed CNS regions after retrograde tracing from the ipsilesional cervical hemicord. Absolute numbers of single-labelled neurons after cervical tracing in intact rats and rats 1, 4, and 12 weeks after spinal cord injury are presented as group mean ± SD. con, contralesional (left side in intact rats); ips, ipsilesional (right side in intact rats); ncl., nucleus; ncll., nuclei; ret., reticular; sec., secondary; LPGi, lateral paragigantocellular nucleus; GiV, gigantocellular reticular nucleus, ventral part; GiA, gigantocellular reticular nucleus, alpha part; RF, reticular formation; C3/C4, cervical spinal cord segments 3 and 4.

Time of tracing after hemisection injury:		No injury	1 week	4 weeks	12 weeks
Region	Side	Mean ± SD	Mean ± SD	Mean ± SD	Mean ± SD
Rostral motor cortex	ips	0 ± 0	0 ± 0	0 ± 0	0 ± 1
Rostral motor cortex	con	5 ± 11	0 ± 0	0 ± 0	0 ± 0
Caudal motor cortex	ips	443 ± 371	2 ± 4	11 ± 16	50 ± 116
Caudal motor cortex	con	3561 ± 2657	2 ± 2	2 ± 4	25 ± 63
Motor cortex, total	ips	443 ± 371	2 ± 4	11 ± 16	51 ± 116
Motor cortex, total	con	3566 ± 2664	2 ± 2	2 ± 4	25 ± 63
Sec. somatosensory cortex	ips	0 ± 0	0 ± 0	0 ± 0	0 ± 0
Sec. somatosensory cortex	con	0 ± 0	0 ± 0	0 ± 0	0 ± 0
Red ncl.	ips	58 ± 34	44 ± 31	55 ± 64	114 ± 87
Red ncl.	con	944 ± 251	0 ± 0	0 ± 1	2 ± 3
Deep mesencephalic RF	ips	166 ± 65	2 ± 5	2 ± 3	2 ± 2
Deep mesencephalic RF	con	46 ± 46	12 ± 10	29 ± 42	58 ± 80
Pontine ret. ncl., oral part	ips	747 ± 335	158 ± 56	124 ± 98	151 ± 95
Pontine ret. ncl., oral part	con	506 ± 392	300 ± 196	357 ± 322	448 ± 289
Pontine ret. ncl., caudal / ventral part	ips	461 ± 60	60 ± 29	65 ± 62	66 ± 56
Pontine ret. ncl., caudal / ventral part	con	218 ± 123	87 ± 72	146 ± 107	175 ± 90
Pontine RF, total	ips	1208 ± 391	218 ± 78	189 ± 156	217 ± 144
Pontine RF, total	con	724 ± 511	387 ± 235	503 ± 422	622 ± 340
Gigantocellular ret. ncl.	ips	1058 ± 324	54 ± 38	45 ± 28	70 ± 42
Gigantocellular ret. ncl.	con	548 ± 277	434 ± 119	710 ± 475	813 ± 407
LPGi / GiV / GiA	ips	2685 ± 1417	66 ± 43	63 ± 59	53 ± 48
LPGi / GiV / GiA	con	1506 ± 1178	1450 ± 452	1369 ± 922	1292 ± 853
Dorsal paragigantocellular ncl.	ips	35 ± 31	10 ± 9	16 ± 26	13 ± 20
Dorsal paragigantocellular ncl.	con	31 ± 29	2 ± 2	1 ± 2	4 ± 5
Medullary ret. ncl., ventral part	ips	538 ± 278	14 ± 14	13 ± 23	15 ± 15
Medullary ret. ncl., ventral part	con	217 ± 169	110 ± 73	104 ± 133	112 ± 82
Medullary ret. ncl., dorsal part	ips	255 ± 123	22 ± 26	36 ± 48	107 ± 79
Medullary ret. ncl., dorsal part	con	178 ± 101	23 ± 16	24 ± 30	56 ± 68
Medull. RF, total	ips	4571 ± 2100	166 ± 113	173 ± 172	258 ± 179
Medull. RF, total	con	2480 ± 1712	2021 ± 437	2208 ± 1447	2276 ± 1376
RF, total	ips	5945 ± 2476	386 ± 166	365 ± 319	476 ± 296
RF, total	con	3250 ± 2177	2420 ± 673	2740 ± 1874	2956 ± 1774
Medial vestibular ncl.	ips	229 ± 61	39 ± 34	44 ± 55	40 ± 50
Medial vestibular ncl.	con	234 ± 47	3 ± 5	8 ± 10	10 ± 14
Lateral vestibular ncl.	ips	257 ± 59	0 ± 0	0 ± 0	0 ± 1
Lateral vestibular ncl.	con	2 ± 4	0 ± 0	0 ± 0	1 ± 4
Locus coeruleus	ips	279 ± 111	10 ± 10	6 ± 8	10 ± 17
Locus coeruleus	con	172 ± 140	159 ± 110	164 ± 158	233 ± 161
Raphe magnus ncl.	ips	1142 ± 733	38 ± 15	27 ± 22	22 ± 21
Raphe magnus ncl.	con	528 ± 472	443 ± 31	427 ± 249	435 ± 247
Raphe obscurus ncl.	ips	577 ± 99	10 ± 9	5 ± 5	6 ± 6
Raphe obscurus ncl.	con	212 ± 108	90 ± 48	90 ± 60	117 ± 88
Raphe pallidus ncl.	ips	95 ± 49	3 ± 3	1 ± 3	2 ± 4
Raphe pallidus ncl.	con	55 ± 39	38 ± 28	29 ± 23	31 ± 21
Raphe Ncll., total	ips	1814 ± 819	51 ± 22	34 ± 25	29 ± 25
Raphe Ncll., total	con	795 ± 603	572 ± 83	546 ± 299	583 ± 336
Spinal cord C3 / C4 (mean / section)	ips	3.2 ± 1.1	0.3 ± 0.2	0.1 ± 0.1	0.2 ± 0.2
Spinal cord C3 / C4 (mean / section)	con	4.4 ± 1.1	0.1 ± 0.1	0.0 ± 0.0	0.2 ± 0.2

Table 3.2. Absolute cell counts for all analysed CNS regions after retrograde tracing from the ipsilesional lumbar hemicord. Absolute numbers of single-labelled neurons after lumbar tracing in intact rats and rats 1, 4, and 12 weeks after spinal cord injury are given as group mean ± SD. con, contralesional (left side in intact rats); ips, ipsilesional (right side in intact rats); ncl., nucleus; ncll., nuclei; ret., reticular; sec., secondary; LPGi, lateral paragigantocellular nucleus; GiV, gigantocellular reticular nucleus, ventral part; GiA, gigantocellular reticular nucleus, alpha part; RF, reticular formation; C3/C4, cervical spinal cord segments 3 and 4.

Anterograde tracing of reticulospinal projections of the gigantocellular reticular nucleus

Intact rats (n=8) and rats with chronic cervical unilateral hemisection injury (n=15; 4 weeks after lesion) received a stereotactic tracer injection into the contralesional (left nucleus in intact rats) gigantocellular reticular nucleus (Figure 3.5 A I-III). Traced fibres entering the contralesional spinal cord grey matter, midline crossing fibres and fibres in the ipsilesional, denervated grey matter at lower cervical (C6-T1) and lumbar (L1-L6) spinal levels were assessed (Figure 3.5 B I-IV). In general, there were significantly more midline crossing fibres in the lumbar spinal cord than in the cervical segments (P=0.0003 for the factor “Segment”, repeated measures two-way ANOVA; Figure 3.5 C). Compared to intact rats, we found a significant increase of the number of midline crossing fibres for all segments in rats with spinal cord injury (P=0.0444 for the factor “Injury”, repeated measures two-way ANOVA;

Figure 3.5 C). In intact rats, there were one to two fibres in the ipsilesional spinal cord grey matter (Figure 3.5 B IV) per midline crossing fibre. These fibres were primarily found in the ventral spinal cord grey matter in intact and lesioned animals. After spinal cord injury, there was a tendency towards a reduction of fibres in the ipsilesional cervical spinal cord per midline crossing fibre but an unchanged ratio in the lumbar spinal cord (Figure 3.5 D).

These findings from anterograde tracing confirmed the previous results of the retrograde tracing experiments demonstrating sprouting of spinal projections of the contralesional gigantocellular reticular nucleus across the spinal cord midline to the denervated side after hemisection. We therefore investigated whether plastic changes including a side-switch were also present in the input systems to the contralesional gigantocellular reticular nucleus in response to spinal cord injury.

Time of tracing after hemisection injury:		No injury	1 week	4 weeks	12 weeks
Region	Side	Mean ± SD	Mean ± SD	Mean ± SD	Mean ± SD
Rostral motor cortex	ips	0.0 ± 0.0	0.0 ± 0.0	0.0 ± 0.0	0.0 ± 0.0
Rostral motor cortex	con	0.0 ± 0.0	0.0 ± 0.0	0.0 ± 0.0	0.0 ± 0.0
Caudal motor cortex	ips	0.0 ± 0.0	0.0 ± 0.0	0.0 ± 0.0	0.0 ± 0.0
Caudal motor cortex	con	11.2 ± 18.6	0.0 ± 0.0	0.0 ± 0.0	0.0 ± 0.0
Motor cortex, total	ips	0.0 ± 0.0	0.0 ± 0.0	0.0 ± 0.0	0.0 ± 0.0
Motor cortex, total	con	11.2 ± 18.6	0.0 ± 0.0	0.0 ± 0.0	0.0 ± 0.0
Sec. somatosensory cortex	ips	0.0 ± 0.0	0.0 ± 0.0	0.0 ± 0.0	0.0 ± 0.0
Sec. somatosensory cortex	con	0.0 ± 0.0	0.0 ± 0.0	0.0 ± 0.0	0.0 ± 0.0
Red ncl.	ips	0.8 ± 1.8	0.0 ± 0.0	0.8 ± 2.5	8.0 ± 6.5
Red ncl.	con	12.8 ± 10.4	0.0 ± 0.0	0.0 ± 0.0	0.0 ± 0.0
Deep mesencephalic RF	ips	46.4 ± 33.8	0.0 ± 0.0	0.0 ± 0.0	0.0 ± 0.0
Deep mesencephalic RF	con	11.2 ± 7.2	0.8 ± 1.8	0.4 ± 1.3	1.6 ± 3.4
Pontine ret. ncl., oral part	ips	73.6 ± 35.8	4.0 ± 6.9	4.8 ± 7.5	9.2 ± 7.3
Pontine ret. ncl., oral part	con	73.6 ± 51.5	50.4 ± 24.8	50.8 ± 27.1	86.0 ± 39.7
Pontine ret. ncl., caudal / ventral part	ips	134.4 ± 53.6	0.8 ± 1.8	1.6 ± 2.8	4.4 ± 2.3
Pontine ret. ncl., caudal / ventral part	con	72.0 ± 55.4	38.4 ± 30.8	68.8 ± 46.6	90.4 ± 46.7
Pontine RF, total	ips	208.0 ± 86.5	4.8 ± 7.2	6.4 ± 9.5	13.6 ± 7.4
Pontine RF, total	con	145.6 ± 101.7	88.8 ± 41.3	119.6 ± 68.2	176.4 ± 79.5
Gigantocellular ret. ncl.	ips	184.8 ± 83.0	7.2 ± 7.2	7.6 ± 9.1	23.6 ± 27.0
Gigantocellular ret. ncl.	con	132.8 ± 92.3	108.8 ± 54.2	158.8 ± 90.5	231.2 ± 92.9
LPGi / GiV / GiA	ips	119.2 ± 35.6	5.6 ± 4.6	1.6 ± 5.1	3.2 ± 4.1
LPGi / GiV / GiA	con	101.6 ± 57.3	193.6 ± 102.0	178.8 ± 110.0	268.0 ± 166.6
Dorsal paragigantocellular ncl.	ips	4.8 ± 3.3	4.0 ± 4.0	2.0 ± 2.8	2.8 ± 4.2
Dorsal paragigantocellular ncl.	con	11.2 ± 10.4	1.6 ± 2.2	0.0 ± 0.0	0.4 ± 1.3
Medullary ret. ncl., ventral part	ips	11.2 ± 14.3	0.0 ± 0.0	0.0 ± 0.0	0.4 ± 1.3
Medullary ret. ncl., ventral part	con	7.2 ± 7.2	5.6 ± 4.6	4.4 ± 5.1	9.2 ± 8.9
Medullary ret. ncl., dorsal part	ips	34.4 ± 20.1	0.0 ± 0.0	0.0 ± 0.0	1.2 ± 1.9
Medullary ret. ncl., dorsal part	con	6.4 ± 6.1	1.6 ± 3.6	1.6 ± 2.8	6.0 ± 6.9
Medull. RF, total	ips	354.4 ± 144.4	16.8 ± 9.1	11.2 ± 12.0	31.2 ± 31.3
Medull. RF, total	con	259.2 ± 159.5	311.2 ± 135.0	343.6 ± 180.8	514.8 ± 257.2
RF, total	ips	608.8 ± 250.0	21.6 ± 11.9	17.6 ± 19.2	44.8 ± 35.1
RF, total	con	416.0 ± 255.2	400.8 ± 140.4	463.6 ± 218.6	692.8 ± 324.9
Medial vestibular ncl.	ips	69.6 ± 31.3	4.8 ± 8.7	3.6 ± 4.4	5.6 ± 5.1
Medial vestibular ncl.	con	14.4 ± 19.3	0.0 ± 0.0	1.2 ± 1.9	1.2 ± 1.9
Lateral vestibular ncl.	ips	33.6 ± 18.5	0.0 ± 0.0	0.0 ± 0.0	0.0 ± 0.0
Lateral vestibular ncl.	con	0.0 ± 0.0	0.0 ± 0.0	0.0 ± 0.0	0.0 ± 0.0
Locus coeruleus	ips	15.2 ± 11.1	0.0 ± 0.0	0.0 ± 0.0	0.0 ± 0.0
Locus coeruleus	con	19.2 ± 19.7	12.0 ± 6.3	26.0 ± 19.0	52.8 ± 33.9
Raphe magnus ncl.	ips	64.0 ± 32.4	3.2 ± 5.2	2.0 ± 2.8	1.2 ± 2.7
Raphe magnus ncl.	con	24.0 ± 26.2	38.4 ± 26.3	28.4 ± 13.9	76.4 ± 45.6
Raphe obscurus ncl.	ips	20.0 ± 11.3	0.0 ± 0.0	0.4 ± 1.3	1.2 ± 1.9
Raphe obscurus ncl.	con	12.8 ± 10.7	11.2 ± 5.9	13.2 ± 9.1	23.6 ± 11.7
Raphe pallidus ncl.	ips	0.0 ± 0.0	0.0 ± 0.0	0.0 ± 0.0	0.0 ± 0.0
Raphe pallidus ncl.	con	0.0 ± 0.0	0.0 ± 0.0	1.2 ± 2.7	3.6 ± 6.9
Raphe Ncll., total	ips	84.0 ± 35.3	3.2 ± 5.2	2.4 ± 2.8	2.4 ± 2.8
Raphe Ncll., total	con	36.8 ± 32.8	49.6 ± 28.4	42.8 ± 17.0	103.6 ± 52.0
Spinal cord C3 / C4 (mean / section)	ips	0.4 ± 0.2	0.0 ± 0.0	0.0 ± 0.0	0.0 ± 0.0
Spinal cord C3 / C4 (mean / section)	con	0.6 ± 0.4	0.0 ± 0.0	0.0 ± 0.0	0.0 ± 0.0

Table 3.3. Absolute cell counts for all analysed CNS regions after retrograde tracing from the ipsilesional cervical and lumbar hemicord. Absolute numbers of double-labelled neurons after cervical and lumbar tracing in intact rats and rats 1, 4, and 12 weeks after spinal cord injury are presented as group mean ± SD. con, contralesional (left side in intact rats); ips, ipsilesional (right side in intact rats); ncl., nucleus; ncll., nuclei; ret., reticular; sec., secondary; LPGi, lateral paragigantocellular nucleus; GiV, gigantocellular reticular nucleus, ventral part; GiA, gigantocellular reticular nucleus, alpha part; RF, reticular formation; C3/C4, cervical spinal cord segments 3 and 4.

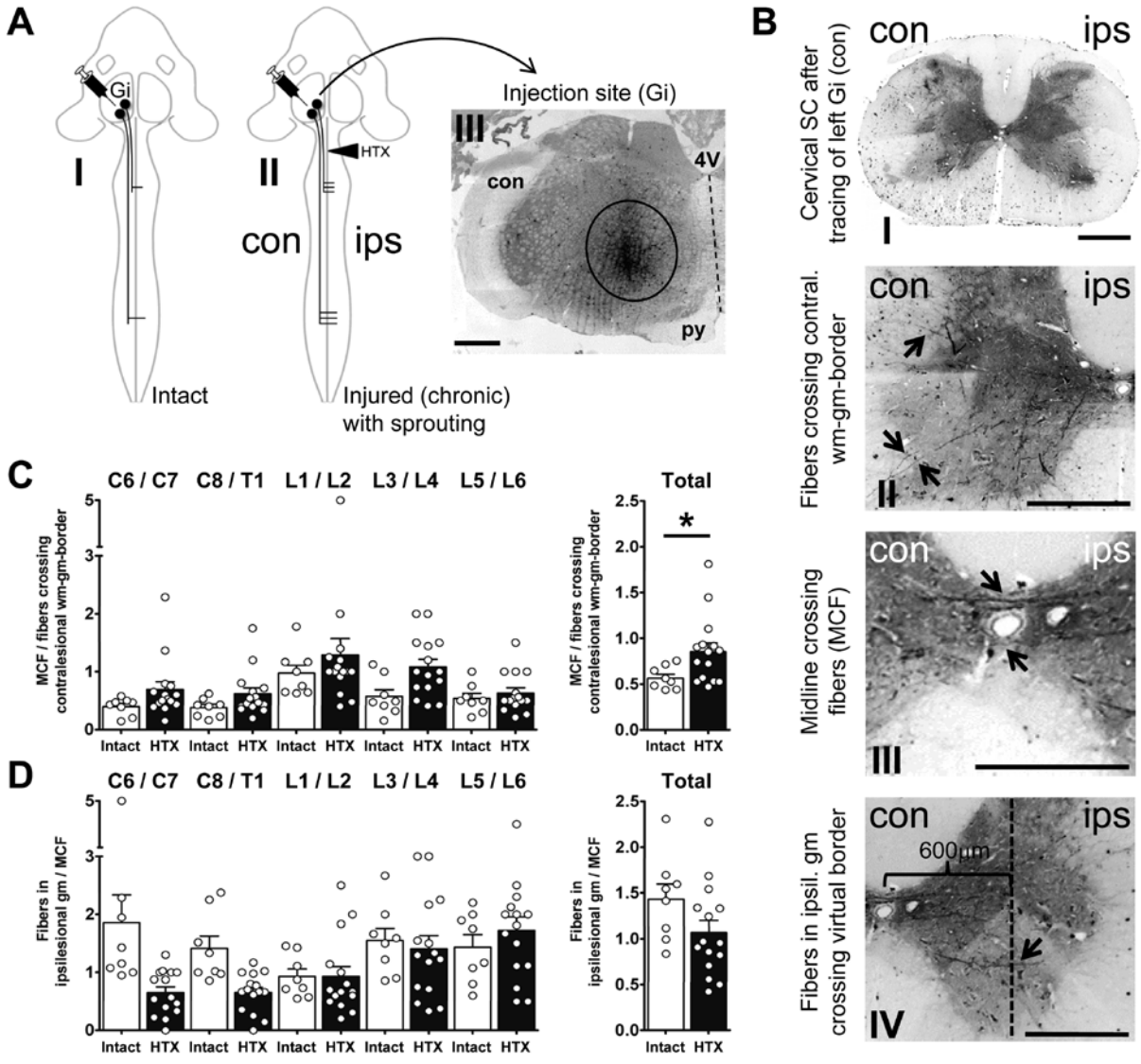

Figure 3.5. Anterograde tracing of reticulospinal projections from the contralesional gigantocellular reticular nucleus. (**A**) Scheme illustrating the anterograde tracing experiment. Intact rats (**A I**) and rats with chronic (4 weeks post lesion; **A II**) cervical unilateral hemisection injury (HTX) received micro-injections of the anterograde tracer mini-emerald into the contralesional (left for intact rats) gigantocellular reticular nucleus (Gi). (**A III**) Fluorescence microscopy image of a brainstem cross section (thickness of 40µm) demonstrating the injection site in an injured rat. The tracer was primarily visible in the region of the gigantocellular reticular nucleus (circle) and the needle tract. In all analysed rats, spreading of the tracer over the midline (dashed line) was not detected. Scale bar, 1mm. Py, pyramidal tract; 4V, 4th ventricle. (**B I**) Fluorescence microscopy image of a cervical spinal cord cross section of an intact rat after anterograde tracing of the left (con) gigantocellular reticular nucleus. Black dots in the spinal cord white matter are traced reticulospinal fibres. Note that we found mainly reticulospinal fibres descending in the ventral, ventrolateral and dorsolateral funiculus on the side of the tracer injection (con). Scale bar, 1mm. (**B II-IV**) Fluorescence microscopy spinal cord images of high magnification of a lesioned rat showing traced fibres (arrows) entering the contralesional spinal cord grey matter (**B II**) as well as midline crossing fibres (**B III**) and fibres passing a virtual border placed in the centre of the ipsilesional grey matter at a distance of 600µm from the central canal (**B IV**). Scale bars, 500µm. (**C**, **D**) Results of the anterograde tracing experiment in intact rats (n=8) and rats with cervical unilateral hemisection injury (n=15). The number of midline crossing fibres normalized to the number of fibres entering the contralesional spinal cord grey matter (**C**) and the number of fibres in the ipsilesional grey matter per midline crossing fibre (**D**) are presented as total mean value for all analysed segments and for the spinal cord segments C6-T1 and L1-L6 separately. Bars show group mean values ± s.e.m. Circles represent individual rats. For differences between groups, repeated measures two-way ANOVA was performed. Mean values (total) were analysed using unpaired 2-tailed *t*-test with **P*<0.05 indicating significantly different results. con, contralesional (left side in intact rats); ips, ipsilesional (right side in intact rats).

Retrograde tracing of the inputs of the gigantocellular reticular nucleus

Intact rats (n=10) and rats four weeks after cervical unilateral hemisection (n=10) received stereotactic injections of the fluorescent tracers mini-emerald (green) into the contralesional (left in intact rats) and tetramethylrhodamine (red) into the ipsilesional (right in intact rats) gigantocellular reticular nucleus.

In intact rats, retrogradely labelled cell bodies were found primarily in the reticular formation in the midbrain, pons and medulla oblongata on both sides as well as in the forebrain cortex. Two brain regions which are functionally and anatomically closely linked to the gigantocellular reticular nucleus were analysed in detail: the rostral motor cortex[170,190], containing the rostral forelimb area and also considered as the premotor region in rats[191-193] and the mesencephalic locomotor region (MLR), a phylogenetically ancient and highly conserved command centre for locomotion[168,194] (Figure 3.6 A I-IV). Based on retrogradely labelled cell counts in intact rats, we found that the gigantocellular reticular nucleus received bilateral projections from the rostral motor cortex with about two-thirds of the traced neurons located in the contralateral and one-third in the ipsilateral cortex (Figure 3.6 A I, III). Projections from the MLR were also bilateral, but with stronger ipsilateral than contralateral projections (Figure 3.6 A II, IV). Since analysis of absolute cell numbers revealed high within-group variability for the same retrograde tracer, and tracers showed different tracing efficiencies, we calculated a lateralization index for each traced region as a measure for contra- versus ipsilateral innervation (Figure 3.6 B I, II).

Compared to intact rats, no statistically significant changes of the projection pattern between the rostral motor cortex and the ipsi- and contralesional gigantocellular reticular nucleus were found as a consequence of spinal cord injury (Figure 3.6 B I). However, for the MLR the lateralization index for projections to the contralesional gigantocellular reticular nucleus increased significantly after hemisection injury (P=0.0302, one-way ANOVA; Figure 3.6 B II). These results suggest that spinal sprouting of reticulospinal fibres originating from the contralesional gigantocellular reticular nucleus is accompanied by modifications of its supraspinal input after spinal hemisection.

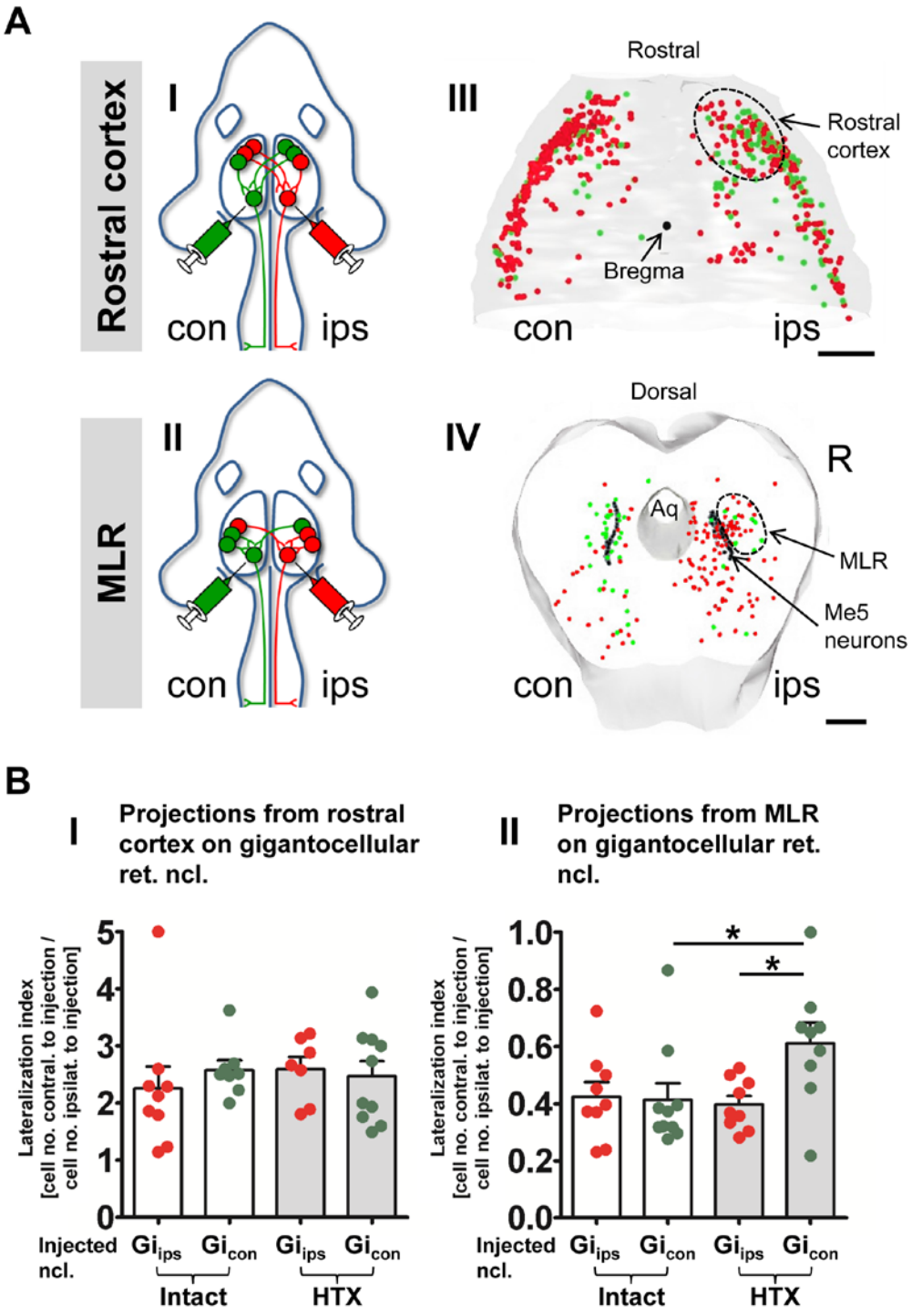

Figure 3.6. Retrograde tracing of the gigantocellular reticular nucleus. (**A I, II**) Scheme illustrating anatomical connections between the gigantocellular reticular nucleus and the rostral motor cortex (**A I**) and the mesencephalic locomotor region (MLR, **A II**) in an intact rat. (**A III, IV**) Three-dimensional Neurolucida reconstruction of the cortex and the midbrain of an intact rat after bilateral retrograde tracings from the left ("con", green cells) and right ("ips", red cells) gigantocellular reticular nucleus (**A III** dorsal view, scale bar, 2mm; **A IV** frontal view, scale bar 1mm). Aq, aqueduct; Me5, mesencephalic trigeminal nucleus (black dots); con, contralesional (left side in intact rats); ips, ipsilesional (right side in intact rats). (**B I, II**) Retrogradely labelled neurons in the rostral motor cortex (**B I**) and MLR (**B II**) were analysed using the lateralization index. Results are presented for intact rats (n=10; intact; white bars) and rats with hemisection injury (n=10; HTX; grey bars). Note that not all injections were placed correctly in the centre of the gigantocellular reticular nucleus. These injections were removed from analysis explaining differences in group size. Bars show group mean values ± s.e.m. for tracing from the ipsilesional (Gi_{ips}; right side in intact rats) and contralesional (Gi_{con}; left side in intact rats) gigantocellular reticular nucleus. Red and green dots represent single rats (colour code as in A). For differences between groups, one-way ANOVA followed by Bonferroni's Multiple Comparison Test was performed. *P<0.05 indicates significantly different results. ret., reticular; ncl., nucleus.

Behavioural changes after micro-lesioning of the gigantocellular reticular nucleus in rats with chronic spinal cord injury

To assess the functional relevance of the observed anatomical changes in the reticular mesencephalic-medullar-spinal system, rats were allowed to recover from unilateral cervical hemisection injury for a period of 16 weeks. Then, spinal cord injured rats received electrolytic micro-lesions of either the ipsilesional (n=5) or contralesional (n=9) gigantocellular reticular nucleus (Figure 3.7 A, B).

For comparison, intact rats of the same age (n=7) were also trained on the behavioural tasks and received a micro-lesion of the left gigantocellular reticular nucleus. Functional testing was performed one day before and two days after the focal brainstem lesion. Following brainstem lesion, intact rats did not demonstrate any functional impairment (Figure 3.7 C-Q, Table 3.4).

Rats with chronic hemisection injury and acute damage to the ipsilesional gigantocellular reticular nucleus showed a significantly reduced shoulder height during wading (see results of the repeated measures two-way ANOVA for all assessed parameters in Table 3.4; Figure 3.7 C) and a significantly reduced toe clearance of both hindpaws during walking (Figure 3.7 F, G). There was a tendency towards an increased external rotation of the ipsilesional (referring to the side of the hemisection), but not the contralesional hindpaw (Figure 3.7 H, I). In these rats, a broader step width (Figure 3.7 J) was mainly due to a laterally displaced ipsilesional hindlimb (Figure 3.7 L).

Rats with chronic hemisection injury and acute damage to the contralesional gigantocellular reticular nucleus demonstrated similar functional deficits to those rats with acute damage to the ipsilesional nucleus including reduced shoulder height during wading as well as dragging of both hindpaws, increased external rotation of the ipsilesional hindpaw and a broader step width during over-ground walking (see Table 3.4; Figure 3.7 C-L). However, only rats with chronic spinal cord injury and damage to the contralesional gigantocellular reticular nucleus showed a significantly decreased swimming velocity and a reduced peak stroke velocity of the ipsilesional (again, referring to the side of the hemisection) hindlimb during swimming (see Table 3.4; Figure 3.7 P, Q). Hip height and basic limb excursions (pro- and retraction) of the ipsilesional fore- and hindlimb during wading were not affected by focal brainstem lesions on either side (Figure 3.7 M-O). Thus, acute lesion of either the ipsi- or the contralesional gigantocellular reticular nucleus in rats with chronic hemisection injury affected bilateral hindlimb function. Damage to the contralesional gigantocellular reticular nucleus produced specific deficits of the ipsilesional hindlimb during swimming.

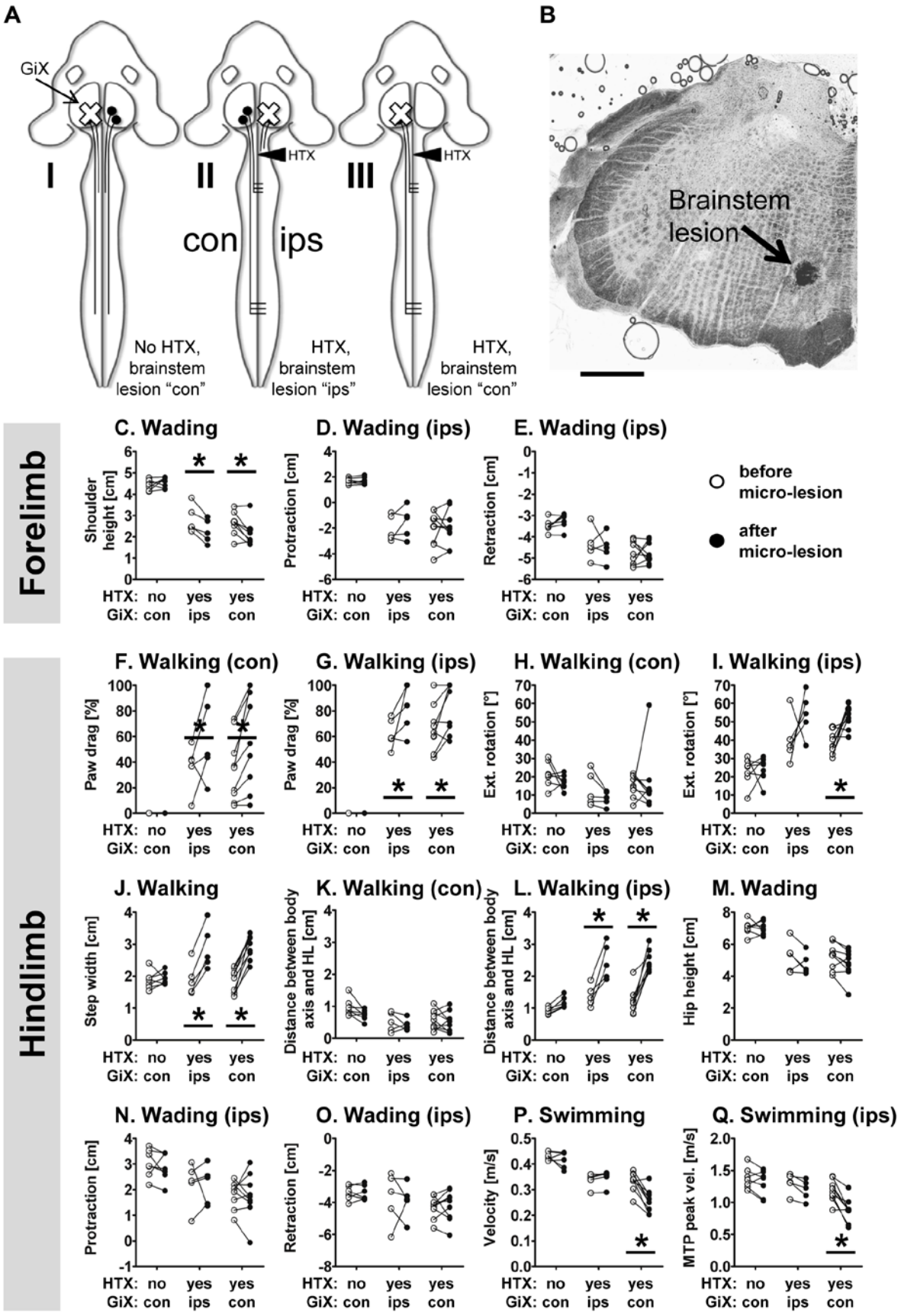

Figure 3.7. Lesioning of the gigantocellular reticular nucleus in recovered rats. (**A I-III**) Scheme illustrating the experimental approach. Intact rats received an electrolytic micro-lesion of the left gigantocellular reticular nucleus while rats that had recovered from hemisection injury for a period of 16 weeks received a lesion of the ipsilesional or the contralesional gigantocellular reticular nucleus. (**B**) Nissl staining demonstrating a representative electrolytic micro-lesion of the ventromedial portion of the contralesional gigantocellular reticular nucleus in

an injured rat. Scale bar, 1mm. (**C-Q**) Functional performance was assessed 1 day before (white dots) and 2 days after focal brainstem lesion (black dots) in intact rats (n=7) and in rats with unilateral hemisection injury and either damage to the ipsilesional (n=5; ips) or contralesional (n=9; con) gigantocellular reticular nucleus. Locomotor performance was assessed during walking, wading and swimming using similar parameters for the fore- (**C-E**) and hindlimbs (**F-Q**) as described for Figure 3.1. Results are presented for each individual rat. For differences between time points (before and after brainstem lesion) and groups, repeated measures two-way ANOVA was performed followed by Bonferroni's Multiple Comparison Test with **P*<0.05 indicating significantly different results between time points. con, contralesional (left side in intact rats); ips, ipsilesional; HTX, hemisection; GiX, micro-lesion of the gigantocellular reticular nucleus.

	Two-Way-ANOVA for repeated measures			Bonferroni *post hoc* tests for each group (pre vs. post brainstem lesion)		
Parameter	**Groups**	**Time**	**Interaction**	**No HTX, Gi lesion left ("con")**	**HTX, Gi lesion ipsilateral to HTX ("ips")**	**HTX, Gi lesion contralateral to HTX ("con")**
Wading: shoulder height	P<0.0001	P=0.0008	P=0.0035	P>0.05	P<0.05	P<0.05
Wading: protraction of ipsilesional forelimb	P<0.0001	P=0.4090	P=0.7119			
Wading: retraction of ipsilesional forelimb	P<0.0001	P=0.8945	P=0.4912			
Walking: dragging of contralesional hindpaw	P=0.0014	P=0.0017	P=0.0465	P>0.05	P<0.05	P<0.05
Walking: dragging of ipsilesional hindpaw	P<0.0001	P=0.0020	P=0.0577	P>0.05	P<0.05	P<0.05
Walking: external rotation of contralesional hindpaw	P=0.1414	P=0.3710	P=0.5921			
Walking: external rotation of ipsilesional hindpaw	P<0.0001	P=0.0096	P=0.2044	P>0.05	P>0.05	P<0.05
Walking: step width	P=0.0384	P<0.0001	P<0.0001	P>0.05	P<0.05	P<0.05
Walking: distance between contralesional hindpaw and body axis	P=0.0179	P=0.0614	P=0.5379			
Walking: distance between ipsilesional hindpaw and body axis	P<0.0001	P<0.0001	P=0.0015	P>0.05	P<0.05	P<0.05
Wading: hip height	P<0.0001	P=0.0306	P=0.2702	P>0.05	P>0.05	P>0.05
Wading: protraction of ipsilesional hindlimb	P<0.0040	P=0.6288	P=0.9697			
Wading: retraction of ipsilesional hindlimb	P=0.1346	P=0.8840	P=0.8741			
Swimming: velocity	P<0.0001	P=0.0038	P=0.0003	P>0.05	P>0.05	P<0.05
Swimming: peak velocity of ipsilesional MTP	P=0.0032	P<0.0001	P=0.0128	P>0.05	P>0.05	P<0.05

Table 3.4: Results of statistical analyses of behavioural testing before and after electrolytic damage to the ipsilesional or contralesional gigantocellular reticular nucleus in rats with cervical unilateral hemisection injury and in intact rats. For the detection of differences between time points (before and after brainstem lesion) and groups, repeated measures two-way ANOVA was used. If significant for the factor "Time", ANOVA was followed by Bonferroni's Multiple Comparison Test for each group. Statistical differences are highlighted in red. HTX, cervical hemisection injury; Gi, gigantocellular reticular nucleus; con, contralesional (left side in intact rats); ips, ipsilesional.

3.5. Discussion

In humans, unilateral spinal cord hemisection causes the Brown-Séquard syndrome which is known to be associated with good recovery of locomotor functions, but poor recovery of hand movements[7]. The rat spinal cord injury model used in the present study reproduced these behavioural findings and showed anatomical plasticity in specific parts of the CNS following the cervical hemisection. The different descending motor tracts were found to vary greatly in their plastic responses; major changes were observed mainly in the medullary reticular system. Retrograde and anterograde tracing showed that reticulospinal fibres originating from the contralesional gigantocellular reticular nucleus sprouted across the spinal cord midline in response to the injury to innervate the denervated hemicord, in particular in the lumbar spinal cord (Figure 3.8). These anatomical changes were accompanied by a high degree of recovery of basic locomotor functions which are believed to be at least partially mediated by the reticulospinal system innervating the spinal CPGs[167,170,195]. Consistent with this, sparing of reticulospinal fibres after contusion injury was found to be associated with a better functional outcome[196]. However, others failed to demonstrate an increase of reticulospinal midline crossing fibres in rodents after spinal cord injury[15,177,178]. We believe that discrepancies between these and our experiments can be mainly attributed to methodological differences (tracing efficacy, type of lesion and analysis).

The rubrospinal system showed a tendency towards an increased number of fibres re-crossing the CNS midline which was, however, not statistically significant. Also, the corticospinal and vestibulospinal system demonstrated no statistically significant increase of midline crossing fibres after hemisection. However, due to high within-group variability, data do not allow to draw the conclusion that these tracts did not respond to the lesion at all. In addition, we did not investigate other forms of anatomical plasticity such as sprouting onto long propriospinal neurons or commissural interneurons which could also provide cortical re-innervation via detour circuits[12,15,197]. We observed a fast recovery of the air-righting reaction within a few days after injury. This reaction is triggered by signals from the labyrinth and mediated via the (lateral) vestibulospinal tract[182]. Since recovery was not associated with significant sprouting of vestibulospinal axons over the midline below the lesion site, optimal use of the spared vestibulospinal-propriospinal connections may allow for rapid recovery of vestibulospinal function in a similar way as the crossed phrenic phenomenon[198]. The decrease of serotonergic projections to the denervated hemicord after hemisection is in line with previous findings in the same spinal cord injury animal model[5] and may explain the beneficial effects of treatment with serotonergic agonists after spinal cord injury[136].

After hemisection injury, the number of reticulospinal midline crossing fibres increased in cervical as well as lumbar spinal segments suggesting growth promoting factors originating from the denervated hemicord and acting on the intact reticulospinal fibres. In development, crossing the midline is regulated by an interplay of attractive and repellent factors[199]. Not much is known about such factors in the adult and injured CNS[200], and more detailed molecular studies are needed to reveal the molecular mechanisms underlying axonal midline crossing in the adult CNS. In the lumbar spinal cord, crossed reticulospinal fibres established a similar structural organization to pre-existing reticulospinal midline crossings in intact rats with an analogous degree of arborisation and a preference for the ventral grey matter[201,202]. Interestingly, in contrast to the lumbar cord there was a tendency towards a reduced arborisation of the midline crossing reticulospinal fibres in the ipsilesional cervical spinal grey matter. This anatomical finding correlates with function: the ipsilesional forelimb remained more impaired and recovered less than the ipsilesional hindlimb after the hemisection injury. The rat model is comparable to the situation in humans, but the mechanisms underlying these segmental differences in plasticity require further investigation.

Crossed reticulospinal neurons innervating new targets in the ipsilesional hemicord may face the problem of an inappropriate or even side-inverted input. After retrograde tracing from the gigantocellular reticular nucleus, we found labelled neurons widely-spread throughout the pontine and medullar reticular formation and, especially, in the contralateral counterpart of the traced gigantocellular reticular nucleus. In addition, the gigantocellular reticular nucleus received bilateral input from higher control centres in particular the MLR, as previously described[168,194] and the rostral motor cortex[170,190]. Electrical stimulation experiments provided evidence that the MLR is capable of initiating basic locomotor behaviours in mammals[166,203] via reticulospinal-interneuronal pathways controlling motoneuron pools of proximal and axial muscles[170,204]. Recent data in primates support the theory that the reticulospinal system is also important for the execution of precise finger and hand movements[205,206], a task typically requiring the involvement of cortical premotor regions[207]. In rats, the rostral motor cortex accommodates primary motor neurons involved in controlling skilled forelimb movements (rostral forelimb area) but is also considered as a premotor region[191,192]. In the present study, hemisection injury was followed by poor recovery of fine motor control, and retrograde tracing revealed that the input from the rostral motor cortex to the gigantocellular reticular nuclei remained unchanged. In contrast, innervation of the contralesional gigantocellular reticular nucleus from the MLR (with a typically stronger ipsilateral input) changed to a more equal bilateral projection pattern, thus extending the influence of the ipsilesional MLR on the

contralesional reticular nucleus (Figure 3.8). We were not able to characterize these changes in more detail due to the limitations of retrograde tracing. Since the measure of lateralization was a ratio and analysis of absolute cell counts was not useful due to high within-group variability, a higher lateralization index may be due to an increase in axons emanating from the ipsilesional MLR or to a reduction of projections from the contralesional MLR. Nevertheless, the balance of the MLRs' innervation pattern was modified in response to hemisection injury which may reflect the input adjustments needed by newly crossed reticulospinal neurons to convey purposeful information to their novel targets in the ipsilesional hemicord. Whether input modification occurred as a consequence of the midline crossing at spinal levels to provide crossed neurons with appropriate information ("bottom-up") or whether, in fact, the changed input from supraspinal control centres enforced the spinal adaptations ("top-down") remains to be elucidated.

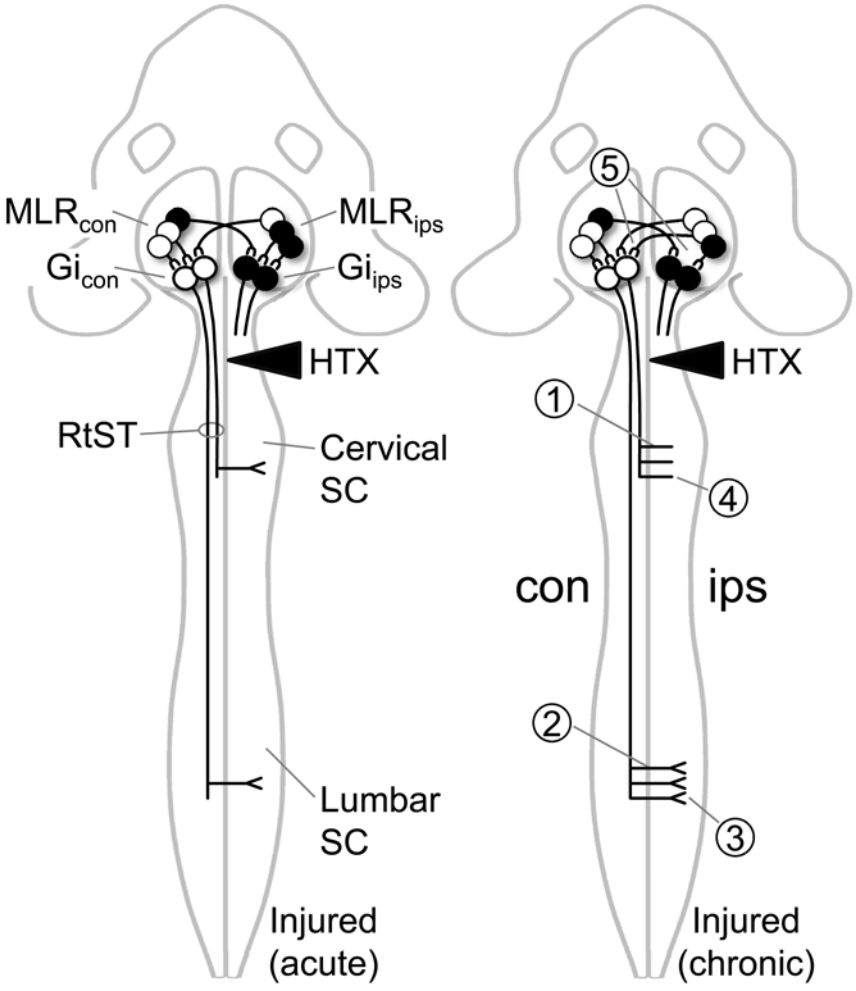

Figure 3.8. Summary of findings on anatomical plasticity in the reticular mesencephalic-medullar-spinal pathway after unilateral spinal cord injury in rats. The scheme shows the supraspinal connections between the mesencephalic locomotor region (MLR) and the gigantocellular reticular nucleus (Gi) located in the medulla oblongata. In addition, spinal projections of the gigantocellular reticular nucleus running in the reticulospinal tract (RtST) are illustrated. An acute cervical unilateral hemisection injury (HTX) severs reticulospinal fibres that descend in the ipsilesional hemicord while contralesional axons are spared. Limited reticular innervation of the ipsilesional hemicord

below the lesion site is provided by a few “pre-existing” midline crossing reticulospinal axons. In rats that recovered from injury over a period of at least 4 weeks (chronic), projections within the reticular network are modified at the level of the brainstem and the spinal cord compared to the acute state. In these rats, more spared contralesional reticulospinal fibres cross the midline at cervical (1) and lumbar (2) spinal segments reaching the ipsilesional spinal cord grey matter below the injury site. In the chronic situation, fibres crossing the midline at lumbar levels demonstrate a degree of branching similar to that of “pre-existing” reticulospinal midline crossing fibres in intact and, most likely, also in acutely injured rats (3). In contrast, fibres that cross the spinal cord midline at cervical segments show a lower degree of branching in the cervical grey matter (4). Changes of the spinal projection pattern of the contralesional gigantocellular reticular nucleus in recovered rats are accompanied by modifications of the nucleus’ input. Normally, the gigantocellular reticular nucleus receives a stronger input from the ipsilateral than from the contralateral MLR (ratio of about 2:1). In rats that have recovered from hemisection injury, this relation is changed implicating a stronger influence of the ipsilesional MLR on the contralesional gigantocellular reticular nucleus (5). MLR_{con}, contralesional mesencephalic locomotor region; MLR_{ips}, ipsilesional mesencephalic locomotor region; Gi_{con}, contralesional gigantocellular reticular nucleus; Gi_{ips}, ipsilesional gigantocellular reticular nucleus; con, contralesional; ips, ipsilesional; SC, spinal cord.

Electrolytic micro-lesioning of the ventromedial portion of the gigantocellular reticular nucleus was performed to determine the functional relevance of the anatomical changes in rats recovered from hemisection injury. Intact rats did not show any behavioural deficits after unilateral destruction of the gigantocellular reticular nucleus and this was most likely due to compensation via other, spared descending CNS systems. In contrast, damage to either the ipsi- or contralesional gigantocellular reticular nucleus in behaviourally recovered, walking rats with chronic unilateral hemisection injury abolished the recovered behaviour. Interestingly, a lesion of the ipsilesional gigantocellular reticular nucleus that had lost all of its ipsilesionally descending projections below C4 led to similar devastating consequences during walking and wading as damage to the contralesional nucleus. Thus, the ipsilesional gigantocellular reticular nucleus may exert some influence on basic locomotor functions after hemisection either via reciprocal connections with its contralesional counterpart or through detour pathways including relay interneurons located in the cervical spinal cord above the lesion[208,209]. However, functional assessment during swimming demonstrated behavioural deficits of the ipsilesional hindlimb which were specific to the inactivation of the contralesional gigantocellular reticular nucleus. This confirms that the observed anatomical changes in the contralesional reticulospinal system made a substantial contribution to functional recovery after hemisection injury.

In conclusion, functionally-relevant anatomical plasticity which can be as drastic as inducing a left-right side switch of axonal projection in the spinal cord and brainstem can also occur in the oldest part of the CNS with its functionally basic neuronal circuits. A deeper knowledge of such elementary adaptations mediating spontaneous recovery after CNS damage is fundamental for the development of new therapeutic approaches aiming for improved recovery in humans[210].

Chapter 4

Clinical algorithm for improved prediction of ambulation and patient stratification after incomplete spinal cord injury

Björn Zörner [1,2], Wolf U. Blanckenhorn [3], Volker Dietz [1],
EM-SCI Study group [4], Armin Curt [1]

[1] Spinal Cord Injury Center, Balgrist University Hospital, Zurich, Switzerland

[2] Brain Research Institute, University of Zurich and Dept. of Health Sciences and Technology, ETH Zurich, Zurich, Switzerland

[3] Zoologisches Museum, University Zurich, Zurich, Switzerland

[4] European Multicenter Study on Human Spinal Cord Injury

The original article was published in *J Neurotrauma* 2010 (27, 241-252).

Author contribution

BZ designed the study, collected and analyzed data, made the figures and wrote the manuscript.

4.1. Abstract

The extent of ambulatory recovery after motor incomplete spinal cord injury (miSCI) differs considerably amongst affected persons. This makes individual outcome prediction difficult and leads to increased within-group variation in clinical trials. The aim of this study on subjects with miSCI was (1) to rank the strongest single predictors and predictor combinations of later walking capacity, (2) to develop a reliable algorithm for clinical prediction, and (3) to identify subgroups with only limited recovery of walking function. Correlation and logistic regression analyses were performed on a dataset of 90 subjects, with tetra- or paraparesis, recruited in a prospective European multicenter study. Eleven measures obtained in the subacute injury period, including clinical examination, tibial somato-sensory evoked potentials (tSSEP) and demographic factors, were related to ambulatory outcome (WISCI II, 6minWT) 6 months after injury. The lower extremity motor score (LEMS) alone and in combination was identified as most predictive for later walking capacity in miSCI. Ambulatory outcome of subjects with tetraparesis was correctly predicted for 92% (WISCI II) or 100% (6minWT) of the cases when LEMS was combined with either tSSEP or the ASIA Impairment Scale, respectively. For individuals with paraparesis, prediction was less distinct mainly due to low prediction rates for individuals with poor walking outcome. A clinical algorithm was generated that allowed for the identification of a subgroup composed of individuals with tetraparesis and poor ambulatory recovery. These data provide evidence that a combination of predictors enables a reliable prediction of walking function and early patient stratification for clinical trials in miSCI.

4.2. Introduction

Sensory-motor impairment after acute spinal cord injury (SCI) is determined by the neurological level of injury and the completeness of the lesion[211,212]. Amongst all subjects with SCI, 40-50% are "motor incomplete"[213] and classified as C or D on the ASIA Impairment Scale (AIS) depending on the degree of preserved motor function below the level of injury (International Standards of Neurological Classification, American Spinal Injury Association (ASIA))[214].

In motor complete SCI (AIS A and B), changes of the AIS (conversion rates) and ASIA motor scores are preferentially used as primary outcome measures. Assessment of walking ability is less applicable as most of these patients are initially non-ambulatory and show only limited spontaneous recovery[3,215,216]. In contrast to motor complete SCI, conversion rates and ASIA motor scores are regarded as less sensitive outcome measures in motor incomplete SCI (miSCI, AIS C and D) due to the substantial improvements often seen after injury (ceiling effect)[3,216]. In miSCI, standardized walking tests (6min, 10m) or qualitative scales of walking ability (walking index for spinal cord injury, WISCI II) are widely used as measures of functional recovery[217-220], even though, a significant proportion of these patients show no or only partial restoration of ambulatory function. Thus, recovery of walking ability is highly variable in miSCI ranging from subjects with very limited standing/stepping capacity (i.e. requiring body weight support, physical assistance, technical aids) to individuals with almost normal walking function[3]. For this reason, prediction of walking outcome at an early stage after injury is difficult[221] but of great value for both selecting an optimal rehabilitation program and for stratifying patients for clinical studies.

The early identification of subgroups based on reliable outcome predictors might enhance the feasibility and success rate of interventional clinical trials in miSCI by reducing the within-group variability and preventing an *a priori* imbalance between different treatment groups[216,222]. These outcome predictors could serve as inclusion or exclusion criteria for defining subgroups of subjects with miSCI[3]. In particular, miSCI subjects with an expected unfavorable outcome of ambulation might benefit from specifically tailored rehabilitation efforts or interventional therapies that enhance neuroplasticity and repair[20,24,47,111]. Therefore, the aim of this study in miSCI was to identify the strongest single and combined predictors of walking outcome in individuals with tetra- or paraparesis allowing reliable prognosis and early subgrouping of patients.

4.3. Methods

Patient selection and general procedures

Subjects were selected from a prospectively gathered European database and admitted between 2001 and 2005 to acute care and rehabilitation hospitals in Switzerland, France or Germany within a European Multicenter project (EM-SCI). Subjects with tetra- or paraparesis were included if full information about all predictive and outcome measures within a 6 month follow-up were available. Ethical approval and informed consent were signed and patients were aged 18 or older at the time of injury. Only patients who were graded C and D according to the ASIA Impairment Scale, i.e. motor incomplete spinal cord injured subjects (miSCI), in the subacute phase (within 16-40 days) after SCI were considered for analysis. Subjects with motor complete SCI (AIS A and B) were excluded from this study. Other exclusion criteria were inconsistent datasets and the presence of general medical, neurological or psychiatric disorders independent of SCI and interfering with clinical recovery. Motor and sensory examinations were performed according to the standards of the American Spinal Injury Association[214]. Correlation and logistic regression analysis, as well as the development of a predictive algorithm, were based on a dataset of 90 subjects with miSCI for the WISCI II based analyses who had at least two combined examinations within the first 6 months after injury. For 3 out of these 90 subjects, 6-min walking test (6minWT) results were not available, this reduced the number of subjects for the 6minWT based analyses to 87. Important characteristics of these subjects are summarized in Figure 4.1 A.

Predictive measures

Eleven predictive measures, obtained in the subacute phase after injury and belonging to three categories (demography, electrophysiology and neurological examination), were considered as potential predictors of walking capacity 6 months after injury. Demographic factors were gender and age at the time of injury. Somato-sensory evoked potentials (SSEP) were recorded after stimulation of the posterior tibial nerves (tSSEP) of both legs and were scored as described previously[223]. Briefly, the P40 latencies and response amplitudes were scored as: 1. no response, 2. pathological P40 latency and pathological configuration of the response, 3. delayed P40 latency with normal amplitude, 4. normal P40 latency with reduced amplitude and 5. normal P40 latency and amplitude. Since stimulation was performed on both legs, asymmetric injuries could result in divergent SSEP scores between legs. In these cases, both scores were used for statistical analysis (tSSEPmin & tSSEPmax) thus in cases of identical scoring of both legs, tSSEPmin and tSSEPmax were equal. Data obtained from clinical

examinations included ASIA motor scores (MS), lower and upper extremity motor subscores (LEMS and UEMS)[224], pin prick (PP), light touch (LT), ASIA impairment scale (AIS) and the neurological level of injury (NLI). In subjects with paraparesis the UEMS was generally 50 (except in one patient). It could be expected that the predictors UEMS and MS do not provide any supplementary information in addition to the LEMS in subjects with paraparesis and were therefore only analyzed for subjects with tetraparesis. Therefore, 11 different single predictors were evaluated for subjects with tetraparesis and 9 for subjects with paraparesis. Clinical and electrophysiological data were acquired in the subacute phase (between day 16 to 40) after miSCI since clinical measurements in this phase are considered reliable and valid[215].

Outcome measures

For evaluation of walking function in the chronic phase after SCI (≥ 6 months post-injury) the walking index for spinal cord injury (WISCI II)[219,220,225,226] and the 6-min walking test (6minWT)[217,227] were used. For the logistic regression analysis, as well as for the development of the algorithm, it was necessary to dichotomize the outcome and to assign subjects to one of two groups according to their walking capacity 6 months after injury. One group consisted of "independent" walkers able to walk without any assistance or device (WISCI II score of 20). In the other group, referred to as "dependent" walkers, subjects required bars, canes/crutches, braces or human assistance (WISCI II score ≤ 19). Another approach used the 6minWT results for the binary classification of miSCI subjects. A walking speed of 0.6m/sec (i.e. 216m/6min) was defined in order to separate "functional" from "non-functional" walkers. The expression "functional" refers to walking ability necessary to overcome some challenges of everyday life, e.g. to cross a road within the green/safety phase of pedestrian traffic lights. An average walking velocity of 0.6 m/sec is regarded sufficient to cross a road within this time period (Swiss standards) and has been used in previous studies to characterize walking capacity[228].

Data analysis

All statistical calculations and data processing were performed with SPSS 14.0 for Windows (SPSS Inc.). Multiple correlation analyses of independent (predictors) and dependent (outcome of walking tests) measures were performed. This provided early evidence for potentially important predictors of walking capacity 6 months after injury and allowed comparisons with other studies in the field. The predictor gender was excluded only for the multiple correlation analysis, which requires ordinal or continuous measures, but was

included for the logistic regression analysis and the generation of the algorithm (see below). In addition, correlations among the different independent measures were evaluated to indicate potential redundancy. Spearman rank correlation coefficients (r_s) were used to determine the relationship between two variables because of the non-parametric properties of the majority of the collected data. The degree of correlation was ranked: $r_s \leq 0.25$ as absent, $r_s > 0.25$ and = 0.5 as poor, $r_s > 0.5$ and = 0.75 as moderate and $r_s > 0.75$ as high.

Multiple logistic regression analyses were performed to identify the most important predictors of walking function and to determine their contribution to prediction[229-232]. This analysis was based on the dichotomous outcome classification and included all predictors. Stepwise forward and backward, as well as single predictor regressions were performed. For stepwise procedures, p-values < 0.05 for entry and removal of a variable were set. The selection of predictors by stepwise forward or backward regression was occasionally inconsistent depending on the type of statistical test applied (Conditional, Wald-test, Likelihood-Ratio test (LR)). To confirm that the models which were suggested by different stepwise procedures do in fact fit the data best, Akaike's information criterion (AIC) corrected for small sample sizes (AICc) and the -2log likelihood were used to compare a total of 66 or 45 different statistical models for subjects with tetraparesis or paraparesis, respectively. These models consisted of either one single predictor or a combination of any two predictors. Akaike's information criterion identifies the most parsimonious model of a large number of models as that with the highest predictive (i.e. r-squared) value whilst minimizing the number of explanatory variables[233,234]. The derived differences of any model to the best model, ΔAICc, enables ranking whereby models with a ΔAICc < 2 can be regarded as equivalent. The best models are characterized by low -2log likelihood and AICc. By means of these values and the percentage of correct classification we were able to identify the models exhibiting the highest predictive potential of walking ability given our data set.

Algorithm

We designed two algorithms for outcome prediction in miSCI by classifying subjects according to their walking performance 6 months after injury (dichotomous classification of WISCI II or 6minWT) and the main predictors as identified by our logistic regression analysis described above. To avoid the formation of subgroups that were too small, thus hindering reliable data interpretation, only the strongest combination of two predictors for subjects with tetra- or paraparesis were considered in the algorithms. Threshold values for the best predictor variable were obtained by the inflection point of the sigmoid curve fitted by the logistic

regression analysis, denoting a predicted probability of 0.5. At this value a subject has an equal probability of being classified as “dependent” vs. “independent” walker (WISCI II) or “non-functional” vs. “functional” (6minWT) walker. The best predictors as well as the respective thresholds differed for subjects with tetra- or paraparesis and were dependent on the outcome measure used (see 4.4. Results). For the WISCI II based algorithm, calculated thresholds for the best predictors were: LEMS = 26.9 and tib.SSEPmin = 2.1 for subjects with tetraparesis and LEMS = 19.2 and PP = 89.9 for subjects with paraparesis. For the 6minWT based algorithm the following thresholds were determined: LEMS = 25.5 for subjects with tetraparesis (the second predictor AIS comprised only two levels, i.e. AIS C or D) and LEMS = 14.1 and age = 61.4 years for subjects with paraparesis. For practical reasons, rounded threshold values were used in the algorithms.

4.4. Results

Outcome of walking function

Subjects with tetra- or paraparesis achieved average WISCI II scores of 13.6 ± 8.4 (median = 20) or 17.9 ± 4.1 (median = 20), respectively, six months after injury. Within 6 minutes (6minWT), subjects with tetraparesis were able to walk a mean distance of 284 ± 235m (paraparetic subjects: 376 ± 209m). Fifty two out of 90 subjects scored 20 on the WISCI II scale 6 months after miSCI, i.e. 58% of the individuals were able to walk independently without any assistance or device. In subjects with tetraparesis, 27 of 51 (53%) reached a WISCI II score of 20. However, 25 out of 39 (64%) subjects with paraparesis achieved the maximal WISCI II score indicating a better outcome of individuals with paraparesis compared to those with tetraparesis (Figure 4.1 B). This was confirmed by the 6minWT results showing that 57% of subjects with tetraparesis and 79% of subjects with paraparesis were able to reach a walking velocity of 0.6m/sec (Figure 4.1 C). In addition, a considerable overlap between WISCI II and 6minWT results was observed when assignment to our dichotomous outcome groups was compared (“independent” vs. “functional” and “dependent” vs. “non-functional” walkers). Only 12% of the subjects were categorized differentially (6% tetraparetic, 18% paraparetic). In particular, for subjects with tetraparesis, results of the 6minWT (57% “functional” walkers) were very similar to the WISCI II outcome (53% “independent” walkers). In contrast, 79% of the subjects with paraparesis were scored as “functional” (6minWT) but only 64% as “independent” walkers (WISCI II). This result is reflected by a stronger correlation between the two walking tests in subjects with tetraparesis (r_s = 0.88) compared to those with paraparesis (r_s = 0.5).

A

	subjects with tetraparesis	subjects with paraparesis
total [#]	51	39
type of injury [#]		
traumatic	43	28
ischemic	5	6
haemorrhagic	1	1
disk herniation	1	4
other	1	0
gender [#]		
male	41	27
female	10	12
age at injury [years]		
mean ± SD	50.27 ± 16.17	43.38 ± 16.46
max.	78	91
min.	20	18
NLI [#]		
	cervical 2: 4 cervical 3: 5 cervical 4: 17 cervical 5: 20 cervical 6: 5	thoracic: 20 lumbar: 19
AIS [#]		
at subacute stage	C:20 D:31	C:19 D:20
at chronic stage	B:1 C:5 D:45	C:2 D:35 E:2

[#] number of subjects

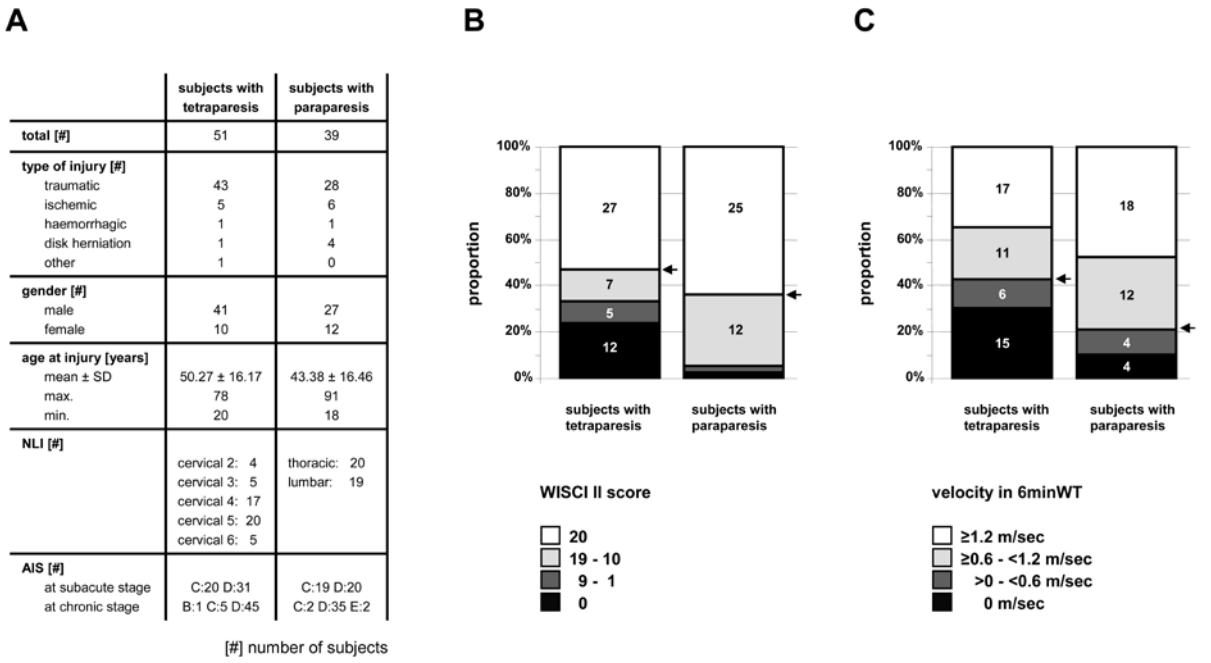

Figure 4.1. Clinical characteristics (A) of subjects with miSCI and walking performance (B, C) 6 months after injury. Most of the subjects who were initially scored as ASIA C in the subacute stage eventually converted to ASIA D. WISCI II scores and walking velocity in the 6minWT indicate an overall better outcome of walking function in subjects with paraparesis. Note that more than 20% of the subjects with tetraparesis did not recover any walking ability (WISCI II score = 0, walking velocity = 0m/sec) 6 months after injury. Box size represents percentage of subjects, with absolute numbers indicated inside. Arrows signify the thresholds used in the algorithms to dichotomize the walking test outcome.

Single predictors of walking capacity

Correlations of all predictor variables, except for the nominal predictor gender, with the WISCI II and the 6minWT outcome are presented in Figure 4.2. In subjects with tetraparesis, MS and LEMS correlated strongly with the outcome of both walking tests. Only weak correlations between walking tests and tSSEP sores were found in these subjects whilst age and NLI were not related to the outcome measures. In subjects with paraparesis, only a moderate correlation (maximal value) between LEMS and the 6minWT result was detected in addition to weak correlations between the ambulatory outcome and PP, AIS or tSSEP. However, a weak negative correlation between the 6minWT outcome and age was observed for subjects with paraparesis. Correlation coefficients between predictors and outcome measures were generally lower for subjects with paraparesis compared to individuals with tetraparesis. In both patient groups, high correlations between some of the predictors were found. In particular, PP and LT were strongly associated (r_s = 0.80 or r_s = 0.69 for subjects with tetraparesis or paraparesis, respectively) suggesting some redundancy in the clinical sensory measures. Interestingly, correlations between tSSEP and PP/LT were generally weak

or absent, except for a moderate correlation of PP and tSSEPmin in subjects with tetraparesis (r_s = 0.65). For subjects with tetraparesis, the outcome of both walking tests was highly correlated (r_s = 0.88, and for subjects with paraparesis r_s = 0.5)

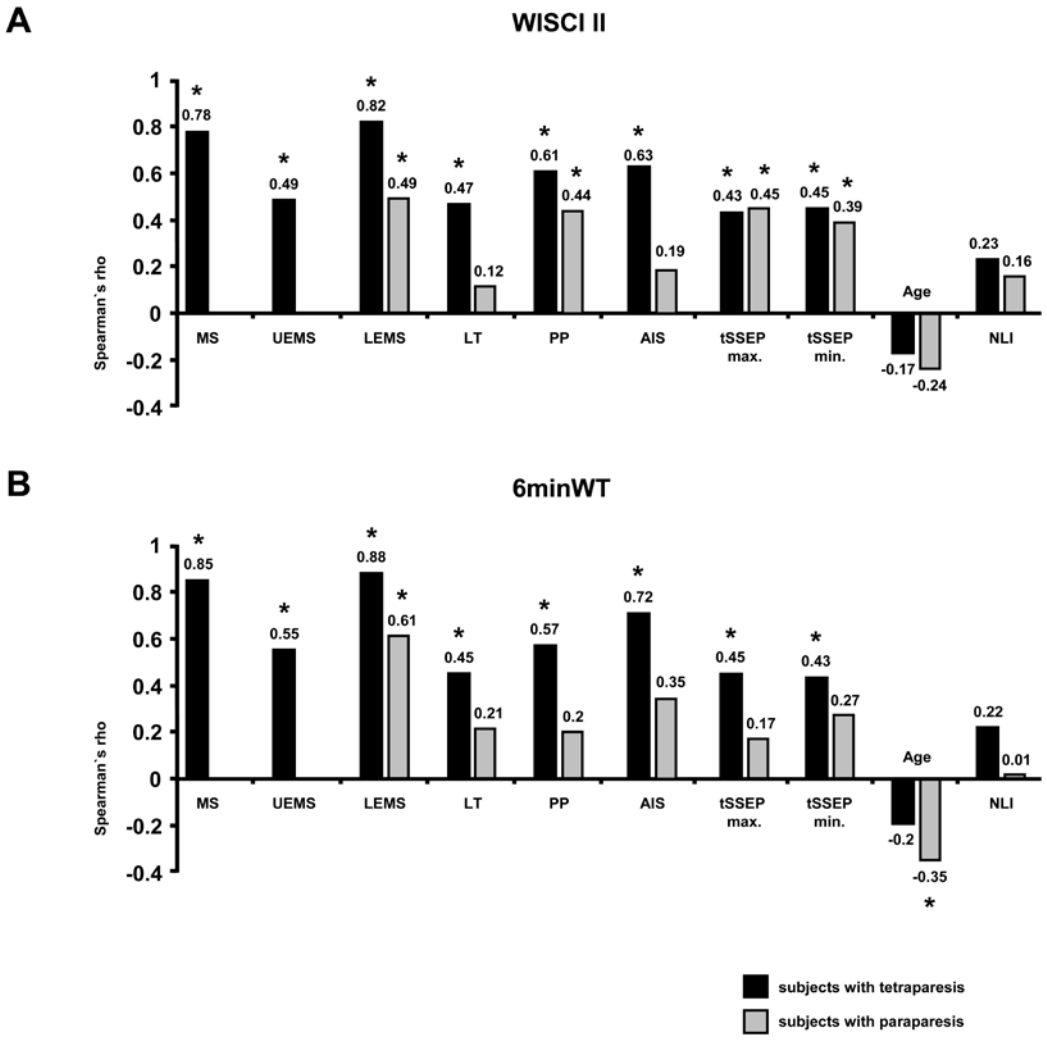

Figure 4.2. Correlation coefficients of different predictors with the WISCI II (A) and 6minWT (B) results obtained 6 months after SCI in subjects with tetra- (black) or paraparesis (grey). ASIA motor scores (MS/LEMS), and to a lesser extent sensory scores (LT/PP) and tSSEPs are strongly correlated with WISCI II and 6minWT outcome. Overall, correlation coefficients are higher in subjects with tetraparesis than with paraparesis. Abbreviations: ASIA motor scores (MS), lower and upper extremity motor subscores (LEMS and UEMS), light touch (LT), pin prick (PP), ASIA Impairment Scale (AIS), lowest and highest tSSEP score (tSSEPmin and tSSEPmax), neurological level of injury (NLI). * Rank correlation is significant at the P <0.01 level, 2-tailed.

In addition to the multiple correlations, logistic regression analyses based on the previous defined dichotomous outcome classification (derived from the WISCI II or the 6minWT results, see 4.3. Methods) were performed separately for every single predictor. Strikingly, for both walking tests and for subjects with tetra- and paraparesis, the LEMS was identified as the

best single predictor of walking outcome (correct prediction rates: subjects with tetraparesis = 90% for WISCI II and 90% for 6minWT, subjects with paraparesis = 67% for WISCI II and 90 % for 6minWT, see also Figure 4.3 and Table 4.2). PP and tSSEPmax were found to be as strong predictors as the LEMS for subjects with paraparesis and the WISCI II based outcome classification.

The result of the logistic regression analysis for single predictors, i.e. LEMS is the most predictive measure for walking outcome, is in line with the results of the multiple correlation analysis (Figure 4.2) demonstrating the highest correlation coefficients between LEMS and the outcome of both walking tests for subjects with tetra- or paraparesis.

Combining predictors of walking capacity

In subjects with tetraparesis, forward (Conditional, Wald & LR) and backward (Wald only) logistic regression analyses identified the combination of LEMS and tSSEPmin as the best statistical model for categorizing patients as “dependent” or “independent” walkers (WISCI II based analysis). For prediction of the 6minWT outcome (“functional” vs. “non-functional” walkers), the combination of LEMS and AIS was found as the most predictive model (forward: Conditional, Wald & LR; backward LR only). To confirm the findings of the stepwise procedure, all models combining two different predictors (55 possible combinations) were compared using the ΔAICc (preferably low) and the percentage of correct prediction (preferably high) as quality criteria (Table 4.2). Combining the LEMS with another predictor resulted in considerably smaller ΔAICc values in comparison to models that include only the LEMS (Figure 4.3). This was true for both walking tests and subjects with tetra- and paraparesis indicating that the combination of the LEMS with another predictor improves outcome prediction. For subjects with tetraparesis, the combinations of LEMS and tSSEPmin (WISCI II) or AIS (6minWT) were superior to all other models (Table 4.2) as suggested by the stepwise procedure. These predictor combinations correctly classified the walking outcome of 92% (WISCI II) or even 100% (6minWT) of the cases with tetraparesis (Table 4.1). The best models for walking outcome prediction in subjects with tetraparesis can be expressed by the equations:

$$Z = -10.96 + 0.28\,(LEMS) + 1.51\,(tSSEPmin) \qquad (WISCI\ II)$$

$$Z = -354.02 + 10.24\,(LEMS) + 61.96\,(AIS) \qquad (6minWT)$$

In subjects with paraparesis, forward (Conditional & LR) and backward (Conditional, Wald & LR) logistic regression identified the combination of LEMS and PP as the most predictive model for the dichotomized WISCI II outcome. Comparison of the models revealed two combinations among the 36 alternatives as the best models (Figure 4.3, Table 4.2). The first model combining LEMS and PP resulted in 82% correct predictions, while the second model with LEMS and AIS correctly predicted 77% of the cases. Despite this difference in the percentages of correct predictions, both models can be regarded as equivalent because $\Delta AICc < 2$. However, for the algorithm the first model combining LEMS and PP was used because of the result of the stepwise logistic regression procedure.

When the ability to achieve an average walking speed of 0.6m/sec in the 6minWT was used as a criterion for recovery of ambulatory capacity ("functional" vs. "non-functional" walkers), forward (Wald only) and backward (Wald only) stepwise logistic regression identified the combination of LEMS and age as the best model. Again, this result was confirmed by comparison of the $\Delta AICc$ values (Table 4.2). However, adding age to the LEMS did not increase the percentage of correct predictions despite the calculated -2log likelihood and AICc values being considerably reduced in comparison to the LEMS only model (Table 4.2). This suggests that the model comprising LEMS and age is more predictive for outcome although, in this case, this is not reflected by a higher percentage of correct predictions. Based on the logistic regression result, i.e. the -2log likelihood and AICc values, age was included as a second outcome predictor in the 6minWT based algorithm. Accordingly, the best models for outcome prognosis of individuals with paraparesis can be described by the following equations:

$$Z = -13.39 + 0.1\,(LEMS) + 0.12\,(PP) \qquad (WISCI\ II)$$

$$Z = -0.28 + 0.28\,(LEMS) - 0.09\,(Age) \qquad (6minWT)$$

Percentages of correct predictions were, in general, lower in subjects with paraparesis compared to subjects with tetraparesis. As illustrated in Table 4.1, this was exclusively due to a weak outcome prediction for subjects with paraparesis and poor recovery of ambulatory capacity ("dependent" or "non-functional" walkers).

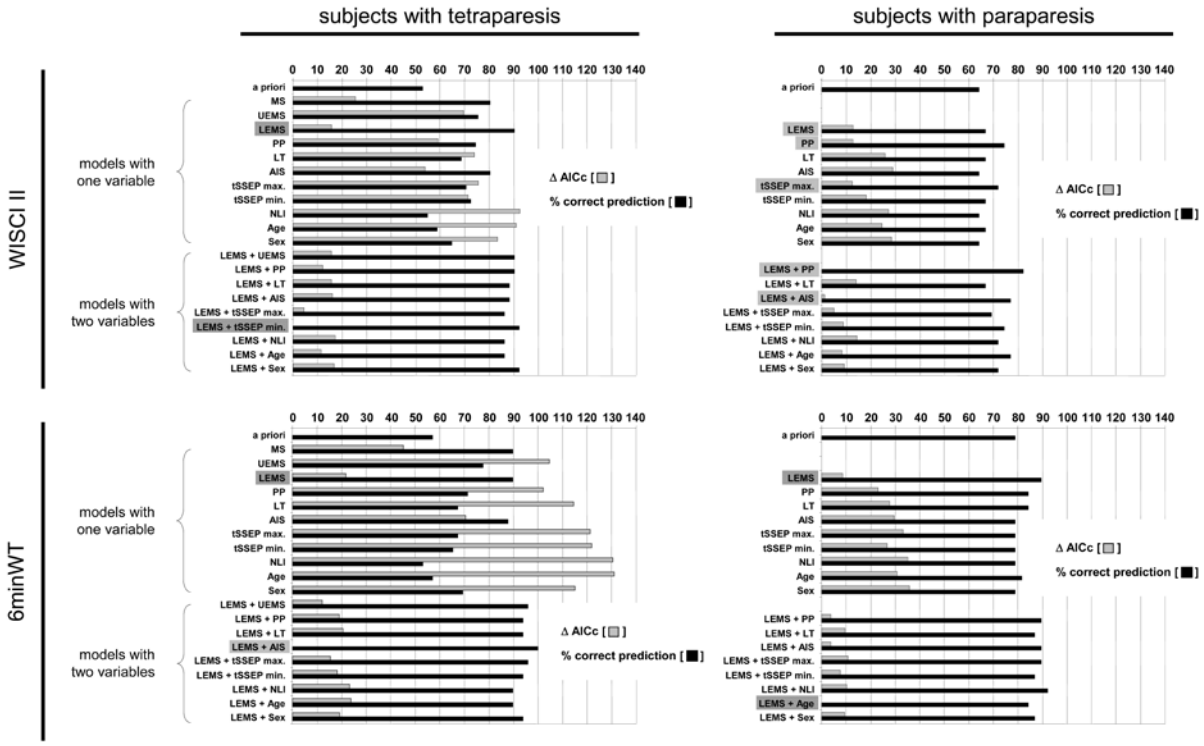

Figure 4.3. Main results of logistic regression analysis are summarized for subjects with tetra- or paraparesis. Based on the WISCI II or 6minWT outcome 6 months after injury, either one or a combination of two predictors was used to classify subjects with miSCI as "dependent" or "independent" and "non-functional" or "functional" walkers, respectively. Good logistic regression models are characterized by high percentages of correct prediction and low ΔAICc values. The AIC is a measure of the "goodness of fit" and allows appraisal and comparison of statistical models. In subjects with tetra- or paraparesis, models including the LEMS in combination with another predictor (tSSEP, PP, AIS or Age) are superior to all other possible combinations (see Table 4.2). The best models, identified by comparison of the ΔAICc values, are highlighted in grey. Abbreviations as in Figure 4.2.

Clinical algorithm for prediction of locomotor outcome

Two algorithms were generated to categorize individuals with miSCI based on the most predictive combinations for walking outcome, namely the LEMS either in combination with tSSEPmin, PP, AIS or age (Figure 4.4). Thresholds were derived from the logistic regression analysis as described in the Method section. Subjects with both predictor scores above threshold were likely to become "independent walkers" (WISCI II) or "functional walkers" (6minWT) 6 months after injury. For instance, this was the case for 16 of 17 subjects with tetraparesis in the WISCI II based algorithm, demonstrating that individuals with miSCI that have initially high predictor scores show a favorable ambulatory outcome. Conversely, patients with both predictive scores below threshold values belonged predominantly to the group of patients that needed support during ambulation 6 months after injury or did not achieve an average walking velocity $\geq$ 0.6m/sec in the 6minWT. By each algorithm, a subgroup of 14 subjects with tetraparesis and both predictive scores below threshold was generated. A striking feature, in common for all of these subjects, was that they demonstrated

only very poor recovery of walking function; 9 (WISCI II) or 12 (6minWT) subjects showed no ambulatory function 6 months after injury, i.e. WISCI II = 0 or walking velocity = 0m/sec, respectively. It should be noted that 10 of the 14 subjects assigned to the subgroups based on either the WISCI II or the 6minWT outcome, were the same individuals.

Subjects with divergent predictor values, i.e. one score below and one score above threshold, showed no clear bias towards either of the outcome groups. In addition, if only one predictor variable was used for algorithmic grouping of the subjects with miSCI, the resulting subgroups were less homogenous with respect to their ambulatory capacity (algorithms not shown). For instance, when only the LEMS was applied for classification of subjects with tetraparesis in the WISCI II based algorithm, the subgroup of patients with LEMS scores ≤ 25 was composed of 3 “independent” and 19 “dependent” walkers. Consequently, the assumption that all subjects with tetraparesis and LEMS scores ≤ 25 early after SCI depend on walking assistance $\geq$ 6 months after injury would have been correct in 86% of the cases (19/22). Including the tSSEPmin classification as a differentiating factor into the WISCI II based algorithm led to a more distinct picture (Figure 4.4); 100% of the patients with LEMS ≤ 25 and tSSEPmin ≤ 2 were “dependent” walkers (14/14). The situation was similar for subjects with tetraparesis, where a LEMS score > 25 and tSSEPmin score > 2 indicated a good walking outcome and also for the 6minWT based algorithm. This suggests that a second variable allowed a more reliable prediction. The typically lower correct prediction rates in the logistic regression analyses for subjects with paraparesis and poor recovery of ambulatory capacity is also reflected in both algorithms showing only a limited stratification of subjects with paraparesis and poor recovery of walking function (left branches for subjects with paraparesis).

In summary, the results suggest that prediction and early patient stratification based on these algorithms is applicable to subjects with both predictor scores either above or below the threshold values (termed “strong prediction” in Figure 4.4) at least for patients with tetraparesis.

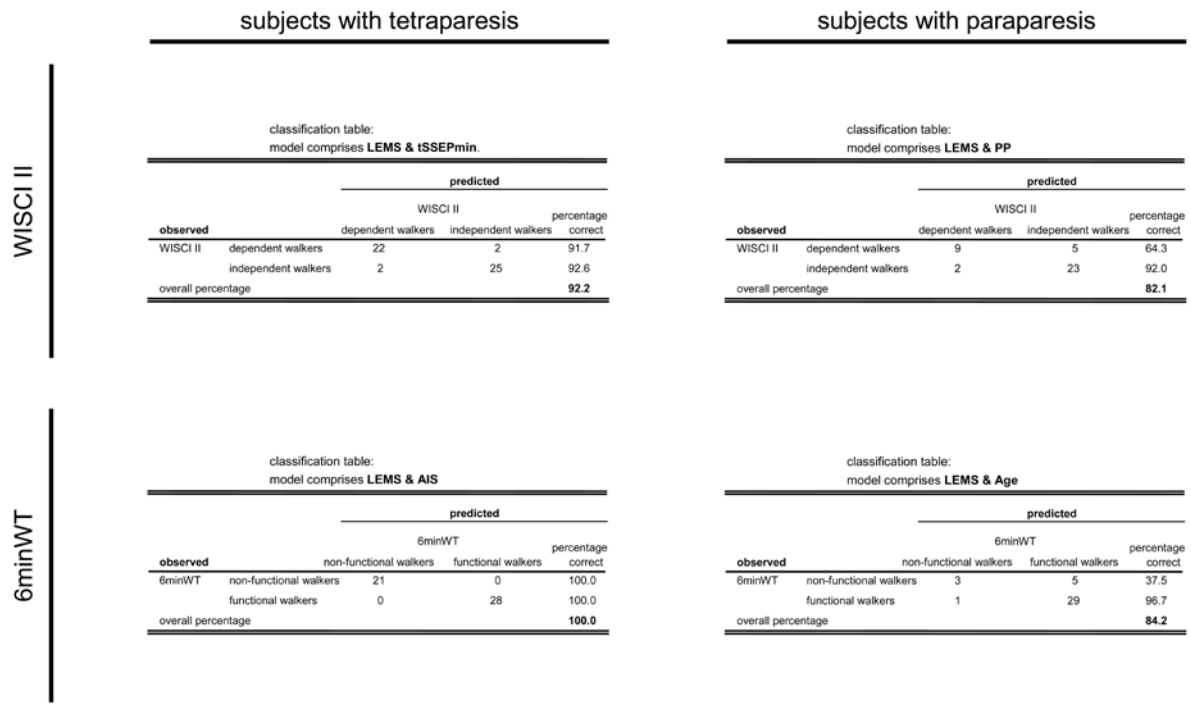

Table 4.1. Classification table for subjects with miSCI. Subjects were either correctly (observed outcome = predicted outcome) or incorrectly (observed outcome ≠ predicted outcome) classified by the best logistic regression models. Regardless of the walking test selected for outcome quantification, percentages of correct prediction were generally lower for subjects with paraparesis than for subjects with tetraparesis. Note that this was mainly due to an inaccurate classification of subjects with actual poor recovery of walking function, i.e. for these subjects a walking status of "independent" or "functional" was incorrectly predicted.

4.5. Discussion

According to a recent study by Ditunno et al.[235] titled "Who wants to walk?" walking function has "a high priority for recovering" after a SCI. Early prediction of later locomotor outcome is of major importance for patients, their families and clinicians. The aim of the study was to identify measures that enable an early prediction of ambulatory outcome in subjects with miSCI. This study showed that a reliable prediction of walking function can be achieved by combining different measures obtained in the subacute phase after injury. Two algorithms were developed that could identify subgroups of patients with either poor or favorable recovery of walking function.

subjects with tetraparesis

WISCI II

model	N	-2 log likelihood	K	AIC	AICc	Δ AICc	% correct predicted
a priori							52,9
one predictor							
MS	51	35,9	1	73,8	73,8	25,5	80,4
UEMS	51	57,9	1	117,8	117,9	69,6	75,5
LEMS	51	31,0	1	63,9	64,0	15,7	90,2
PP	51	52,7	1	107,4	107,4	59,1	74,5
LT	51	60,1	1	122,1	122,2	73,9	68,6
AIS	51	50,0	1	102,1	102,1	53,8	80,4
tib. SSEPmax	51	60,9	1	123,8	123,9	75,6	70,6
tib. SSEPmin	51	58,8	1	119,6	119,7	71,4	72,5
NLI	51	69,4	1	140,7	140,8	92,5	54,9
Age	51	68,7	1	139,3	139,4	91,1	58,8
Sex	51	64,9	1	131,7	131,8	83,5	64,7
two predictors							
MS + UEMS	51	29,9	2	63,7	64,0	15,7	90,2
MS + LEMS	51	29,9	2	63,7	64,0	15,7	90,2
MS + PP	51	31,5	2	67,0	67,3	19,0	84,3
MS + LT	51	35,1	2	74,3	74,5	26,2	82,4
MS + AIS	51	35,6	2	75,3	75,5	27,2	82,4
MS + tib. SSEPmax	51	31,3	2	66,6	66,8	18,5	86,3
MS + tib. SSEPmin	51	27,2	2	58,5	58,7	10,4	86,3
MS + NLI	51	35,8	2	75,6	75,8	27,5	82,4
MS + Age	51	32,8	2	69,6	69,8	21,5	78,4
MS + Sex	51	35,0	2	74,0	74,2	25,9	84,3
UEMS + LEMS	51	29,9	2	63,7	64,0	15,7	90,2
UEMS + PP	51	45,5	2	95,0	95,3	47,0	80,4
UEMS+ LT	51	52,0	2	108,0	108,3	59,9	72,5
UEMS + AIS	51	50,0	2	104,0	104,3	56,0	80,4
UEMS + tib. SSEPmax	51	51,4	2	106,9	107,1	58,8	76,5
UEMS + tib. SSEPmin	51	47,3	2	98,5	98,8	50,5	76,5
UEMS + NLI	51	57,7	2	119,3	119,6	71,3	72,5
UEMS + Age	51	56,0	2	116,0	116,3	67,9	72,5
UEMS + Sex	51	51,8	2	107,5	107,8	59,5	74,5
LEMS + PP	51	28,1	2	60,2	60,5	12,2	90,2
LEMS + LT	51	29,9	2	63,8	64,0	15,7	88,2
LEMS + AIS	51	30,1	2	64,2	64,4	16,1	88,2
LEMS + tib. SSEPmax	51	24,3	2	52,6	52,9	4,5	86,3
LEMS + tib. SSEPmin	51	22,0	2	48,1	48,3	0,0	92,2
LEMS + NLI	51	30,7	2	65,3	65,6	17,3	86,3
LEMS + Age	51	27,7	2	59,5	59,7	11,4	86,3
LEMS + Sex	51	30,4	2	64,9	65,1	16,8	92,2
PP + LT	51	52,7	2	109,3	109,6	61,2	74,5
PP + AIS	51	41,3	2	86,5	86,8	38,5	80,4
PP + tib. SSEPmax	51	51,0	2	106,0	106,3	58,0	78,4
PP + tib. SSEPmin	51	51,4	2	106,7	107,0	58,6	78,4
PP + NLI	51	52,0	2	108,1	108,3	60,0	74,5
PP + Age	51	49,5	2	103,1	103,3	55,0	72,5
PP + Sex	51	51,6	2	107,3	107,5	59,2	72,5
LT + AIS	51	46,2	2	96,5	96,7	48,4	82,4
LT + tib. SSEPmax	51	55,2	2	114,4	114,6	66,3	76,5
LT + tib. SSEPmin	51	54,7	2	113,4	113,6	65,3	74,5
LT + NLI	51	59,5	2	123,0	123,3	75,0	62,7
LT + Age	51	53,8	2	111,6	111,9	63,6	72,5
LT + Sex	51	57,9	2	119,8	120,1	71,7	68,6
AIS + tib. SSEPmax	51	57,9	2	119,8	120,1	71,7	80,4
AIS + tib. SSEPmin	51	39,9	2	83,8	84,1	35,8	82,4
AIS + NLI	51	49,1	2	102,2	102,4	54,1	80,4
AIS + Age	51	47,5	2	99,1	99,3	51,0	80,4
AIS + Sex	51	46,6	2	97,1	97,4	49,0	84,3
tib. SSEPmax + tib. SSEPmin	51	58,4	2	120,9	121,1	72,8	72,5
tib. SSEPmax + NLI	51	59,5	2	123,0	123,3	75,0	68,8
tib. SSEPmax + Age	51	60,3	2	124,6	124,8	76,5	68,6
tib. SSEPmax + Sex	51	56,7	2	117,4	117,7	69,4	72,5
tib. SSEPmin + NLI	51	57,6	2	119,3	119,5	71,2	70,6
tib. SSEPmin + Age	51	58,2	2	120,4	120,6	72,3	72,5
tib. SSEPmin + Sex	51	54,1	2	112,2	112,4	64,1	72,5
NLI + Age	51	67,9	2	139,8	140,0	91,7	56,9
NLI + Sex	51	63,4	2	130,8	131,0	82,7	60,8
Age + Sex	51	63,5	2	130,9	131,2	82,9	60,8

6minWT

model	N	-2 log likelihood	K	AIC	AICc	Δ AICc	% correct predicted
a priori							57,1
one predictor							
MS	49	23,7	1	49,4	49,4	45,2	89,8
UEMS	49	53,4	1	108,8	108,9	104,6	77,6
LEMS	49	12,0	1	25,9	26,0	21,7	89,8
PP	49	52,2	1	106,3	106,4	102,2	71,4
LT	49	58,3	1	118,6	118,7	114,4	67,3
AIS	49	36,3	1	74,7	74,8	70,5	87,8
tib. SSEPmax	49	61,7	1	125,4	125,5	121,3	67,3
tib. SSEPmin	49	62,1	1	126,2	126,3	122,0	65,3
NLI	49	66,4	1	134,7	134,8	130,5	53,1
Age	49	66,6	1	135,3	135,4	131,1	57,1
Sex	49	58,7	1	119,3	119,4	115,2	69,4
two predictors							
MS + UEMS	49	6,0	2	16,1	16,3	12,1	95,9
MS + LEMS	49	6,0	2	16,1	16,3	12,1	95,9
MS + PP	49	21,9	2	47,8	48,1	43,8	85,7
MS + LT	49	23,6	2	51,3	51,5	47,3	87,8
MS + AIS	49	23,7	2	51,4	51,6	47,4	89,8
MS + tib. SSEPmax	49	22,9	2	49,9	50,1	45,9	89,8
MS + tib. SSEPmin	49	22,0	2	48,0	48,3	44,0	87,8
MS + NLI	49	23,7	2	51,4	51,6	47,4	89,8
MS + Age	49	23,2	2	50,3	50,6	46,3	85,7
MS + Sex	49	19,8	2	43,6	43,9	39,6	89,8
UEMS + LEMS	49	6,0	2	16,1	16,3	12,1	95,9
UEMS + PP	49	44,0	2	92,0	92,3	88,0	75,5
UEMS+ LT	49	49,1	2	102,2	102,4	98,2	75,5
UEMS + AIS	49	34,2	2	72,4	72,7	68,4	87,8
UEMS + tib. SSEPmax	49	50,9	2	105,8	106,0	101,8	71,4
UEMS + tib. SSEPmin	49	49,6	2	103,2	103,5	99,2	69,4
UEMS + NLI	49	53,4	2	110,8	111,0	106,8	77,6
UEMS + Age	49	53,2	2	110,3	110,6	106,3	75,5
UEMS + Sex	49	42,8	2	89,6	89,8	85,6	79,6
LEMS + PP	49	9,5	2	23,1	23,3	19,1	93,9
LEMS + LT	49	10,3	2	24,5	24,8	20,5	93,9
LEMS + AIS	49	0,0	2	4,0	4,3	0,0	100,0
LEMS + tib. SSEPmax	49	7,8	2	19,5	19,8	15,5	95,9
LEMS + tib. SSEPmin	49	9,1	2	22,3	22,5	18,3	93,9
LEMS + NLI	49	11,6	2	27,2	27,4	23,2	89,8
LEMS + Age	49	11,9	2	27,9	28,1	23,9	89,8
LEMS + Sex	49	9,6	2	23,3	23,5	19,3	93,9
PP + LT	49	52,1	2	108,2	108,5	104,2	71,4
PP + AIS	49	32,2	2	68,5	68,7	64,5	87,8
PP + tib. SSEPmax	49	52,1	2	108,3	108,5	104,3	69,4
PP + tib. SSEPmin	49	52,0	2	108,1	108,3	104,1	71,4
PP + NLI	49	51,9	2	107,8	108,1	103,8	69,4
PP + Age	49	51,7	2	107,3	107,6	103,3	71,4
PP + Sex	49	48,4	2	100,7	101,0	96,7	77,6
LT + AIS	49	34,7	2	73,5	73,7	69,5	87,8
LT + tib. SSEPmax	49	56,7	2	117,4	117,6	113,4	69,4
LT + tib. SSEPmin	49	57,1	2	118,3	118,6	114,3	73,5
LT + NLI	49	58,0	2	120,1	120,3	116,1	67,3
LT + Age	49	55,9	2	115,8	116,1	111,8	69,4
LT + Sex	49	53,1	2	110,1	110,4	106,1	67,3
AIS + tib. SSEPmax	49	33,7	2	71,4	71,6	67,4	87,8
AIS + tib. SSEPmin	49	32,6	2	69,2	69,5	65,2	87,8
AIS + NLI	49	35,7	2	75,4	75,7	71,4	87,8
AIS + Age	49	35,3	2	74,6	74,9	70,6	87,8
AIS + Sex	49	29,6	2	63,2	63,5	59,2	89,8
tib. SSEPmax + tib. SSEPmin	49	61,4	2	126,8	127,0	122,8	67,3
tib. SSEPmax + NLI	49	61,1	2	126,2	126,5	122,2	65,3
tib. SSEPmax + Age	49	61,7	2	127,4	127,7	123,4	67,3
tib. SSEPmax + Sex	49	55,7	2	115,4	115,6	111,4	67,3
tib. SSEPmin + NLI	49	61,5	2	127,0	127,3	123,0	63,3
tib. SSEPmin + Age	49	62,1	2	128,1	128,4	124,1	65,3
tib. SSEPmin + Sex	49	54,6	2	113,2	113,5	109,2	69,4
NLI + Age	49	66,2	2	136,3	136,6	132,3	57,1
NLI + Sex	49	57,4	2	118,8	119,0	114,8	65,3
Age + Sex	49	58,6	2	121,1	121,4	117,1	69,4

Table 4.2. For legend, see next page.

subjects with paraparesis

WISCI II

model	N	-2 log likelihood	K	AIC	AICc	Δ AICc	% correct predicted
a priori							64,1
one predictor							
LEMS	39	42,2	1	86,5	86,6	12,8	66,7
PP	39	42,2	1	86,3	86,4	12,7	74,4
LT	39	48,7	1	99,4	99,5	25,7	66,7
AIS	39	50,3	1	102,6	102,7	29,0	64,1
tib. SSEPmax	39	42,0	1	86,1	86,2	12,4	71,8
tib. SSEPmin	39	44,8	1	91,7	91,8	18,1	66,7
NLI	39	49,4	1	100,9	101,0	27,2	64,1
Age	39	48,1	1	98,2	98,3	24,6	66,7
Sex	39	50,0	1	102,0	102,1	28,3	64,1
two predictors							
LEMS + PP	39	34,7	2	73,4	73,8	0,0	82,1
LEMS + LT	39	41,7	2	87,4	87,8	14,0	66,7
LEMS + AIS	39	35,3	2	74,6	74,9	1,1	76,9
LEMS + tib. SSEPmax	39	37,2	2	78,5	78,8	5,0	69,2
LEMS + tib. SSEPmin	39	39,1	2	82,2	82,5	8,7	74,4
LEMS + NLI	39	41,9	2	87,7	88,1	14,3	71,8
LEMS + Age	39	38,8	2	81,6	81,9	8,2	76,9
LEMS + Sex	39	39,3	2	82,6	82,9	9,1	71,8
PP + LT	39	40,6	2	85,2	85,5	11,7	74,4
PP + AIS	39	40,8	2	85,6	85,9	12,2	74,4
PP + tib. SSEPmax	39	36,7	2	77,4	77,8	4,0	79,5
PP + tib. SSEPmin	39	38,7	2	81,4	81,8	8,0	79,5
PP + NLI	39	42,1	2	88,3	88,6	14,9	71,8
PP + Age	39	40,2	2	84,5	84,8	11,0	74,4
PP + Sex	39	41,2	2	86,4	86,7	12,9	74,4
LT + AIS	39	48,3	2	100,5	100,8	27,1	69,2
LT + tib. SSEPmax	39	41,1	2	86,1	86,5	12,7	71,8
LT + tib. SSEPmin	39	43,7	2	91,4	91,8	18,0	69,2
LT + NLI	39	48,3	2	100,5	100,9	27,1	69,2
LT + Age	39	44,9	2	93,7	94,1	20,3	74,4
LT + Sex	39	47,4	2	98,8	99,2	25,4	69,2
AIS + tib. SSEPmax	39	41,9	2	87,7	88,1	14,3	71,8
AIS + tib. SSEPmin	39	44,5	2	93,0	93,3	19,6	69,2
AIS + NLI	39	48,8	2	101,7	102,0	28,2	64,1
AIS + Age	39	46,9	2	97,8	98,1	24,3	69,2
AIS + Sex	39	48,5	2	101,1	101,4	27,6	64,1
tib. SSEPmax + tib. SSEPmin	39	42,0	2	88,0	88,4	14,6	71,8
tib. SSEPmax + NLI	39	41,3	2	86,6	86,9	13,2	71,8
tib. SSEPmax + Age	39	41,7	2	87,3	87,6	13,9	71,8
tib. SSEPmax + Sex	39	41,7	2	87,5	87,8	14,0	71,8
tib. SSEPmin + NLI	39	44,5	2	93,0	93,3	19,6	69,2
tib. SSEPmin + Age	39	44,1	2	92,1	92,4	18,7	66,7
tib. SSEPmin + Sex	39	44,7	2	93,3	93,6	19,9	69,2
NLI + Age	39	45,8	2	95,6	96,0	22,2	71,8
NLI + Sex	39	49,1	2	102,2	102,5	28,8	64,1
Age + Sex	39	47,4	2	98,7	99,1	25,3	69,2

6minWT

model	N	-2 log likelihood	K	AIC	AICc	Δ AICc	% correct predicted
a priori							78,9
one predictor							
LEMS	38	25,4	1	52,9	53,0	8,6	89,5
PP	38	32,6	1	67,3	67,4	23,0	84,2
LT	38	35,1	1	72,2	72,3	27,9	84,2
AIS	38	35,9	1	73,8	73,9	29,6	78,9
tib. SSEPmax	38	37,7	1	77,4	77,6	33,2	78,9
tib. SSEPmin	38	34,5	1	71,0	71,2	26,8	78,9
NLI	38	38,7	1	79,4	79,5	35,2	78,9
Age	38	36,5	1	75,1	75,2	30,8	81,6
Sex	38	39,0	1	80,1	80,2	35,8	78,9
two predictors							
LEMS + PP	38	21,9	2	47,9	48,2	3,8	89,5
LEMS + LT	38	24,8	2	53,7	54,0	9,6	86,8
LEMS + AIS	38	21,9	2	47,8	48,2	3,8	89,5
LEMS + tib. SSEPmax	38	25,4	2	54,8	55,2	10,8	89,5
LEMS + tib. SSEPmin	38	23,8	2	51,6	52,0	7,6	86,8
LEMS + NLI	38	25,2	2	54,3	54,6	10,3	92,1
LEMS + Age	38	20,0	2	44,0	44,4	0,0	84,2
LEMS + Sex	38	24,7	2	53,5	53,8	9,4	86,8
PP + LT	38	32,6	2	69,2	69,5	25,2	81,6
PP + AIS	38	28,3	2	60,6	61,0	16,6	84,2
PP + tib. SSEPmax	38	32,4	2	68,8	69,2	24,8	84,2
PP + tib. SSEPmin	38	29,8	2	63,7	64,0	19,6	84,2
PP + NLI	38	32,4	2	68,8	69,1	24,7	81,6
PP + Age	38	30,2	2	64,4	64,7	20,3	89,5
PP + Sex	38	32,5	2	69,0	69,3	25,0	84,2
LT + AIS	38	32,7	2	69,5	69,8	25,4	84,2
LT + tib. SSEPmax	38	34,6	2	73,2	73,6	29,2	84,2
LT + tib. SSEPmin	38	31,8	2	67,7	68,0	23,6	86,8
LT + NLI	38	35,0	2	73,9	74,3	29,9	84,2
LT + Age	38	31,3	2	66,6	66,9	22,5	86,8
LT + Sex	38	34,7	2	73,4	73,7	29,3	84,2
AIS + tib. SSEPmax	38	34,8	2	73,7	74,0	29,6	78,9
AIS + tib. SSEPmin	38	31,4	2	66,8	67,2	22,8	86,8
AIS + NLI	38	35,6	2	75,2	75,6	31,2	78,9
AIS + Age	38	30,5	2	64,9	65,2	20,9	84,2
AIS + Sex	38	35,1	2	74,2	74,6	30,2	78,9
tib. SSEPmax + tib. SSEPmin	38	33,8	2	71,6	72,0	27,6	81,6
tib. SSEPmax + NLI	38	37,6	2	79,1	79,5	35,1	78,9
tib. SSEPmax + Age	38	36,0	2	76,0	76,3	31,9	81,6
tib. SSEPmax + Sex	38	37,7	2	79,4	79,8	35,4	78,9
tib. SSEPmin + NLI	38	34,5	2	73,0	73,4	29,0	78,9
tib. SSEPmin + Age	38	33,2	2	70,4	70,8	26,4	81,6
tib. SSEPmin + Sex	38	34,3	2	72,6	73,0	28,6	76,3
NLI + Age	38	35,8	2	75,6	75,9	31,6	81,6
NLI + Sex	38	38,7	2	81,4	81,8	37,4	78,9
Age + Sex	38	36,5	2	77,1	77,4	33,0	81,6

Table 4.2. Detailed results of logistic regression analyses are given for subjects with tetra- or paraparesis and both walking tests analyzed in this study. The predictive value of a model is measured by the -2log likelihood and *Akaike's information criterion* (AIC) corrected for small sample sizes (AICc). ΔAICc values enable direct comparison of different models in which models with ΔAICc values ≤ 2 can be regarded as equivalent. Results for all possible models are shown; e.g. for subjects with tetraparesis 11 or 55 models are possible when either one or two predictors are used, respectively. The best models are highlighted in grey. Abbreviations: number of subjects analyzed (N), number of variables in a model (K), ASIA motor scores (MS), lower and upper extremity motor subscores (LEMS and UEMS), light touch (LT), pin prick (PP), ASIA Impairment Scale (AIS), lowest and highest tSSEP score (tSSEPmin & tSSEPmax), neurological level of injury (NLI).

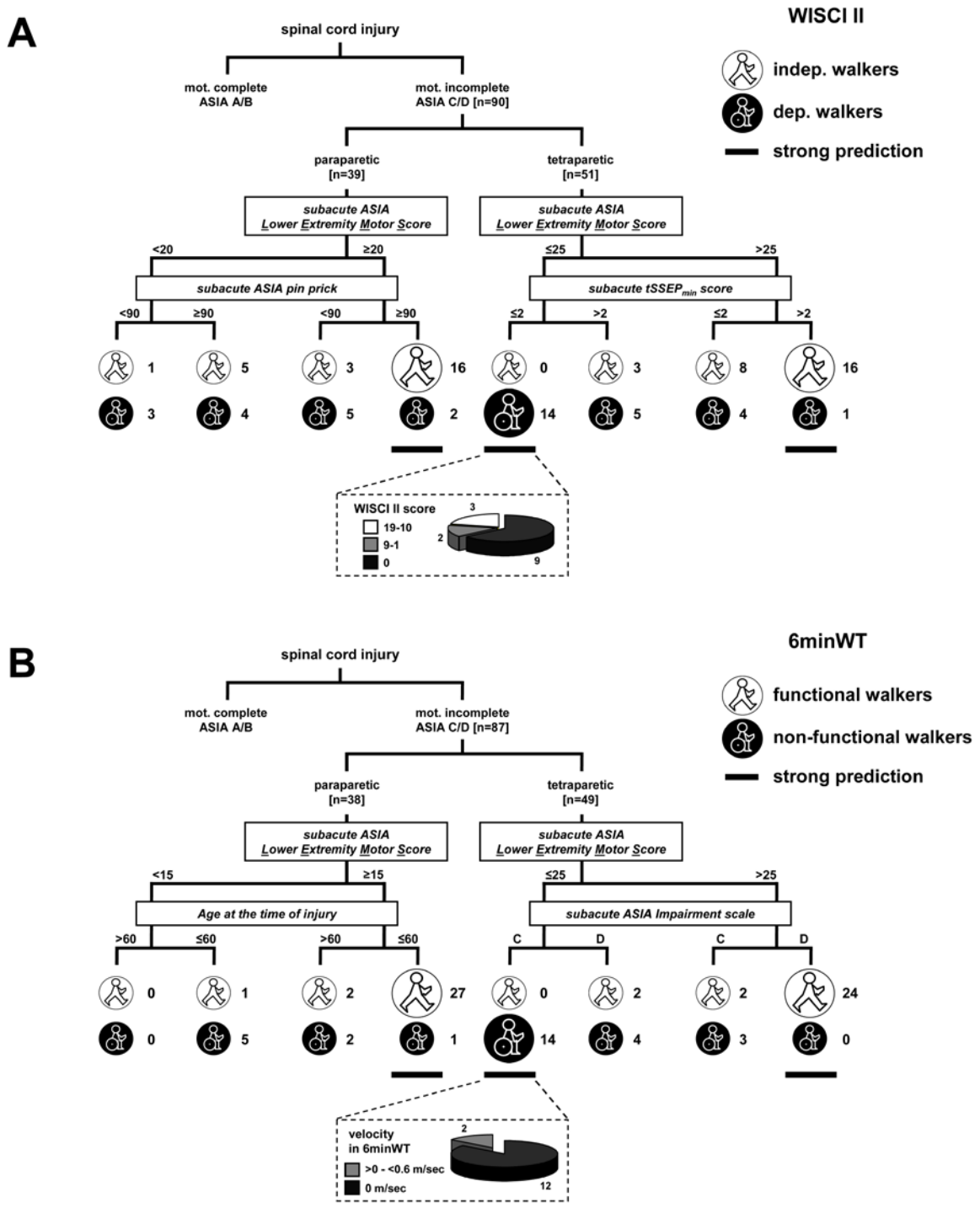

Figure 4.4. Proposed algorithm for predicting walking capacity by means of predictors obtained in the subacute phase after miSCI. Dichotomization of walking outcome was either based on the WISCI II (**A**) or the 6minWT (**B**) performed 6 months after injury. The main predictors and threshold values were separately identified in the logistic regression analysis for both walking tests and subjects with para- or tetraparesis. The likelihood of correct prediction of walking capacity is higher for subjects with predictor scores either above or below the threshold values (outer branches of trees for subjects with tetra- or paraparesis) with the exception of subjects with paraparesis and poor walking outcome (see also Table 4.1). The branches with strong prediction of walking outcome are indicated by a bold line at the bottom of the algorithms. For instance, it could be assumed that all subjects with tetraparesis and both predictor scores above the threshold would be able to walk independently 6 months after injury (**A**). This assumption is supported by the finding that 16 out of 17 subjects were in fact scored as "independent" walkers at this time (follow far right branch). Vice versa, the general assumption that subjects with tetraparesis and both scores below the threshold would need assistance for ambulation 6 months after injury, appears correct since all of the patients in this subgroup (14 out of 14) were indeed scored as "dependent" walkers. The insets show detailed WISCI II scores and walking velocity during the 6minWT for subjects with tetraparesis who did not recover "independent" or "functional" walking capacity and were revealed by the algorithms. These latter subgroups could be targeted for early intense rehabilitation and interventional treatments. Numbers indicate the amount of subjects categorized for each branch.

Outcome prediction in motor-incomplete spinal cord injury

A broad range of different factors such as neurological deficit, age, gender and electrophysiological measurements have been shown in previous studies to be closely related to functional outcome and, in particular, to walking ability after SCI[215,236-243]. The general characteristics of our patients, such as neurological level of injury, type of injury or gender (predominantly men), were similar to these studies, although the mean age of 47.3 years in this study was slightly higher. In the literature, the importance of early clinical examination for outcome prediction is highly emphasized[215,244,245]. Motor scores, in particular the LEMS, have been shown to correlate with and are predictive for ambulatory outcome[246,247]. Preserved PP sensation was shown to be associated with the recovery of motor function[237,248]. Studies on subjects with miSCI that assess the significance of combined clinical parameters to improve the predictability of ambulatory function do not exist. A comprehensive examination of this approach is, however, of importance. Nevertheless, it has to be taken into consideration that a combination of correlated predictors might not necessarily improve prediction as they might provide the same, possibly redundant information. Approaches using multiple correlations do not account for such redundancy. Therefore, we used multiple logistic regression, which is considered the gold standard for developing predictive models, in addition to multiple correlation analysis which is more commonly used in the literature[229-232]. Both types of analyses were performed independently from each other to demonstrate similarities and/or differences of the results. On the one hand, we found for subjects with tetraparesis that the LEMS was strongly correlated with the walking test outcome and was also identified by the logistic regression as the best single predictor for later walking performance demonstrating its importance for outcome prediction by two independent statistical approaches. On the other hand, the logistic regression approach revealed that improved prediction is not simply achieved by combining the two measures that show the strongest correlation with the walking tests outcome (see Figure 4.2 and Table 4.2). Logistic regression analysis followed by a ranking procedure (ΔAICc) provided the first evidence that the combination of the LEMS with another predictor such as PP, tSSEP, AIS or age considerably increased outcome prediction in miSCI. The importance of tSSEP for walking outcome prediction can be explained by the fact that tSSEPs provide information about the functional integrity of the dorsal columns, which is crucial for movement control and locomotion. However, why tSSEPs were more predictive than LT remains debatable. Stimulation of both proprioceptive and exteroceptive afferent fibers contribute to the tSSEP signal while the LT gives only information about exteroception. Although subjective responses to LT are likewise dependent on posterior cord function, tSSEP recordings might be more objective and more sensitive to

subtle nerve fiber damage[223,240]. In addition, LT represents rather gross measures with only 3 levels of discrimination.

For outcome prediction, in particular for the 6minWT, it has to be emphasized that usually 90% of the subjects were already correctly categorized by using only the LEMS as a classification parameter, except for subjects with paraparesis in the WISCI II based analysis (only 67%), indicating that the contribution of the second predictor in the combined models was minor but nevertheless significant. This can be explained by the inherent properties of this approach, i.e. the first predictor in the model accounts for most of the outcome variability whilst the contribution of the second variable is typically smaller. However, using only the strongest predictor, the LEMS, in the algorithms led to a less homogenous distribution of "independent or functional" and "dependent or non-functional" walkers in the branches of the algorithms that suggest either a favorable or unfavorable outcome (algorithms not shown). In addition, the presented algorithms can easily be reduced to a one-predictor-algorithm, if required, by simply summing the numbers of subjects with either good or poor outcome for each branch generated by the additional predictor.

The result of the 6minWT based analysis which demonstrated that the best model for outcome prediction in subjects with tetraparesis combined LEMS and AIS might be surprising since for both scores examination of the strength of defined key muscles is crucial but, however, rated and evaluated very differentially (see ASIA standards[214]). Adding information about whether more than half of the key muscles below the NLI have a muscle grade $< \text{or} \geq 3$ (AIS) to the sum of the grades of the lower extremity key muscles (LEMS) increased the percentage of correctly classified subjects from 90 to 100%.

As reported previously by others[249], we found that outcome prediction was less successful in subjects with paraparesis, in particular for those with poor functional outcome, than in individuals with tetraparesis. This suggests that other factors not investigated in this study might be crucial for prediction of ambulatory capacity in subjects with paraparesis. Additional measurements, such as motor evoked potentials or MR-imaging, for which a prognostic value has been demonstrated[247,250-254] might be included in further studies to improve prediction in individuals with paraparesis.

The decision to convert the walking test outcome into a dichotomous outcome measure ("dependent" vs. "independent" walkers or "non-functional" vs. "functional" walkers) might oversimplify the complexity of the recovery pattern of walking after miSCI. However, it was used because it is simple and obvious to both patients and clinicians. In addition, the goal of the study was not to describe precisely the course and outcome of

subjects after SCI; instead we aimed for a rather abstract approach that guides outcome prediction and allows simple stratification of subjects with incomplete SCI. The final decision to include or exclude a subject from a clinical study is usually either positive or negative and ultimately dichotomous; that is, at some point in the recruitment process for a clinical trial data reduction has to take place. In this study, two different walking tests were used as outcome measures describing and evaluating different characteristics of the subject's walking capability after SCI. Both are widely applied and accepted in SCI rehabilitation centers. Selection of one of these walking tests as a primary outcome measure as well as the corresponding threshold depends on the aim of a given clinical trial or the type of outcome prediction a clinician wants to make. Nevertheless, there was a high correlation between both walking tests, at least for subjects with tetraparesis, and results of the logistic regression analyses were highly similar for both tests.

Time window for acquisition of predictive data

The time point of predictor assessment is of particular importance with respect to clinical care and trials[255]. Here, we chose the subacute post-injury phase (16 - 40 days after injury) for data collection, since clinical measurements are considered very reliable at 1 month after injury[215]. We acknowledge that in several translational studies predictive measures need to be obtained at earlier time points (< 16 days) as therapeutic interventions might start early (3 - 14 days) or almost immediately (1 - 2 days) after trauma[4]. Since SSEP recordings are less dependent on the active cooperation of the patient and even feasible during surgery, they might be applicable at early time points after injury as objective and reliable predictors in miSCI[223,256-260]. A similar approach represents motor evoked potentials (MEPs) where initial assessments can either be performed in awake and cooperative patients or under anesthetics as developed for intraoperative monitoring[259,260].

Patient stratification for clinical trials in motor-incomplete spinal cord injury

In accordance with the literature, the majority of the subjects with miSCI in this study showed excellent spontaneous recovery of walking function[228,239,261-263]. However, the high standard deviations for walking test results should be noted as they challenge the execution of clinical trials in miSCI[3]. After simple randomization, putative treatment effects might be diluted by large within-group variability. Posthoc statistical analysis of subgroups that compensates for outcome variability is considered problematic with respect to bias and the guidelines of good clinical practice[263]. A better strategy might involve early patient stratification by using in- and

exclusion criteria that are strong predictors of functional outcome[255]. However, only a limited number of predictors can be considered in the study design since a large amount of exclusion criteria might hinder patient recruitment and reasonable sample sizes. To avoid expensive and time-consuming screening protocols, combinations of a few potent and complementary predictors are required for efficient patient stratification. We demonstrated that only two predictors are required to achieve 92-100% of correct predictions in subjects with tetraparesis. Adding a third predictive measure resulted in either no or only a small increase in correct predictions (not shown) but would however amplify the number of patient sub-groups, each with reduced sample sizes, in a clinical trial. An advantage of our approach is that the thresholds in the two proposed algorithms were based on clinical data and not theoretical assumptions. For the WISCI II based classification, using LEMS and tSSEP as predictors, the algorithm selected 14 of 24 subjects with tetraparesis and poor functional outcome; nine of these scored 0 on the WISCI II scale. The 6minWT based algorithm, gathered 14 from 21 non-functional walkers with tetraparesis. We suggest that these subjects with miSCI would be suitable for interventional clinical trials aiming at functional improvement through the enhancement of neural repair and plasticity[20,264]. Clearly, this approach affects patient recruitment since only 1/3 of the subjects with tetraparesis would be eligible trial candidates. However, the classification system promises a more homogenous study population and a higher sensitivity with respect to potential treatment effects.

Study limitations and perspectives

A limitation of the present study is that we have focused on the first 6 months after injury and thus further improvement of walking function might occur after this time period[265]. Long-term follow up studies are required to confirm these results. Furthermore, future investigations should attempt to improve the predictability of other outcome measures, which are important for activities of daily living[266]. A possible divergent outcome of patients with specific clinical SCI syndromes, e.g. central cord or Brown-Séquard syndrome, was not addressed. The Brown-Séquard syndrome was shown to have the best outcome prognosis with regard to walking capacity after injury[267]. In addition, we did not distinguish between subjects affected by traumatic or non-traumatic SCI. Although the initial neurological deficits and the general course of functional recovery were shown to be similar[268-270], however, we cannot exclude that the value of individual predictive measures for reliable outcome prognosis differs between the two patient groups. Future perspectives include the validation of the algorithm by applying the classification system to other miSCI populations.

Conclusion

The prediction of walking outcome after miSCI is improved by combining different measures obtained in the subacute phase after injury. The proposed clinical algorithms represent a method to enable an early patient stratification for clinical trials in miSCI. However, this approach needs further confirmation in independent patient cohorts.

Chapter 5

Basic mechanisms of functional recovery in multiple sclerosis

Björn Zörner and Martin E. Schwab

Brain Research Institute, University of Zurich and Dept. of Health Sciences and Technology, ETH Zurich, Zurich, Switzerland

The original article was published in *Kesselring, Comi and Thompson, Multiple Sclerosis: Recovery of Function and Neurorehabilitation,* Cambridge University Press, 2010 (44-52).

Author contributions

BZ wrote the manuscript. MES revised the manuscript.

5.1. Introduction

In multiple sclerosis (MS), inflammatory and immuno-mediated processes cause local destruction of glial and neuronal components of the central nervous system (CNS). Accordingly, MS is a chronic inflammatory and neurodegenerative disorder. Symptoms in patients are due to the formation of disseminated focal lesions or so-called MS plaques in the gray and white matter of the brain and spinal cord. Neuropathological characteristics of such lesions are destruction of oligodendrocytes, demyelination of axons, axon degeneration, axon loss and neuronal damage[271,272]. Functional impairments during the inflammatory episodes and subsequent irreversible neurological disabilities are due to variable degrees of nervous tissue damage and differentially affected cell types, but neither clinical nor pathological criteria are currently predictive of the extent of recovery during the course of MS. Nevertheless, recession of the causative pathological processes, repair of and substitution for damaged nervous tissue as well as substantial compensatory reorganization of neuronal networks are thought to be strategies utilized by the CNS to re-establish function.

For the development of effective therapies it is essential to understand MS etiology, pathology and, in particular, endogenous recovery strategies. It is likely that the fundamental mechanisms responsible for functional recovery from lesions associated with diseases such as MS or traumatic CNS injuries share common characteristics. Therefore, in this chapter we summarize recent concepts of functional recovery after CNS damage focusing on insights obtained from animal models and human studies of demyelinating disorders and traumatic injuries to the CNS.

5.2. Recession of pathophysiological processes

Local inflammatory activity has been linked to the emergence and remission of many of the functional impairments in MS patients. Local endothelial damage due to inflammation or mechanical stress causes breakdown of the blood-brain barrier (BBB). Increased BBB permeability can impede neuronal function through a number of mechanisms. Extravasation of fluid leads to myelin swelling, edema formation, tissue compression and metabolic disturbances. Therefore, restitution of BBB integrity and subsequent edema resolution can contribute to improvements observed in the acute phase of recovery.

A short-lasting, reversible inhibition of axonal impulse conduction can be observed in MS patients and after traumatic CNS injury, e.g. spinal cord injury, and is associated with transient neurological symptoms in patients. The underlying mechanisms leading to

conduction block and its disappearance are currently unknown, however a potential role for nitric oxide, several cytokines and ionic disequilibrium has been postulated[273,274].

5.3. Repair of damaged nervous tissue

In rodent models of experimentally induced demyelination, significant spontaneous remyelination can be observed three weeks post-lesion[275]. By contrast, spontaneous myelin repair in humans is limited and often restricted to the margins of lesions. However, in MS patients, a few areas of extensive remyelination can be found in the white matter. These remyelinated regions, referred to as shadow plaques, are sharply circumscribed and characterized by thin myelin sheets and gliosis[276]. In addition to remyelination, the compensatory reassembly of sodium channels along demyelinated axons can contribute, at least partially, to functional recovery in the subacute phase after injury[277]. A prerequisite for remyelination is the availability of axon-myelinating oligodendrocytes at the site of the lesion. Thus, one line of experimental therapeutic attempts to enhance remyelination currently focuses on optimizing the recruitment of endogenous oligodendrocytes or their precursors[278]. A second approach is based on cell transplantation strategies which will be discussed below.

5.4. Replacement of lost nervous tissue

Permanent functional deficits seen in progressive MS or following traumatic CNS injury have been ascribed to irreversible neuronal and axonal degeneration. Encouragingly, recent findings in stem cell research suggest that some replacement of lost or degenerated cells by newly born cells might be feasible at least in some regions of the adult CNS. Multipotent neural stem cells reside especially in specific germinal regions in the brain including the subventricular zone of the lateral ventricles and the subgranular zone of the hippocampal dentate gyrus[279,280]. In addition, in other parts of the CNS, e.g. the spinal cord, dividing cells which show *in-vitro*-multipotency are also present[281]. These endogenous stem cell pools are a potential source of cellular replacement following injury[282,283]. After induction of local axon demyelination in the CNS of adult rats endogenous progenitor cells were shown to proliferate and to differentiate into mature oligodendrocytes which have the ability to remyelinate axons[278]. Increased proliferation of progenitor cells as well as migration of these cells from germinal regions towards lesioned areas has been reported after CNS injury in various animal models[284,285]. However, it is evident clinically that after severe insults newly generated cells derived from endogenous stem cells are insufficient to compensate entirely for lost CNS tissue.

Transplantation of embryonic or adult stem cells has been considered as an alternative strategy to substitute for damaged CNS tissue[286]. Despite promising results obtained in animal studies, where migration and differentiation of transplanted stem cells has been demonstrated, this approach faces a number of key challenges and safety issues with regards to clinical translation[283,286,287]. Crucial prerequisites for successful transplantation in human trials include identification of the most appropriate stem cell type and transplantation paradigm; adequate cell survival and immunological tolerance by the host tissue, precise control of proliferation and region-specific differentiation of grafted cells. In multifocal CNS diseases, such as MS, the feasibility of multiple stem cell injections into lesion sites is limited. Systemic applications of cells into the blood-stream or the cerebrospinal fluid might overcome this problem[287,288]. Whether these cells are eventually able to migrate to their appropriate target tissue ("specific homing") or become distributed to other organs is an open question. In addition, many underlying mechanisms for the reported beneficial effects are unknown; for example grafted stem cells could act as a source of trophic factors or differentiate into glial cells or neurons which might be integrated into neuronal networks. Finally, it should be considered that only a few studies have conclusively demonstrated that effects observed following transplantation are directly linked to functional recovery[289,290]. Therefore, whereas pharmacological manipulation of endogenous stem cell pools or transplantation of stem cell grafts might provide therapeutic options in the future, more basic research in this field is required before clinical application becomes safe and feasible.

5.5. Regeneration of damaged axons

A strict definition of "successful axonal regeneration" might include the following: the lesioned axon has (1) to form growth cones and sprouts close to the transection site; (2) to elongate long distances past the lesion and to reach the denervated areas; and (3) to be integrated into functional neuronal circuitries (Figure 5.1 A-C). Since central networks can be plastic and undergo structural adaptations that contribute to functional recovery after CNS lesion (see below), one has to consider that the original local circuitries might experience major changes before re-growth of axons is accomplished.

Axonal damage is a common feature in MS and traumatic CNS injury

In MS, injured axons are not only present within, and adjacent to, the plaques but can also be found in normal-appearing white matter[291]. The precise mechanisms involved in axonal damage in MS are not well understood, whereas processes following traumatic injury have

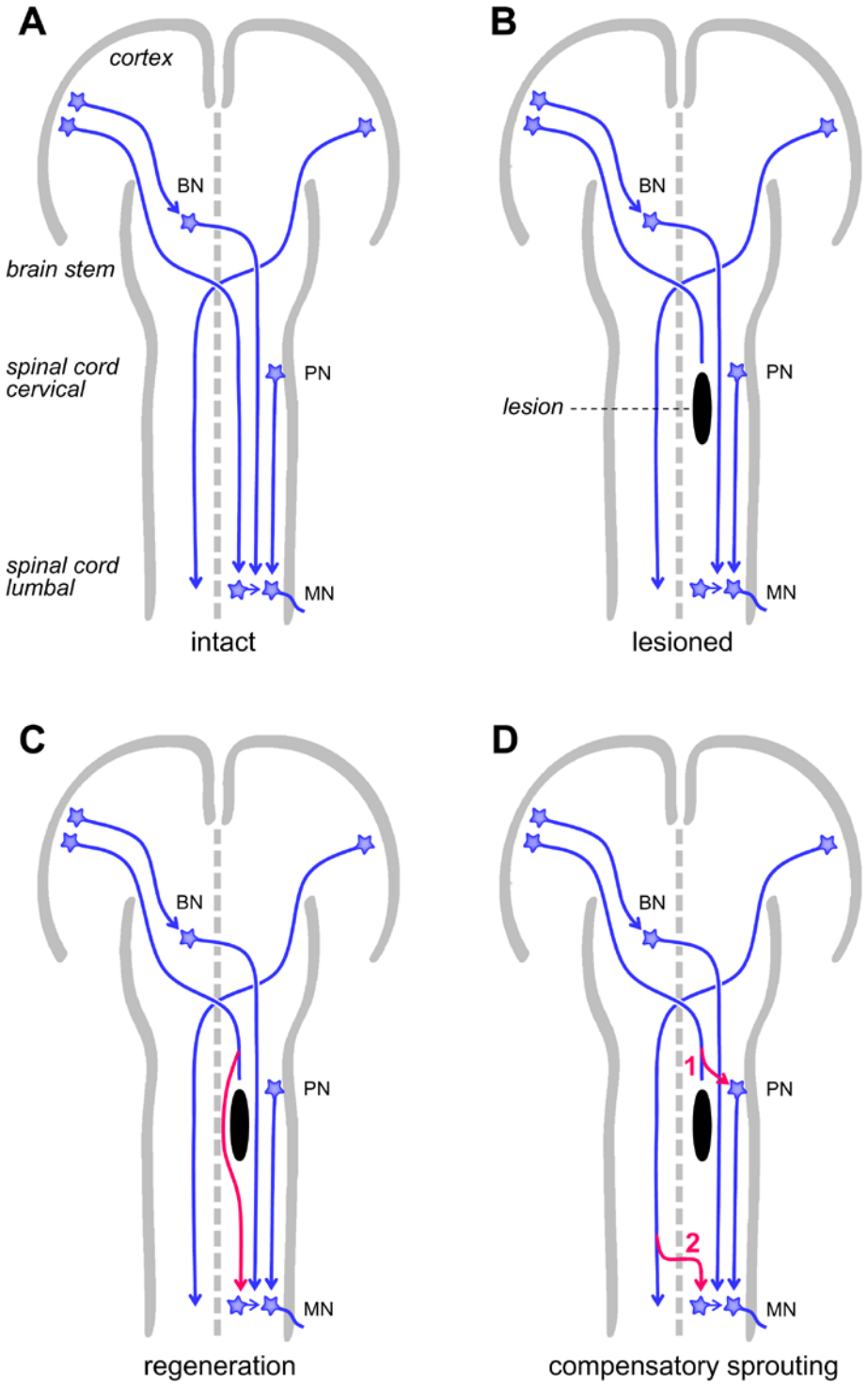

Figure 5.1. Focal damage to the corticospinal tract (CST) in the adult CNS leads to compensatory anatomical changes which are accompanied by functional recovery after injury. Neurons in the cortex, brainstem and propriospinal interneurons project to spinal circuitries in the lumbar spinal cord and are important for hind limb control (**A**). After selective transection of hind limb CST fibers at the midthoracic level of the spinal cord, spontaneous regeneration of lesioned fibers is restricted by growth-inhibitory factors in the adult mammalian CNS, but some control of hind limb function is maintained via spared bulbospinal and propriospinal pathways (**B**). Application of antibodies against the growth-inhibitory protein Nogo-A promotes regeneration of the injured axons. Lesioned fibers show enhanced regenerative sprouting rostral to the lesion site and are able to bypass it to re-innervate lumbar circuitries (**C**). In addition, damaged axons can spontaneously form detour pathways by contacting spared descending propriospinal interneurons rostral to the lesion site which relay cortical control to lumbar neuronal networks (**D**, 1). After Nogo-A neutralization, intact contralateral CST fibers show collateral sprouting at spinal levels, cross the midline and contact lumbar motoneurons and interneurons in the partially deafferented hemicord (**D**, 2). BN, brainstem neuron; PN, propriospinal (inter)neuron; MN, motoneuron.

been characterized in more detail[37]. After transection, central axons undergo a series of time-dependent modifications. In the acute phase after lesion the proximal part of the axon retracts up to several millimeters, a process referred to as “axonal die back”, eventually resulting in the formation of a retraction bulb. The section of the axon separated from its cell body is subject to Wallerian degeneration. Interestingly, lesioned central fibers can show a transient growth response which is associated with the upregulation of cytoskeletal and growth-associated proteins (e.g. GAP-43) in injured cell bodies[292]; however, this response subsides after 7-14 days[37]. Axons can form growth-cone like structures at the lesion site, but are not capable to grow beyond it, illustrating the limited potential of axons to regenerate in the adult mammalian CNS[37]. Therefore, in contrast to the situation in the peripheral nervous system or during CNS development, regeneration of axons has traditionally not been considered to contribute to functional recovery after CNS injury[293]. Given that premise, several questions arise such as, why do central axons fail to regenerate? What are the underlying mechanisms of this failure? And, how can we, by inducing axonal regeneration, improve functional recovery after CNS injury?

First insights into the answers for these questions arose from experiments performed by Tello in 1911 and Aguayo in the early 1980s suggesting that adult central neurons have some regenerative potential[293,294]. In adult rabbits or rats, peripheral nerve grafts were transplanted into the CNS, e.g. the cortex or spinal cord. Axons that entered the graft grew over long distances, i.e. several centimeters, thereby demonstrating that damaged central axons are able to re-grow in the presence of a growth-promoting environment. Thus, growth inhibitory factors were postulated to be present in the adult CNS[65]. Components of central myelin were found to impede axonal outgrowth and, eventually, the existence of myelin-associated, growth-restricting proteins was demonstrated[66]. Antibodies raised against the most important one of these, Nogo-A, were shown to block its inhibitory activity *in vitro*[67] and to promote axonal regeneration *in vivo*[24,36] (Figure 5.2 A,B). To date, 6-8 additional molecules with some neurite growth-restricting properties *in vitro* have been identified[79,295-297]. This group of central growth inhibitors comprises Ephrins, Semaphorins, Proteoglycans and myelin proteins such as MAG (myelin-associated glycoprotein) and OMgp (oligodendrocyte myelin glycoprotein). Whether axonal regeneration can be induced by blocking these molecules *in vivo* is still unclear[298].

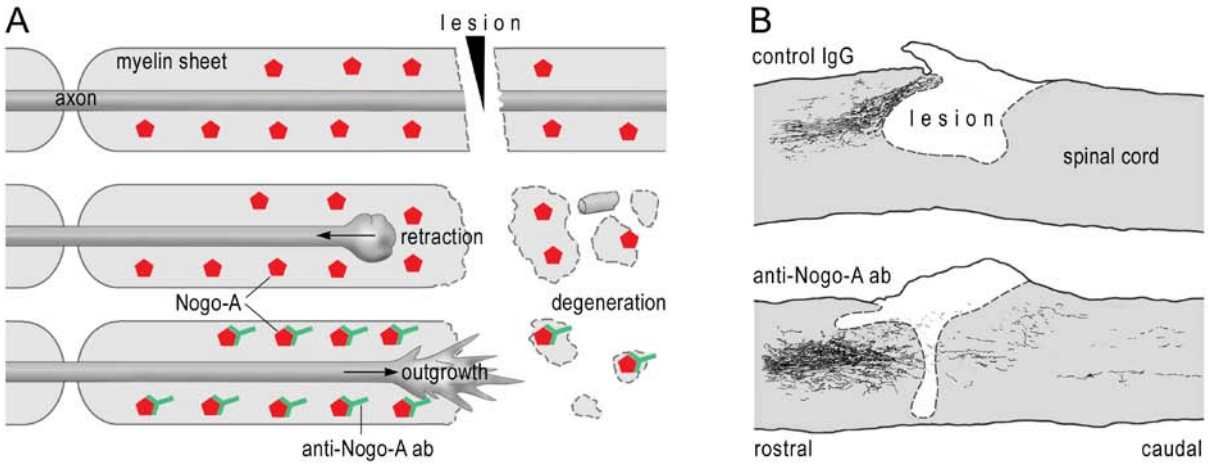

Figure 5.2. Treatment with anti-Nogo-A antibodies after CNS injury promotes axonal regeneration *in vivo.* (**A**) The growth-inhibitory protein Nogo-A is expressed mainly by oligodendrocytes which form the myelin sheets surrounding central axons. Nogo-A signaling leads to retraction of the proximal section of the axon which is still connected to its cell body whereas the separated distal section undergoes Wallerian degeneration. Application of Nogo-A neutralizing antibodies leads to the formation of growth cones and axonal outgrowth after CNS lesion. (**B**) After experimental spinal cord injury in rats, anti-Nogo-A antibodies delivered via an intrathecal catheter induce regenerative sprouting and long-distance elongation of lesioned CST fibers (labeled in black) whereas axonal regeneration is absent after treatment with control antibodies. Regenerating fibers bypass the lesion site in spared tissue bridges and extend caudally on an irregular course up to 5 millimeters in the spinal cord as demonstrated by camera lucida reconstructions of the spinal cord. In addition, massive sprouting of CST fibers and growth cone formation rostral to the lesion site can be observed in anti-Nogo-A antibody-treated animals. The growth response after blocking Nogo-A signaling was accompanied by substantial functional recovery in several behavior tests. Adapted with kind permission from Annals of Neurology (2005) Vol.58, No 5, pp. 706-719, copyright (2005) Wiley-Liss, Inc.

The Nogo-A signaling pathway

The transmembrane protein Nogo-A is expressed predominantly on the surface of oligodendrocytes and some subpopulations of central neurons[69-71,73]. Growth-inhibition is attributed to at least two regions within the Nogo-A protein; one located close to the C-terminus, the so-called Nogo-66 region, and the other termed the Nogo-A specific domain[76]. Nogo-66, present in all Nogo-isoforms, exerts its inhibitory potential via a specific binding site in the neuronal membranes, the Nogo-66-receptor (NgR)[75,77]. Interestingly, binding of MAG and OMgp to NgR has also been demonstrated *in vitro*[78,79]. For signal transmission NgR interacts with several co-receptors (Lingo-1, TROY and the low-affinity neurotrophin receptor p75) leading to activation of the small intracellular GTPase RhoA[27,299]. Downstream targets of RhoA, which eventually transmit the growth inhibitory signal to the cytoskeleton and induce growth arrest and growth cone collapse, are kinases like ROCK and LimK and the actin-binding protein Cofilin[87,88]. Enhanced axonal regeneration accompanied by functional improvements has been reported after *nogo* gene deletions (Nogo-A-KO mice)[100], blockade of different components of the Nogo-66-receptor-complex[89,92] and downstream messengers in rodent models of spinal cord injury[96].

Effects of Nogo-A inactivation after CNS injury

For blocking Nogo-A activity *in vivo,* monoclonal antibodies against Nogo-A can be applied to the cerebrospinal fluid. These antibodies bind to and mask their molecular targets and are, together with Nogo-A, then internalized from the cell surface decreasing the Nogo-A tissue levels[94]. By using this approach in different animal models of CNS injury enhanced regenerative sprouting and fiber growth has been demonstrated and was shown to be closely associated with enhanced functional recovery[31,32,36] (Figure 5.2 A). For example, after transection of the corticospinal tract (CST) at thoracic level, adult rats were either treated with anti-Nogo-A or control antibodies[31]. Motor recovery was tested in various behavior tasks at different post-lesional time points. Sensory testing demonstrated that there were no severe malfunctions such as hypersensitivity or increased pain which might be a result of aberrant fiber sprouting. Animals which received a Nogo-A neutralizing antibody showed a faster and more complete hind limb motor recovery, e.g. during running over a horizontal ladder or a narrow beam, but also of precision movements, e.g. skilled reaching, while pain and allodynia were absent[31,32]. Quantification of regenerative sprouts rostral to and regenerated fibers caudal to the lesion site revealed a massive increase of CST branches and fibers in anti-Nogo-A antibody-treated animals. Most importantly, profound long-distance regeneration of lesioned CST axons was only present after Nogo-A neutralization. By using spared tissue bridges as scaffolds, these fibers grew irregularly around the lesion site, elongated and arborised up to 5 millimeters caudal to the lesion (Figure 5.2 B). Similarly, a proof-of-concept study in adult macaque monkeys demonstrated that application of anti-Nogo-A antibodies delivered intrathecally over a period of four weeks after unilateral cervical spinal cord injury resulted in enhanced recovery of manual dexterity and was found to promote re-growth of CST fibers. Again, CST axons bypassed the lesion site and grew into the denervated hemicord[32]. These pre-clinical findings implicate a major role for Nogo-A Nogo-receptor signaling in restriction of neurite regeneration and neuronal plasticity in the adult CNS and suggest what remains to be proven in the currently ongoing clinical trials: Nogo-A neutralization might be a novel medical strategy to enhance axonal regeneration in humans with the potential to substantially alleviate the patients' suffering from CNS injury.

5.6. Reorganization and neuronal plasticity in damaged and spared systems

Cortical neuronal networks and representational maps are subject to permanent modifications in the adult CNS[48,300]. After injury, compensatory adaptations in intact and damaged neuronal networks have been shown to contribute to functional recovery[20,108,301]. The potential of the

CNS to change and adapt is described as “neuronal plasticity”. Neuronal plasticity can occur at different levels ranging from intracellular to neuroanatomical alterations. Modifications of synaptic transmission include changes in neurotransmitter release, receptor number and function, and second messenger cascades. Activity-dependent changes in synaptic strength can be short- or long-lasting. Long-term potentiation (LTP) and long-term depression (LTD) are examples of activity-dependent alterations in synaptic connectivity important for memory formation. It has been suggested that synaptic plasticity and changes in the balance between inhibition and excitation in cortical horizontal connections, i.e. connections between neurons in different subregions of the motor cortex, are responsible for rapid reorganization of cortical maps after lesion[47]. Single synapses or entire dendritic spines can be newly generated, remodeled or eliminated[302]. Finally, whole neuronal circuitries have been shown to be plastic. Anatomical or structural plasticity involves sprouting, outgrowth and pruning of axonal or dendritic processes leading to the reorganization and formation of new networks.

Spontaneous anatomical plasticity at different CNS levels has been extensively documented in animal models of spinal cord injury and stroke and is thought to be a major mechanism accounting for functional improvements at later stages in the recovery process[47,108]. Neutralization of the growth-inhibitory protein Nogo-A facilitates axonal outgrowth, compensatory sprouting of lesioned and intact fibers and anatomical rearrangements after CNS injury[23,116]. Axons lesioned at the midthoracic level of the spinal cord, which ordinarily project to the lumbar spinal cord, can show spontaneous collateral sprouting into the cervical spinal cord[40]. Such sprouts can contact unlesioned propriospinal neurons, which bypass the lesion site, and form functional detour pathways. Formation of detour circuits was observed after traumatic spinal cord injury and in MS models, i.e. EAE[12,39]. In the presence of Nogo-A blocking antibodies collateral sprouts of lesioned axons cross the midline at the brainstem level to innervate contralateral nuclei[119]. Therefore, injured neurons are able to retain motor control by collateral sprouting and the formation of new supraspinal and intraspinal circuits relaying cortical input to spinal targets (Figure 5.1 D). In addition, reactive collateral sprouting after CNS injury is present in spared fiber tracts. Following unilateral stroke or transection of CST fibers and anti-Nogo-A treatment, contralateral unlesioned CST fibers sprout and cross the midline at spinal levels to innervate the deafferented hemicord. These midline-crossing fibers show topographically appropriate innervation patterns and are functionally integrated into local spinal circuitries indicated by improved behavioral outcome[23]. After stroke, neurons of the intact cortex form new axonal projections to contralateral subcortical targets, e.g. the striatum or the red nucleus, resulting in

a bilateral corticofugal innervation pattern[101,118,121,303]. These findings suggest that descending projections emanating from cortical regions contralateral to the lesion site are able to compensate for functions lost due to injury (Figure 5.1 D). How far activity drives these changes, e.g. by training of the impaired limb, is currently subject of intense investigation.

Several descending fiber tracts are important for motor functions, i.e. the corticospinal, rubrospinal, vestibulospinal and reticulospinal system as well as serotonergic and dopaminergic projections from the brainstem. Each system is considered to be partially specialized for motor control, whereby some degree of functional overlap and parallel processing can be assumed. Both the red nucleus and the motor cortex share common features with regard to target neurons in the spinal cord and also function, i.e. control of skilled movements. Interestingly, after bilateral CST transection, rubrospinal projections sprout into deafferented spinal regions in the presence of Nogo-A neutralizing antibodies and this is correlated with functional recovery[110]. This demonstrates that parallel, anatomically separate systems are able to compensate, at least partially, for the loss of another system. One could hypothesize that re-learning of motor tasks in the rehabilitation phase after CNS injury is partially based on the functional switch between neuronal systems. In patients, physical training during rehabilitation is crucial and might contribute to activity-dependent fine-tuning of newly formed neural circuitries.

Here, we have emphasized that ample evidence has been provided for anatomical reorganization of neuronal networks in the cortex, subcortical systems and in the spinal cord after CNS injury in animals. Studies performed in MS and stroke patients using functional magnetic resonance imaging or transcranial magnetic stimulation techniques have demonstrated that functionally relevant adaptive changes and processes of reorganization can also occur in the human CNS[59,304]. However, patients with large or progressive CNS lesions often show only limited functional recovery, a clinical observation which might be explained by the “concept of reserve capacity”[39]. According to this, functional recovery continues as long as a sufficient number of plastic pathways exist that are capable of functionally compensating for lost neurons or entire neuronal networks. By enhancing the plastic potential of the CNS, e.g. by suppression of growth-inhibitory proteins like Nogo-A, and by the incorporation of additional neuronal networks in the recovery process, new therapeutic approaches might be able to increase the endogenous reserve capacity.

5.7. Conclusion

Recession, repair, replacement, regeneration and reorganization are basic repair strategies of the adult CNS in order to achieve functional recovery after injury. It is not only the absolute number of neurons and fibers spared or repaired after lesion that accounts for functional outcome, but the capability of the CNS to adapt, reorganize and establish new neural networks that also play a key role in functional improvements. Knowledge about spontaneous mechanisms of functional recovery is crucial for the identification of therapeutic targets and for the development of new therapies. Interventions can support the recovery process but could also interfere with inherent mechanisms of recovery. Therapies that have proven efficient in animal models face the hurdle of secure translation to human patients, but recent progress in this field gives hope that we will be able to substantially support the damaged CNS in its efforts to repair itself in the future.

General discussion and outlook

The phenomenon of midline crossing fibers after CNS injury and its implications for neurorehabilitation

Corticospinal fibers cross the spinal cord midline after pyramidotomy[19,42] and spinal hemisection[18] in rats. Corticofugal fibers traverse the midline at the level of the pons in the brainstem following pyramidotomy and neutralization of the neurite growth inhibitor Nogo-A[119]. As described in ***Chapter 3***, we found that also reticulospinal fibers spontaneously cross the midline of the spinal cord after cervical hemisection injury in rats. The increase of midline crossing fibers correlates with improved functional outcome after lesion. However, a direct causal link between these anatomical changes and improved function has not yet been demonstrated mainly due to methodological limitations. Previous restrictions may be overcome in the future by using novel innovative approaches, for example two-photon excitation microscopy and optogenetics or other genetic engineering techniques allowing for selective activation and inactivation of neurons crossing the CNS midline in an awake behaving animal[305].

Nonetheless, an increased number of midline crossing fibers was found in different CNS regions and after different types of lesion[18,19,42,47,119]. Axons sprouting over the CNS midline can originate from anatomically and functionally different subpopulations of neurons. Therefore, increasing the number of midline crossing fibers may represent a common mechanism of the adult CNS to restore function after injury. To become functionally relevant, midline crossing axons have to pass through several stages: first, collaterals of spared projecting fibers sprout and grow over the CNS midline; second, having arrived on the other side, collaterals branch and grow towards their (appropriate) target neuron(s); third, axon terminals establish synaptic contacts with their target(s); finally, inappropriate connections on both sides of the CNS are pruned. In analogy to processes in the developing CNS such as the formation of the pyramidal decussation or commissural projections, each of these steps may be tightly regulated in space and time by an interplay of attractive and repellent factors[199,306]. During development, growth cones of crossing neurons are guided by various long- and short-range cues[199,306] like Netrins[307,308] and Slit[309] as well as Semaphorins[310] and Ephrins[311,312]. However, only little information is available on the factors and receptors guiding axons across the midline in the adult and injured CNS[19,199]. Results in young mice indicate that ephrin-B3-

EphA4 signaling is important for corticospinal axons that (re-)cross the CNS midline in the ventral spinal cord after unilateral ablation of the motor cortex[200].

In contrast to the precisely regulated growth and guidance machinery in the developing CNS, instead, lesioned and unlesioned fibers may also sprout in a rather chaotic way, in particular, at an early time point after CNS damage[313]. Here, sprouting could be induced by growth-promoting factors rashly up-regulated in response to the lesion. A temporary rank growth of collaterals, *inter alia* across the midline, could initially lead to the formation of numerous random connections between neurons. This first "cluttered" reaction may be followed by a second, activity-dependent selection phase characterized by pruning of unnecessary and stabilization of useful connections.

Certainly, the molecular mechanisms underlying the phenomenon of midline crossing fibers in the adult and injured CNS require further investigations using *state-of-the-art* techniques like transcriptomics, proteomics and metabolomics[314,315]. Unraveling the complex molecular processes permitting axonal growth over the CNS midline may open up new avenues for tailored therapies of neurological diseases in which further, treatment induced, compensatory sprouting of spared fibers augment spontaneous recovery.

Basic animal studies support the clinical view that training of lost functions is essential to improve outcome after brain and spinal cord injury in neurorehabilitation[316]. Our group showed that forced use of the affected forelimb after unilateral pyramidotomy in rats further improved behavioral recovery in tasks requiring fine motor control[19]. Interestingly, the number of unlesioned corticospinal fibers crossing the spinal cord midline was increased three weeks after lesion in comparison to intact rats but was not influenced by training or inactivity. However, after lesion, forced limb use increased branching of midline crossing fibers in the denervated spinal gray matter. These findings suggest that an increase of midline crossing fibers is primarily induced by the lesion itself, that arborization of these fibers is mainly driven by activity and that both processes eventually leading to well-branched midline crossing fibers are important for functional recovery. Although the neurobiological basis of training after CNS injury was not specifically addressed in the present work, this is in line with the results presented in ***Chapter 3***. We found in our - presumably "self-training"[317] - rats with hemisection injury an increased number of reticulospinal fibers crossing the spinal cord midline. However, arborization of these fibers was significantly reduced in the cervical spinal cord and unchanged in lumbar segments in comparison to pre-existing reticulospinal midline crossing fibers in intact rats. This was correlated with poor functional recovery of the ipsilesional forelimb and substantial improvements of hindlimb function. Whether reduced

branching of cervical reticulospinal midline crossing fibers is the cause or the consequence - for example due to inactivity - of the observed poor recovery of the ipsilesional forelimb remains to be determined. Deeper insights into the basic mechanisms of spontaneous recovery and training may also help to identify the best way of combining new pharmacological treatments enhancing neuronal plasticity with different types of training to further promote spontaneous recovery in humans with CNS injury[112,113].

New approaches for the treatment of incomplete spinal cord injury

Effects of dopaminergic, noradrenergic and serotonergic agonists on fore- and hindlimb function after cervical hemisection in rats

As described in detail in ***Chapter 2 and 3***, we found a characteristic pattern of recovery after cervical unilateral spinal cord hemisection injury in rats which was similar to humans with Brown-Séquard syndrome. In brief, the ipsilesional forelimb showed only poor recovery in all motor tasks while hindlimbs demonstrated excellent recovery of basic locomotor functions required for overground walking, wading and swimming. A number of previous studies reported that treatment with dopaminergic, noradrenergic and serotonergic agonists improves hindlimb function after complete spinal cord transections in rodents, cats and monkeys by modulating local spinal circuits including the lumbar central pattern generator (CPG)[136,318-323]. In rats, CPGs located in the lumbar and also the cervical spinal cord mediate coordinated quadruple locomotion[324]. With the intention to improve especially the deficits of the ipsilesional forelimb, our group investigated the effects of different monoaminergic agonists on fore- and hindlimb function in recovered rats with cervical hemisection injury[5]. Rats were treated intrathecally with different dopaminergic, noradrenergic and serotonergic agonists, namely clonidine, methoxamine, apomorphine, quipazine and 8-OHDPAT, more than four weeks after hemisection. Following injections, recovered hindlimb stepping was changed, mainly so that locomotion was aggravated, while almost no effects were detected on forelimb function. From these unexpected findings two important insights were gained: firstly, there are major differences between cervical and lumbar locomotor centers regarding the monoaminergic drive needed, and secondly there are major differences of the effects of monoamines in complete and incomplete spinal cord injury.

Deep brain stimulation improves locomotion after thoracic spinal cord injury in rats

From mice to primates[325], important components of the basic CNS locomotor network which allows mammals to walk, run or swim[326,327] are the mesencephalic locomotor region[171,194], the

ventromedial medullar reticular formation with its gigantic reticulospinal neurons[170,328,329] as well as spinal interneurons including those which are part of the CPG[153,167,172]. Our finding that anatomical plasticity in the mesencephalo-reticulo-spinal system significantly contributed to locomotor recovery after incomplete spinal cord injury in rats underlines its significance for locomotor behavior (see ***Chapter 3***).

In rodents, reticulospinal projections typically descend broadly distributed within the spinal cord white matter in the ventral and ventrolateral funiculus[201,330]. After incomplete spinal cord injury, it is likely that some of these fibers may be spared by the lesion and remain intact. Encouraged by the finding that relatively few reticulospinal midline crossing fibers mediated significant functional recovery in rats with hemisection injury (see ***Chapter 3***), our group further studied this important locomotor network.

Excitatory deep brain stimulation of the mesencephalic locomotor region in awake behaving rats with chronic incomplete thoracic spinal cord injury improved hindlimb movements during walking and swimming in an intensity-dependent manner[330]. Rats with subtotal spinal cord injuries at midthoracic level with a total of loss of more than 90% of the white matter tissue and only a few remaining fibers in the ventrolateral funiculus showed severely and permanently impaired hindlimb function. In these almost paraplegic rats, electrical stimulation of the mesencephalic locomotor region elicited functional hindlimb strokes during swimming[330]. The mechanisms underlying these effects may include: firstly, a rather global and unspecific excitation of the lumbar spinal circuits[136] through various types of spared fibers leading to enhanced sensitivity of the CPG to sensory input and, secondly, an increased recruitment or more efficient use of the remaining reticulospinal fibers due to supraphysiological excitation in the brainstem, thereby, conveying “pacemaker” information from the mesencephalic locomotor region to the lumbar CPG network.

Permanent excitatory or inhibitory electric stimulation of different brain regions is already successfully used in the clinic to treat patients with Parkinson’s disease[331-333], dementia[334-336], major depression[337-339] and many other neuropsychiatric diseases[340,341]. Therefore, stimulation of parts of the MLR in humans[342] may not only improve walking function in Parkinson’s disease[343,344] but also in humans with severe but anatomical incomplete chronic spinal cord injury. A first pilot study pursuing this approach in subjects with spinal cord injury is in preparation as a cooperation project of the Department of Neurosurgery, University Hospital Zurich, the Brain Research Institute, University and ETH Zurich, and the Spinal Cord Injury Center, Balgrist University Hospital Zurich.

Treatment with anti-Nogo-A antibodies in multiple sclerosis

Studies on the natural history on MS suggest that it is a two-stage disease[345]. The early phase is characterised by focal inflammatory CNS lesions causing acute, but often transient impairments (relapse and remission). After relapse, recovery of function is achieved by different processes, as discussed in ***Chapter 5***. In the late phase about 10 to 20 years after first manifestation of the disease, diffuse inflammation and neurodegeneration are predominant leading to slow, but continuous deterioration of cognition and walking function. Available treatments can reduce the frequency of relapses through modulation of the immune system but do not completely stop disease activity[346]. So far, treatments facilitating recovery in MS are not available. As discussed in ***Chapter 1***, neutralization of Nogo-A results in enhanced axonal sprouting and increased functional recovery after spinal cord injury and stroke in rodents and primates. In the view of these findings, blockade of Nogo-A seems to be a promising therapeutic option in stroke but also in MS. Studies in mice showed that neutralization of Nogo-A promotes functional recovery in an animal model of MS, that is experimental autoimmune encephalomyelitis[347,348]. However, results on the underlying mechanisms were less distinct suggesting enhanced remyelination in MS plaques as well as increased axonal outgrowth after Nogo-A blockade[347-349]. Determination of whether increased remyelination, enhanced neuronal plasticity or even neuroprotection is the predominant mode of action of this therapy in MS will influence its clinical application. More efficient remyelination appears desirable following a severe ("spinal") relapse or optic neuritis at early disease stages, whereas increased plasticity and neuroprotection may be needed to counteract neurodegeneration and deterioration of function at later stages of the disease. This issue includes the question of the optimal time window for treatment. Intrathecal or intravenous infusions of anti-Nogo-A antibodies may be performed once during or shortly after a relapse or even repeatedly for long-term treatment. As a prerequisite for a clinical trial in MS, an currently ongoing preclinical joint project of the Department of Neurology, University Hospital Zurich, and the Brain Research Institute, University and ETH Zurich, addresses these clinically relevant questions using a rat model of targeted experimental autoimmune encephalomyelitis.

Acknowledgements / Danksagung

Dankesworte müssen kurz sein wie eine Liebeserklärung.

nach Theodor Fontane

I want to sincerely thank Professor Martin Schwab for teaching and supervising me during my doctoral studies. I thank Martin for guiding me safely through the complex and occasionally "inhibitory" environment of basic neuroscience research. I thank the committee members of my PhD, Professor Wolf Blanckenhorn, Professor Armin Curt and Professor Volker Dietz for their continuing and invaluable support.

Ich bedanke mich ganz herzlich bei meinen Freunden und Kollegen Linard Filli, Sandra Kapitza, Roman Gonzenbach, Lukas Bachmann und Marc Bolliger für ihre tatkräftige Hilfe bei den verschiedenen Projekten und für ihren liebenswürdigen, jahrelangen Beistand. I warmly thank Michelle Starkey who read and revised all manuscripts with enormous patience. I also want to thank Lisa Schnell for her pioneering work in Martin's lab and excellent suggestions during my doctoral studies. Many thanks go to my dear colleagues at the Brain Research Institute. Especially, I thank Martina Röthlisberger, Jeannette Scholl, Regula Schneider, Mirijam Gullo, Hansjörg Kasper, Stefan Giger and Oliver Weinmann for their excellent technical support and for their extraordinary high degree of commitment to our projects. Also, I would like to remember with utmost respect and gratitude our late colleague and friend Eva Hochreutener who contributed excellent graphical work and suggestions essential to all of the presented studies.

Sehr herzlich danke ich Regula Wälchli für ihre liebevolle Unterstützung, ihr Verständnis und ihre unendliche Geduld mit mir. Ganz besonders möchte ich mich noch bei meinen Eltern für ihre unermüdliche Hilfe und ihren uneingeschränkten Beistand bedanken und dafür, dass sie immer für mich da sind. Diese Arbeit ist ihnen gewidmet.

References

1. Wyndaele M, Wyndaele JJ. Incidence, prevalence and epidemiology of spinal cord injury: what learns a worldwide literature survey? Spinal Cord 2006;44:523-9.
2. Selvarajah S, Hammond ER, Haider AH, et al. The Burden of Acute Traumatic Spinal Cord Injury among Adults in the United States: An Update. J Neurotrauma 2014;31:228-38.
3. Fawcett JW, Curt A, Steeves JD, et al. Guidelines for the conduct of clinical trials for spinal cord injury as developed by the ICCP panel: spontaneous recovery after spinal cord injury and statistical power needed for therapeutic clinical trials. Spinal Cord 2007;45:190-205.
4. Dietz V, Curt A. Neurological aspects of spinal-cord repair: promises and challenges. Lancet Neurol 2006;5:688-94.
5. Filli L, Zorner B, Weinmann O, Schwab ME. Motor deficits and recovery in rats with unilateral spinal cord hemisection mimic the Brown-Sequard syndrome. Brain 2011;134:2261-73.
6. Taylor RG, Gleave JR. Incomplete spinal cord injuries; with Brown-Sequard phenomena. J Bone Joint Surg Br 1957;39-B:438-50.
7. Little JW, Halar E. Temporal course of motor recovery after Brown-Sequard spinal cord injuries. Paraplegia 1985;23:39-46.
8. James ND, Bartus K, Grist J, Bennett DL, McMahon SB, Bradbury EJ. Conduction failure following spinal cord injury: functional and anatomical changes from acute to chronic stages. J Neurosci 2011;31:18543-55.
9. Waxman SG. Demyelination in spinal cord injury. J Neurol Sci 1989;91:1-14.
10. Liu Y, Rouiller EM. Mechanisms of recovery of dexterity following unilateral lesion of the sensorimotor cortex in adult monkeys. Exp Brain Res 1999;128:149-59.
11. Weidner N, Ner A, Salimi N, Tuszynski MH. Spontaneous corticospinal axonal plasticity and functional recovery after adult central nervous system injury. Proc Natl Acad Sci U S A 2001;98:3513-8.
12. Bareyre FM, Kerschensteiner M, Raineteau O, Mettenleiter TC, Weinmann O, Schwab ME. The injured spinal cord spontaneously forms a new intraspinal circuit in adult rats. Nat Neurosci 2004;7:269-77.
13. Dancause N, Barbay S, Frost SB, et al. Extensive cortical rewiring after brain injury. J Neurosci 2005;25:10167-79.
14. Rossignol S. Plasticity of connections underlying locomotor recovery after central and/or peripheral lesions in the adult mammals. Philos Trans R Soc Lond B Biol Sci 2006;361:1647-71.
15. Courtine G, Song B, Roy RR, et al. Recovery of supraspinal control of stepping via indirect propriospinal relay connections after spinal cord injury. Nat Med 2008;14:69-74.
16. Ghosh A, Haiss F, Sydekum E, et al. Rewiring of hindlimb corticospinal neurons after spinal cord injury. Nat Neurosci 2010;13:97-104.
17. Barriere G, Leblond H, Provencher J, Rossignol S. Prominent role of the spinal central pattern generator in the recovery of locomotion after partial spinal cord injuries. J Neurosci 2008;28:3976-87.
18. Ghosh A, Sydekum E, Haiss F, et al. Functional and anatomical reorganization of the sensory-motor cortex after incomplete spinal cord injury in adult rats. J Neurosci 2009;29:12210-9.
19. Maier IC, Baumann K, Thallmair M, Weinmann O, Scholl J, Schwab ME. Constraint-induced movement therapy in the adult rat after unilateral corticospinal tract injury. J Neurosci 2008;28:9386-403.

20. Bradbury EJ, McMahon SB. Spinal cord repair strategies: why do they work? Nat Rev Neurosci 2006;7:644-53.

21. Courtine G, van den Brand R, Musienko P. Spinal cord injury: time to move. Lancet 2011;377:1896-8.

22. Edgerton VR, Roy RR. A new age for rehabilitation. Eur J Phys Rehabil Med 2012;48:99-109.

23. Thallmair M, Metz GA, Z'Graggen WJ, Raineteau O, Kartje GL, Schwab ME. Neurite growth inhibitors restrict plasticity and functional recovery following corticospinal tract lesions. Nat Neurosci 1998;1:124-31.

24. Schwab ME. Nogo and axon regeneration. Curr Opin Neurobiol 2004;14:118-24.

25. Freund P, Wannier T, Schmidlin E, et al. Anti-Nogo-A antibody treatment enhances sprouting of corticospinal axons rostral to a unilateral cervical spinal cord lesion in adult macaque monkey. J Comp Neurol 2007;502:644-59.

26. Nudo RJ. Plasticity. NeuroRx 2006;3:420-7.

27. Yiu G, He Z. Glial inhibition of CNS axon regeneration. Nat Rev Neurosci 2006;7:617-27.

28. Liu BP, Cafferty WB, Budel SO, Strittmatter SM. Extracellular regulators of axonal growth in the adult central nervous system. Philos Trans R Soc Lond B Biol Sci 2006;361:1593-610.

29. Maier IC, Schwab ME. Sprouting, regeneration and circuit formation in the injured spinal cord: factors and activity. Philos Trans R Soc Lond B Biol Sci 2006;361:1611-34.

30. Gonzenbach RR, Schwab ME. Disinhibition of neurite growth to repair the injured adult CNS: focusing on Nogo. Cell Mol Life Sci 2008;65:161-76.

31. Liebscher T, Schnell L, Schnell D, et al. Nogo-A antibody improves regeneration and locomotion of spinal cord-injured rats. Ann Neurol 2005;58:706-19.

32. Freund P, Schmidlin E, Wannier T, et al. Nogo-A-specific antibody treatment enhances sprouting and functional recovery after cervical lesion in adult primates. Nat Med 2006;12:790-2.

33. Carulli D, Laabs T, Geller HM, Fawcett JW. Chondroitin sulfate proteoglycans in neural development and regeneration. Curr Opin Neurobiol 2005;15:116-20.

34. Galtrey CM, Fawcett JW. The role of chondroitin sulfate proteoglycans in regeneration and plasticity in the central nervous system. Brain Res Rev 2007;54:1-18.

35. Seif GI, Nomura H, Tator CH. Retrograde axonal degeneration "dieback" in the corticospinal tract after transection injury of the rat spinal cord: a confocal microscopy study. J Neurotrauma 2007;24:1513-28.

36. Schnell L, Schwab ME. Axonal regeneration in the rat spinal cord produced by an antibody against myelin-associated neurite growth inhibitors. Nature 1990;343:269-72.

37. Kerschensteiner M, Schwab ME, Lichtman JW, Misgeld T. In vivo imaging of axonal degeneration and regeneration in the injured spinal cord. Nat Med 2005;11:572-7.

38. Fenrich KK, Rose PK. Spinal interneuron axons spontaneously regenerate after spinal cord injury in the adult feline. J Neurosci 2009;29:12145-58.

39. Kerschensteiner M, Bareyre FM, Buddeberg BS, et al. Remodeling of axonal connections contributes to recovery in an animal model of multiple sclerosis. J Exp Med 2004;200:1027-38.

40. Fouad K, Pedersen V, Schwab ME, Brosamle C. Cervical sprouting of corticospinal fibers after thoracic spinal cord injury accompanies shifts in evoked motor responses. Curr Biol 2001;11:1766-70.

41. Ekstrand MI, Enquist LW, Pomeranz LE. The alpha-herpesviruses: molecular pathfinders in nervous system circuits. Trends Mol Med 2008;14:134-40.

42. Brus-Ramer M, Carmel JB, Chakrabarty S, Martin JH. Electrical stimulation of spared corticospinal axons augments connections with ipsilateral spinal motor circuits after injury. J Neurosci 2007;27:13793-801.

43. Rossignol S, Barriere G, Alluin O, Frigon A. Re-expression of locomotor function after partial spinal cord injury. Physiology (Bethesda) 2009;24:127-39.

44. Nudo RJ. Mechanisms for recovery of motor function following cortical damage. Curr Opin Neurobiol 2006;16:638-44.

45. Strick PL. Anatomical organization of multiple motor areas in the frontal lobe: implications for recovery of function. Adv Neurol 1988;47:293-312.

46. Ward NS, Frackowiak RS. The functional anatomy of cerebral reorganisation after focal brain injury. J Physiol Paris 2006;99:425-36.

47. Raineteau O, Schwab ME. Plasticity of motor systems after incomplete spinal cord injury. Nat Rev Neurosci 2001;2:263-73.

48. Nudo RJ, Milliken GW, Jenkins WM, Merzenich MM. Use-dependent alterations of movement representations in primary motor cortex of adult squirrel monkeys. J Neurosci 1996;16:785-807.

49. Brown CE, Li P, Boyd JD, Delaney KR, Murphy TH. Extensive turnover of dendritic spines and vascular remodeling in cortical tissues recovering from stroke. J Neurosci 2007;27:4101-9.

50. Frost SB, Barbay S, Friel KM, Plautz EJ, Nudo RJ. Reorganization of remote cortical regions after ischemic brain injury: a potential substrate for stroke recovery. J Neurophysiol 2003;89:3205-14.

51. Weiller C, Ramsay SC, Wise RJ, Friston KJ, Frackowiak RS. Individual patterns of functional reorganization in the human cerebral cortex after capsular infarction. Ann Neurol 1993;33:181-9.

52. Schallert T, Kozlowski DA, Humm JL, Cocke RR. Use-dependent structural events in recovery of function. Adv Neurol 1997;73:229-38.

53. Kozlowski DA, Schallert T. Relationship between dendritic pruning and behavioral recovery following sensorimotor cortex lesions. Behav Brain Res 1998;97:89-98.

54. Seitz RJ, Hoflich P, Binkofski F, Tellmann L, Herzog H, Freund HJ. Role of the premotor cortex in recovery from middle cerebral artery infarction. Arch Neurol 1998;55:1081-8.

55. Jones TA. Multiple synapse formation in the motor cortex opposite unilateral sensorimotor cortex lesions in adult rats. J Comp Neurol 1999;414:57-66.

56. Dancause N, Barbay S, Frost SB, et al. Effects of small ischemic lesions in the primary motor cortex on neurophysiological organization in ventral premotor cortex. J Neurophysiol 2006;96:3506-11.

57. Miyai I, Yagura H, Oda I, et al. Premotor cortex is involved in restoration of gait in stroke. Ann Neurol 2002;52:188-94.

58. Fridman EA, Hanakawa T, Chung M, Hummel F, Leiguarda RC, Cohen LG. Reorganization of the human ipsilesional premotor cortex after stroke. Brain 2004;127:747-58.

59. Ward NS. Functional reorganization of the cerebral motor system after stroke. Curr Opin Neurol 2004;17:725-30.

60. Rossini PM, Calautti C, Pauri F, Baron JC. Post-stroke plastic reorganisation in the adult brain. Lancet Neurol 2003;2:493-502.

61. Ward NS. Plasticity and the functional reorganization of the human brain. Int J Psychophysiol 2005;58:158-61.

62. Rouiller EM, Olivier E. Functional recovery after lesions of the primary motor cortex. Prog Brain Res 2004;143:467-75.

63. Hallett M. Plasticity of the human motor cortex and recovery from stroke. Brain Res Brain Res Rev 2001;36:169-74.

64. Schwab ME, Caroni P. Oligodendrocytes and CNS myelin are nonpermissive substrates for neurite growth and fibroblast spreading in vitro. J Neurosci 1988;8:2381-93.

65. Schwab ME, Thoenen H. Dissociated neurons regenerate into sciatic but not optic nerve explants in culture irrespective of neurotrophic factors. J Neurosci 1985;5:2415-23.

66. Caroni P, Schwab ME. Two membrane protein fractions from rat central myelin with inhibitory properties for neurite growth and fibroblast spreading. J Cell Biol 1988;106:1281-8.

67. Caroni P, Schwab ME. Antibody against myelin-associated inhibitor of neurite growth neutralizes nonpermissive substrate properties of CNS white matter. Neuron 1988;1:85-96.

68. Spillmann AA, Bandtlow CE, Lottspeich F, Keller F, Schwab ME. Identification and characterization of a bovine neurite growth inhibitor (bNI-220). J Biol Chem 1998;273:19283-93.

69. Chen MS, Huber AB, van der Haar ME, et al. Nogo-A is a myelin-associated neurite outgrowth inhibitor and an antigen for monoclonal antibody IN-1. Nature 2000;403:434-9.

70. GrandPre T, Nakamura F, Vartanian T, Strittmatter SM. Identification of the Nogo inhibitor of axon regeneration as a Reticulon protein. Nature 2000;403:439-44.

71. Prinjha R, Moore SE, Vinson M, et al. Inhibitor of neurite outgrowth in humans. Nature 2000;403:383-4.

72. Low K, Culbertson M, Bradke F, Tessier-Lavigne M, Tuszynski MH. Netrin-1 is a novel myelin-associated inhibitor to axon growth. J Neurosci 2008;28:1099-108.

73. Wang X, Chun SJ, Treloar H, Vartanian T, Greer CA, Strittmatter SM. Localization of Nogo-A and Nogo-66 receptor proteins at sites of axon-myelin and synaptic contact. J Neurosci 2002;22:5505-15.

74. Oertle T, Schwab ME. Nogo and its paRTNers. Trends Cell Biol 2003;13:187-94.

75. Fournier AE, GrandPre T, Gould G, Wang X, Strittmatter SM. Nogo and the Nogo-66 receptor. Prog Brain Res 2002;137:361-9.

76. Oertle T, van der Haar ME, Bandtlow CE, et al. Nogo-A inhibits neurite outgrowth and cell spreading with three discrete regions. J Neurosci 2003;23:5393-406.

77. Fournier AE, GrandPre T, Strittmatter SM. Identification of a receptor mediating Nogo-66 inhibition of axonal regeneration. Nature 2001;409:341-6.

78. Liu BP, Fournier A, GrandPre T, Strittmatter SM. Myelin-associated glycoprotein as a functional ligand for the Nogo-66 receptor. Science 2002;297:1190-3.

79. Wang KC, Koprivica V, Kim JA, et al. Oligodendrocyte-myelin glycoprotein is a Nogo receptor ligand that inhibits neurite outgrowth. Nature 2002;417:941-4.

80. Venkatesh K, Chivatakarn O, Lee H, et al. The Nogo-66 receptor homolog NgR2 is a sialic acid-dependent receptor selective for myelin-associated glycoprotein. J Neurosci 2005;25:808-22.

81. Venkatesh K, Chivatakarn O, Sheu SS, Giger RJ. Molecular dissection of the myelin-associated glycoprotein receptor complex reveals cell type-specific mechanisms for neurite outgrowth inhibition. J Cell Biol 2007;177:393-9.

82. Joset A, Dodd DA, Halegoua S, Schwab ME. Pincher-generated Nogo-A endosomes mediate growth cone collapse and retrograde signaling. J Cell Biol 2010;188:271-85.

83. Montani L, Gerrits B, Gehrig P, et al. Neuronal Nogo-A modulates growth cone motility via Rho-GTP/LIMK1/cofilin in the unlesioned adult nervous system. J Biol Chem 2009;284:10793-807.

84. Niederost B, Oertle T, Fritsche J, McKinney RA, Bandtlow CE. Nogo-A and myelin-associated glycoprotein mediate neurite growth inhibition by antagonistic regulation of RhoA and Rac1. J Neurosci 2002;22:10368-76.

85. Fournier AE, Takizawa BT, Strittmatter SM. Rho kinase inhibition enhances axonal regeneration in the injured CNS. J Neurosci 2003;23:1416-23.

86. Yiu G, He Z. Signaling mechanisms of the myelin inhibitors of axon regeneration. Curr Opin Neurobiol 2003;13:545-51.

87. Alabed YZ, Grados-Munro E, Ferraro GB, Hsieh SH, Fournier AE. Neuronal responses to myelin are mediated by rho kinase. J Neurochem 2006;96:1616-25.

88. Hsieh SH, Ferraro GB, Fournier AE. Myelin-associated inhibitors regulate cofilin phosphorylation and neuronal inhibition through LIM kinase and Slingshot phosphatase. J Neurosci 2006;26:1006-15.

89. GrandPre T, Li S, Strittmatter SM. Nogo-66 receptor antagonist peptide promotes axonal regeneration. Nature 2002;417:547-51.

90. Li S, Strittmatter SM. Delayed systemic Nogo-66 receptor antagonist promotes recovery from spinal cord injury. J Neurosci 2003;23:4219-27.

91. Fournier AE, Gould GC, Liu BP, Strittmatter SM. Truncated soluble Nogo receptor binds Nogo-66 and blocks inhibition of axon growth by myelin. J Neurosci 2002;22:8876-83.

92. Ji B, Li M, Wu WT, et al. LINGO-1 antagonist promotes functional recovery and axonal sprouting after spinal cord injury. Mol Cell Neurosci 2006;33:311-20.

93. Mullner A, Gonzenbach RR, Weinmann O, Schnell L, Liebscher T, Schwab ME. Lamina-specific restoration of serotonergic projections after Nogo-A antibody treatment of spinal cord injury in rats. Eur J Neurosci 2008;27:326-33.

94. Weinmann O, Schnell L, Ghosh A, et al. Intrathecally infused antibodies against Nogo-A penetrate the CNS and downregulate the endogenous neurite growth inhibitor Nogo-A. Mol Cell Neurosci 2006;32:161-73.

95. Freund P, Schmidlin E, Wannier T, et al. Anti-Nogo-A antibody treatment promotes recovery of manual dexterity after unilateral cervical lesion in adult primates--re-examination and extension of behavioral data. Eur J Neurosci 2009;29:983-96.

96. McKerracher L, Higuchi H. Targeting Rho to stimulate repair after spinal cord injury. J Neurotrauma 2006;23:309-17.

97. Simonen M, Pedersen V, Weinmann O, et al. Systemic deletion of the myelin-associated outgrowth inhibitor Nogo-A improves regenerative and plastic responses after spinal cord injury. Neuron 2003;38:201-11.

98. Kim JE, Li S, GrandPre T, Qiu D, Strittmatter SM. Axon regeneration in young adult mice lacking Nogo-A/B. Neuron 2003;38:187-99.

99. Zheng B, Ho C, Li S, Keirstead H, Steward O, Tessier-Lavigne M. Lack of enhanced spinal regeneration in Nogo-deficient mice. Neuron 2003;38:213-24.

100. Dimou L, Schnell L, Montani L, et al. Nogo-A-deficient mice reveal strain-dependent differences in axonal regeneration. J Neurosci 2006;26:5591-603.

101. Lee JK, Kim JE, Sivula M, Strittmatter SM. Nogo receptor antagonism promotes stroke recovery by enhancing axonal plasticity. J Neurosci 2004;24:6209-17.

102. Crespo D, Asher RA, Lin R, Rhodes KE, Fawcett JW. How does chondroitinase promote functional recovery in the damaged CNS? Exp Neurol 2007;206:159-71.

103. Shen Y, Tenney AP, Busch SA, et al. PTPsigma is a receptor for chondroitin sulfate proteoglycan, an inhibitor of neural regeneration. Science 2009;326:592-6.

104. Bradbury EJ, Moon LD, Popat RJ, et al. Chondroitinase ABC promotes functional recovery after spinal cord injury. Nature 2002;416:636-40.

105. Cafferty WB, Yang SH, Duffy PJ, Li S, Strittmatter SM. Functional axonal regeneration through astrocytic scar genetically modified to digest chondroitin sulfate proteoglycans. J Neurosci 2007;27:2176-85.

106. Fouad K, Schnell L, Bunge MB, Schwab ME, Liebscher T, Pearse DD. Combining Schwann cell bridges and olfactory-ensheathing glia grafts with chondroitinase promotes locomotor recovery after complete transection of the spinal cord. J Neurosci 2005;25:1169-78.

107. Farmer SF, Harrison LM, Ingram DA, Stephens JA. Plasticity of central motor pathways in children with hemiplegic cerebral palsy. Neurology 1991;41:1505-10.

108. Payne BR, Lomber SG. Reconstructing functional systems after lesions of cerebral cortex. Nat Rev Neurosci 2001;2:911-9.

109. Kapfhammer JP, Schwab ME. Inverse patterns of myelination and GAP-43 expression in the adult CNS: neurite growth inhibitors as regulators of neuronal plasticity? J Comp Neurol 1994;340:194-206.

110. Raineteau O, Fouad K, Noth P, Thallmair M, Schwab ME. Functional switch between motor tracts in the presence of the mAb IN-1 in the adult rat. Proc Natl Acad Sci U S A 2001;98:6929-34.

111. Barritt AW, Davies M, Marchand F, et al. Chondroitinase ABC promotes sprouting of intact and injured spinal systems after spinal cord injury. J Neurosci 2006;26:10856-67.

112. Maier IC, Ichiyama RM, Courtine G, et al. Differential effects of anti-Nogo-A antibody treatment and treadmill training in rats with incomplete spinal cord injury. Brain 2009;132:1426-40.

113. Garcia-Alias G, Barkhuysen S, Buckle M, Fawcett JW. Chondroitinase ABC treatment opens a window of opportunity for task-specific rehabilitation. Nat Neurosci 2009;12:1145-51.

114. Fawcett JW, Curt A. Damage control in the nervous system: rehabilitation in a plastic environment. Nat Med 2009;15:735-6.

115. Wiessner C, Bareyre FM, Allegrini PR, et al. Anti-Nogo-A antibody infusion 24 hours after experimental stroke improved behavioral outcome and corticospinal plasticity in normotensive and spontaneously hypertensive rats. J Cereb Blood Flow Metab 2003;23:154-65.

116. Emerick AJ, Neafsey EJ, Schwab ME, Kartje GL. Functional reorganization of the motor cortex in adult rats after cortical lesion and treatment with monoclonal antibody IN-1. J Neurosci 2003;23:4826-30.

117. Markus TM, Tsai SY, Bollnow MR, et al. Recovery and brain reorganization after stroke in adult and aged rats. Ann Neurol 2005;58:950-3.

118. Wenk CA, Thallmair M, Kartje GL, Schwab ME. Increased corticofugal plasticity after unilateral cortical lesions combined with neutralization of the IN-1 antigen in adult rats. J Comp Neurol 1999;410:143-57.

119. Blochlinger S, Weinmann O, Schwab ME, Thallmair M. Neuronal plasticity and formation of new synaptic contacts follow pyramidal lesions and neutralization of Nogo-A: a light and electron microscopic study in the pontine nuclei of adult rats. J Comp Neurol 2001;433:426-36.

120. Papadopoulos CM, Tsai SY, Alsbiei T, O'Brien TE, Schwab ME, Kartje GL. Functional recovery and neuroanatomical plasticity following middle cerebral artery occlusion and IN-1 antibody treatment in the adult rat. Ann Neurol 2002;51:433-41.

121. Seymour AB, Andrews EM, Tsai SY, et al. Delayed treatment with monoclonal antibody IN-1 1 week after stroke results in recovery of function and corticorubral plasticity in adult rats. J Cereb Blood Flow Metab 2005;25:1366-75.

122. Kartje GL, Schulz MK, Lopez-Yunez A, Schnell L, Schwab ME. Corticostriatal plasticity is restricted by myelin-associated neurite growth inhibitors in the adult rat. Ann Neurol 1999;45:778-86.

123. Bareyre FM, Haudenschild B, Schwab ME. Long-lasting sprouting and gene expression changes induced by the monoclonal antibody IN-1 in the adult spinal cord. J Neurosci 2002;22:7097-110.

124. Harel NY, Strittmatter SM. Can regenerating axons recapitulate developmental guidance during recovery from spinal cord injury? Nat Rev Neurosci 2006;7:603-16.

125. Martin JH, Friel KM, Salimi I, Chakrabarty S. Activity- and use-dependent plasticity of the developing corticospinal system. Neurosci Biobehav Rev 2007;31:1125-35.

126. Friel KM, Martin JH. Bilateral activity-dependent interactions in the developing corticospinal system. J Neurosci 2007;27:11083-90.

127. Curt A, Schwab ME, Dietz V. Providing the clinical basis for new interventional therapies: refined diagnosis and assessment of recovery after spinal cord injury. Spinal Cord 2004;42:1-6.

128. Zorner B, Blanckenhorn WU, Dietz V, Curt A. Clinical algorithm for improved prediction of ambulation and patient stratification after incomplete spinal cord injury. J Neurotrauma 2010;27:241-52.

129. Basso DM. Neuroanatomical substrates of functional recovery after experimental spinal cord injury: implications of basic science research for human spinal cord injury. Phys Ther 2000;80:808-17.

130. McEwen ML, Springer JE. Quantification of locomotor recovery following spinal cord contusion in adult rats. J Neurotrauma 2006;23:1632-53.

131. Muir GD, Webb AA. Mini-review: assessment of behavioural recovery following spinal cord injury in rats. Eur J Neurosci 2000;12:3079-86.

132. Metz GA, Merkler D, Dietz V, Schwab ME, Fouad K. Efficient testing of motor function in spinal cord injured rats. Brain Res 2000;883:165-77.

133. Kunkel-Bagden E, Dai HN, Bregman BS. Methods to assess the development and recovery of locomotor function after spinal cord injury in rats. Exp Neurol 1993;119:153-64.

134. Basso DM, Beattie MS, Bresnahan JC. A sensitive and reliable locomotor rating scale for open field testing in rats. J Neurotrauma 1995;12:1-21.

135. Hamers FP, Lankhorst AJ, van Laar TJ, Veldhuis WB, Gispen WH. Automated quantitative gait analysis during overground locomotion in the rat: its application to spinal cord contusion and transection injuries. J Neurotrauma 2001;18:187-201.

136. Courtine G, Gerasimenko Y, van den Brand R, et al. Transformation of nonfunctional spinal circuits into functional states after the loss of brain input. Nat Neurosci 2009;12:1333-42.

137. Magnuson DS, Smith RR, Brown EH, et al. Swimming as a model of task-specific locomotor retraining after spinal cord injury in the rat. Neurorehabil Neural Repair 2009;23:535-45.

138. Gorska T, Chojnicka-Gittins B, Majczynski H, Zmyslowski W. Recovery of overground locomotion following partial spinal lesions of different extent in the rat. Behav Brain Res 2009;196:286-96.

139. Basso DM. Behavioral testing after spinal cord injury: congruities, complexities, and controversies. J Neurotrauma 2004;21:395-404.

140. Roy RR, Hutchison DL, Pierotti DJ, Hodgson JA, Edgerton VR. EMG patterns of rat ankle extensors and flexors during treadmill locomotion and swimming. J Appl Physiol 1991;70:2522-9.

141. Bolton DA, Tse AD, Ballermann M, Misiaszek JE, Fouad K. Task specific adaptations in rat locomotion: runway versus horizontal ladder. Behav Brain Res 2006;168:272-9.

142. Garnier C, Falempin M, Canu MH. A 3D analysis of fore- and hindlimb motion during locomotion: comparison of overground and ladder walking in rats. Behav Brain Res 2008;186:57-65.

143. Kanagal SG, Muir GD. Task-dependent compensation after pyramidal tract and dorsolateral spinal lesions in rats. Exp Neurol 2009;216:193-206.

144. Schucht P, Raineteau O, Schwab ME, Fouad K. Anatomical correlates of locomotor recovery following dorsal and ventral lesions of the rat spinal cord. Exp Neurol 2002;176:143-53.

145. Kaegi S, Schwab ME, Dietz V, Fouad K. Electromyographic activity associated with spontaneous functional recovery after spinal cord injury in rats. Eur J Neurosci 2002;16:249-58.

146. Fischer MS, Schilling N, Schmidt M, Haarhaus D, Witte H. Basic limb kinematics of small therian mammals. J Exp Biol 2002;205:1315-38.

147. Filipe VM, Pereira JE, Costa LM, et al. Effect of skin movement on the analysis of hindlimb kinematics during treadmill locomotion in rats. J Neurosci Methods 2006;153:55-61.

148. Gruner JA, Altman J. Swimming in the rat: analysis of locomotor performance in comparison to stepping. Exp Brain Res 1980;40:374-82.

149. Kloos AD, Fisher LC, Detloff MR, Hassenzahl DL, Basso DM. Stepwise motor and all-or-none sensory recovery is associated with nonlinear sparing after incremental spinal cord injury in rats. Exp Neurol 2005;191:251-65.

150. Metz GA, Whishaw IQ. Cortical and subcortical lesions impair skilled walking in the ladder rung walking test: a new task to evaluate fore- and hindlimb stepping, placing, and co-ordination. J Neurosci Methods 2002;115:169-79.

151. Dottori M, Hartley L, Galea M, et al. EphA4 (Sek1) receptor tyrosine kinase is required for the development of the corticospinal tract. Proc Natl Acad Sci U S A 1998;95:13248-53.

152. Schapiro S, Salas M, Vukovich K. Hormonal effects on ontogeny of swimming ability in the rat: assessment of central nervous system development. Science 1970;168:147-50.

153. Kiehn O. Locomotor circuits in the mammalian spinal cord. Annu Rev Neurosci 2006;29:279-306.

154. Goulding M. Circuits controlling vertebrate locomotion: moving in a new direction. Nat Rev Neurosci 2009;10:507-18.

155. Juvin L, Simmers J, Morin D. Propriospinal circuitry underlying interlimb coordination in mammalian quadrupedal locomotion. J Neurosci 2005;25:6025-35.

156. Grillner S, Wallen P, Saitoh K, Kozlov A, Robertson B. Neural bases of goal-directed locomotion in vertebrates--an overview. Brain Res Rev 2008;57:2-12.

157. Hagglund M, Borgius L, Dougherty KJ, Kiehn O. Activation of groups of excitatory neurons in the mammalian spinal cord or hindbrain evokes locomotion. Nat Neurosci;13:246-52.

158. Frigon A, Rossignol S. Experiments and models of sensorimotor interactions during locomotion. Biol Cybern 2006;95:607-27.

159. Butt SJ, Lundfald L, Kiehn O. EphA4 defines a class of excitatory locomotor-related interneurons. Proc Natl Acad Sci U S A 2005;102:14098-103.
160. Yamaguchi T. The central pattern generator for forelimb locomotion in the cat. Prog Brain Res 2004;143:115-22.
161. Metz GA, Whishaw IQ. The ladder rung walking task: a scoring system and its practical application. Journal of visualized experiments : JoVE 2009.
162. de Seze M, Falgairolle M, Viel S, Assaiante C, Cazalets JR. Sequential activation of axial muscles during different forms of rhythmic behavior in man. Exp Brain Res 2008;185:237-47.
163. Ceccato JC, de Seze M, Azevedo C, Cazalets JR. Comparison of trunk activity during gait initiation and walking in humans. PloS one 2009;4:e8193.
164. Rossignol S, Frigon A. Recovery of locomotion after spinal cord injury: some facts and mechanisms. Annu Rev Neurosci 2011;34:413-40.
165. Zorner B, Schwab ME. Anti-Nogo on the go: from animal models to a clinical trial. Ann N Y Acad Sci 2010;1198 Suppl 1:E22-34.
166. Shik ML, Severin FV, Orlovsky GN. Control of walking and running by means of electrical stimulation of the mesencephalon. Electroencephalogr Clin Neurophysiol 1969;26:549.
167. Grillner S. Neural networks for vertebrate locomotion. Sci Am 1996;274:64-9.
168. Garcia-Rill E, Skinner RD, Conrad C, Mosley D, Campbell C. Projections of the mesencephalic locomotor region in the rat. Brain Res Bull 1986;17:33-40.
169. Webster DM, Steeves JD. Funicular organization of avian brainstem-spinal projections. J Comp Neurol 1991;312:467-76.
170. Matsuyama K, Mori F, Nakajima K, Drew T, Aoki M, Mori S. Locomotor role of the corticoreticular-reticulospinal-spinal interneuronal system. Prog Brain Res 2004;143:239-49.
171. Ryczko D, Dubuc R. The multifunctional mesencephalic locomotor region. Curr Pharm Des 2013;19:4448-70.
172. Grillner S, Wallen P. Central pattern generators for locomotion, with special reference to vertebrates. Annu Rev Neurosci 1985;8:233-61.
173. McCrea DA, Rybak IA. Organization of mammalian locomotor rhythm and pattern generation. Brain Res Rev 2008;57:134-46.
174. Markham CH. Vestibular control of muscular tone and posture. Can J Neurol Sci 1987;14:493-6.
175. Armstrong DM. The supraspinal control of mammalian locomotion. J Physiol 1988;405:1-37.
176. Whishaw IQ, Gorny B, Sarna J. Paw and limb use in skilled and spontaneous reaching after pyramidal tract, red nucleus and combined lesions in the rat: behavioral and anatomical dissociations. Behav Brain Res 1998;93:167-83.
177. Ballermann M, Fouad K. Spontaneous locomotor recovery in spinal cord injured rats is accompanied by anatomical plasticity of reticulospinal fibers. Eur J Neurosci 2006;23:1988-96.
178. Weishaupt N, Hurd C, Wei DZ, Fouad K. Reticulospinal plasticity after cervical spinal cord injury in the rat involves withdrawal of projections below the injury. Exp Neurol 2013;247C:241-9.
179. Sayad WY, Harvey SC. The Regeneration of the Meninges: The Dura Mater. Ann Surg 1923;77:129-41.

180. Kapitza S, Zorner B, Weinmann O, et al. Tail spasms in rat spinal cord injury: changes in interneuronal connectivity. Exp Neurol 2012;236:179-89.

181. Gensel JC, Tovar CA, Hamers FP, Deibert RJ, Beattie MS, Bresnahan JC. Behavioral and histological characterization of unilateral cervical spinal cord contusion injury in rats. J Neurotrauma 2006;23:36-54.

182. Pellis SM, Pellis VC, Teitelbaum P. Air righting without the cervical righting reflex in adult rats. Behav Brain Res 1991;45:185-8.

183. Laouris Y, Kalli-Laouri J, Schwartze P. The postnatal development of the air-righting reaction in albino rats. Quantitative analysis of normal development and the effect of preventing neck-torso and torso-pelvis rotations. Behav Brain Res 1990;37:37-44.

184. Bertelli JA, Mira JC. Behavioral evaluating methods in the objective clinical assessment of motor function after experimental brachial plexus reconstruction in the rat. J Neurosci Methods 1993;46:203-8.

185. Zorner B, Filli L, Starkey ML, et al. Profiling locomotor recovery: comprehensive quantification of impairments after CNS damage in rodents. Nat Methods 2010;7:701-8.

186. Gelderd JB, Chopin SF. The vertebral level of origin of spinal nerves in the rat. Anat Rec 1977;188:45-7.

187. Paxinos G, Watson C. The rat brain in stereotaxic coordinates. Academic Press 1998;Fourth Edition.

188. Starkey ML, Bleul C, Zorner B, et al. Back seat driving: hindlimb corticospinal neurons assume forelimb control following ischaemic stroke. Brain 2012;135:3265-81.

189. Lindau NT, Banninger BJ, Gullo M, et al. Rewiring of the corticospinal tract in the adult rat after unilateral stroke and anti-Nogo-A therapy. Brain 2013.

190. Antal M. Termination areas of corticobulbar and corticospinal fibres in the rat. J Hirnforsch 1984;25:647-59.

191. Passingham RE, Myers C, Rawlins N, Lightfoot V, Fearn S. Premotor cortex in the rat. Behav Neurosci 1988;102:101-9.

192. Rouiller EM, Moret V, Liang F. Comparison of the connectional properties of the two forelimb areas of the rat sensorimotor cortex: support for the presence of a premotor or supplementary motor cortical area. Somatosens Mot Res 1993;10:269-89.

193. Smith NJ, Horst NK, Liu B, Caetano MS, Laubach M. Reversible Inactivation of Rat Premotor Cortex Impairs Temporal Preparation, but not Inhibitory Control, During Simple Reaction-Time Performance. Front Integr Neurosci 2010;4:124.

194. Steeves JD, Jordan LM. Autoradiographic demonstration of the projections from the mesencephalic locomotor region. Brain Res 1984;307:263-76.

195. Hagglund M, Borgius L, Dougherty KJ, Kiehn O. Activation of groups of excitatory neurons in the mammalian spinal cord or hindbrain evokes locomotion. Nat Neurosci 2010;13:246-52.

196. Basso DM, Beattie MS, Bresnahan JC. Descending systems contributing to locomotor recovery after mild or moderate spinal cord injury in rats: experimental evidence and a review of literature. Restor Neurol Neurosci 2002;20:189-218.

197. Jankowska E, Stecina K, Cabaj A, Pettersson LG, Edgley SA. Neuronal relays in double crossed pathways between feline motor cortex and ipsilateral hindlimb motoneurones. J Physiol 2006;575:527-41.

198. Goshgarian HG. The crossed phrenic phenomenon: a model for plasticity in the respiratory pathways following spinal cord injury. J Appl Physiol 2003;94:795-810.

199. Evans TA, Bashaw GJ. Axon guidance at the midline: of mice and flies. Curr Opin Neurobiol 2010;20:79-85.

200. Omoto S, Ueno M, Mochio S, Yamashita T. Corticospinal tract fibers cross the ephrin-B3-negative part of the midline of the spinal cord after brain injury. Neurosci Res 2011;69:187-95.

201. Zemlan FP, Behbehani MM, Beckstead RM. Ascending and descending projections from nucleus reticularis magnocellularis and nucleus reticularis gigantocellularis: an autoradiographic and horseradish peroxidase study in the rat. Brain Res 1984;292:207-20.

202. Martin GF, Vertes RP, Waltzer R. Spinal projections of the gigantocellular reticular formation in the rat. Evidence for projections from different areas to laminae I and II and lamina IX. Exp Brain Res 1985;58:154-62.

203. Ross GS, Sinnamon HM. Forelimb and hindlimb stepping by the anesthetized rat elicited by electrical stimulation of the pons and medulla. Physiol Behav 1984;33:201-8.

204. Noga BR, Kriellaars DJ, Brownstone RM, Jordan LM. Mechanism for activation of locomotor centers in the spinal cord by stimulation of the mesencephalic locomotor region. J Neurophysiol 2003;90:1464-78.

205. Davidson AG, Buford JA. Bilateral actions of the reticulospinal tract on arm and shoulder muscles in the monkey: stimulus triggered averaging. Exp Brain Res 2006;173:25-39.

206. Alstermark B, Isa T. Circuits for skilled reaching and grasping. Annu Rev Neurosci 2012;35:559-78.

207. Kaas JH, Stepniewska I, Gharbawie O. Cortical networks subserving upper limb movements in primates. Eur J Phys Rehabil Med 2012;48:299-306.

208. Reed WR, Shum-Siu A, Onifer SM, Magnuson DS. Inter-enlargement pathways in the ventrolateral funiculus of the adult rat spinal cord. Neuroscience 2006;142:1195-207.

209. Cowley KC, Zaporozhets E, Schmidt BJ. Propriospinal neurons are sufficient for bulbospinal transmission of the locomotor command signal in the neonatal rat spinal cord. J Physiol 2008;586:1623-35.

210. Lu P, Blesch A, Graham L, et al. Motor axonal regeneration after partial and complete spinal cord transection. J Neurosci 2012;32:8208-18.

211. Bracken MB, Hildreth N, Freeman DH, Jr., Webb SB. Relationship between neurological and functional status after acute spinal cord injury: an epidemiological study. J Chronic Dis 1980;33:115-25.

212. Coleman WP, Geisler FH. Injury severity as primary predictor of outcome in acute spinal cord injury: retrospective results from a large multicenter clinical trial. Spine J 2004;4:373-8.

213. DeVivo MJ. Sir Ludwig Guttmann Lecture: trends in spinal cord injury rehabilitation outcomes from model systems in the United States: 1973-2006. Spinal Cord 2007;45:713-21.

214. Marino RJ, Barros T, Biering-Sorensen F, et al. International standards for neurological classification of spinal cord injury. J Spinal Cord Med 2003;26 Suppl 1:S50-6.

215. Waters RL. Functional prognosis of spinal cord injuries. J Spinal Cord Med 1996;19:89-92.

216. Geisler FH, Coleman WP, Grieco G, Poonian D. Measurements and recovery patterns in a multicenter study of acute spinal cord injury. Spine 2001;26:S68-86.

217. van Hedel HJ, Wirz M, Dietz V. Assessing walking ability in subjects with spinal cord injury: validity and reliability of 3 walking tests. Arch Phys Med Rehabil 2005;86:190-6.

218. Ditunno JF, Jr., Barbeau H, Dobkin BH, et al. Validity of the Walking Scale for Spinal Cord Injury and Other Domains of Function in a Multicenter Clinical Trial. Neurorehabil Neural Repair 2007.

219. Ditunno JF, Scivoletto G, Patrick M, Biering-Sorensen F, Abel R, Marino R. Validation of the walking index for spinal cord injury in a US and European clinical population. Spinal Cord 2007.

220. Jackson AB, Carnel CT, Ditunno JF, et al. Outcome measures for gait and ambulation in the spinal cord injury population. J Spinal Cord Med 2008;31:487-99.

221. Schonherr MC, Groothoff JW, Mulder GA, Eisma WH. Prediction of functional outcome after spinal cord injury: a task for the rehabilitation team and the patient. Spinal Cord 2000;38:185-91.

222. Ragnarsson KT, Wuermser LA, Cardenas DD, Marino RJ. Spinal cord injury clinical trials for neurologic restoration: improving care through clinical research. Am J Phys Med Rehabil 2005;84:S77-97; quiz S8-100.

223. Curt A, Dietz V. Ambulatory capacity in spinal cord injury: significance of somatosensory evoked potentials and ASIA protocol in predicting outcome. Arch Phys Med Rehabil 1997;78:39-43.

224. Marino RJ, Graves DE. Metric properties of the ASIA motor score: subscales improve correlation with functional activities. Arch Phys Med Rehabil 2004;85:1804-10.

225. Ditunno JF, Jr., Ditunno PL, Graziani V, et al. Walking index for spinal cord injury (WISCI): an international multicenter validity and reliability study. Spinal Cord 2000;38:234-43.

226. Morganti B, Scivoletto G, Ditunno P, Ditunno JF, Molinari M. Walking index for spinal cord injury (WISCI): criterion validation. Spinal Cord 2005;43:27-33.

227. van Hedel HJ, Wirz M, Curt A. Improving walking assessment in subjects with an incomplete spinal cord injury: responsiveness. Spinal Cord 2006;44:352-6.

228. Dobkin B, Barbeau H, Deforge D, et al. The evolution of walking-related outcomes over the first 12 weeks of rehabilitation for incomplete traumatic spinal cord injury: the multicenter randomized Spinal Cord Injury Locomotor Trial. Neurorehabil Neural Repair 2007;21:25-35.

229. Rowland T, Ohno-Machado L, Ohrn A. Comparison of multiple prediction models for ambulation following spinal cord injury. Proc AMIA Symp 1998:528-32.

230. Burnett DM, Kolakowsky-Hayner SA, Gourley EV, 3rd, Cifu DX. Spinal cord injury "outliers": an analysis of etiology, outcomes, and length of stay. J Neurotrauma 2000;17:765-72.

231. Eftekhar B, Mohammad K, Ardebili HE, Ghodsi M, Ketabchi E. Comparison of artificial neural network and logistic regression models for prediction of mortality in head trauma based on initial clinical data. BMC Med Inform Decis Mak 2005;5:3.

232. Linder R, Konig IR, Weimar C, Diener HC, Poppl SJ, Ziegler A. Two models for outcome prediction - a comparison of logistic regression and neural networks. Methods Inf Med 2006;45:536-40.

233. Akaike H. A new look at the statistical model identification. IEEE Trans Automatic Control 1974;19:716-23.

234. Burnham KP, Anderson, D. R. Model selection and multimodel inference: A practical information-theoretic approach. New York, Springer-Verlag 2002.

235. Ditunno PL, Patrick M, Stineman M, Ditunno JF. Who wants to walk? Preferences for recovery after SCI: a longitudinal and cross-sectional study. Spinal Cord 2008;46:500-6.

236. Daverat P, Sibrac MC, Dartigues JF, et al. Early prognostic factors for walking in spinal cord injuries. Paraplegia 1988;26:255-61.

237. Crozier KS, Graziani V, Ditunno JF, Jr., Herbison GJ. Spinal cord injury: prognosis for ambulation based on sensory examination in patients who are initially motor complete. Arch Phys Med Rehabil 1991;72:119-21.

238. Jacobs SR, Yeaney NK, Herbison GJ, Ditunno JF, Jr. Future ambulation prognosis as predicted by somatosensory evoked potentials in motor complete and incomplete quadriplegia. Arch Phys Med Rehabil 1995;76:635-41.

239. Burns SP, Golding DG, Rolle WA, Jr., Graziani V, Ditunno JF, Jr. Recovery of ambulation in motor-incomplete tetraplegia. Arch Phys Med Rehabil 1997;78:1169-72.

240. Curt A, Dietz V. Electrophysiological recordings in patients with spinal cord injury: significance for predicting outcome. Spinal Cord 1999;37:157-65.

241. Scivoletto G, Morganti B, Ditunno P, Ditunno JF, Molinari M. Effects on age on spinal cord lesion patients' rehabilitation. Spinal Cord 2003;41:457-64.

242. Sipski ML, Jackson AB, Gomez-Marin O, Estores I, Stein A. Effects of gender on neurologic and functional recovery after spinal cord injury. Arch Phys Med Rehabil 2004;85:1826-36.

243. Kay ED, Deutsch A, Wuermser LA. Predicting walking at discharge from inpatient rehabilitation after a traumatic spinal cord injury. Arch Phys Med Rehabil 2007;88:745-50.

244. Kirshblum SC, O'Connor KC. Predicting neurologic recovery in traumatic cervical spinal cord injury. Arch Phys Med Rehabil 1998;79:1456-66.

245. Kirshblum SC, O'Connor KC. Levels of spinal cord injury and predictors of neurologic recovery. Phys Med Rehabil Clin N Am 2000;11:1-27, vii.

246. Waters RL, Adkins R, Yakura J, Vigil D. Prediction of ambulatory performance based on motor scores derived from standards of the American Spinal Injury Association. Arch Phys Med Rehabil 1994;75:756-60.

247. Curt A, Keck ME, Dietz V. Functional outcome following spinal cord injury: significance of motor-evoked potentials and ASIA scores. Arch Phys Med Rehabil 1998;79:81-6.

248. Oleson CV, Burns AS, Ditunno JF, Geisler FH, Coleman WP. Prognostic value of pinprick preservation in motor complete, sensory incomplete spinal cord injury. Arch Phys Med Rehabil 2005;86:988-92.

249. Kim CM, Eng JJ, Whittaker MW. Level walking and ambulatory capacity in persons with incomplete spinal cord injury: relationship with muscle strength. Spinal Cord 2004;42:156-62.

250. Silberstein M, Tress BM, Hennessy O. Prediction of neurologic outcome in acute spinal cord injury: the role of CT and MR. AJNR Am J Neuroradiol 1992;13:1597-608.

251. Flanders AE, Spettell CM, Tartaglino LM, Friedman DP, Herbison GJ. Forecasting motor recovery after cervical spinal cord injury: value of MR imaging. Radiology 1996;201:649-55.

252. Flanders AE, Spettell CM, Friedman DP, Marino RJ, Herbison GJ. The relationship between the functional abilities of patients with cervical spinal cord injury and the severity of damage revealed by MR imaging. AJNR Am J Neuroradiol 1999;20:926-34.

253. Metz GA, Curt A, van de Meent H, Klusman I, Schwab ME, Dietz V. Validation of the weight-drop contusion model in rats: a comparative study of human spinal cord injury. J Neurotrauma 2000;17:1-17.

254. Miyanji F, Furlan JC, Aarabi B, Arnold PM, Fehlings MG. Acute cervical traumatic spinal cord injury: MR imaging findings correlated with neurologic outcome--prospective study with 100 consecutive patients. Radiology 2007;243:820-7.

255. Tuszynski MH, Steeves JD, Fawcett JW, et al. Guidelines for the conduct of clinical trials for spinal cord injury as developed by the ICCP Panel: clinical trial inclusion/exclusion criteria and ethics. Spinal Cord 2007;45:222-31.

256. Grundy BL, Friedman W. Electrophysiological evaluation of the patient with acute spinal cord injury. Crit Care Clin 1987;3:519-48.

257. Houlden DA, Schwartz ML, Klettke KA. Neurophysiologic diagnosis in uncooperative trauma patients: confounding factors. J Trauma 1992;33:244-51.

258. Curt A, Van Hedel HJ, Klaus D, Dietz V. Recovery from a spinal cord injury: significance of compensation, neural plasticity, and repair. J Neurotrauma 2008;25:677-85.

259. Deletis V, Sala F. Intraoperative neurophysiological monitoring of the spinal cord during spinal cord and spine surgery: a review focus on the corticospinal tracts. Clin Neurophysiol 2008;119:248-64.

260. Kelleher MO, Tan G, Sarjeant R, Fehlings MG. Predictive value of intraoperative neurophysiological monitoring during cervical spine surgery: a prospective analysis of 1055 consecutive patients. J Neurosurg Spine 2008;8:215-21.

261. Bosch A, Stauffer ES, Nickel VL. Incomplete traumatic quadriplegia. A ten-year review. Jama 1971;216:473-8.

262. Maynard FM, Reynolds GG, Fountain S, Wilmot C, Hamilton R. Neurological prognosis after traumatic quadriplegia. Three-year experience of California Regional Spinal Cord Injury Care System. J Neurosurg 1979;50:611-6.

263. Geisler FH, Coleman WP, Grieco G, Poonian D. The Sygen multicenter acute spinal cord injury study. Spine 2001;26:S87-98.

264. Buchli AD, Rouiller E, Mueller R, Dietz V, Schwab ME. Repair of the injured spinal cord. A joint approach of basic and clinical research. Neurodegener Dis 2007;4:51-6.

265. Kirshblum S, Millis S, McKinley W, Tulsky D. Late neurologic recovery after traumatic spinal cord injury. Arch Phys Med Rehabil 2004;85:1811-7.

266. Anderson KD. Targeting recovery: priorities of the spinal cord-injured population. J Neurotrauma 2004;21:1371-83.

267. McKinley W, Santos K, Meade M, Brooke K. Incidence and outcomes of spinal cord injury clinical syndromes. J Spinal Cord Med 2007;30:215-24.

268. Iseli E, Cavigelli A, Dietz V, Curt A. Prognosis and recovery in ischaemic and traumatic spinal cord injury: clinical and electrophysiological evaluation. J Neurol Neurosurg Psychiatry 1999;67:567-71.

269. McKinley WO, Huang ME, Tewksbury MA. Neoplastic vs. traumatic spinal cord injury: an inpatient rehabilitation comparison. Am J Phys Med Rehabil 2000;79:138-44.

270. McKinley WO, Seel RT, Gadi RK, Tewksbury MA. Nontraumatic vs. traumatic spinal cord injury: a rehabilitation outcome comparison. Am J Phys Med Rehabil 2001;80:693-9; quiz 700, 16.

271. Dutta R, Trapp BD. Pathogenesis of axonal and neuronal damage in multiple sclerosis. Neurology 2007;68:S22-31; discussion S43-54.

272. Dhib-Jalbut S. Pathogenesis of myelin/oligodendrocyte damage in multiple sclerosis. Neurology 2007;68:S13-21; discussion S43-54.

273. Moreau T, Coles A, Wing M, et al. Transient increase in symptoms associated with cytokine release in patients with multiple sclerosis. Brain 1996;119 (Pt 1):225-37.

274. Kapoor R, Davies M, Smith KJ. Temporary axonal conduction block and axonal loss in inflammatory neurological disease. A potential role for nitric oxide? Ann N Y Acad Sci 1999;893:304-8.

275. Radtke C, Spies M, Sasaki M, Vogt PM, Kocsis JD. Demyelinating diseases and potential repair strategies. Int J Dev Neurosci 2007;25:149-53.

276. Bruck W, Kuhlmann T, Stadelmann C. Remyelination in multiple sclerosis. J Neurol Sci 2003;206:181-5.

277. Waxman SG. Demyelinating diseases--new pathological insights, new therapeutic targets. N Engl J Med 1998;338:323-5.

278. Gensert JM, Goldman JE. Endogenous progenitors remyelinate demyelinated axons in the adult CNS. Neuron 1997;19:197-203.

279. Alvarez-Buylla A, Temple S. Stem cells in the developing and adult nervous system. J Neurobiol 1998;36:105-10.

280. Gage FH. Mammalian neural stem cells. Science 2000;287:1433-8.

281. Shihabuddin LS, Ray J, Gage FH. FGF-2 is sufficient to isolate progenitors found in the adult mammalian spinal cord. Exp Neurol 1997;148:577-86.

282. Martino G, Pluchino S. The therapeutic potential of neural stem cells. Nat Rev Neurosci 2006;7:395-406.

283. Miller RH. The promise of stem cells for neural repair. Brain Res 2006;1091:258-64.

284. Gould E, Tanapat P. Lesion-induced proliferation of neuronal progenitors in the dentate gyrus of the adult rat. Neuroscience 1997;80:427-36.

285. Picard-Riera N, Decker L, Delarasse C, et al. Experimental autoimmune encephalomyelitis mobilizes neural progenitors from the subventricular zone to undergo oligodendrogenesis in adult mice. Proc Natl Acad Sci U S A 2002;99:13211-6.

286. Lassmann H. Stem cell and progenitor cell transplantation in multiple sclerosis: the discrepancy between neurobiological attraction and clinical feasibility. J Neurol Sci 2005;233:83-6.

287. Magnus T, Rao MS. Neural stem cells in inflammatory CNS diseases: mechanisms and therapy. J Cell Mol Med 2005;9:303-19.

288. Pluchino S, Furlan R, Martino G. Cell-based remyelinating therapies in multiple sclerosis: evidence from experimental studies. Curr Opin Neurol 2004;17:247-55.

289. McDonald JW, Liu XZ, Qu Y, et al. Transplanted embryonic stem cells survive, differentiate and promote recovery in injured rat spinal cord. Nat Med 1999;5:1410-2.

290. Cummings BJ, Uchida N, Tamaki SJ, et al. Human neural stem cells differentiate and promote locomotor recovery in spinal cord-injured mice. Proc Natl Acad Sci U S A 2005;102:14069-74.

291. Kutzelnigg A, Lucchinetti CF, Stadelmann C, et al. Cortical demyelination and diffuse white matter injury in multiple sclerosis. Brain 2005;128:2705-12.

292. Plunet W, Kwon BK, Tetzlaff W. Promoting axonal regeneration in the central nervous system by enhancing the cell body response to axotomy. J Neurosci Res 2002;68:1-6.

293. Ramon y Cajal S. Degeneration and Regeneration of the Nervous System. Hafner, New York 1928.

294. David S, Aguayo AJ. Axonal elongation into peripheral nervous system "bridges" after central nervous system injury in adult rats. Science 1981;214:931-3.

295. Mukhopadhyay G, Doherty P, Walsh FS, Crocker PR, Filbin MT. A novel role for myelin-associated glycoprotein as an inhibitor of axonal regeneration. Neuron 1994;13:757-67.

296. Niederost BP, Zimmermann DR, Schwab ME, Bandtlow CE. Bovine CNS myelin contains neurite growth-inhibitory activity associated with chondroitin sulfate proteoglycans. J Neurosci 1999;19:8979-89.

297. Benson MD, Romero MI, Lush ME, Lu QR, Henkemeyer M, Parada LF. Ephrin-B3 is a myelin-based inhibitor of neurite outgrowth. Proc Natl Acad Sci U S A 2005;102:10694-9.

298. Bartsch U, Bandtlow CE, Schnell L, et al. Lack of evidence that myelin-associated glycoprotein is a major inhibitor of axonal regeneration in the CNS. Neuron 1995;15:1375-81.

299. Buchli AD, Schwab ME. Inhibition of Nogo: a key strategy to increase regeneration, plasticity and functional recovery of the lesioned central nervous system. Ann Med 2005;37:556-67.

300. Johansson BB. Brain plasticity and stroke rehabilitation. The Willis lecture. Stroke 2000;31:223-30.

301. Ward NS, Cohen LG. Mechanisms underlying recovery of motor function after stroke. Arch Neurol 2004;61:1844-8.

302. Holtmaat AJ, Trachtenberg JT, Wilbrecht L, et al. Transient and persistent dendritic spines in the neocortex in vivo. Neuron 2005;45:279-91.

303. Cafferty WB, Strittmatter SM. The Nogo-Nogo receptor pathway limits a spectrum of adult CNS axonal growth. J Neurosci 2006;26:12242-50.

304. Cifelli A, Matthews PM. Cerebral plasticity in multiple sclerosis: insights from fMRI. Mult Scler 2002;8:193-9.

305. Deisseroth K. Controlling the brain with light. Sci Am 2010;303:48-55.

306. Vulliemoz S, Raineteau O, Jabaudon D. Reaching beyond the midline: why are human brains cross wired? Lancet Neurol 2005;4:87-99.

307. Serafini T, Colamarino SA, Leonardo ED, et al. Netrin-1 is required for commissural axon guidance in the developing vertebrate nervous system. Cell 1996;87:1001-14.

308. Finger JH, Bronson RT, Harris B, Johnson K, Przyborski SA, Ackerman SL. The netrin 1 receptors Unc5h3 and Dcc are necessary at multiple choice points for the guidance of corticospinal tract axons. J Neurosci 2002;22:10346-56.

309. Sabatier C, Plump AS, Le M, et al. The divergent Robo family protein rig-1/Robo3 is a negative regulator of slit responsiveness required for midline crossing by commissural axons. Cell 2004;117:157-69.

310. Castellani V, Chedotal A, Schachner M, Faivre-Sarrailh C, Rougon G. Analysis of the L1-deficient mouse phenotype reveals cross-talk between Sema3A and L1 signaling pathways in axonal guidance. Neuron 2000;27:237-49.

311. Kullander K, Croll SD, Zimmer M, et al. Ephrin-B3 is the midline barrier that prevents corticospinal tract axons from recrossing, allowing for unilateral motor control. Genes & development 2001;15:877-88.

312. Yokoyama N, Romero MI, Cowan CA, et al. Forward signaling mediated by ephrin-B3 prevents contralateral corticospinal axons from recrossing the spinal cord midline. Neuron 2001;29:85-97.

313. Beauparlant J, van den Brand R, Barraud Q, et al. Undirected compensatory plasticity contributes to neuronal dysfunction after severe spinal cord injury. Brain 2013;136:3347-61.

314. Raad M, El Tal T, Gul R, et al. Neuroproteomics approach and neurosystems biology analysis: ROCK inhibitors as promising therapeutic targets in neurodegeneration and neurotrauma. Electrophoresis 2012;33:3659-68.

315. Caudle WM, Bammler TK, Lin Y, Pan S, Zhang J. Using 'omics' to define pathogenesis and biomarkers of Parkinson's disease. Expert review of neurotherapeutics 2010;10:925-42.

316. Lovely RG, Gregor RJ, Roy RR, Edgerton VR. Effects of training on the recovery of full-weight-bearing stepping in the adult spinal cat. Exp Neurol 1986;92:421-35.
317. Starkey ML, Bleul C, Kasper H, et al. High-Impact, Self-Motivated Training Within an Enriched Environment With Single Animal Tracking Dose-Dependently Promotes Motor Skill Acquisition and Functional Recovery. Neurorehabil Neural Repair 2014.
318. Forssberg H, Grillner S. The locomotion of the acute spinal cat injected with clonidine i.v. Brain Res 1973;50:184-6.
319. Barbeau H, Rossignol S. Initiation and modulation of the locomotor pattern in the adult chronic spinal cat by noradrenergic, serotonergic and dopaminergic drugs. Brain Res 1991;546:250-60.
320. Fedirchuk B, Nielsen J, Petersen N, Hultborn H. Pharmacologically evoked fictive motor patterns in the acutely spinalized marmoset monkey (Callithrix jacchus). Exp Brain Res 1998;122:351-61.
321. Antri M, Mouffle C, Orsal D, Barthe JY. 5-HT1A receptors are involved in short- and long-term processes responsible for 5-HT-induced locomotor function recovery in chronic spinal rat. Eur J Neurosci 2003;18:1963-72.
322. Musienko P, van den Brand R, Marzendorfer O, et al. Controlling specific locomotor behaviors through multidimensional monoaminergic modulation of spinal circuitries. J Neurosci 2011;31:9264-78.
323. Brustein E, Rossignol S. Recovery of locomotion after ventral and ventrolateral spinal lesions in the cat. II. Effects of noradrenergic and serotoninergic drugs. J Neurophysiol 1999;81:1513-30.
324. Ballion B, Morin D, Viala D. Forelimb locomotor generators and quadrupedal locomotion in the neonatal rat. Eur J Neurosci 2001;14:1727-38.
325. Nudo RJ, Masterton RB. Descending pathways to the spinal cord: a comparative study of 22 mammals. J Comp Neurol 1988;277:53-79.
326. Jordan LM. Initiation of locomotion in mammals. Ann N Y Acad Sci 1998;860:83-93.
327. Jordan LM, Liu J, Hedlund PB, Akay T, Pearson KG. Descending command systems for the initiation of locomotion in mammals. Brain Res Rev 2008;57:183-91.
328. Matsuyama K, Nakajima K, Mori F, Aoki M, Mori S. Lumbar commissural interneurons with reticulospinal inputs in the cat: morphology and discharge patterns during fictive locomotion. J Comp Neurol 2004;474:546-61.
329. Shefchyk SJ, Jell RM, Jordan LM. Reversible cooling of the brainstem reveals areas required for mesencephalic locomotor region evoked treadmill locomotion. Exp Brain Res 1984;56:257-62.
330. Bachmann LC, Matis A, Lindau NT, Felder P, Gullo M, Schwab ME. Deep brain stimulation of the midbrain locomotor region improves paretic hindlimb function after spinal cord injury in rats. Science translational medicine 2013;5:208ra146.
331. Deuschl G, Agid Y. Subthalamic neurostimulation for Parkinson's disease with early fluctuations: balancing the risks and benefits. Lancet Neurol 2013;12:1025-34.
332. Anderson D, Kartha N. Deep brain stimulation in nonparkinsonian movement disorders and emerging technologies, targets, and therapeutic promises in deep brain stimulation. Neurol Clin 2013;31:809-26.
333. Kalia SK, Sankar T, Lozano AM. Deep brain stimulation for Parkinson's disease and other movement disorders. Curr Opin Neurol 2013;26:374-80.
334. Hardenacke K, Shubina E, Buhrle CP, et al. Deep Brain Stimulation as a Tool for Improving Cognitive Functioning in Alzheimer's Dementia: A Systematic Review. Frontiers in psychiatry 2013;4:159.

335. Hardenacke K, Kuhn J, Lenartz D, et al. Stimulate or degenerate: deep brain stimulation of the nucleus basalis Meynert in Alzheimer dementia. World neurosurgery 2013;80:S27 e35-43.
336. Salma A, Vasilakis M, Tracy PT. Deep brain stimulation for cognitive disorders: insights into targeting nucleus basalis of meynert in Alzheimer dementia. World neurosurgery 2014;81:e4-5.
337. Schlaepfer TE, Bewernick BH, Kayser S, Madler B, Coenen VA. Rapid effects of deep brain stimulation for treatment-resistant major depression. Biological psychiatry 2013;73:1204-12.
338. Anderson RJ, Frye MA, Abulseoud OA, et al. Deep brain stimulation for treatment-resistant depression: efficacy, safety and mechanisms of action. Neurosci Biobehav Rev 2012;36:1920-33.
339. Bewernick BH, Kayser S, Sturm V, Schlaepfer TE. Long-term effects of nucleus accumbens deep brain stimulation in treatment-resistant depression: evidence for sustained efficacy. Neuropsychopharmacology : official publication of the American College of Neuropsychopharmacology 2012;37:1975-85.
340. Williams NR, Okun MS. Deep brain stimulation (DBS) at the interface of neurology and psychiatry. The Journal of clinical investigation 2013;123:4546-56.
341. Tierney TS, Sankar T, Lozano AM. Deep brain stimulation emerging indications. Prog Brain Res 2011;194:83-95.
342. Benarroch EE. Pedunculopontine nucleus: functional organization and clinical implications. Neurology 2013;80:1148-55.
343. Plaha P, Gill SS. Bilateral deep brain stimulation of the pedunculopontine nucleus for Parkinson's disease. Neuroreport 2005;16:1883-7.
344. Stefani A, Lozano AM, Peppe A, et al. Bilateral deep brain stimulation of the pedunculopontine and subthalamic nuclei in severe Parkinson's disease. Brain 2007;130:1596-607.
345. Leray E, Yaouanq J, Le Page E, et al. Evidence for a two-stage disability progression in multiple sclerosis. Brain 2010;133:1900-13.
346. Markowitz CE. The current landscape and unmet needs in multiple sclerosis. The American journal of managed care 2010;16:S211-8.
347. Yang Y, Liu Y, Wei P, et al. Silencing Nogo-A promotes functional recovery in demyelinating disease. Ann Neurol 2010;67:498-507.
348. Karnezis T, Mandemakers W, McQualter JL, et al. The neurite outgrowth inhibitor Nogo A is involved in autoimmune-mediated demyelination. Nat Neurosci 2004;7:736-44.
349. Chong SY, Rosenberg SS, Fancy SP, et al. Neurite outgrowth inhibitor Nogo-A establishes spatial segregation and extent of oligodendrocyte myelination. Proc Natl Acad Sci U S A 2012;109:1299-304.

Publications

1. Chasing CNS plasticity: the brainstem's contribution to locomotor recovery in spinal cord injured rats.
Zörner B, Bachmann LC, Filli L, Kapitza S, Gullo M, Bolliger M, Starkey ML, Röthlisberger M, Gonzenbach RR, Schwab ME.
Brain *in press*.

2. High-Impact, Self-Motivated Training Within an Enriched Environment With Single Animal Tracking Dose-Dependently Promotes Motor Skill Acquisition and Functional Recovery.
Starkey ML, Bleul C, Kasper H, Mosberger AC, **Zörner B**, Giger S, Gullo M, Buschmann F, Schwab ME.
Neurorehabil Neural Repair. 2014. [Epub ahead of print].

3. Infusion of anti-Nogo-A antibodies in adult rats increases growth and synapse related proteins in the absence of behavioral alterations.
Craveiro LM, Weinmann O, Roschitzki B, Gonzenbach RR, **Zörner B**, Montani L, Yee BK, Feldon J, Willi R, Schwab ME.
Exp Neurol. 2013. 250; 52-68.

4. Back seat driving: hindlimb corticospinal neurons assume forelimb control following ischaemic stroke.
Starkey ML, Bleul C, **Zörner B**, Lindau NT, Mueggler T, Rudin M, Schwab ME.
Brain. 2012. 135; 3265-3281.

5. Tail spasms in rat spinal cord injury: Changes in interneuronal connectivity.
Kapitza S, **Zörner B**, Weinmann O, Bolliger M, Filli L, Dietz V, Schwab ME.
Exp Neurol. 2012. 236; 179-189.

6. Sustained Efficacy of Natalizumab in the Treatment of Relapsing-Remitting Multiple Sclerosis Independent of Disease Activity and Disability at Baseline: Real-Life Data From a Swiss Cohort.
Kallweit U, Jelcic I, Braun N, Fischer H, **Zörner B**, Schreiner B, Sokolov AA, Martin R, Weller M, Linnebank M.
Clin Neuropharmacol. 2012. 35; 77-80.

7. Delayed anti-nogo-a antibody application after spinal cord injury shows progressive loss of responsiveness.
Gonzenbach RR, **Zoerner B**, Schnell L, Weinmann O, Mir AK, Schwab ME.
J Neurotrauma. 2012. 29; 567-578.

8. Motor deficits and recovery in rats with unilateral spinal cord hemisection mimic the Brown-Sequard syndrome.
Filli L, **Zörner B**, Weinmann O, Schwab ME.
Brain. 2011. 134: 2261-2273.

9. Profiling locomotor recovery: comprehensive quantification of impairments after CNS damage in rodents.
Zörner B, Filli L, Starkey ML, Gonzenbach R, Kasper H, Röthlisberger M, Bolliger M, Schwab ME.
Nat Methods. 2010. 7: 701-708.

10. A novel classification of quiescent and transit amplifying adult neural stem cells by surface and metabolic markers permits a defined simultaneous isolation.
Obermair FJ, Fiorelli R, Schroeter A, Beyeler S, Blatti C, **Zoerner B**, Thallmair M.
Stem Cell Res. 2010. 5: 131-143.

11. Anti-Nogo on the go: from animal models to a clinical trial.
Zörner B, Schwab ME.
Ann N Y Acad Sci. 2010. 1198 Suppl 1: E22-34. Review.

12. Nogo-A antibodies and training reduce muscle spasms in spinal cord-injured rats.
Gonzenbach RR, Gasser P, **Zörner B**, Hochreutener E, Dietz V, Schwab ME.
Ann Neurol. 2010. 68: 48-57.

13. Modulation of spinal reflex by assisted locomotion in humans with chronic complete spinal cord injury.
Bolliger M, Trepp A, **Zörner B**, Dietz V.
Clin Neurophysiol. 2010. 121:2152-2158.

14. Outcome after incomplete spinal cord injury: central cord versus Brown-Sequard syndrome.
Wirz M, **Zörner B**, Rupp R, Dietz V.
Spinal Cord. 2010. 48: 407-414.

15. Basic mechanisms of functional recovery.
Zörner B, Schwab ME.
In Kesselring, Comi and Thompson;
Multiple Sclerosis: Recovery of Function and Neurorehabilitation.
Cambridge University Press. 2010. 5; 44-52. Textbook Article.

16. Functional and anatomical reorganization of the sensory-motor cortex after
incomplete spinal cord injury in adult rats.
Ghosh A, Sydekum E, Haiss F, Peduzzi S, **Zörner B**, Schneider R, Baltes C,
Rudin M, Weber B, Schwab ME.
J Neurosci. 2009. 29: 12210-12219.

17. Mice with a mutation in the dynein heavy chain 1 gene display sensory neuropathy
but lack motor neuron disease.
Dupuis L, Fergani A, Braunstein KE, Eschbach J, Holl N, Rene F, Gonzalez De Aguilar JL,
Zoerner B, Schwalenstocker B, Ludolph AC, Loeffler JP.
Exp Neurol. 2009. 215: 146-152.

18. Clinical algorithm for improved prediction of ambulation and patient stratification
after incomplete spinal cord injury.
Zörner B, Blanckenhorn WU, Dietz V; EM-SCI Study Group, Curt A.
J Neurotrauma. 2010. 27: 241-252.

19. Levodopa therapy in incomplete spinal cord injury.
Maric O, **Zörner B**, Dietz V.
J Neurotrauma. 2008. 25: 1303-1307.

20. Reduced expression of brain-derived neurotrophic factor in mice deficient for pituitary
adenylate cyclase activating polypeptide type-I-receptor.
Zink M, Otto C, **Zörner B**, Zacher C, Schütz G, Henn FA, Gass P.
Neurosci Lett. 2004. 360: 106-108.

21. Mice with reduced brain-derived neurotrophic factor expression show decreased choline acetyltransferase activity, but regular brain monoamine levels and unaltered emotional behavior.
Chourbaji S, Hellweg R, Brandis D, **Zörner B**, Zacher C, Lang UE, Henn FA, Hörtnagl H, Gass P.
Brain Res Mol Brain Res. 2004. 121: 28-36.

22. Forebrain-specific trkB-receptor knockout mice: behaviorally more hyperactive than "depressive".
Zörner B, Wolfer DP, Brandis D, Kretz O, Zacher C, Madani R, Grunwald I, Lipp HP, Klein R, Henn FA, Gass P.
Biol Psychiatry. 2003. 54: 972-982.

23. Memory retrieval after contextual fear conditioning induces c-Fos and JunB expression in CA1 hippocampus.
Strekalova T, **Zörner B**, Zacher C, Sadovska G, Herdegen T, Gass P.
Genes Brain Behav. 2003. 2: 3-10.